AGITATION, MIXING AND MASS TRANSFER IN SIMULATED HIGH VISCOSITY FERMENTATION BROTHS

by

ALAN DOUGLAS HICKMAN

A thesis submitted to the Faculty of Science and Engineering of the University of Birmingham for the Degree of Doctor of Philosophy

Chemical Engineering Department
University of Birmingham - 1985

ABSTRACT

Gas-liquid mass transfer, agitator power consumption, rheology, gas-liquid mixing and gas hold-up have been studied in an agitated, sparged vessel of diameter, T = 0.3 m, with a liquid capacity of 0.02 m^3, unaerated liquid height = 0.3 m. The solutions of sodium carboxymethylcellulose used exhibit moderate viscoelasticity and shear thinning behaviour, obeying the power law over the range of shear rates studied. The gas-liquid mass transfer was studied using a steady state technique. This involves monitoring the gas and liquid phase oxygen concentrations when a microorganism (yeast) is cultured in the solutions of interest. Agitator power consumption was measured using strain gauges mounted on the impeller shaft. Various agitator geometries were used. These were: Rushton turbines (D = T/3 and D = T/2), used singly and in pairs; Intermig impellers (D = 0.58T), used as a pair; and a 45° pitched blade turbine (D = T/2), used in combination with a Rushton turbine. Gas hold-up and gas-liquid flow patterns were visually observed. In addition, the state of the culture variables, (oxygen uptake rate and carbon dioxide production rate), were used to provide a respiratory quotient, the value of which can be linked to the degree of gas-liquid mixing in the vessel. Measurement of point values of the liquid phase oxygen concentration is also used to indicate the degree of liquid mixing attained.

The volumetric mass transfer coefficient, $k_L a$, was found to be dependent on the conditions in which the yeast was cultivated, as well as being a function of time. These variations were associated with variations in solution composition seen over the course of each experiment. Steps were taken to ensure that further $k_L a$ values were measured under identical conditions of the culture variables, in order to determine the effect on $k_L a$ of varying viscosity, agitator speed and type and air flow rate.

Increasing solution viscosity results in poorer gas-liquid mixing and a reduction in $k_L a$, as has been found by earlier workers. Thus high agitator speeds and power inputs are required to maintain adequate mass transfer rates. In the more viscous solutions used, large diameter dual impeller systems were required, to mix the gas and liquid phases. Of these a pair of Rushton turbines (D = T/2) gave the highest $k_L a$ values at a given power input. In these solutions the dependence of $k_L a$ on the gassing rate, which is seen in intermediate and low viscosity solutions, virtually disappears, with $k_L a$ highly dependent on the power input and the apparent viscosity. At intermediate viscosities a smaller pair of Rushton turbines showed the most efficient mass transfer characteristics, here $k_L a$ is dependent on the power input and the gassing rate, but independent of viscosity. This is linked to the flow regime in force in the vessel, which at intermediate viscosities lies in the transition region between the laminar and turbulent flow regimes. Variations in gas hold-up, rising then falling with increasing impeller speed, were linked to variations in the gassed power number, falling then rising with increasing impeller speed. These effects are considered to be due to variations in the size of the gas filled cavities behind the impeller blades.

TO MY WIFE: SUE

ACKNOWLEDGEMENTS

Firstly, I would like to thank Professor A.W. Nienow for all his invaluable help and encouragement over the last three years.

I am also grateful to the following members of the department for their interest and help given:

Bob Badham and Sid Chatwin for their technical expertise.

Stan Ward for constructing the equipment.

Paul Wilkinson for the photographs.

In addition I would like to say a big thank you to all the other members of the department and my fellow postgraduates who have shown an interest or offered advice regarding this work.

Finally, I gratefully acknowledge the financial support of the Science and Engineering Research Council, who provided a CASE award and Tate and Lyle Ltd. for acting as a collaborating body for the CASE award.

CONTENTS

CHAPTER 1

INTRODUCTION

1.1) Motivation and the Areas of Interest

The absorption of a gas into a liquid is an important step in many major industrial processes. These processes include reactions such as chlorination, hydrogenation, carbonation and oxidation, as well as processes which utilise microorganisms, such as in aerobic fermentations and in waste water treatment. Gas absorption is usually limited by the interfacial area and the liquid phase mass transfer coefficient, especially when the gas is sparingly soluble (see Chapter 4, section 1). The interfacial area available for absorption is increased in many continuous processes by passing the liquid over a solid support of large surface area; otherwise it is common to sparge the gas through the bulk liquid.

Mechanically agitated vessels are in common use in processes involving gas-liquid contact, since air sparging alone may not promote sufficient liquid turbulence to break up the gas bubbles[1]. Mechanical agitation breaks up the bubbles and circulates them around the vessel, increasing interfacial area. Mechanical agitation also enhances heat transfer, reduces inhomogeneity within the liquid and aids suspension of solid particles. Its limitations include increased costs for installation and power consumption, although to obtain the same mass transfer by air sparging alone may be more costly[2].

This present work concentrates on oxygen transfer from air into aqueous solutions contained in a sparged agitated vessel. This situation is commonly found in the fermentation industry; in the production of biomass, e.g. Bakers Yeast or single cell protein, metabolites such as citric acid or antibiotics, and macromolecules, e.g. enzymes and polysaccharides. Oxygen is utilised for growth and product formation, but

mainly as the final step in the provision of energy, through respiration. As oxygen is only slightly soluble, it needs to be supplied continuously from the gas phase to cope with the high demand of actively growing micro-organisms. The amount of oxygen dissolved in the culture fluid may typically last for only ten seconds[3]. A shortage of oxygen can cause formation of unwanted by-products, reducing yield and may cause cell death.

Microbiological cultures are often rheologically complex and highly viscous. This can be caused by high substrate or product concentration, or cell morphology, or a combination of these factors (see Chapter 2, section 3). The rheological properties of the liquid can have a large effect on the performance of a process[4], (see Chapters 3 and 4). High viscosity reduces the degree of turbulence at a particular agitation speed, thus reducing heat and mass transport rates. Increasing agitator speed increases costs by raising the power input and the amount of heat which has to be removed. The rheological properties affect the bubble coalescence rate and equilibrium bubble size which in turn alters the interfacial area.[13] In addition, increasing the concentration of the solutes associated with increasing viscosity often diminishes the diffusivity of gases, which in turn reduces the mass transfer coefficient. Mixing times are increased with increasing viscosity, which can lead to a marked variation in oxygen concentration throughout the vessel. Viscous culture fluids often exhibit shear thinning behaviour and sometimes a yield stress (see Chapter 2). These features combine to give a rapid fall off of shear rate away from the turbulent impeller regions leaving large dead zones, particularly around baffles and other internal surfaces such as heat exchanger coils.

A study of mass transfer in rheologically complex cultures is hampered by the variations of rheological properties with time, as most large scale cultures of interest are carried out in batch or semi-batch fashion. In this present study, model fluids are employed to reproduce

some of the rheological properties observed in culture broths, enabling mass transfer to be studied in conjunction with power consumption, mixing and hold-up of gas within these liquids, under different agitation and aeration conditions.

1.2) Layout of Thesis

The thesis can be divided into two main parts. The first part, Chapter 1 to 4, covers the background and literature, which is sub-divided under these headings: Rheology (Chapter 2), Power and Mixing (Chapter 3) and Mass Transfer (Chapter 4). Some overlap occurs between the chapters, for example a discussion of "apparent viscosity" and its determination occurs in Chapter 3 with an outline of the dimensionless numbers related to power consumption. Where necessary cross references have been made between the subsections to aid the reader.

The second part, Chapter 5 onwards, contains a description of the experimental work carried out and a discussion of that work in relation to the literature. As a variety of methods are available for the measurement of mass transfer coefficients in gas-liquid systems, their relative merits for use in viscous liquid systems are outlined in Chapter 4. The presentation and discussion of the results obtained using the chosen methods is divided into several parts: In Chapter 6 the results which are of relevance in the development of the experimental methods used are presented, whilst the mass transfer coefficients obtained are related to the power consumption, the rheological properties, the aeration rate and the agitation conditions within the vessel in Chapter 8. Prior to this, in Chapter 7, the mixing of the gas and liquid phases and the power consumption is analysed under various aeration and agitation conditions.

The overall conclusions which are drawn are contained in Chapter 9, with a discussion of their relevance to industrial scale practices and results. This leads to some suggestions for further work.

CHAPTER 2

RHEOLOGY

2.1) General Background

There are many texts dealing with the theoretical and practical aspects of rheology (see references 4 - 8), so this chapter deals only with the parts of the subject which are of direct relevance to the work carried out. Rheology can be defined as "the study of the deformation and the flow of matter"; this work exclusively deals with the rheology of liquids. From the rheological viewpoint, fluids can be subdivided into two main classes: Newtonian and non-Newtonian. Non-Newtonian fluids contain many sub-classes, which are described in the following sections. Newtonian fluids are defined as exhibiting a direct proportionality between an applied shear stress, τ, and the corresponding resultant shear rate, $\dot{\gamma}$. Such that:

$$\frac{\tau}{\dot{\gamma}} = \mu = \text{a constant} \qquad (2.1)$$

Where μ is termed the "coefficient of viscosity", or just the "viscosity" of the fluid, and is independent of shear, dependent only on temperature and pressure. The properties of non-Newtonian liquids which are of interest are their viscous properties, their elastic properties and their time dependent properties. These are each dealt with in turn.

2.1.1) Viscous Properties of Non-Newtonian fluids

A plot of shear stress versus shear rate is termed a rheogram. For a Newtonian fluid this yields a straight line of slope μ, passing through the origin. Similar plots for non-Newtonian fluids give lines which may be curved, or which do not pass through the origin, or both.

In general, non-Newtonian fluids have variable coefficients of viscosity, termed the apparent viscosity, μ_a, which is dependent on the value of the shear rate. As the shear rate in many pieces of equipment which are used with non-Newtonian fluids is not uniform, it is often necessary to use an average value, see section 3.1.

By analogy with Newtonian fluids, the apparent viscosity is defined as:

$$\frac{\tau}{\dot{\gamma}} = \mu_a = \text{a variable} \qquad (2.2)$$

Figure 2.1 shows some representative rheograms for Newtonian and non-Newtonian fluids. The group labelled "plastic" will not flow until a critical yield stress, τ_y, is exceeded. If the τ versus $\dot{\gamma}$ graph follows a straight line when τ_y, is exceeded then the fluid is termed a Bingham Plastic.

Most rheologically complex materials, including the solutions used in this work, show the type of behaviour labelled shear thinning in figure 2.1. These shear thinning materials are often termed pseudo-plastic, from comparison with plastic behaviour, with the ratio of the shear stress to the shear rate falling with increasing shear rate, so the apparent viscosity is reduced with increasing shear. Figure 2.2 shows the variation of the apparent viscosity with shear rate for a typical shear thinning fluid. It can be seen that there are regions at low and high shear rate where Newtonian behaviour is approximated, i.e. the apparent viscosity remains constant with changing shear rate. One means used to explain these regions of constant viscosity is to consider the orientation of large asymmetric molecules within the liquid. The shear effects at low shear rates which tend to organise the entangled molecules into parallel lines are overcome by the random motion of the molecules. This provides a high resistance to shear and hence a high

Figure 2.1 Representative Rheograms for Classes of Non-Newtonian Fluids

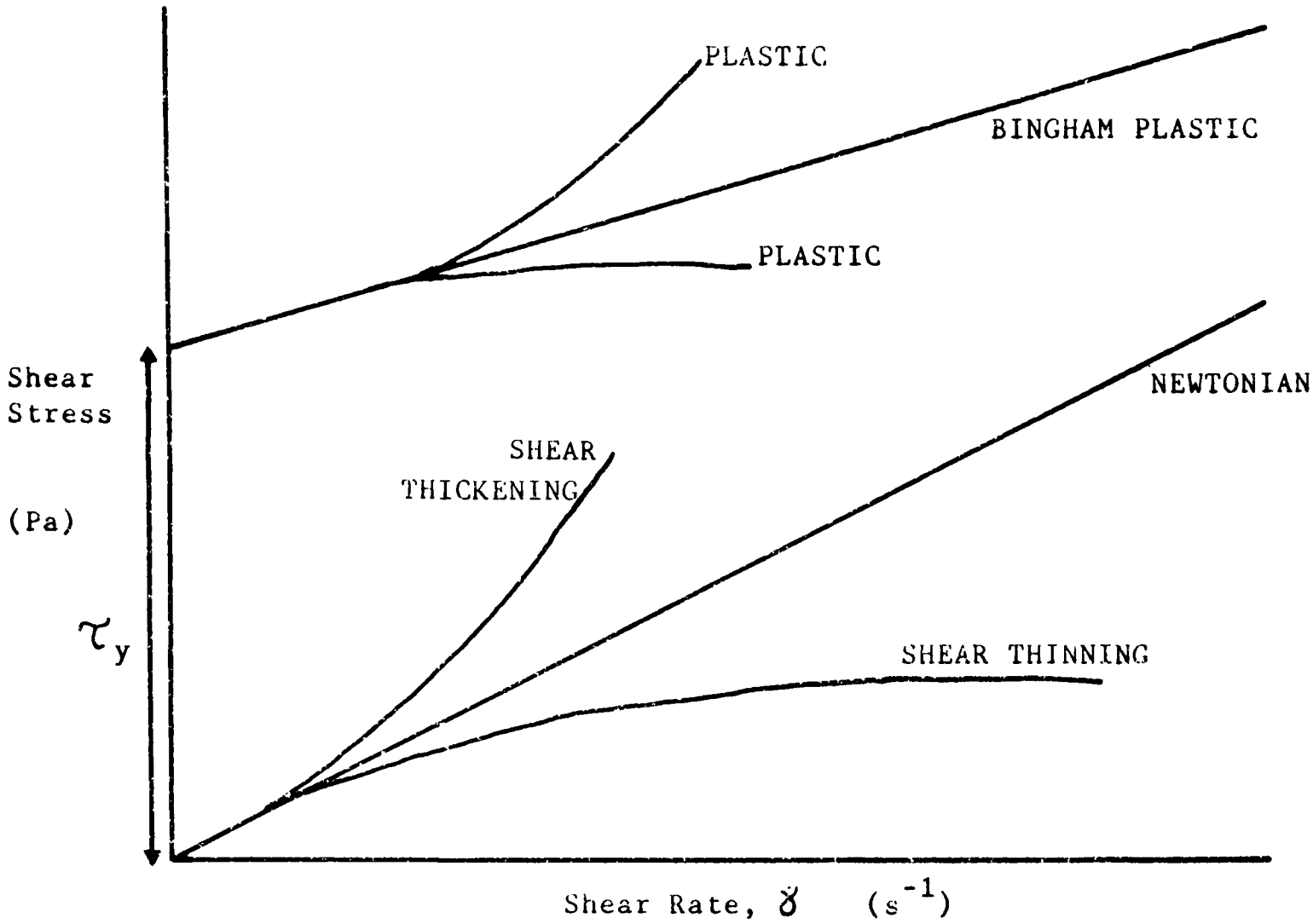

Figure 2.2 Flow Curve for a Typical Shear Thinning Fluid

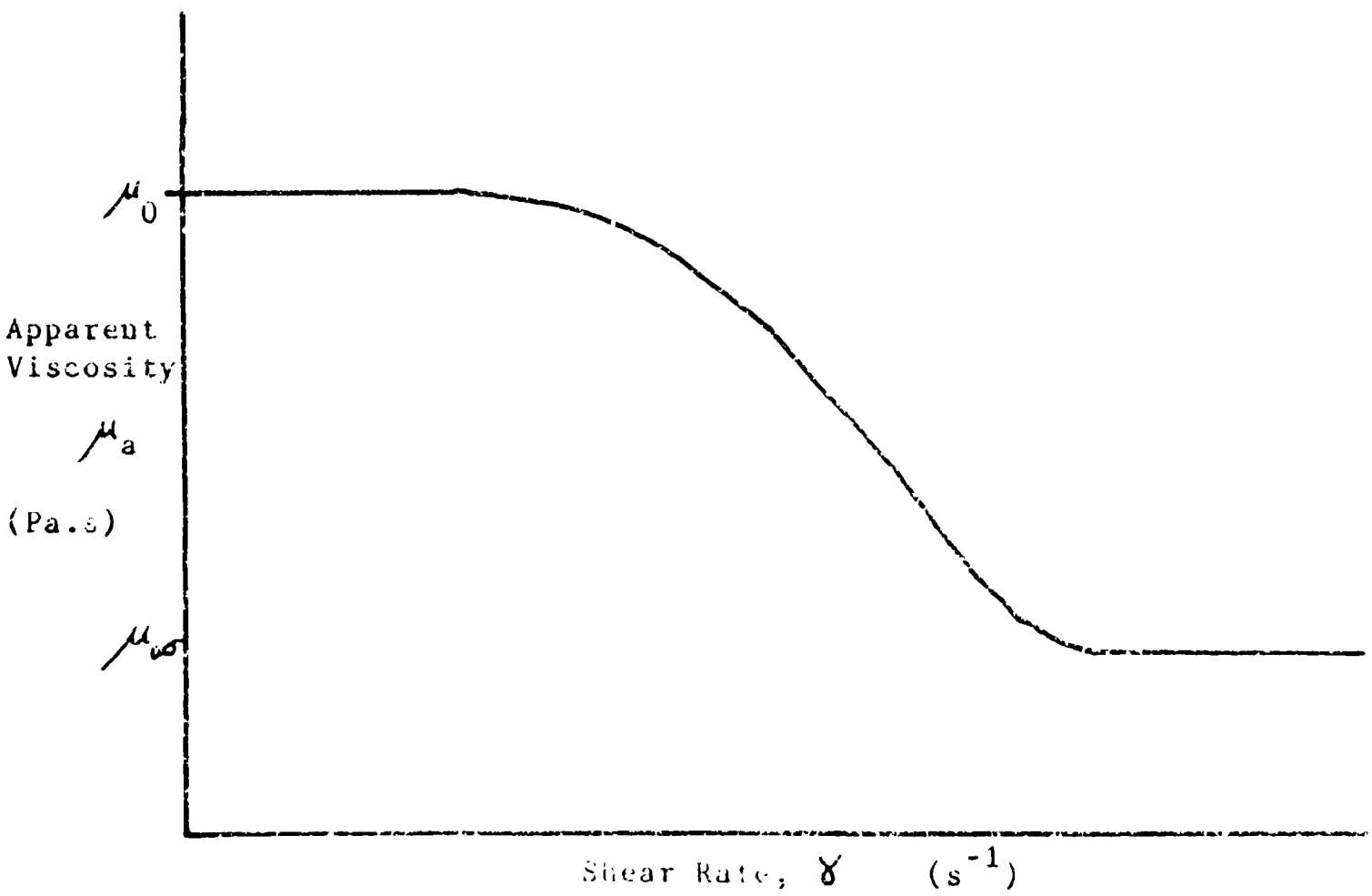

μ_a , termed the zero shear viscosity μ_0 . Increasing shear progressively organises the molecules and μ_a monotonically falls as the major axes of the large molecules are brought into line with the flow direction. At high shear rates the molecules are thought to be completely aligned, and the apparent viscosity becomes independent of the shear rate again at a lower value than μ_0 , which is termed μ_∞, "the infinite shear viscosity". The difference between μ_0 and μ_∞ can be large, covering several orders of magnitude. In the region of falling μ_a , a double logarithmic plot of τ versus $\dot{\gamma}$ often reveals linearity over several decades of shear rate. Where this is the case, the Power-Law or Otswald-de Waele equation is often used. It takes the form:

$$\tau = K \dot{\gamma}^n \quad , \quad n<1 \qquad (2.3)$$

giving:

$$\mu_a = K \dot{\gamma}^{n-1} \qquad (2.4)$$

Where K is termed the consistency index and n is the flow behaviour index. For a shear thinning fluid n<1 ; where n=1 the equation describes a Newtonian fluid. Some fluids demonstrate shear thickening behaviour, e.g. some sand and clay suspensions at high solids concentration. These fluids have values for n>1.

Equation 2.3 does not accommodate the first and second Newtonian regions shown in figure 2.2. It is also criticised because it is dimensionally unsound. Other models have been developed, some of which accommodate the yield stress which is shown by some fluids. A selection of these are given in table 2.1, with a more complete description available in Whorlow[6].

Table 2.1

Some Mathematical Models for the Viscous Behaviour of Non-Newtonian Fluids. (Taken from Whorlow[6])

Equation Number	Mathematical Format	Name of Model	Comments
2.3	$\tau = K \dot{\gamma}^{n}$	Power Law or Otswald-de Waele	See text
2.5	$\dot{\gamma} = K_1 \tau + K_2 \tau^{n_E}$	Ellis	($n_E > 1$) Shows Newtonian Behaviour at low $\dot{\gamma}$
2.6	$\tau - \tau_y = \mu_B \dot{\gamma}$	Bingham Plastic	Accommodates yield stress and shows linear shear stress - shear rate behaviour above τ_y.
2.7	$\tau - \tau_y = K_{HB} \dot{\gamma}^{n_{HB}}$	Herschel-Buckley	Similar to power law, but includes yield stress.
2.8	$\tau^{\frac{1}{2}} = \tau_y^{\frac{1}{2}} + K_C \dot{\gamma}^{\frac{1}{2}}$	Casson	Semi-empirical, used mainly for suspensions.

The subscripted variables K and n are constants

2.1.2) Time Dependent Properties of Non-Newtonian Fluids

From a practical point of view it is generally the shear stress and the associated viscosity, as described in the previous section, which are the rheological properties of greatest interest. For many non-Newtonian fluids the measured apparent viscosity and the variation of the apparent viscosity with the shear rate depend upon the recent shear history of the fluid. In some materials a constant rate of shear can result in a substantial lowering of the apparent viscosity with time. This effect is termed thixotropy. If the same fluid is then left to stand, after a time the initial apparent viscosity is recovered. The opposite effect, termed anti-thixotropy or rheopexy, is characterised by an increase in apparent viscosity with time at constant shear.

If rheograms are determined for such fluids starting at zero shear stress, going to a high shear stress and then back to zero again, then the result is a hysteresis loop as shown in figure 2.3, where the arrows indicate the direction of change in shear stress. A fluid which has been left to stand will show a larger hysteresis loop than one which has recently been subjected to a great deal of shear stress. If the shearing process is continued to equilibrium, then thixotropic fluids yield rheograms which are characteristic of shear thinning fluids.

Figure 2.3 Rheograms of Time Dependent Non-Newtonian Fluids

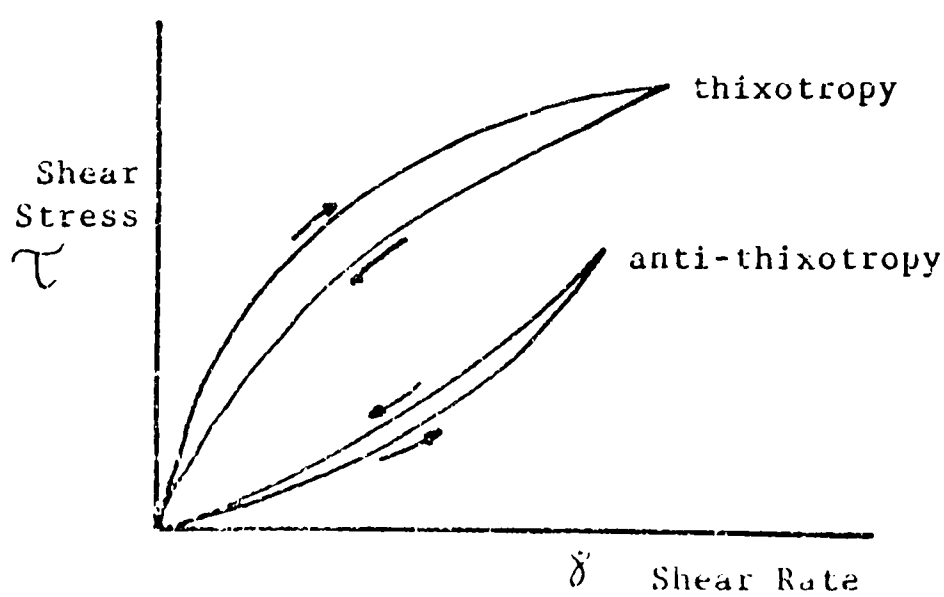

2.1.3) Viscoelastic Properties of Non-Newtonian Fluids

Some non-Newtonian fluids exhibit viscous behaviour and show time dependent elastic effects. They will flow when subjected to a shear stress, but part of their deformation is recovered upon removal of that stress. These fluids are termed viscoelastic fluids and they can be classified as somewhere between elastic solids and purely viscous liquids. Several methods are available to estimate the viscoelastic properties of a fluid. The major ones in use are creep compliance measurements, which involves measuring the deformation (strain) at constant stress as a function of time, and normal force measurement, which is measurement of the forces produced in directions normal to the direction of an imposed stress. Each of these is described in turn, although only normal force measurements have been used to characterise the fluids used in this work.

a) Creep Compliance

When a material loaded into a rheometer is subjected to a constant stress of low enough magnitude so as to produce only small deformations, then the increase of deformation or strain as a function of time is termed creep, and the ratio of the strain to the constant stress is termed creep compliance. Figure 2.4 shows an ideal creep compliance versus time curve, where the stress is imposed instantaneously at time t_0 , and removed at time t_1 .

The creep portion of the curve between t_0 and t_1 can be divided into three main regions[5]:

1) J_0 : Instantaneous Compliance, region A - B. In which the primary structural units or bonds within the material are stretched elastically. If the stress were removed at B, the original structure would be completely recovered.

2) J_R : Retarded Elastic Compliance, region B-C. In which bonds break and are reformed, with weaker bonds breaking earlier than strong ones.

Figure 2.4

Idealised Creep Compliance versus Time for a Viscoelastic Material.[5]

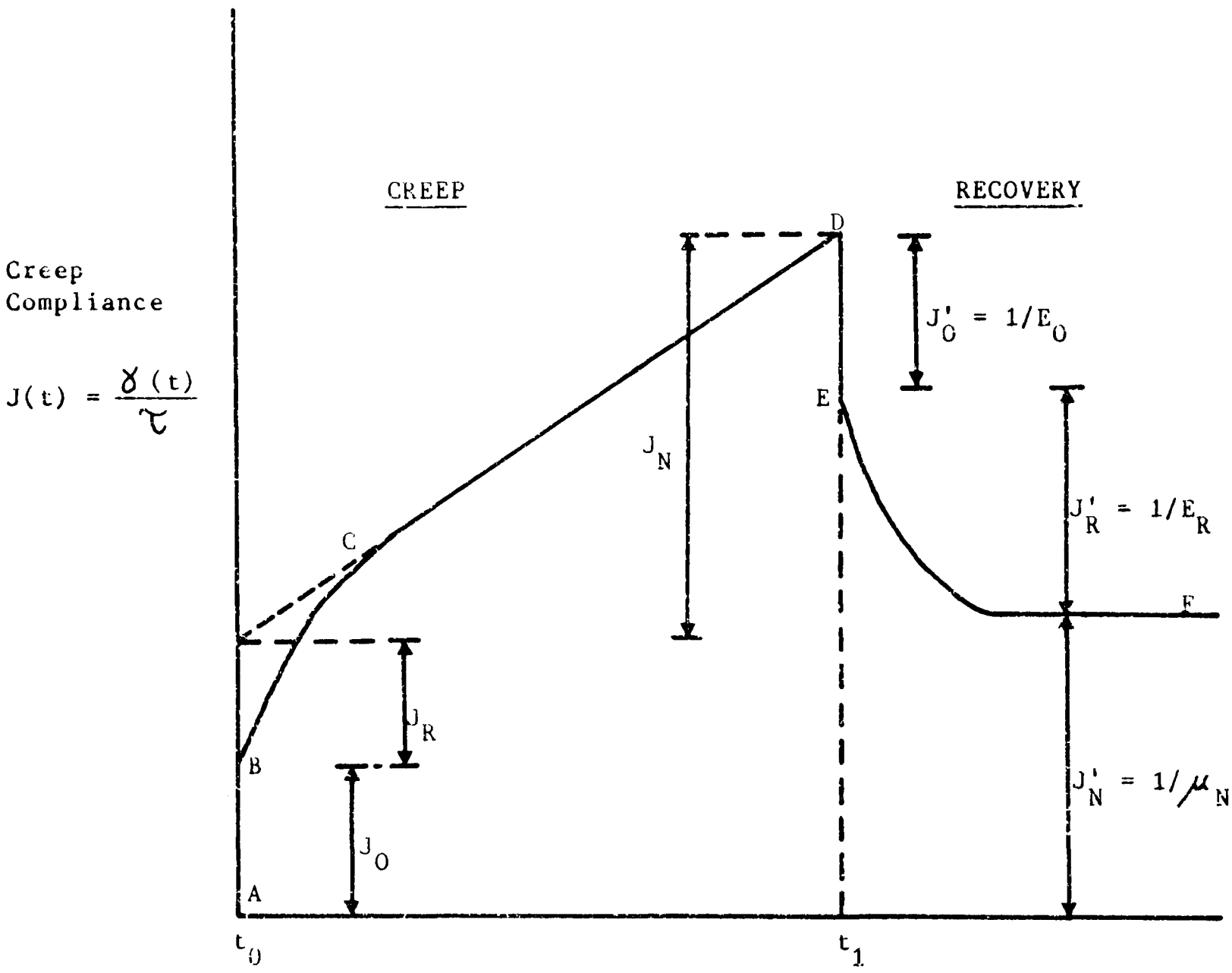

3) J_N : Newtonian Compliance, region C - D. Following rupture of some of the bonds, the particles or units flow past each other.

Removal of the stress at time t_1 allows the fluid to recover, following a similar pattern to the compliance:

1) J'_O : Instantaneous Elastic Recovery, region D - E. Corresponding to the Instantaneous Compliance.

2) J'_R : Retarded Elastic Recovery, region E - F

Since bonds were broken which did not reform and flow occurred in the C - D region, part of the structure is not recovered. This is represented by J'_N. In theory $J_O = J'_O$, $J_R = J'_R$ and $J_N = J'_N$. However in practice discrepancies can occur. In particular, the position of C is difficult to determine, as the C - D portion of the compliance may be slightly curved when the stress is applied for a long time.

If the creep compliance versus time curves for different shear stresses coincide then the behaviour is termed linear viscoelasticity. For the majority of materials the behaviour is non-linear, i.e. the creep compliance at time t, where $t > 0$, increases with increasing shear stress. For many cases of non-linear behaviour, where the deformation is small, linear behaviour is shown over a narrow range of shear stress, enabling the experimental results to be readily interpreted.

Mechanical and electrical analogues can be used to describe linear viscoelastic behaviour in creep compliance. In common use are mechanical models which take the form of combinations of helical springs, obeying Hooke's Law of Elasticity (i.e. elongation is proportional to stress or tension), and dashpots of Newtonian liquids, consisting of a cylinder with a loosely fitting plunger immersed in the liquid. Thus the friction constant of a dashpot represents Newtonian viscosity.

Two basic combinations of spring and dashpots are used: The Maxwell element, consisting of a spring and dashpot in series, and the Kelvin-Voigt element, consisting of a spring and dashpot in parallel. Figure 2.5 shows these elements and figure 2.6 shows the strain versus time curve for these elements if a constant stress is instantaneously applied at t_0 and removed at t_1. In the Maxwell element the spring stretches spontaneously and the plunger in the dashpot moves at a constant rate, which is dependent on the applied stress. At t_1 the spring contracts and the plunger remains stationary. Thus it provides a model for the Instantaneous Compliance and the Newtonian Compliance.

In the Kelvin-Voigt element the damping resistance of the dashpot prevents instantaneous extension of the spring. The combination of a Kelvin-Voigt element and a Maxwell element in series produces a strain-time curve where the Retarded Elastic Compliance is modelled by the Kelvin-Voigt element. This is the simplest mechanical analogue of viscoelastic behaviour. Close analysis of creep compliance versus time data indicate that a very large number of Kelvin-Voigt elements in series are required to produce a reasonable model of the behaviour of most real fluids. This suggests a series of discrete mechanisms contributing to the Retarded Elastic Compliance, whereas in reality a continuous spectrum of retardation mechanisms and times is required[5].

b) Normal Force Measurements

The most commonly described flow for rheometrical analysis is steady simple shear flow. Study of such a flow, within a rectangular Cartesian representation, having velocity components of:

$$v_1 = \dot{\gamma} . x_2 \quad , \quad v_2 = v_3 = 0 \qquad (2.9)$$

Figure 2.5

Mechanical Analogues for Creep Compliance

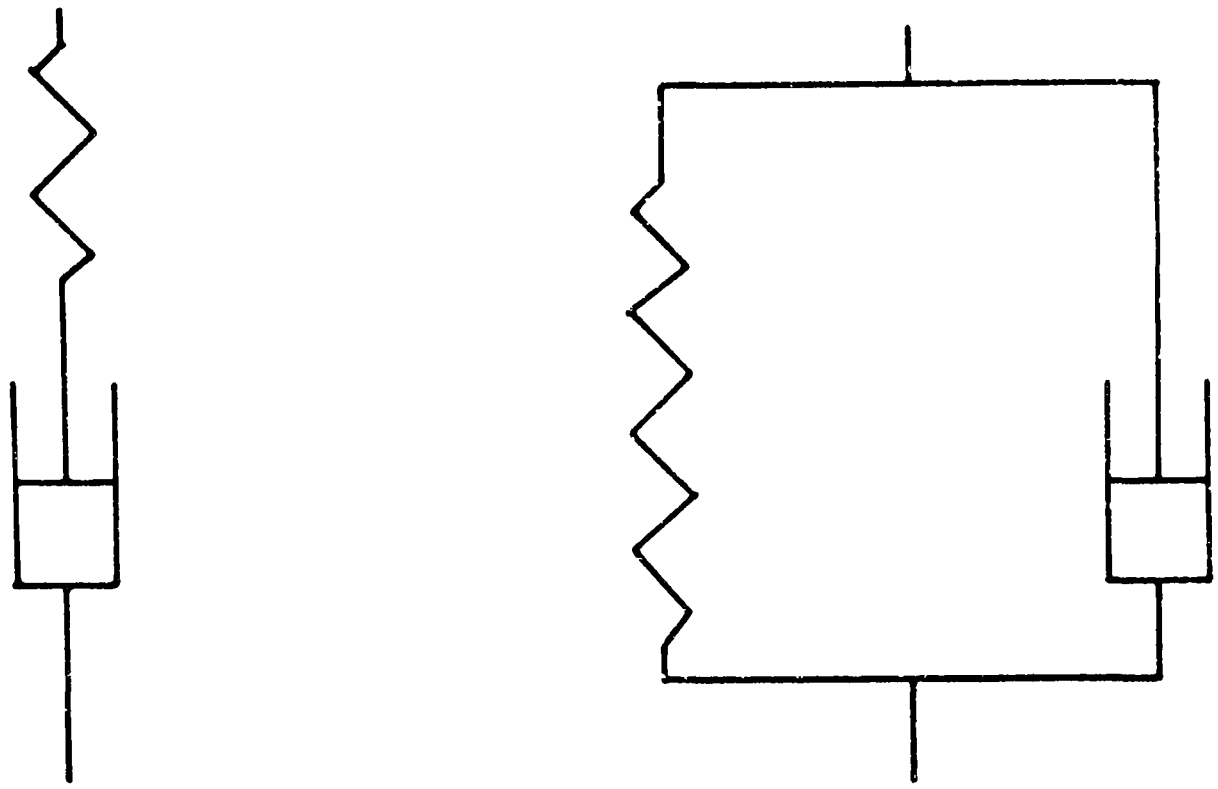

i) Maxwell Element

ii) Kelvin-Voigt Element

Figure 2.6

Strain versus Time Curves for Spring and Dashpot Models

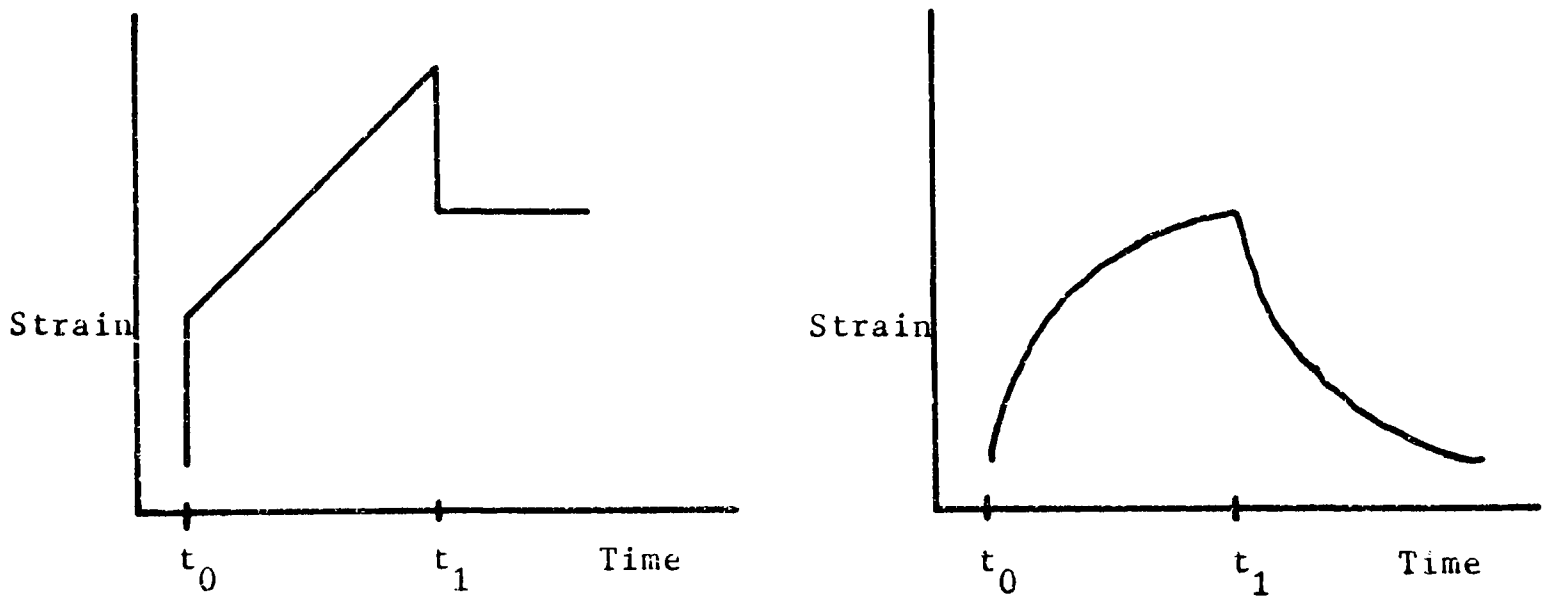

i) Maxwell Element

ii) Kelvin-Voigt Element

gives the corresponding stress distribution in the form[6]:

$$P_{11} = \tau(\dot{\gamma}) = \dot{\gamma} \cdot \mu(\dot{\gamma})$$

$$P_{13} = P_{23} = 0$$

$$P_{11} - P_{22} = N_1(\dot{\gamma}) \qquad (2.10)$$

$$P_{22} - P_{33} = N_2(\dot{\gamma})$$

where P_{ij} is the stress tensor, $N_1(\dot{\gamma})$ The 1st normal stress difference

$N_2(\dot{\gamma})$ The 2nd normal stress difference

$\mu(\dot{\gamma})$ The apparent viscosity, μ_a

$\tau(\dot{\gamma})$ The shear stress in steady simple shear flow.

For a Newtonian liquid, $N_1 = N_2 = 0$, μ = a constant

For an inelastic non-Newtonian liquid, $N_1 = N_2 = 0$, μ is dependent on $\dot{\gamma}$

For a non-linear elastic liquid, μ, N_1 and N_2 are all dependent on $\dot{\gamma}$

Also if the fluid does not have a yield stress, then in the limit as $\dot{\gamma} \to 0$; $\mu \to \mu_0$, $N_1 \to 0$, $N_2 \to 0$. Thus, at small rates of shear, this analysis implies that viscoelastic liquids will behave as Newtonian liquids.

The effect of a finite positive 1st normal stress difference can be remarkable. A vertical cylinder or rod rotated in a viscoelastic liquid can cause the liquid to climb up the rod. This is because of the tension along streamlines in the liquid, which form closed loops around the rod and contract. If there is a free surface, then the liquid will rise, however if the surface is enclosed then a pressure is developed. This rise of liquid is known as the Weissenberg Effect and the pressure developed is measured as a normal force in instruments such as the Weissenberg Rheogoniometer. For a cone and plate geometry, the 1st normal stress difference is related to the total normal force, F, by:

$$F = \frac{\pi Rc^2}{2} \cdot N_1 - \frac{3\pi\rho\Omega^2 Rc^4}{40} \qquad (2.11)$$

Where Rc is the radius of the cone and Ω the rotational speed. The negative term on the right hand side of equation 2.11 is the correction necessary to account for the pressure attributed to centrifugal forces[7]. Thus measurement of the total normal force generated as a function of the rotational speed can be used to determine the variation of N_1 with shear rate, $\dot{\gamma}$.

N_1 can be much larger than the shear stress in highly elastic fluids, and it is often fitted by a power-law type equation over limited ranges of shear rate:

$$N_1 = A \dot{\gamma}^{b} \qquad (2.12)$$

Where the degree of deviation of b from zero gives an indication of the non-linearity of the viscoelastic behaviour. The 2nd normal stress difference, N_2, is much smaller than N_1 and in general it is negative. It can be determined from the pressure profile on the plate in a cone and plate geometry. Accurate determination of N_2 is made difficult by edge effects and the necessity to measure the difference between two large quantities.

It is generally accepted that substantial normal stress effects and shear thinning behaviour are characteristic features of viscoelastic liquids in steady simple shear flow. The two manifestations of non-Newtonian behaviour are generally related to each other in practical terms, i.e. the greater the normal stress levels, the greater the shear thinning behaviour of the liquid. One significant exception is the Boger fluid, which is a solution of polyacrylamide in a Newtonian sugar syrup solution. The viscosity is virtually constant over a wide range of shear rates, with high N_1 values. Quadratic viscoelastic behaviour, that is b = 2 , occurs at low shear rates[9,10].

2.2) Measurement of Rheological Properties

Many commercial instruments are available for the measurement of rheological properties; in particular viscosity measurement is well catered for. Many of these instruments are used in conjunction with specific fluids and provide data which cannot be generally interpreted, or readily compared to the data provided by other instruments. Quantitative data can be obtained using four principale categories of commercially available instruments. The theoretical basis and limitations of these categories of instruments are dealt with in detail by Whorlow[6], while Sherman[5] provides a description of many instruments, with details of the manufacturers. The four main categories are:

a) Tube or Capillary viscometers

b) Falling sphere viscometers

c) Coaxial cylinder viscometers

d) Cone and plate viscometers

In this present work only instruments in categories c and d have been used, see Chapter 5. Termed rotational instruments, they have the principal advantage over other types of viscometer in that both the duration and magnitude of the shear which a sample is subjected to can be varied at will. This enables changes in rheology with time to be easily monitored.

The rotational instruments can also be designed to provide an approximately uniform shear rate throughout the sample. For cone and plate viscometers the rate of shear, $\dot{\gamma}$, is given by:

$$\dot{\gamma} = \Omega / \theta \qquad \text{for } \theta < 5^{\circ} \qquad (2.13)$$

where θ is the cone angle and Ω the rotational speed. The shear stress, τ, is given by:

$$\tau = 3G_T / 2\pi Rc^3 \qquad (2.14)$$

where G_T is the torque and Rc the cone radius. For coaxial viscometers, the relative radii of the cylinders needs to be taken into account,with

the resulting equations complicated by end effects. Several solutions are given by Whorlow[6]. In general correction factors are required which are specific to the instrument in use.

Viscoelastic properties can be measured in some rotational viscometers. Measurement of the total force exerted on the plate in cone and plate viscometers can be used to obtain N_1 values, according to equation 2.11, if adjustments are made to accommodate errors due to secondary flow, (see below). N_2 can be measured if pressure transducers are flush mounted on the plate to measure the distribution of pressure. Creep compliance data can be obtained in rotational instruments in which very small shear stresses and shear rates can be applied and measured.

There are some effects which may introduce errors into the results of rheological measurements[6]. These include wall effects such as slippage; end or edge effects, due to interfacial tension, geometry and evaporation; secondary flow within the fluid, caused by inertia of the fluid; and temperature rise due to the shearing process. Slippage at the wall is thought to occur mainly in greases, where an oil film may be present on the metal surface, or in slurries, or in very stiff materials such as partly vulcanised rubber. Slippage is characterised by erratic torque readings, due to the variation in friction at the wall. Where more than one geometry can be used to determine the rheogram of a material, inconsistent results indicate that slippage may be occurring[6]. End or edge effects are common in rotational viscometers. In coaxial instruments the ends of the inner cylinder will affect the results obtained. To eliminate this error cylinders of various lengths should be used , if this is possible. For cone and plate geometries, edge and end effects are generally considered to be negligible in shear stress-shear rate measurements where the cone angle is small. This also requires that the material being tested reaches or exceeds the edge of the cone. Evaporation can have a major effect, causing formation of a surface

skin in some fluids. This can be prevented by applying a film of another liquid, such as silicone oil, to the edge of the cone and plate.

In cone and plate geometries secondary flow effects can be important, particularly in viscoelastic liquids[7]. In purely viscous fluids, secondary flow stream lines are directed outwards near the rotating cone and inwards near the stationary plate. For viscoelastic liquids there is an additional region near the apex of the cone where closed streamlines flow in the opposite direction to those for the purely viscous case. This will increase the torque on the cone and plate, particularly at high shear rates[11]. If a liquid of relatively low viscosity is subjected to a high rotational speed in a cone and plate geometry this secondary flow effect will, even in Newtonian liquids, produce apparently shear thickening behaviour. An empirical approach can be used to determine the effects of secondary flow in real fluids, by carrying out tests with different cone angles. If consistent results are obtained then it can be inferred that secondary flow is not introducing a significant error.

In coaxial geometries no correction is required for secondary flow effects in torque measurements provided the laminar flow regime is not affected by turbulence or instabilities of the Taylor vortex type[6]. Taylor vortices are inertial effects, which occur because the fast moving fluid near the inner cylinder tries to move outwards. This produces circulation loops, which increases the torque applied for a given rotational speed. The occurrence of these vortices is related to the coaxial cylinder Reynolds number, Re_c :

$$Re_c = \Omega R_1(R_2 - R_1) / \mu \qquad (2.15)$$

where R_2 and R_1 are the radii of the outer and inner cylinders respectively and Ω is the rotational speed. For $Re_c > 41.3(R_2/[R_2 - R_1])^{\frac{1}{2}}$ Taylor vortices will occur. To avoid this, measurements at high rotational speeds with low viscosity fluids require a narrow gap coaxial geometry.

The shear induced heating of a test liquid leads to a rise in

temperature within the liquid. This can lead to considerable error if high shear rates are used and if the material properties of the liquid are very temperature sensitive. Cone and plate geometries have only a thin liquid layer, so it is the thermal capacity of the cone and the plate which dominate the changes in temperature due to the shearing process. For coaxial instruments the liquid properties are more important. With care it is possible to reduce or eliminate errors due to shear induced heating. Constant temperature water can be circulated under a cone or plate, or around the outer cylinder, depending on the geometry. Otherwise the whole instrument can be contained in a constant temperature room or cabinet, to enable measurements to be carried out at the temperatures of interest.

Other factors which can introduce errors into rheological measurements include:

i) Inhomogeneity within the test sample and separation of particles within the flow field. This is particularly relevant where the rheology of the liquid is dependent on the type and size of the particles it contains, for example in mycelial broth cultures[12].

ii) Instrument imperfections, e.g. non concentric axes in coaxial flow, or bending of the frame in normal force measurement.

iii) Poor sample preparation and loading, e.g. air bubbles trapped in the sample or sample flung out at high rotational speeds.

2.3) Rheological Properties of Fluids of Interest

Viscous non-Newtonian behaviour is often encountered within the fermentation industry. There are several constituents of culture broths which can contribute to this behaviour; they are high substrate concentration, particularly at the start of a batch culture; cell morphology and extra cellular product formation[13]. The most important and

widespread of these categories are where cell morphology and product formation cause rheologically complex behaviour[14].

Cultures where cell morphology is important are characterised by the formation of filaments and agglomerates of cells, e.g. fermentations of Streptomyces and Aspergillus species, where the broth produced is markedly shear thinning, even at low cell concentrations[15,16]. Measurement of the rheological properties of such cultures can be difficult in conventional viscometers[12,17]. In coaxial viscometers settling of the biomass or phase separation at the cylinder surfaces can occur. In narrow gap viscometers the relatively large pellets impair measurement and can break up in the flow field. To overcome these difficulties, turbine impellers have been used in place of the rotating cylinder[12]. It is the mycelial structure in these cultures which cause the complex rheological behaviour, with the continuous phase essentially aqueous.

For cultures where product formation determines the rheological properties, it is generally the continuous phase which exhibits viscous non-Newtonian behaviour. This major difference can cause markedly different heat and mass transfer characteristics between these categories[18]. In some cultures, for example the production of Pullulan by Pullularia pullulans[19], it is a combination of product formation and mycelial structure which determines the rheological properties.

A major example of cultures where it is the product which determines the rheological properties is in the production of extra-cellular polysaccharides. These generally water soluble polymers are important as thickeners, gelling agents and suspending agents[15,20,21]. Examples include Dextran, Curdlan and Pullulan, which are neutral microbial polysaccharides, and Alginate and Xanthan which are anionic microbial polysaccharides. They all form viscous solutions, with shear thinning exhibited to a greater or lesser degree.

Of primary interest to this work is the anionic microbial poly-

saccharide Xanthan. This gum is produced by the microorganism Xanthamonas campestris (NRRL B - 1459). The gum is resistant to acid, alkali and biodegradation[20], and stable at temperatures up to 150°C [21]. The stability to biodegradation is thought to be enhanced by the trisaccharide side chains, which cause steric hindrance to enzymic depolymerisation. Xanthan is composed of five groups; glucose, mannose, gluceronic acid, acetyl and pyruvate groups. In solution it acts as a stabiliser, emulsifier and thickening agent. It is used in the food industry in products such as sauces and salad dressings and in canned food. In the oil industry it is used as a drilling mud additive and has potential for use in tertiary oil recovery. Solutions of Xanthan are highly viscous and shear thinning, fitting the power law model over a wide range of shear rates. They show an apparent yield stress, with good evidence of viscoelastic properties[15,22], including a slight Weissenberg effect and measurable 1st normal stress difference, although the yield stress makes measurement of N_1 values difficult and reduces the Weissenberg effect[22].

2.4) Non-Newtonian Solutions Used in This Work

Microbially produced polysaccharides such as Xanthan can be used in experiments to determine the effects that rheology has on mass transfer rates. However their complex rheological properties would hinder interpretation of the results obtained. In addition polysaccharide solutions are often opaque, hindering visualisation of flow patterns and mixing. Using model fluids which share some of the properties of Xanthan but not all of them, leads more readily to specific interpretation of results. To this end the material chosen was sodium carboxy-methyl cellulose (CMC), supplied by Hercules ltd., type 7H4C. CMC solutions have been used in other mass transfer studies (see Chapter 4). It is a cellulose ether produced by reacting alkali cellulose with sodium monochloroacetate.

It acts as a thickener, stabiliser, suspending agent and as a protective colloid, with applications in the food, pharmaceutical and other industries. Examples of uses are in salad dressings, low calorie foods, shampoos, lotions and ointments, as a laxative and in wallpaper paste.

CMC solutions have similar rheological behaviour to Xanthan solutions. They are shear thinning and slightly viscoelastic, but do not exhibit a yield stress. CMC solutions are also slightly thixotropic. Table 2.2 shows some data obtained for CMC and Xanthan solutions by Solomon[22] over a range of shear rates from 30 to 280 s^{-1}. Data for CMC solutions used in this work are similar (see Chapter 6).

It can be seen from the table that good agreement is obtained for the viscoelastic parameters measured, with 1.4% CMC giving results close to 4.5% Xanthan and 0.8% CMC giving results close to 2.0% Xanthan. The shear thinning behaviour is not modelled as closely, with Xanthan giving much higher values of the consistency index and lower values of the flow behaviour index than the corresponding CMC solution. However, an examination of the apparent viscosity of these solutions at the shear rates of interest here (around 100s^{-1}) shows that similar apparent viscosities are obtained, although at higher and lower shear rates the apparent viscosities of the solutions deviate. These values are tabulated below.

Table 2.3

Apparent Viscosities of Xanthan and CMC Solutions

Solution	Apparent Viscosity @ =30s^{-1}	@ =100s^{-1}	@ =280s^{-1}
4.5% Xanthan	2.59	0.91	0.37
1.4% CMC	2.23	1.10	0.60
2.0% Xanthan	1.15	0.42	0.18
0.8% CMC	0.83	0.47	0.29

Table 2.2

Rheological Data for Solutions of Xanthan and CMC

Fluid	Concentration (% w/w)	Power Law Equation Parameters (Equation 2.3)		1st Normal Stress Difference Parameters (Equation 2.12)		Yield Stress τ_y	
		K $Pa.s^n$	n —	A $Pa.s^n$	b —	Herschel-Buckley Equation 2.7 Pa	Casson Equation 2.8 Pa
Xanthan	4.5	50.0	0.13	6.73	0.46	8.3	19.4
CMC	1.4	16.6	0.41	6.37	0.52	0	0
Xanthan	2.0	20.0	0.16	2.13	0.57	5.8	11.47
CMC	0.8	4.11	0.53	2.33	0.57	0	0

CHAPTER 3

POWER CONSUMPTION AND MIXING OF NON-NEWTONIAN FLUIDS

The area of interest covers work carried out in unaerated and aerated liquids contained in vessels typified by that shown in figure 3.1. In general four baffles are used which prevent the formation of a vortex around the impeller shaft. This shaft is centrally located and is fitted with one or more impellers of various types. The height to diameter ratios used can be varied, but most studies concentrate on a ratio of one. Several dimensionless numbers have been used in the analysis of the results obtained in this geometry, which are described below.

3.1) Dimensionless Numbers Used in This Area of Study

Some of the dimensionless numbers used require a knowledge of the rheological properies of the fluid, the most widely used example being the Reynolds number, which requires a value for the liquid viscosity. For a Newtonian liquid, the viscosity is fixed at a given temperature and pressure; for non-Newtonian liquids, the viscosity is also dependent upon the shear rate, as outlined in Chapter 2. So in order to determine the apparent viscosity , it is first necessary to determine the shear rate within the vessel. However, as the shear rate is highly non-uniform, an average value must be used, γ_{AV} , which must first be determined.

In order to determine γ_{AV} , Metzner and Otto[23], measured the power input for a series of non-Newtonian fluids and Newtonian fluids under the same conditions of geometry, impeller speed, etc. in the laminar flow regime. By matching the resulting power numbers (see section 3.1.2) they obtained the Reynolds numbers applicable to the non-Newtonian fluids and from these they determined the apparent viscosity. By defining the average shear rate, γ_{AV} , as:

$$\gamma_{AV} = \tau / \mu_a \qquad (3.1)$$

Figure 3.1

Diagram of a Vessel Typical of Those Used in These Studies

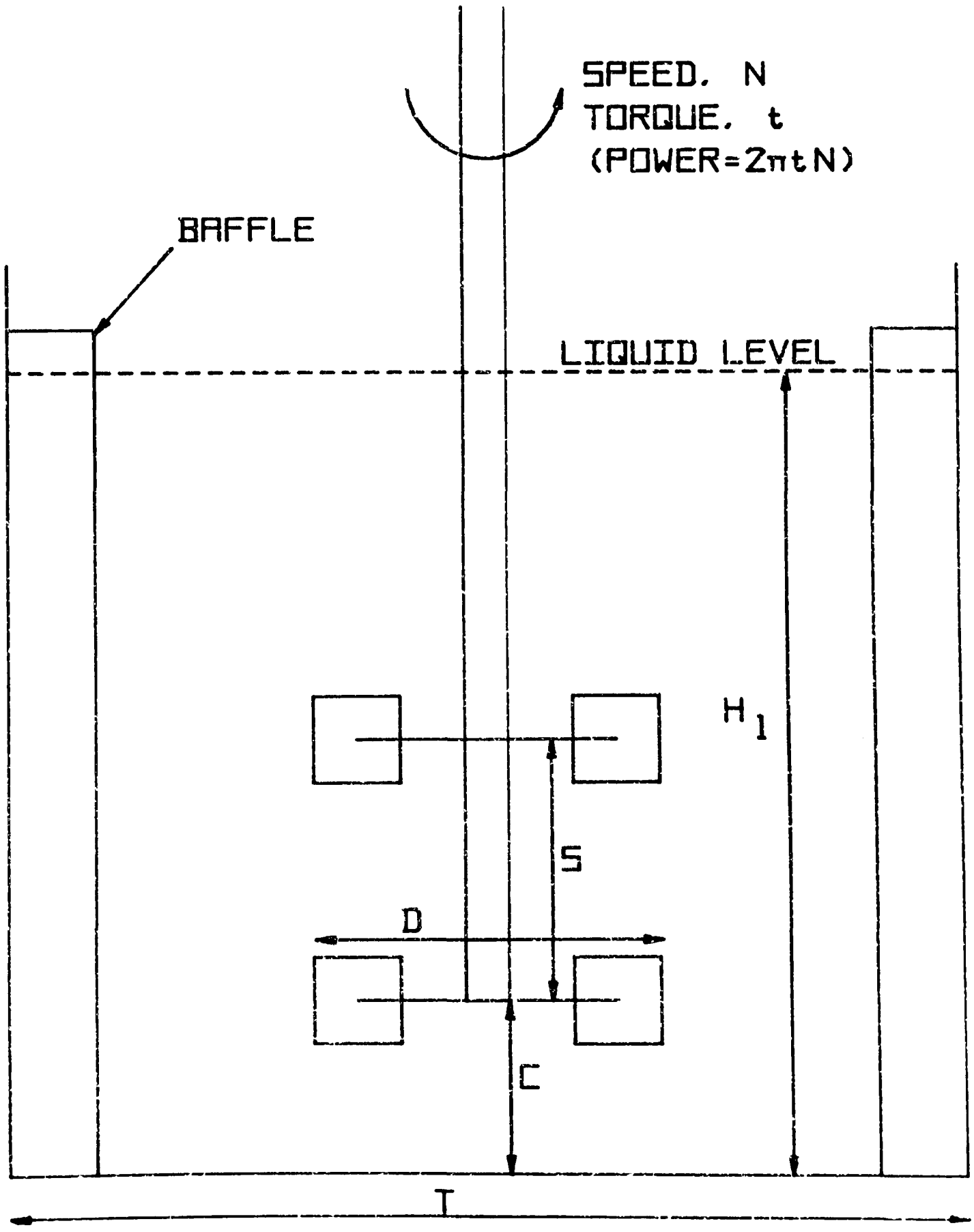

They found that γ_{AV} was linearly related to the impeller speed:

$$\gamma_{AV} = k_s N \qquad (3.2)$$

With the value of k_s dependent on the type of agitator, having a value of 13 for turbines. In a fuller study Metzner et al[24] determined $k_s = 11.5 \pm 10\%$ for disc turbines, $k_s = 10.0 \pm 10\%$ for propellers and $k_s = 13.0 \pm 15\%$ for pitched blade turbines. Calderbank and Moo-Young[25 & 26] found that $k_s \simeq 10$ for shear thinning fluids, with the value of k_s being slightly dependent on the flow behaviour index, n, giving:

$$\gamma_{AV} = k'_s N \left(\frac{4n}{3n + 1} \right)^{n/1-n} \qquad (3.3)$$

Which combined with the power law equation (equation 2.3) gives:

$$\mu_a = \frac{K}{(k'_s N)^{1 - n}} \cdot \left(\frac{3n + 1}{4n} \right)^n \qquad (3.4)$$

Whereas equation 3.2 yields:

$$\mu_a = K (k_s N)^{n-1} \qquad (3.5)$$

Ducla et al.[27] found that k_s is constant for shear thinning inelastic liquids but is reduced in viscoelastic liquids. In 1% and 1.25% CMC solutions very similar to those used here, they found $k_s = 6.1$ to 7.1, depending on the type of turbine used. Further discussion of k_s values in viscoelastic liquids is contained in Chapter 7,section 2.

Once a value of k_s has been determined or chosen, it is then possible to determine the apparent viscosity and hence the Reynolds number (see below).

3.1.1) Reynolds Number, Re

This represents the ratio of inertial to viscous forces, which determine whether the liquid flow is laminar, transitional or turbulent. In agitated vessels it takes the form:

$$Re = \frac{\rho N D^2}{\mu_a} \qquad (3.6)$$

Where the apparent viscosity, μ_a , is replaced by the viscosity, μ , for Newtonian liquids. The density, ρ , is the density of the liquid, even in gas-liquid dispersions. N is the impeller speed and D the impeller diameter.

Where the liquid obeys the Power Law, equation 3.6 and 3.5 can be combined to give:

$$Re = \frac{\rho \cdot N^{2-n} \cdot D^2}{K \cdot k_s^{n-1}} \qquad (3.7)$$

Doubt about the precise value of k_s lead Ranade and Ulbrecht[28] to use:

$$Re = \frac{\rho \cdot N^{2-n} \cdot D^2}{K} \qquad (3.8)$$

In this work equation 3.7 is used, with a value taken for k_s of 11.5, which enables a comparison of experimental results with other workers, (see Chapters 7 and 8). It can be seen from equation 3.7 that the chosen value of k_s is not of great importance, particularly when comparing fluids with similar rheological properties. Changing the value of k_s has the effect of shifting the data to slightly lower or higher Reynolds number whilst the shape of the curves produced is not significantly altered.

3.1.2) Power or Newton Number, Po

Representing the ratio of pressure differences producing flow to inertial forces it is usually based on the power input by the impeller for agitated vessels, P, and takes the form:

$$Po = \frac{P}{\rho N^3 D^5} \qquad (3.9)$$

Where ρ ,N and D are the same as in the Reynolds number.

Po is often plotted as a function of Reynolds number, or in aerated

systems it is sometimes plotted as a function of the Galilei number, with Froude and Aeration numbers as parameters (see below).

3.1.3) Froude Number, Fr

This represents the ratio of inertial forces to gravitational forces, where g is the gravitational constant:

$$Fr = \frac{N^2 D}{g} \qquad (3.10)$$

The effect of Froude number on the Power number is generally limited to the movement of the liquid surface or vortex formation. The Froude number is generally considered to be unimportant in unaerated fluids at low Reynolds numbers, or at any Reynolds number in baffled vessels (see section 3.2.1).

3.1.4) Aeration Number, Fl_g

This relates the gas flow rate, Q with the impeller pumping rate:

$$Fl_g = Q \ / \ ND^3 \qquad (3.11)$$

Fl_g is used as a parameter in plots of Po versus the Galilei number, or Po is plotted against Fl_g with Fr as a parameter.

3.1.5) Galilei Number, Ga

This has been used to show the effect of viscosity on power consumption[29]. It is represented as:

$$Ga = \frac{Re^2}{Fr} = \frac{g D^3 \rho^2}{\mu_a^2} \qquad (3.12)$$

It has the advantage of removing the impeller speed, N from one of the groups produced in a dimensional analysis, enabling the variations in Po due to other factors to be analysed independently.

3.1.6) The Weissenberg Number, Wi

This is used to relate the elastic properties of the material to the viscous properties. Wi is the ratio of the 1st normal stress difference, N_1 , to the shear stress, τ :

$$Wi = N_1 / \tau \qquad (3.13)$$

By substituting equations 3.4 and 2.12 into equation 3.13, Wi can be expressed as:

$$Wi = \frac{A}{K} \dot{\gamma}^{b-n} \qquad (3.14)$$

For stirred tanks the shear rate can be replaced by $\dot{\gamma}_{AV}$ as discussed earlier for the Reynolds number, allowing Wi to be related to the impeller speed within the vessel.

3.1.7) The Deborah Number, De

For transient and reciprocating processes, or for processes with a residence time, the Deborah number, De, is used to relate the characteristic time of the process, t_p, to the characteristic time of the material, λ :

$$De = \frac{\lambda}{t_p} \qquad (3.15)$$

For an ideal elastic solid, λ is infinite and in principle λ is zero for an ideal viscous liquid, e.g. for water $\lambda \simeq 10^{-13}$ sec. which is close to zero[8]. In between these two extreme values of λ , lie the viscoelastic liquids. These can appear to be solid-like when they are exposed to fast processes with a low t_p. This raises De to high levels which correspond to solid-like behaviour. For agitation of viscoelastic liquids the process time can be expressed as the reciprocal of the agitation speed, 1/N. The characteristic material time can be expressed as the fluid relaxation time[30], $N_1 / \mu_a \dot{\gamma}^2$. This gives:

$$De = \frac{N_1 N}{\mu_a \dot{\gamma}^2} \qquad (3.16)$$

Substitution of equation 2.4 and 2.12 in equation 3.16 gives:

$$De = N \cdot \frac{A}{K} \dot{\gamma}^{b-n-1} \qquad (3.17)$$

Clearly an average value for $\dot{\gamma}$ can be used which is related to the stirrer speed, N. The similarity of De and Wi where N can be related to $\dot{\gamma}$ is clear, and De can be considered to be a special case of Wi under these conditions[31].

Dimensionless numbers related to mass transfer studies are described in Chapter 4, section 5.

3.2) Studies Carried Out of Power Consumption and Mixing in Non-Newtonian Fluids

The power consumed in an agitated tank can be determined by measuring the torque on the impeller shaft, t, and its rotational speed, N. The power is given by:

$$P = 2\pi t.N \qquad (3.18)$$

LeGrys[2] recommends the inclusion of the power input due to the sparged gas, P', although this is usually insignificant when compared to P, the power due to agitation, particularly in laboratory studies: (see Schugerl[13])

$$P' = M_G RT \ln (P_{in}/P_{out}) \qquad (3.19)$$

Where M_G is the mass flow of gas, R is the gas constant, T, the absolute temperature, and P_{in} and P_{out} are the inlet and exit gas pressures.

Flow patterns have been studied using solid tracer particles[22,32] and liquid tracer droplets[33]. Blend times can be investigated by several methods[34], including dye addition[35], conductivity measurement[36] and pH measurement[37]. For opaque fluids Hot-film Probe Anemometry has been used to investigate mixing[22], measuring the velocity profiles of the fluid within the vessel.

3.2.1) Unaerated Mixing

A lot of work has been carried out using Newtonian liquids. Rushton et al.[38] and Bates et al.[39] studied mixing and power consumption over a range of geometries, viscosities and impeller types. Sachs and Rushton[33] gathered photographic evidence of flow patterns produced by disc turbines in Newtonian fluids. Some work has been done with non-Newtonian fluids. Godleski and Smith[35] investigated blend times in shear thinning fluids, finding that the presence of baffles increased the time needed to fully mix the vessel contents. Metzner and Taylor[32] compared flow patterns in viscous Newtonian and shear thinning fluids. They observed a rapid reduction in fluid velocity outside the impeller region, particularly in the non-Newtonian fluids. With increasing distance from the impeller a fall in fluid velocity reduces the shear rate, this increases the apparent viscosity, so the turbulent flow regime only exists near the impeller, with the flow becoming laminar and even stagnant near the walls of the vessel. The turbulent impeller region has been described as a cavern[22,40], with its diameter linked to the Reynolds number[41].

Viscoelastic fluids can exhibit flow reversal at low impeller speeds[22,28]. This is associated with the normal stress developed in laminar flow overcoming the centrifugal force. For disc turbines an intermediate flow pattern has been described as well[28], it consists of reversed flow in the bulk of the vessel with rotational flow in the cavern region. A small increase in the impeller speed causes the formation of small recirculation loops, with fluid approaching the top and bottom of the impeller blades at an angle of 45°, with the precise Reynolds number at which these flow patterns are obtained being dependent on the impeller diameter[22].

The results of studies of power consumption in unaerated mixing are usually presented in terms of the dimensionless groups: Reynolds

number, Froude number and Power number. Geometric effects can be included by reference to standard dimensions, but if geometric similarity is assumed then:

$$Po = f(Re, Fr) \qquad (3.20)$$

For unaerated mixing the Froude number is found to have no significant effect. Rushton et al.[38] produced Po versus Re curves for unaerated Newtonian liquids. They show that in the laminar regime (Re<10), Po is inversely proportional to Re. In the turbulent regime ($Re>10^4$), Po is constant, i.e.independent of Re. For non-Newtonian fluids average shear rates are used to determine the apparent viscosity. This enables the production of Po versus Re curves (see section 3.1). Several workers[22,24,28] have noted that for inelastic shear thinning fluids the Po versus Re curves pass through a minimum in the transition region. This area has been termed the extended laminar regime. Ranade and Ulbrecht[28] found that viscoelastic fluids do not show a minimum in this region, but exhibit significantly lower Po values than shear thinning or Newtonian liquids. Solomon[22] found that slightly viscoelastic fluids, those having low 1st normal stress differences, exhibited a minimum in the extended laminar region, but fluids with high 1st normal stress differences do not.

Nienow et al.[42] carried out studies of unaerated power consumption in Newtonian, shear thinning and viscoelastic fluids. They found similar results to other workers, but in addition they noted that the power consumption in the laminar regime was much higher when viscoelastic fluids were used. Hocker et al.[43] have found similar results. Both publications made use of k_s values similar to Metzner et al.[24]. If lower values had been chosen, as determined by Ducla et al.[27], then the viscoelastic data would have coincided with the data for Newtonian and shear thinning liquids, thus supporting the results of Ducla et al.[27], as described in Chapter 3, section 1. Prud'homme and Shaqfeh[44] measured

the torque required to agitate Boger fluids, which have virtually constant viscosity yet exhibit viscoelastic properties. They found that increasing viscoelasticity increased the torque required, suggesting that the presence of secondary flows within the liquid are responsible for these effects seen with viscoelastic liquids.

3.2.2) Aerated Mixing

Aeration of fluids is generally found to cause a reduction in power consumption when compared with the unaerated fluid. Investigators have shown that this is linked with the formation of gas filled cavities behind the impeller blades[28,45-48]. Gas bubbles entering the impeller region coalesce in these cavities, with small bubbles being broken off in the turbulent region at their trailing edges. In low viscosity liquids the air flow rate is found to have a large effect on the power consumption[42,46], increasing air flow rate reducing the power drawn at a particular agitator speed. Further increases in air flow rate causes flooding of the impeller[48], with the impeller no longer able to promote gas dispersion throughout the vessel. The power drawn has been related to the size and shape of the gas filled cavities behind the agitator blades[46,48]. In viscous fluids these cavities are much more stable than in low viscosity fluids and can remain after the air supply is removed[22,46]. This causes the effect of altering air flow rate to be considerably reduced in viscous fluids, with power consumption virtually independent of air flow rate. Yagi and Yoshida[49] described the impeller region becoming enveloped in gas when shear thinning fluids are studied. They describe this gas envelope as similar in shape to a doughnut, and report that bubble break up in the impeller region is reduced when compared to Newtonian liquids. Schugerl[13] noted that increasing viscosity is accompanied by an increasing tendency for very large and very small bubbles to be formed. This can have a significant effect on mass transfer,

as large bubbles ascend rapidly, quickly leaving the liquid. Small bubbles however have a much lower ascending velocity and are rapidly in equilibrium with the liquid. Thus they form the bulk of the gas hold-up without contributing significantly to mass transfer. Acharya and Ulbrecht[50] have found that increasing viscosity reduces collision and coalescence times, enhancing large bubble formation, also increasing viscoelasticity increases collision and coalescence times, favouring smaller bubble formation. Blakeborough and Sambamurthy[51] found lower than expected power consumption when aerating shear thinning pulp suspensions. They gave an explanation for this by considering the aerated fluid density in the impeller region. Nienow et al.[42] have determined that the gassed power number, Po_g, is related in a complex manner to the size of the gas filled cavities behind the blades, the pumping capacity of the impeller and the amount of gas held in the impeller region. These in turn depend upon the rheological characteristics of the liquid. For example the presence of a yield stress was found to reduce Po_g at low Re. This is due to the increased stability of the gas filled cavities at low Re, when compared to fluids without a yield stress. In addition increasing viscoelasticity of the fluid leads to a lowering of the minimum Po_g attained.

Hocker et al.[43] investigated power consumption in several aerated agitated fluids and showed that inelastic shear thinning CMC solutions gave similar results to Newtonian glycerol-water mixtures, i.e. the dependence of power consumption on air flow rate diminishes as the viscosity increases. For viscoelastic polyacrylamide solutions the effect of altering air flow rate on power consumption is diminished at much lower viscosities than for inelastic fluids. With stable gas filled cavities promoted at lower viscosities in viscoelastic liquids, the power consumption is reduced and gas dispersion inhibited. Similar results were found by Ranade and Ulbrecht[28], whilst other workers[36,42,52]

found that above a minimum low air flow rate, altering air flow rate had no effect on power consumed in viscous non-Newtonian fluids. Solomon[22] found that in CMC and Xanthan solutions air flow rate did not affect the ratio of gassed to ungassed power, P_g / P. However at high Reynolds numbers in medium viscosity Carbopol solutions, which are shear thinning and exhibit a yield stress, a marked effect was obtained, with P_g / P being reduced with increasing air flow rate.

CHAPTER 4

GAS-LIQUID MASS TRANSFER

4.1) Introduction

The rate of mass transfer, r, across a gas-liquid interface is determined by the mass transfer coefficients (k_G for the gas phase and k_L for the liquid phase), the area of contact between the phases, A' and the concentration gradient available as the driving force[53]. These are equated as:

$$r = k_G A'(p_G - p_i) \qquad (4.1)$$

$$= k_L A'(C_i - C_L) \qquad (4.2)$$

Where the driving force for the gas phase is given by the difference between the partial pressures of the transferring species in the bulk gas phase, p_G, and at the interface, p_i. For the liquid phase the driving force is given by the difference in the concentrations of the transferring species at the interface, C_i, and in the bulk liquid, C_L. This is shown diagrammatically in figure 4.1, where $p_G > p_i$ and $C_i > C_L$. The interfacial concentrations are assumed to be in equilibrium, implying that C_i is equivalent to the solubility of the transferring species at its partial pressure p_i. For sparingly soluble species, such as oxygen, a linear partition coefficient exists between its partial pressure in the gas phase and its solubility in the liquid. This relates the interfacial concentrations according to:

$$p_i = HC_i \qquad (4.3)$$

Where H is the Henry's Law Constant.

Combination of equations 4.1 to 4.3 allows the elimination of the unknown interfacial concentrations. This gives:

$$r = A'\left(p_G/H - C_L\right) \cdot \left[\frac{1}{k_L} + \frac{1}{Hk_G}\right]^{-1} \qquad (4.4)$$

As the partition coefficient, H is independent of the partial pressure

Figure 4.1

Interfacial Behaviour for Purely Physical Absorption, or Absorption with Slow Reaction.

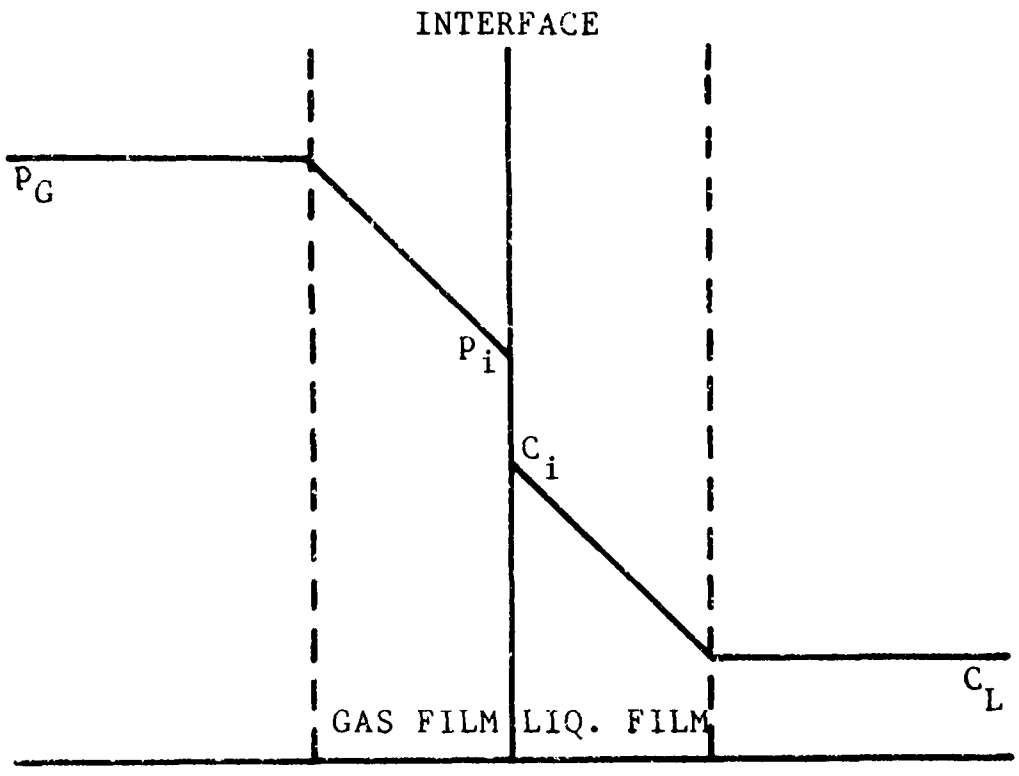

and concentration of the transferring species, then:

$$C^* = p_G / H \qquad (4.5)$$

Where C^* is the liquid phase concentration of the transferring species which is in equilibrium with the bulk gas phase. As we are considering only sparingly soluble species, the value of H is much greater than unity[54], in addition k_L and k_G are dependent on the diffusivity of the transferring species in the interfacial region, as shown below. As the diffusion coefficient in the gas phase is much higher than that in the liquid phase[54], then $k_G > k_L$. Overall this provides:

$$\frac{1}{k_L} >> \frac{1}{Hk_G} \qquad (4.6)$$

Thus

$$\left[\frac{1}{k_L} + \frac{1}{Hk_G}\right] \simeq \frac{1}{k_L} \qquad (4.6a)$$

Combination of equations 4.4 to 4.6a yields:

$$r = k_L A' . (C^* - C_L) \qquad (4.7)$$

That k_L and k_G are a function of the diffusion coefficients in the gas and liquid phases is shown by the various models applied to gas-liquid mass transfer in the interfacial region. Classically two theories, the film theory and the penetration theory have been used to describe this process[55]. The film theory assumes that thin films of stagnant gas and liquid exist either side of the gas-liquid interface, through which the transferring species diffuses when passing from one bulk phase to the other. This results in a linear dependence of the mass transfer coefficient on the diffusion coefficient, D_L, i.e.:[55]

$$k_L \propto D_L \qquad (4.8)$$

The penetration theory takes into account transient mass transfer conditions, assuming that the liquid at the interface is continually stripped away and replaced with fresh liquid from the bulk, due to the action of turbulent eddies. This results in[56]:

$$k_L \propto \sqrt{D_L} \qquad (4.9)$$

Boundary layer theories could also be used in the analysis of gas-liquid mass transfer, though this is not generally practised[57]. These would suggest:

$$k_L \propto (D_L)^{\frac{2}{3}} \qquad (4.10)$$

All these models predict a different exponent in the k_L - D_L relationship, however the precise value is not of great importance in the consideration of simple systems where few species are being absorbed/desorbed at the same time[55]. All models show that k_L will be increased by increased turbulence in the liquid phase which will reduce the thickness of the stagnant film, or increase the rate of surface renewal, or reduce the thickness of the boundary layer, depending on which model is chosen. In the area of gas-liquid mass transfer in sparged agitated systems, the film model is generally applied, due to its simplicity[56]. This is particularly the case where mass transfer with chemical reaction[58] or biochemical reaction[54] is considered.

The expression given in equation 4.7 for the mass transfer rate can be further developed to provide the overall mass flux, N_A, with dimensions of amount transferred per unit volume per unit time, i.e.:

$$N_A = r / V \qquad (4.11)$$

Where V is the volume of the system of interest, usually taken as the liquid volume. This yields:

$$N_A = k_L a \, (C^* - C_L) \qquad (4.12)$$

Where a is the specific interfacial area, or the interfacial area per unit volume (A'/V). Equation 4.12 can be applied to a system where C^* and C_L are independent of position and time. This is however not always the case and equation 4.12 must be considered to be the summation or integration of the point values within the system[54]. Manipulation of C^* and C_L to increase the driving force and hence increase the overall

mass flux is constrained, particularly in fermentations where conditions of pressure, temperature and minimum critical dissolved oxygen concentration required to sustain life are manipulated to meet the physiological requirements of the microorganisms[54]. Thus the main parameters of interest for design purposes are k_L and a. These can be determined separately, as outlined in the following section, however most studies concentrate on the determination of their product k_La, termed the volumetric mass transfer coefficient. This is partly because this is simpler to carry out, particularly in the gas-liquid dispersions which are of interest here, because the alteration of a process variable will often affect both k_L and a.

The measurement of k_La is the major aim of this present work, which focusses on mass transfer in viscous non-Newtonian liquids. The methods which are available for the measurement of k_La are outlined in section 4.2. They were all developed for use in low viscosity systems, so their usefulness in viscous or non-Newtonian liquids is dependent on the effects which the alteration in rheology has on their accuracy. Section 4.3 deals with some of the problems encountered in using the various methods in rheologically complex liquids. From equation 4.12 it can be seen that the measurement of the solubility of the transferred species as well as its concentration is important in mass transfer. This work concentrates on oxygen transfer, so section 4.4 is devoted to the techniques available for measuring dissolved oxygen concentration and oxygen solubility. Finally section 4.6 surveys the results of the mass transfer studies carried out in viscous and non-Newtonian liquids, which are then compared in Chapter 8 with the results obtained in this study.

4.2) Measuring Methods Used to Determine $k_L a$

k_L and a can be measured separately, as shown below. However this is not generally done and several methods have been developed which determine their product $k_L a$. These methods, which were developed in low viscosity systems, can be divided into three categories, which are: a) Chemical Methods, b) Steady State Methods and c) Unsteady state or Dynamic Methods. Each is dealt with in turn.

4.2.1) Separate Determination of k_L and a

Examination of equation 4.12 shows that k_L can only be determined either by maintaining a constant interfacial area, or by simultaneous measurement of $k_L a$ and a. Levenspiel and Godfrey[59] used a stirred cell of fixed interfacial area. In this apparatus both the gas and liquid phases flowed continuously, producing a steady state flux of oxygen transfer from air to pure water. The k_L values obtained varied between $2.7 - 4.5 \times 10^{-5}$ $m.s^{-1}$ depending on the agitation rate within the liquid phase. Calderbank et al.[60] studied single bubbles of carbon dioxide rising freely in a sealed column of liquid. They obtained k_L values through photographic measurement of the bubble volume and area, whilst monitoring the pressure change in the column using a transducer. The k_L values obtained were found to be dependent on bubble size and liquid composition, ranging from $15 - 30 \times 10^{-5}$ $m.s^{-1}$ in water to $1 - 5 \times 10^{-5}$ $m.s^{-1}$ in 99% glycerol. The bubble diameters used ranged from 4 - 35 $\times 10^{-3}$ m. Koide et al.[61] used the same technique as Calderbank et al.[60] in a variety of solutions. They noted that bubble age had a pronounced effect on the k_L values when the liquid contained low molecular weight organic compounds. This is presumed to be due to interfacial accumulation of the dissolved species. Using a stirred cell contacter, with fixed interfacial area, Elstner and Onken[62] determined the effect on k_L of the addition of various salts and alcohols. For salts they determined

that k_L is inversely related to the viscosity of the solution whilst k_L is directly related to the diffusivity in alcohol solutions. They also found that the addition of surface active compounds, such as sodium alkyl sulphate, affected k_L, as did impurities in the liquid. Removal of the surface layer of the liquid by suction with a capillary produced higher k_L values, comparable to those obtained by Calderbank et al.[60]

The interfacial area in aerated vessels has been determined using light transmission and scattering measurements[63,64]. Initially suspensions of solid spheres and bubble swarms of known interfacial area were used to test the technique. Bubble sizes have been measured by removal of liquid and bubbles in a capillary tube under suction, with simultaneous measurement of gas hold-up used to provide an estimate of the interfacial area[65 - 67]. Chemical methods have also been used to measure the interfacial area. These are similar to the chemical methods used to measure k_La, as described in the next section, but they rely on fast chemical reactions. In terms of the fiim model of mass transfer, a chemical reaction between an absorbing species A and a dissolved species B can occur within the liquid film, or at the gas-liquid interface[58]. This relies on the chemical reaction rate and the diffusion rate of B in stagnant liquid film being fast enough to remove all of the species A as it enters the liquid. Under these circumstances the influence of k_L disappears, with the interfacial area and the reaction rate determining the rate of mass transfer. Suitable systems which have been used include the absorption of carbon dioxide at low partial pressures in air into dilute sodium hydroxide solutions[68,69] and absorption of oxygen into aqueous alkaline sodium dithionite solutions[69,70]. However the results obtained using these methods can be susceptible to influence of k_G, the gas mass transfer coefficient[68].

4.2.2) Chemical Methods for Determining $k_L a$

The most common chemical method in use for the determination of $k_L a$ is that of sulphite oxidation[54]. Aqueous sodium sulphite is oxidised by dissolved molecular oxygen in the presence of cobalt or copper ions as a catalyst. Conditions are chosen such that the reaction is sufficiently fast for there to be no oxygen accumulated within the liquid, giving $C_L = 0$. This means that that the rate of reaction, which is measured by frequent sampling and titration of the unreacted sulphite, is determined by $k_L a.C^*$. The reaction kinetics are complex, with the overall reaction order depending on the choice of catalyst and its concentration[69,71]. As the reaction is fast, a significant proportion of the oxygen absorbed can undergo reaction in the interfacial region, which gives rise to enhanced $k_L a$ values[69,72]. Carbon dioxide absorption into sodium carbonate/bicarbonate buffer solutions has been used to measure $k_L a$ in water[69] and in non-Newtonian solutions[30]. When using this method it has been found that the total ionic strength of the liquids used needs to be maintained at approximately $2M.l^{-1}$ and the ratio of carbonate to bicarbonate needs to be maintained at approximately 4, in order to ensure that the chemical reaction of the carbon dioxide is slow enough to be controlled by $k_L a$, even though the concentration of carbon dioxide in the liquid is effectively zero. Apart from problems associated with enhancement of $k_L a$ due to a high rate of reaction, these two methods are criticised because of the high concentration of salts used. In general salt addition, or addition of other chemicals, will have a major effect on the bubble coalescence behaviour[71,66], which will affect the interfacial area. Chemicals can also reduce the diffusivity and solubility of the transferring species[54], which will alter the mass transfer coefficient.

To counter these problems, Zlokarnik[73] used the hydrazine method to measure $k_L a$. It has two principal advantages; the first is that the

chemical reaction is slow, leaving a finite oxygen concentration in the liquid which is measured using a dissolved oxygen probe (see section 4.4). The second advantage is that it utilises a very low concentration of chemicals. Copper sulphate is used as the catalyst at a concentration of 0.01M. and the hydrazine (N_2H_4) is added slowly to the solution at a constant rate to prevent accumulation of oxygen within the liquid. In addition the reaction products are nitrogen and water, which should not significantly affect the mass transfer behaviour.

4.2.3) Steady State Methods for Determining $k_L a$

In order to maintain a mass flux it is necessary to maintain a driving force for mass transfer. This can be done using chemical methods, as described above, to continually remove the transferred species from the liquid, or a non-chemical reaction of the transferred component can be used e.g. biochemical removal of oxygen. Alternatively, the partially saturated liquid can be continuously replaced with fresh liquid which contains less of the absorbed component. If these processes are continued for a reasonable period of time then a steady state can be produced when the rate of removal is equivalent to the rate of transfer for the component of interest. This allows $k_L a$ to be determined, using equation 4.12, providing the mass flux and the concentration difference of the absorbed species can be measured or estimated.

Perez and Sandall[74] used a steady state method to determine $k_L a$ values in non-Newtonian Carbopol solutions, this involved the use of two vessels. In the agitated vessel of interest carbon dioxide was absorbed from the gas phase. At the same time liquid was continuously withdrawn and passed through a desorption column, where the carbon dioxide was removed under vacuum, before returning the liquid to the absorption vessel. Metering of gas and liquid flow rates combined with analysis of the inlet and exit liquid streams for carbon dioxide content allowed $k_L a$

values to be determined. Voigt and Schugerl[75] and Konig et al.[76] used a similar method, which combined oxygen absorption in one vessel with oxygen stripping using a gas stream of nitrogen in a second vessel. Keitel and Onken[77] analysed the steps involved in the determination of $k_L a$ using this method, and show that gross errors can result unless high liquid flow rates are used. This is necessary to maintain a low dissolved oxygen concentration and hence a high driving force, otherwise a small error in dissolved oxygen measurement can result in a large error in the determination of the driving force and hence $k_L a$. This observation applies to any steady state method used to determine $k_L a$, which relies on the measurement of the dissolved oxygen concentration[22].

Liquids which contain living microorganisms have been utilised to provide $k_L a$ values. The simplest methods involve monitoring real fermentation systems under steady state conditions, measuring the dissolved oxygen concentration and the oxygen uptake rate (OUR), i.e. the rate of removal of oxygen from the gas stream which is equivalent to the mass flux, N_A, of the transferring species[78 - 81]. This method can also be used in non-fermenting systems, by the addition of a suitable micro-organism and the substrates which are required by that microorganism. Solomon[22] used Bakers Yeast in solutions of Carbopol, Xanthan Gum and CMC to measure $k_L a$ values. Kappeli and Fiechter[82] used a special strain of yeast which was unable to grow or produce by-products in the absence of dissolved oxygen. They ensured that the demand for oxygen was higher than the rate of supply, thus the dissolved oxygen concentration remained at zero. This eliminated the need to measure the dissolved oxygen concentration. However this procedure may cause higher $k_L a$ values to be obtained than are found for purely physical absorption, due to the accumulation of microorganisms within the interfacial region[83 - 88]. This effect is only considered to be significant where $k_L a$ is very low and the interface is very stable, as may occur in surface aerated liquids

of fixed interfacial area[54,89 - 92]. Under conditions of low dissolved oxygen concentration $k_L a$ can also be affected by the formation of by-products such as alcohol, due to anaerobic conditions being produced[93,94], (see Chapter 7,section 4). This is due to the desorption of the alcohol occurring at the gas-liquid interface, which causes eddies in the surface due to the formation of surface tension gradients[55].

4.2.4) Unsteady State Determination of $k_L a$

The development of the dissolved oxygen probe provided a simple means to continuously monitor the concentration of oxygen within a liquid. These probes can be used in steady state methods of $k_L a$ determination to ascertain the steady state value of the dissolved oxygen concentration, as described above, in this case the rate of accumulation of oxygen within the liquid is zero. For unsteady state methods the rate of accumulation of oxygen in the liquid phase is not zero. A mass balance formulation for oxygen in the liquid phase is:

$$\begin{bmatrix}\text{Accumulation rate of} \\ O_2 \text{ in the liquid}\end{bmatrix} = \begin{bmatrix}\text{rate of transfer of} \\ O_2 \text{ into the liquid}\end{bmatrix} - \begin{bmatrix}\text{rate of removal of} \\ O_2 \text{ from the liquid}\end{bmatrix}$$

For an aerobic fermentation, where no liquid flow occurs, i.e. a batch liquid, this results in the expression[78,95]:

$$\frac{dC_L}{dt} = k_L a\ (C^* - C_L) - r_c \qquad (4.13)$$

where t is time and r_c is the volumetric rate of consumption of oxygen by the microorganisms (moles.m^{-3}.s^{-1}). Clearly where $\frac{dC_L}{dt} = 0$, i.e. no net accumulation, the rate of consumption is balanced by the rate of transfer and the steady state equation 4.12 results. Where no oxygen is consumed, i.e. in batch liquids which do not contain any microorganisms or chemicals which react with oxygen, then equation 4.13 becomes:

$$\frac{dC_L}{dt} = k_L a \ (C^* - C_L) \qquad (4.14)$$

These equations (4.13 & 4.14) form the basis of the unsteady state methods used to determine $k_L a$. In general any dissolved oxygen contained in the liquid is first reduced to a low value, or removed completely. Then air is sparged into the liquid and the increase in C_L with time is noted. Where aerobic microorganisms are contained in the liquid, removal of the dissolved oxygen is accomplished simply by switching off the air supply. This gives a removal rate equivalent to the rate of consumption by the microorganisms, allowing the determination of r_c in equation 4.13. Recommencing aeration allows $k_L a$ to be found from equation 4.13[78,95]. Where no microorganisms are present, the dissolved oxygen is removed by sparging nitrogen through the liquid, in the so called Dynamic Gassing Out Method[71], prior to aeration and determination of $k_L a$ using equation 4.14. Alternatively a step change in the impeller speed during a steady state fermentation will alter $k_L a$[96]. This in turn causes C_L to alter to a new steady state value and the rate of change of C_L during the unsteady state period allows $k_L a$ to be found, using equation 4.13. This has the advantage of eliminating any significant variation in C^* which can affect the $k_L a$ value determined, as shown below.

In all of the unsteady state methods described, complications can arise which generally result in $k_L a$ being underestimated[97]. They all use dissolved oxygen probes to measure the rate of change of C_L. When this change is fast, the response of the probe will lag behind the actual dissolved oxygen concentration in the liquid. This is due to diffusional resistances associated with the probe membrane[98,99] and with the presence of a stagnant liquid film around the probe membrane[99,100]. It is possible to determine the probe response lag, by measuring the response time of the probe when subjected to a sudden change in dissolved oxygen

concentration, e.g. by rapidly moving the probe from a liquid depleted in oxygen to a liquid which is saturated with oxygen. This can then be incorporated in the determination of k_La[100 - 102], although probes with fast response times enable this lag to be ignored when measuring low k_La values[71]. Similarly several methods have been used in an attempt to overcome the response lag due to the stagnant liquid layer[22,100,103-106]. Another area in which considerable error can be introduced into the k_La values determined, is in modelling the gas phase dynamics. This has an effect on the value of C^* which is used. Generally C^* is assumed to be constant and equal to the oxygen concentration which is in equilibrium with the partial pressure of oxygen in the inlet gas stream. However Lopes de Figueiredo and Calderbank[107], when measuring k_La values in water-air systems, demonstrated that the k_La values obtained are much higher if the actual gas phase composition is taken into account. Dunn and Einsele[108] have developed several models to account for the gas phase dynamics in systems with well mixed gas and liquid phases. Shoiya and Dunn[109] extended this consideration to a variety of gas and liquid flows, whilst Linek and Vacek[110] considered the start up effects of switching gas streams. Chapman et al.[111] adapted the dynamic gassing out method to enable the gas phase dynamics to be incorporated. It involved monitoring the dynamic oxygen concentration in the outlet gas stream, using an oxygen electrode, in addition to monitoring the dissolved oxygen concentration.

The unsteady state method of Mignone and Ertola[96] produces a virtually constant gas phase oxygen concentration, removing problems associated with gas phase dynamics. Similarly Vardar and Lilly[112] have developed a method which removes the errors associated with the variation in the gas phase concentration of oxygen and the probe response lags. It involves producing a sinusoidal variation in pressure within the vessel, which in turn causes the dissolved oxygen concentration to vary

sinusoidally. This allows $k_L a$ to be calculated, although the variation in pressure may affect the results[113].

4.3) Measurement of $k_L a$ in Viscous and Rheologically Complex Systems

Steady state[22,74,76], unsteady state[22,43,49,100,114 - 116] and chemical methods[30,36,70] have all been used for the measurement of $k_L a$ in viscous and non-Newtonian model systems. Chemical methods have the disadvantage of altering the rheological and physical properties of the liquid. Ranade and Ulbrecht[30] found that the addition of ionic compounds during carbon dioxide absorption studies removed any measureable non-Newtonian behaviour and reduced the viscosity markedly in shear thinning CMC and viscoelastic polyacrylamide solutions. In general the addition of salts or any chemicals can have a major effect on bubble coalescence behaviour[66,71], which in turn affects the interfacial area. Chemicals will also reduce the diffusivity and solubility of the transferring species[54], which alters the mass transfer coefficient.

Dissolved oxygen electrodes or probes are widely used in the measurement of $k_L a$, although some serious problems are encountered in viscous liquids. The presence of a stagnant film of liquid around the probe tip, which produces a response lag, is much more important than in low viscosity systems[22], as the degree of turbulence is generally lower in viscous liquids, especially when the liquid is shear thinning, as the shear rate in agitated vessels is lower away from the impeller region and near to solid surfaces. This increased response lag will have the greatest effect on unsteady state measurements of $k_L a$, however it may be offset by the fact that $k_L a$ values are generally lower in viscous liquids[13]. In viscous liquids the thickness of the stagnant film will be highly dependent on the agitation conditions[22]. This will affect the readings in both steady state and unsteady state methods of $k_L a$ determination, making positioning of the probe within the vessel

important in determining the reading obtained. Positioning of the probe will also affect the readings obtained due to variations in pressure with altering liquid height[117], or variations in the actual dissolved oxygen concentration due to poor liquid mixing [104]. These effects can be judged by the use of more than one dissolved oxygen electrode[49]. Kipke[114] overcame the effect of the impeller speed on probe response by positioning a small impeller close to the tip of the probe, which ensured a high liquid flow across the tip. This also removed any gas bubbles which would otherwise adhere to the membrane on the probe, which can cause a higher reading of dissolved oxygen to be registered[105,119 - 122]. This is particularly important when fast response dissolved oxygen probes are used, such as those required in the unsteady state determination of $k_L a$.

For the dynamic gassing out method, which uses nitrogen to remove the oxygen prior to aeration, the hold-up of tiny bubbles of nitrogen in the viscous liquid can reduce the $k_L a$ values obtained by up to 80%[123]. These bubbles act as an additional oxygen sink, removing oxygen from the liquid and reducing the dissolved oxygen reading.

In the steady state determination of $k_L a$, the factors discussed above which affect the probe reading can be important in determining high $k_L a$ values accurately[22], as these require high dissolved oxygen readings. When these conditions occur a small error in C_L will produce a large error in the driving force, as the values of C^* and C_L will be very similar. Otherwise steady state methods which involve the addition of microorganisms to model fluids would appear to give a reasonable system of $k_L a$ measurement[22]. Care must be taken to ensure that the model fluid properties are not unduly altered, particularly where they are sensitive to variations in pH which may be caused by the addition of the microorganisms[22]. In fact the maintenance of similar rheological, physical and chemical properties between the model fluid and the system of interest is important in all $k_L a$ measurements[54]. Thus where the

system being modelled is a fermentation system, it may be an advantage to utilise a real fermentation as a model.

4.4) Measurement of Oxygen Concentration and Solubility in Aqueous Solutions

In order to determine $k_L a$ it is necessary to measure both the solubility and the concentration of the transferring species in the liquid. Schumpe and Quicker[124] have reviewed the general area of gas solubility in fermentation broths, paying particular attention to oxygen solubility measurement. For a sparingly soluble species such as oxygen, Henry's Law holds. This relates the equilibrium concentration of the species in the liquid phase to its partial pressure in the gas phase through the partition coefficient, H, as shown in equation 4.3. H, known as Henry's Constant, is independent of pressure over a limited range, but is dependent on temperature and solution composition[125]. Some values for H are known for oxygen in water and in some simple solutions[126].

The most commonly used method for determining the concentration or solubility of oxygen in a liquid, is the Winkler method[127]. It is a chemical method that is extensively used in natural and waste waters. In use care must be taken with this method to ensure that no competing reactions with oxidative or reductive species present in the liquid take place. Hikita et al.[128] developed a non chemical method for the measurement of oxygen concentration in sucrose solutions. After degassing the solution of interest under vacuum, it is agitated with a known amount of oxygen gas in a sealed system at a stated pressure. The reduction in volume of the gas phase at constant pressure gives a direct measure of the amount of oxygen which has dissolved in the liquid. Quicker et al.[129] used a similar method, keeping the volume constant and noting the change in pressure due to the dissolution of oxygen in the liquid. This method was successfully used in fermentation media, even if it contained viable microorganisms. Kappeli and Fiechter[130] developed a method which made use of a dissolved oxygen electrode. These electrodes do not directly measure the concentration of oxygen within a liquid[99], the reading they give is dependent on the activity of the dissolved oxygen. Thus the

reading is proportional to the partial pressure of oxygen which is required to produce the oxygen concentration found in the solution. This means that an electrode calibrated to give a reading of 100% at a certain temperature and oxygen pressure will give the same reading in any solution with the same temperature and oxygen pressure, regardless of the solubility of oxygen in those solutions. Kappeli and Fiechter[130] introduced a known concentration of oxygen into the solution of interest by enzymic degradation of a known amount of hydrogen peroxide. Comparison of the reading obtained on the meter with the 100% saturation reading obtained at a known pressure and temperature gave a measure of the solubility of oxygen in the solution.

It has been suggested[125,129], that it is possible to calculate the solubility of oxygen in a given solution. This requires a knowledge of the salting out effect which the other species present in the solution will have on the oxygen. The effects which some species have has been determined[124,125,129], however these are mostly electrolytes. The effects of most non-electrolytes, such as polymeric materials and organic compounds are not well known[124].

From the above consideration of solubility measurement and the procedures described in the previous sections, it can be seen that dissolved oxygen electrodes are powerful tools in enabling $k_L a$ values to be estimated. In a comprehensive study, Lee and Tsao[99] describe their design and operation, sources of error and applications. In principle they utilise the reduction of molecular oxygen at a cathode to produce a current which can be measured and is proportional to the rate of this reduction. At the anode the balancing reaction which occurs depends upon the electrode type: Polarographic probes, which require an external voltage of ca. 600 mV to be applied, utilise the formation of silver chloride from chlorine ions in solution and the silver metal anode;

Galvanic probes rely upon the dissolution of the lead metal anode as lead ions, requiring no external voltage to be applied. The electrodes and their surrounding electrolyte are separated from the test liquid or gas by an oxygen permeable membrane. This prevents poisoning of the electrodes by most impurities and ensures that no harm is done to the test sample by the electrodes and the electrolyte . The main variables in the design of the probes are the area and position of the anode and cathode, the thickness and type of material of the membrane and the principle of operation. In practice all the desirable characteristics which a probe can have, i.e. low flow dependency, long term stability, fast response, high sensitivity, etc., are mutually exclusive in probe design. For example a thin membrane provides a fast response, but also makes the probe sensitive to the velocity of the surrounding liquid. Thus each probe must be designed for a specific use. As the response of dissolved oxygen electrodes is dependent in part on the rate of diffusion of oxygen through the membrane, they are very sensitive to variations in temperature. This has lead to the incorporation of temperature compensation circuits in their design, however it is still very important to ensure accurate temperature control or measurements when measuring dissolved oxygen, particularly because the solubility of oxygen varies with temperature[99].

4.5) Techniques for Correlating $k_L a$ Values in Viscous / Non-Newtonian Solutions

The preceding sections give some details of the methods used to measure $k_L a$ values in agitated gas-liquid systems. As can be seen from the discussion in section 3, their use in viscous or non-Newtonian solutions can be problematic. However several comprehensive studies have been carried out and the variations in $k_L a$ with varying rheological properties, agitation rates and gas flow rates have been determined. The results are reported and compared in the following sections. In general dimensionless numbers are used to correlate the data, some of these are described in Chapter 3, section 1, the remainder are described below.

The means used to report mass transfer results in terms of dimensionless numbers can be split into two main groups, depending on the approach adopted. The principal difference between the two is that one makes use of the impeller speed and diameter to represent the agitation conditions whilst the other uses the power consumption of the impeller to describe the agitation conditions. Each is dealt with in turn:

4.5.1) Dimensionless Correlations for $k_L a$ Using the Impeller Speed

Dimensional analysis carried out by Sideman et al.[131] lead to the following correlation for mass transfer results:

$$Sh' = f(\ Re,\ Sc,\ v_s . \mu/\sigma\ ,\ \mu_g / \mu\ ) \qquad (4.15)$$

Where Sh' is a modified Sherwood Number

Re is the Reynold Number (described in Chapter 3, section 1)

Sc is the Schmidt Number

$v_s . \mu/\sigma$ is a gas flow group with v_s = superficial gas velocity
μ = liquid viscosity
σ = Interfacial tension

μ_g / μ is the ratio of the viscosities of the dispersed phase (gas) to the continuous phase (liquid).

The Sherwood number, Sh, represents the ratio of the mass diffusivity to the molecular diffusivity and is used in the study of absorption of a molecular species across a defined interface:

$$Sh = k_c L / D_m \qquad (4.16)$$

where D_m is the diffusion coefficient for the species of interest, L is a characteristic length within the system and k_c is the mass transfer coefficient.

For use in gas-liquid mass transfer where the area of the interface cannot be readily separated from the mass transfer coefficient, i.e. in mechanically agitated sparged vessels, the Sherwood number is modified to include the specific interfacial area, giving:

$$Sh' = k_L a \, D^2 / D_L \qquad (4.17)$$

where $k_L a$ is the volumetric mass transfer coefficient and D, the impeller diameter. D_L is the diffusion coefficient in the liquid.

The Schmidt number represents the ratio of the momentum diffusivity to the molecular diffusivity, through the use of the kinematic viscosity and the diffusion coefficient:

$$Sc = \mu / \rho \, D_L \qquad (4.18)$$

It is used in the above correlation proposed by Sideman et al.[131] and also in correlations which make use of the impeller power requirements, (see below).

In correlations involving results obtained in non-Newtonian liquids, the shear thinning nature of the solutions requires the use of the apparent viscosity μ_a rather than the viscosity, μ . This substitution

is carried out as described in Chapter 3, section 1. In addition the viscoelastic properties of the solutions have been incorporated in the correlation using the Deborah number, De, which is also described in Chapter 3. These and other modifications to the Sideman correlation are described as appropriate in the relevant sections.

4.5.2) Correlations Involving the Use of the Agitator Power Input

Through a consideration of the functional dependence of $k_L a$ on the material and process parameters, Zlokarnik[73] obtained the following:

$$k_L a = f(\rho , \mu , \sigma , D_L, P/Q, Q/V, g, Si) \qquad (4.19)$$

where ρ = density, μ = viscosity (μ_a for non-Newtonian fluids), σ = surface tension, D_L = diffusion coefficient, P = agitator power input, V = volume, Q = air flow rate, g = gravitational constant and Si is a measure of the bubble coalescence behaviour in the solution of interest. This in turn gives the following:

$$k_L a^* = f((P/Q)^*, (Q/V)^*, \sigma^*, Sc, Si^*) \qquad (4.20)$$

$$\text{where } k_L a^* = k_L a \left(\mu / \rho g^2 \right)^{\frac{1}{3}} \qquad (4.21)$$

$$(P/Q)^* = P/Q \left[\rho \left(\mu g/\rho \right)^{\frac{2}{3}} \right]^{-1} \qquad (4.22)$$

$$(Q/V)^* = Q/V \left[\mu / \rho g^2 \right]^{\frac{1}{3}} \qquad (4.23)$$

$$\sigma^* = \sigma / \rho . \left[\left(\mu/\rho \right)^4 g \right]^{\frac{1}{3}} \qquad (4.23a)$$

where Sc = Schmidt number (as above) and Si^* is a material dimensionless group which describes the coalescence behaviour of the solutions. The parameters included in the group Si^* are unknown, so it is usual to compare results obtained in solutions of similar coalescence behaviour, allowing Si^* to be ignored. In addition the variation in surface tension found in the studies carried out is minimal (see following section) allowing the group, σ^* to be removed from the correlation. This leaves:

$$(k_La)^* = f_1(\ (P/Q)^*,\ (Q/V)^*,\ Sc\ ) \qquad (4.24)$$

which can be further reduced, if no dependence of k_La on Q is found, to:

$$(k_La)^* = f_2(\ (P/V)^*,\ Sc\ ) \qquad (4.25)$$

$$\text{where } (P/V)^* = (P/Q)^*.(Q/V)^*$$

$$= (P/V).\ [\rho\ (\mu g^4/\rho)^{\frac{1}{3}}]^{-1} \qquad (4.26)$$

Thus the dependence of k_La on variations in process parameters and viscosity can be described through the use of three dimensionless groups (equation 4.25) or four dimensionless groups (equation 4.24) where air flow rate is important. Several authors find that this dependence can be further reduced by combining the groups $(k_La)^*$ and $(Q/V)^*$, this gives:

$$K^* = f_3(\ (P/Q)^*,\ Sc\ ) \qquad (4.27)$$

$$\text{where } K^* = (k_La)^*.(Q/V)^{*-1} = k_La\ V\ /\ Q \qquad (4.28)$$

This requires that the exponent on the group $(Q/V)^*$ in equation 4.24 is determined to be 1, or is set to 1. This can affect the exponents on the other dimensionless groups, although it offers the advantage of reducing the number of groups in the overall correlation. This is dealt with in more detail in Chapter 8, section 5.

4.6) $k_L a$ Values in Agitated Viscous/Non-Newtonian Liquids: Studies Carried Out

There have been several studies carried out on a similar scale to that used here which have attempted to determine $k_L a$ values in viscous and non-Newtonian systems. Several of these are of only limited interest here. Solomon[22] used both the dynamic gassing out method and a steady state method similar to that used here, in viscous solutions of CMC, Carbopol and Xanthan Gum. The results obtained were limited, with no measurement of agitator power consumption. However he showed that the dynamic method yielded lower $k_L a$ values than the steady state method, even if lags due to the electrode response time and the liquid film resistance were eliminated. The reason for this was determined to be related to the gas phase dynamics, in particular the hold-up of small nitrogen bubbles as first described by Heijnen et al.[123]. Tanaka[116] used a dynamic gassing out method in granulated agar broths and shear thinning broths of plant cells at high concentrations. Again no power consumption measurements were made, though he found that $k_L a$ decreased gradually with increasing viscosity up to 0.05 Pa.s. At higher viscosities $k_L a$ was highly dependent on the viscosity, falling rapidly to very low levels. Joshi and Kale[70] and Konig et al.[76] used tube agitators, which cause the aeration rate to be intricately linked to the agitator speed and the liquid rheology. Neither report any power consumption measurements, or measurements of the rheological properties of the liquids used.

Joshi and Kale[70] used a chemical method, similar to that of Ranade and Ulbrecht[30], to measure $k_L a$ in dilute solutions (<100p.p.m.) of CMC, Cuar Gum and polyethylene oxide. In addition they measured the interfacial area (see section 4.2). They found that increasing solute concentration raised both $k_L a$ and a, although k_L was reduced slightly at the higher concentrations used. Konig et al.[76] used a steady state method in solutions of propanol, CMC, glycerol and polyacrylamide, PAA. Their few results

show that k_La is drastically reduced by increasing viscosity in glycerol and PAA. In CMC solutions the k_La results for solutions of 1.0% (K = 0.06 Pa.s^n, n = 0.85) and 1.4% (K = 0.1 Pa.s^n, n = 0.81) were virtually the same. In 2% CMC (K = 0.27 Pa.s^n, n = 0.67) k_La values were significantly lower. The tube stirrer was found to be ineffective at mixing the liquid at higher PAA concentrations (1%, K = 2.5 Pa.s^n, n = 0.38), being flooded rapidly by any but very low air flows. In addition they found that the viscous liquids required up to 2½ hours before the steady state was established. This is indicative of poor liquid mixing, or long circulation times and may suggest that the use of two vessels, one for absorbing and one for desorbing the transferring oxygen is not suitable in rheologically complex solutions, particularly as disengagement of the gas bubbles in the solution can be a problem.

Paca et al.[36] used the dynamic gassing out and sulphite oxidation methods in colloidal starch solutions. They found that k_La was highly dependent on the impeller speed and virtually independent of the gassing rate at μ = 0.2 Pa.s. Dang et al.[100] used a dynamic gassing out method. The k_La values obtained were much lower than in water and less dependent on the impeller speed in a 2% CMC solution although the air flow rate still had a major effect on k_La. No power consumption or rheological data were reported.

The remaining studies, which are much more comprehensive, can be divided into two main categories, depending on the means used to correlate the results. The first group use the dimensionless numbers Sh', Re, Fr, Sc, etc., which essentially relate k_La to the geometric variables N and D and the properties of the liquid. Thus use of this method may be expected to produce different correlations depending on the agitator type and vessel geometry. The second group use the dimensionless numbers $(k_La)^*$, $(P/Q)^*$, $(Q/V)^*$, Sc, etc. These give k_La in terms of the process

variables, such as the power input and the air flow rate, as well as incorporating the liquid properties, This allows greater flexibility in the comparison of different agitator types and vessel geometries. It should be noted that, where surface tension and diffusivity data are used, they are generally taken as being the same as that found in water, for the non-Newtonian polymer solutions studied. This is not unreasonable, as the concentration of these polymer solutions are relatively low, even at high viscosities, when compared to the concentration of Newtonian solutions of similar viscosities. Thus in the literature cited below, where such data have been determined, the values are near to that of water.

Comparison of the results of the various studies carried out is a difficult task, as the raw data which has been determined, i.e. $k_L a$, P, etc., are rarely presented in terms of the operating variables: N, Q and μ_a. In general terms it is usually possible to distinguish the dependence of $k_L a$ on P or N, Q and μ_a from the correlations used. This has been done and the results are shown in table 4.1. No discussion of the influence of the measuring methods used on the results obtained will be carried out here, as the methods have been discussed in the previous sections. Where a method is thought to have unduly influenced a result, this will be noted in the conclusions to this chapter.

Perez and Sandall[74] determined $k_L a$ values in solutions of Carbopol (0 - 1% w/w), using a six bladed disc turbine (D = T/3) in a baffled cylindrical vessel, H_l = T = 0.152 m. They found that $k_L a$ was unaffected by agitation below an impeller speed of 3.3 s^{-1} in water, above this speed $k_L a$ increased rapidly with increasing agitator speed. In Carbopol solutions the critical speed at which $k_L a$ became dependent on the agitator speed was reduced slightly reaching 3.0 s^{-1} in 1% Carbopol. On going from water to 0.25% Carbopol (K = 0.0428 Pa.s^n, n = 0.916), $k_L a$ was

Table 4.1

Mass Transfer Results from the Literature

Ref.	Author	Measuring Method	Solution	Range of Viscosity (Pa.s x 10^3)	Generalised Results	Effects of Viscoelasticity
74	Perez & Sandall	St.St. CO_2 abs. (Chemical)	Carbopol	1 - 40	$k_La \propto N^{1.11} . Q^{0.447} . \mu_a^{-1.3}$	—
30	Ranade & Ulbrecht	Chemical, Dyn. CO_2 abs.	CMC PAA	1 - 5.3 1 - 5.3	$k_La \propto N^{1.8} . \mu_a^{-0.41}$	reduces k_La
49	Yagi & Yoshida	Dyn. O_2 desorb.	Glycerol Millet Jelly CMC PAN	1 - 5.1 1 - 70 1 - 347 1 - 50	$k_La \propto N^{2.2} . Q^{0.28} . \mu_a^{-0.40}$	reduces k_La
115	Nishikawa et al.	Dyn. O_2 abs.	Millet Jelly CMC	1 - 42 1 - 2000	$k_La \propto N^{2.4} . Q^{0.33} . \mu_a^{-0.5}$ also $k_La \propto (P/V)^{0.8}$	No effect
114	Kipke	Dyn. O_2 abs.	CMC	370 - 1500	$k_La \propto P/V^{0.7} . Q^{0.3} . \mu_a^{-0.47}$	—
43	Hocker et al.	Dyn. O_2 abs.	Glucose CMC PAA	1 - 267 1 - 291 1 - 503	$\overline{k_La} \propto P^{0.59} . Q^{0.41} . \mu^{-0.69}$	Increased Impeller Speed dependency
132	Henzler	Dyn. O_2 abs.	Glucose Glycerol Millet Jelly CMC PAA	12 - 207 1 - 5.1 1 - 70 9 - 342 —	$k_La \propto P^{0.5} . Q^{0.5} . \mu^{-0.63}$ $k_La \propto P^{0.6} . Q^{0.4} . \mu^{-0.57}$ $\overline{k_La} \propto P^{0.6} . Q^{0.4} . \mu^{-0.69}$	Increased Impeller Speed dependency
135	Jurecic et al.	Dyn./St.St.	Fermentation broths	K=0.0139 n=0.678	$k_La \propto P^{0.35} . Q^{0.65}$ large scale $k_La \propto P^{0.5} . Q^{0.7}$ pilot scale	—

reduced by a factor of 2 at each impeller speed. Further increases in concentration to 0.75% (K = 0.507 Pa.s^n, n = 0.773) did not reduce k_La further. In a 1% Carbopol solution (K = 5.29 Pa.s^n, n = 0.594) k_La was reduced at low impeller speeds (< 5s^{-1}), but actually increased compared to 0.25 and 0.75% Carbopol at higher speeds, approaching that of water at N = 8s^{-1}. They reported a large foam build up in the 0.75% and 1.0% Carbopol solutions, which would be expected to increase k_La through the increase in interfacial area which this causes, this may explain the higher than expected k_La values in the 0.75% and 1% solutions. For water and 0.25% Carbopol solutions, sufficient results were obtained at N > 3.3s^{-1}, to be able to correlate the data according to:

$$Sh' = 21.1\ Re^{1.11}.\ Sc^{0.5}.\ (\ D.v_s/\ \sigma\ )^{0.447}.\ (\ \mu_g/\mu_a\ )^{0.694} \qquad (4.29)$$

Where μ_a was determined using the equations of Calderbank and Moo-Young[25], as described in Chapter 3, section 1; and μ_g is the viscosity of the gas phase. The gas viscosity was not varied and the liquid viscosity varied by less than a factor of 40 in determining this correlation, which is not completely dimensionless. It gives a dependence of k_La on viscosity of $k_La \propto \mu_a^{-1.3}$, if the solutions of higher apparent viscosity were included, then k_La would be less dependent on the viscosity. They found that k_La was dependent on the air flow rate, as can be seen from the correlation, however lack of data on power consumption prevents any precise determination of the effects of P and Q on k_La. As $k_La \propto N^{1.11}$, which is determined from the correlation, the dependence of k_La on P can be estimated by assuming that the gassed power number, Po_g, remains constant for the small variation in viscosity. This gives $k_La \propto P^{0.37}$ from $P = Po_g.\rho.N^3.D^5$ (equation 3.9).

Yagi and Yoshida[49] used a dynamic gassing out technique which varied slightly from that used by other workers in general. They sparged air

through the solutions until equilibrium was reached, then left the solution to stand until the air bubbles had left the solution. They then sparged nitrogen gas and determined $k_L a$ from the desorption of the oxygen in the solution. Shear thinning polyacrylate (PAN) and CMC solutions, which showed evidence of viscoelastic properties, were used, in addition to Newtonian solutions of Millet Jelly and glycerol. The vessel of H_l = T = 0.25m was fitted with a single disc turbine (D = 0.1m). In the Newtonian solutions $k_L a$ was reduced with increasing viscosity over the range 0.001 - 0.07 Pa.s, yet showed the same dependence on N and Q at 0.07 Pa.s as in water. For non-Newtonian fluids the dependence of $k_L a$ on N reduced with increasing apparent viscosity, which lead to a reduction in $k_L a$ compared to Newtonian fluids of the same viscosity. In order to correlate the data using one equation, a Deborah number was incorporated. In addition they measured the effect of the gas viscosity on $k_L a$ and determined that it was negligible. This lead to a correlation of:

$$Sh' = \frac{0.060\ Re^{1.5}.\ Fr^{0.19}.\ Sc^{0.5}.\ (\mu_a.v_s/\sigma)^{0.6}.(\ N.D/v_s\ )^{0.32}}{(\ 1 + 2De^{0.5}\ )^{0.67}} \qquad (4.30)$$

The manner in which they arrived at values for De did not depend on the measurement of the viscoelastic properties of the fluid, but was related to the shear rate at which the ratio of the apparent viscosity to the viscosity at zero shear rate, μ_0, equalled 0.67. This shear rate at which $\mu_a/\mu_0 = 0.67$ was taken to be the reciprocal of the characteristic material time which is used to determine the Deborah number. Equation 4.30 implies that the non-Newtonian fluids showed a similar dependence of $k_L a$ on the gas flow rate as that found in the Newtonian liquids. In addition the effect due to varying viscosity can be determined. This gives $k_L a \propto N^{2.2}.\ v_s^{0.28}.\mu^{-0.4}$.

Nishikawa et al.[115] also used the dynamic gassing out method in Millet Jelly and CMC solutions, in vessels of $H_1 = T = 0.15 - 0.6m$ with turbines and disc turbines ($D = 0.33T - 0.5T$). They found no effect of viscoelasticity in their results and could correlate all the non-Newtonian data with that of the Newtonian solutions using the apparent viscosity determined according to the results of Nagata et al.[133]. For a range of 0.001 - 2.0 Pa.s they obtained:

$$Sh' \propto Re^{1.5} . Sc^{0.5} . (\mu_a . v_s / \sigma)^{0.5} . Fr^{0.37} . (ND/v_s)^{.167} . (T/D)^2 . Po_g^{0.8} \qquad (4.31)$$

This gives $k_La \propto N^{2.4} . v_s^{0.33} . \mu^{-0.5}$ and they also measured the power consumption, obtaining $k_La \propto (P/V)^{0.8}$.

Ranade and Ulbrecht[30] found that k_La was independent of the gas flow rate in non-Newtonian solutions of CMC (0.01 - 0.12%) and polyacrylamide (PAA, 0.01 - 0.1%). They used a chemical method to determine k_La in a vessel of $T = 0.3m$ using a single disc turbine ($D = 0.27T - 0.47T$) and gas flow rates of 1 - 4 vvm. The chemicals used were found to affect the rheological properties of the solutions, reducing the viscosity and removing any non-Newtonian behaviour, so their properties were measured before addition of the salts. These measurements included measurement of the viscoelastic properties of the liquids, enabling them to use a correct form of the Deborah number as described in Chapter 3, section 1. This gave:

$$Sh' = 2.5 \times 10^{-4} Re^{1.8} . (\mu_a / \mu_w)^{1.39} . [1 + 100 De]^{-0.67} \qquad (4.32)$$

Which shows a similar dependence of k_La on N and μ_a as that found by Yagi and Yoshida[49], although no dependence on air flow rate was found.

Kipke[114] studied k_La in very viscous solutions of CMC, $\mu_a = 0.56 - 4.0$ Pa.s (at a shear rate of 21 s^{-1}). He used the dynamic gassing

out method in a vessel of $H_1 = T = 0.4$ m with a disc turbine, ($D = T/3$) and dual Intermig impellers, ($D = 0.4T - 0.6T$). He found that k_La was rapidly reduced at high viscosities ($\mu_a > 0.80$ Pa.s), where N was kept constant. In addition the dependence of k_La on Q was reduced, though not entirely eliminated, at higher viscosities. He correlates his data according to equation 4.27, ignoring Sc. This gave:

$$K^* \propto (P/Q)^m \qquad (4.33)$$

Where m = 0.5 in water and 0.7 in the CMC solutions, for both the disc turbines and the Intermig impellers. Based on this value of 0.7, the following relationship can be derived:

$$k_La \propto P^{0.7} . Q^{0.3} . \mu_a^{-0.47} \qquad (4.34)$$

Hocker et al.[43] carried out a similar study to that of Kipke[114], extending the range of variables used to include viscous Newtonian solutions of glucose and highly viscoelastic polyacrylamide (PAA), as well as shear thinning CMC solutions. For CMC, agitated using a disc turbine ($D = T/3$) in a vessel of $H_1 = T = 0.4$ m, they found that increasing CMC concentration reduces k_La compared to that in water and also reduces but does not eliminate the dependence of k_La on Q. Using correlations of the type shown in equation 4.27, they obtain:

$$K^* = 0.105\ (P/Q)^{*0.59} . Sc^{0.3} \qquad (4.35)$$

which gives: $$k_La \propto P^{0.59} . Q^{0.41} . \mu^{-0.69} \qquad (4.36)$$

for CMC solutions agitated by a disc turbine. This shows a higher dependence on the viscosity than previously reported by other workers. Similar results were obtained for a disc turbine in glucose solutions with k_La values reduced due to reduced diffusivity when compared to CMC solutions of the same viscosity. In 0.75% CMC and in water they found little

difference between a disc impeller, a disc turbine, and two sizes of MIG agitator. In PAA solutions an additional effect of impeller speed was found which prevented $(P/Q)^*$ correlating the data for the disc impeller or the disc turbine. This impeller speed dependence increased with increasing PAA concentration, indicating that the effect was due to the increasing viscoelasticity found in these solutions compared to CMC solutions. In contrast the MIG agitators were able to correlate the data for various gas flow rates and power inputs in the PAA solutions, giving a regression line which fell in the middle of the data collected for disc turbines, which was in turn comparable with that collected in CMC.

Hocker et al.[43] also investigated different gas distributor types, to assess their effects on $k_L a$. Using a point sparger, a ring sparger, a three ring sparger and sintered elements, in a 1.5% CMC solution, ($K = 1.5$ Pa.s^n, $n = 0.67$), agitated using a disc turbine, they found a slight improvement on increasing the area over which gas entered the vessel. When using a MIG agitator a large improvement in $k_L a$ was found with increasing area of gas distribution, particularly at low power inputs.

In a study of mass transfer using a dynamic gassing out technique, Henzler[132] incorporated the data of Yagi and Yoshida[49], Hocker et al.[43] and Kipke[114], which has already been described. For disc turbines ($D = 0.25T - 0.33T$) in vessels of $T/H_1 = 1$ he obtains:

$$K^* = c_1 \, (P/Q)^{*c_2} . \, Sc^{-c_3} \qquad (4.37)$$

Where $c_1 = 0.045$, $c_2 = 0.5$ and $c_3 = 0.3$ for glucose and glycerol solutions, ($\mu = 0.001 - 0.2$ Pa.s). For the Millet Jelly solution of Yagi and Yoshida[49] he obtains: $c_1 = 0.0125$, $c_2 = 0.6$, $c_3 = 0.17$ ($\mu = 0.001 - 0.07$ Pa.s). For CMC solutions $c_1 = 0.082$, $c_2 = 0.6$, $c_3 = 0.3$ ($\mu_a = 0.016 - 1.5$ Pa.s), although the data of Kipke[114] shows considerable scatter around this correlation line. For PAA solutions no such correlation could be

developed, due to the effects of viscoelasticity, which were particularly pronounced when using large diameter impellers, D > 0.4 T. In general the data obtained in PAA solutions was scattered around the correlation produced for the CMC solutions.

Few papers have been published describing mass transfer into rheologically complex liquids on the industrial or pilot plant scale. In general insufficient data regarding the rheological properties and process variables of interest is given, thus information regarding the applicability of the correlations developed using smaller scale data is scant. Paca et al.[134] studied mass transfer in a vessel of 0.17 m^3 liquid volume, with $H_l/T = 1.7$. Three disc turbines ($D = \frac{1}{3} T$) were used at a spacing of 1.3 D. They found that k_La was highly dependent on P/V and Q in pure water, although the addition of antifoam (sperm whale oil), reduced k_La and the dependence of k_La on P/V and Q. In colloidal starch solutions of μ = 0.02 Pa.s and μ = 0.05 Pa.s, chosen to model an erythromycin fermentation, k_La was reduced by increasing viscosity, particularly at low agitator power inputs, where a large dependence on Q was observed. At higher power inputs the dependence of k_La on P/V was reduced compared with that found in water, particularly in the intermediate viscosity solution. In media used in the production of erythromycin, the complex, ill-defined formulation leads to foam production and a complex interaction between the constituents and the resultant k_La values produced. During actual fermentations it was found that the yield of erythromycin finally obtained was directly related to the agitator power input used during the growth of an inoculum culture, which was then used to seed a production fermenter.

Jurecic et al.[135] measured k_La values during an antibiotic fermentation process on a pilot and production scale with liquid volumes of 0.1 m^3

(T = 0.41 m, H_1 = 0.86 m) and 67.5 m^3 (T = 3.3 m, $H_1 \cong$ 8 m). Two disc turbines fitted with four curved blades (D = 0.22 m) were used in the pilot vessel, whilst four disc turbines fitted with six flat blades (D = 1.1 m) were used in the larger vessel. The fermentation medium which contained up to 20% by volume of solids including biomass, was distinctly shear thinning, although not highly viscous; with power law parameters: n = 0.678 and K = 0.0139 Pa.s^n, at the time when the k_La values were measured using an unsteady state technique. In order to correlate the results produced using the parameters proposed by Zlokarnik[73] (see previous section), they divided the volume of the liquid by the number of impellers within the vessel and determined the power input of the top and bottom impellers separately. This gave overall for both sizes of vessel:

$$K^* = 0.30 \ (P/Q)^{*0.35} . Sc^{-0.3} . (\sigma / \sigma_w)^{-0.5} \quad (4.37)$$

Where σ is the surface tension of the solution used and σ_w is the surface tension of water. Close examination of the separate k_La values in the top and bottom regions of the production scale vessel reveals a higher dependence of k_La on P/V in the bottom region than is found in the top region. In addition k_La was independent of Q near the bottom impeller, although k_La was highly dependent on Q near the top impeller. From this they surmise that the upper impellers act merely to circulate the liquid and the gas bubbles, whilst the lower impeller disperses all the gas. Thus the upper regions behave in a similar manner to a bubble column, with gentle stirring. Overall, extrapolation of the pilot plant data to the larger scale resulted in k_La being underestimated slightly.

4.7) Conclusions Regarding the Mass Transfer Results Available in the Literature for Viscous/Non-Newtonian Solutions

It is not possible to make a direct comparison of the k_La values obtained by the various authors without some knowledge of the agitation rate, power input, gas flow rate and rheological properties used. These are rarely given in full, however the overall trends can be compared. Of greatest interest are the effects which varying power input, apparent viscosity and air flow rate have on k_La and also the effect of visco-elasticity. These are compiled for the different small scale studies in table 4.1. In general the effect of varying power consumption is found to be approximately the same for all the solutions studied, i.e. $k_La \propto P^{\beta}$ where $0.5 < \beta < 0.7$. The values of β can be gauged from the studies which only quote the impeller speed dependence, by assuming that $P \propto N^3$, which can be derived from the power number - Reynolds number relationship in both the turbulent and transitional regimes: i.e. Po_g is constant and $P = Po_g \rho N^3 D^5$ (from equation 3.9). All the studies except one predict that k_La is dependent on the gas flow rate for all conditions of rheology. In general the effect is reduced at higher viscosities, as reported by Kipke[114] but this is not shown in the correlations presented by the various authors.

That Ranade and Ulbrecht[30] find no dependence of k_La on Q is surprising, particularly as the viscosity of the solutions used is very low. However this may be related to the method of measurement used, which required the addition of salts to their polymer solutions, which in general would be expected to reduce the effect of altering gas flow rate[71]. Most of the other authors use a dynamic gassing out technique to measure k_La values. These can also be subject to error as outlined in the earlier sections of this chapter. In particular the gross dependency of k_La on the operational variables may be distorted due to the errors inherent in the use of these techniques, as described in

Chapter 8, section 5.

The dependence of k_La on viscosity can be adequately described by $k_La \propto \mu_a^{-m}$ where $0.4 < m < 0.7$ for the majority of the studies carried out. It is interesting to note that the low values of m are obtained for the correlations which use Sh', Re, De, etc., whilst those which use the correlation proposed by Zlokarnik[73] obtain higher values of m. Particularly worthy of examination is the values of m quoted for Millet Jelly. The original work was carried out by Yagi and Yoshida[49], Henzler[132] merely reinterpreted their results and obtained a higher value for m.

Shear thinning behaviour has not been seen to affect the k_La values obtained when compared to Newtonian behaviour. However increasing viscoelasticity has had an effect, reducing k_La according to Yagi and Yoshida[49] and Ranade and Ulbrecht[30]. This however is probably a consequence of their correlating method, as they do not account for the effect of the lowered power consumption seen in aerated viscoelastic fluids (see Chapter 3). k_La is affected in viscoelastic PAA solutions, according to Hocker et al.[43], but the effect depends upon the impeller speed and type, with k_La values higher and lower than those in CMC, for a range of power consumptions, depending on the agitation speed required.

The studies reported do show similar k_La values under similar conditions, supported by the global correlation carried out by Henzler[132] which covered most of the work of any significance. One can expect that increases in viscosity and non-Newtonian behaviour will drastically reduce mass transfer coefficients when compared to water, requiring higher impeller speeds and increased power consumption to maintain reasonable levels of mass transfer.

A comparison of the literature data with the results obtained in this study is contained in Chapter 8, section 5, where some of the results contained in the literature are presented diagramatically.

CHAPTER 5

EQUIPMENT EMPLOYED

This chapter has been divided into three sections, each covering a different area of the work carried out. The first describes the equipment used in the main study of mass transfer, mixing and power consumption. The second describes the rheometers used to determine the viscous and viscoelastic properties of the liquids studied and the third section describes the equipment used in the measurement of the oxygen solubility within the liquids. The methods used in these experiments are described in Chapter 6.

5.1) Equipment Used in Mass Transfer, Mixing and Power Consumption Studies

5.1.1) Vessels Used

Two vessels were used, a 5 litre capacity vessel and a 20 litre capacity vessel. The smaller vessel was used in the initial study of mass transfer carried out to determine the feasibility of the method. From the lessons learnt in those studies the 20 litre vessel and its ancillary equipment was designed and chosen. The dimensions of these two vessels are shown in table 5.1.

The 5 litre vessel is shown in figure 5.1. It consisted of a QVF glass pipe section of internal diameter, T = 0.16 m. It was fitted with stainless steel end plates. For a liquid height of 0.17 m the liquid volume, V was 3×10^{-3} m^3, although a liquid height of 0.227 m was also used, giving V = 4×10^{-3} m^3. Four equally spaced baffles were fitted of width 0.015 m; in addition several threaded holes in the top plate were used to fit a dissolved oxygen electrode, a mercury manometer, a thermometer and a resistance thermometer. The resistance thermometer provided a signal for the temperature control unit and recorder. Temperature control was achieved using heating rods fitted

Table 5.1 Dimensions of Vessels Used in This Work

	5 litre Vessel	20 litre Vessel
Overall Internal Height	0.300 m	0.400 m
Overall Internal Width : T	0.160 m	0.300 m
Liquid Height : H_l	0.170 - 0.227 m	0.300 m (= T)
Working Volume : V	3 - 4 litres	20 litres
Baffle Width	0.015 m	0.030 m
Shaft Diameter	0.015 m	0.019 m
Sparger Type	pipe	ring & pipe
Material	glass & st.st.	perspex & st.st.
Impeller Type	8 bladed disc turbine	see text
Impeller Diameter	0.076 m	see table 5.2
Impeller Clearance : c	0.040 m	0.075 m (= T/4)
Impeller Separation : s	—	3T/8 or T/2

Figure 5.1

The 5 litre Vessel

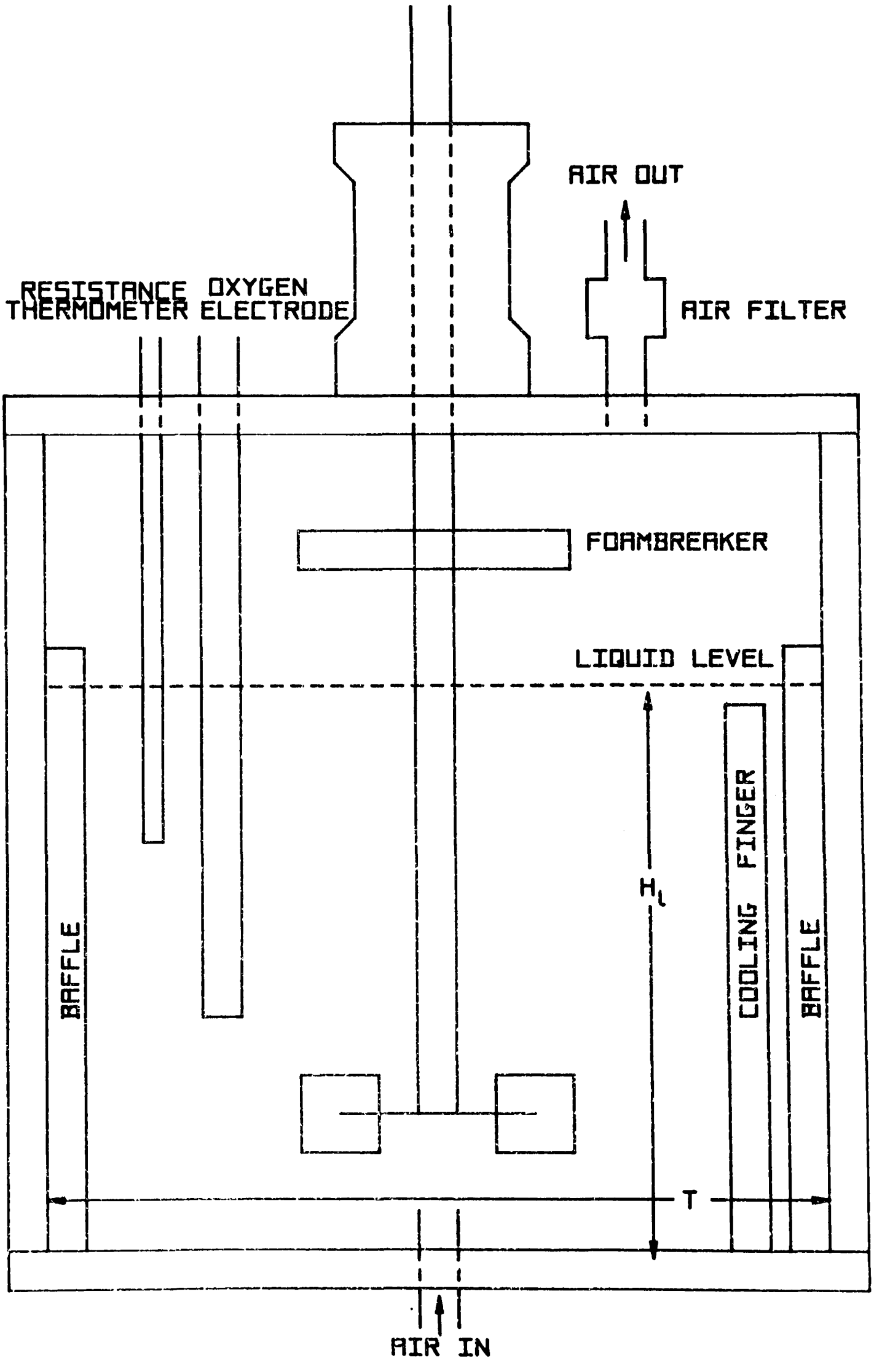

in the base plate of the vessel and a stainless steel cooling finger supplied with cold water from the mains. A 400 W d.c. motor fitted with a variable speed control was connected to the impeller shaft via a flexible coupling. The shaft entered the vessel through a bearing mounted on the top plate. In the air space above the liquid the shaft was fitted with a mechanical foam breaker, diameter 0.078 m, made according to the design of Kok and Zajic[136]. At a clearance from the base of the vessel of 0.04 m was fitted the 8 bladed disc turbine impeller (D = 0.076 m).

The 20 litre vessel, shown in figure 5.2 and plate 1 was constructed from a perspex tube internal diameter, T = 0.3 m, height 0.4 m mounted in a square perspex box width 0.4 m. The outer box acted as a water jacket for heating and cooling of the inner vessel and also aided distortion free observation of the inner vessel contents. The base of the vessel was made of a flat perspex sheet to enable visual observation of the vessel contents from beneath. For this purpose, the vessel was mounted in a frame 1.2 m above the floor (see plate 3). In the base of the vessel, a valve was fitted to enable the inner vessel to be drained and also for removal of liquid samples.

The top plate was constructed of stainless steel. This carried the impeller shaft bearing housing and various threaded holes for the probes etc. These consisted of: dissolved oxygen electrodes which could be positioned virtually anywhere in the vessel due to the multiplicity of holes available; a thermocouple to supply a signal for the temperature controller; the sparger tube which entered through the top plate at the back of the vessel close to the vessel wall; the exit gas line; a tapping for a mercury manometer and a narrow stainless steel tube inserted into the central region of the vessel, through which glucose was pumped. In the vessel four baffles were fitted of width 0.03 m (T/10), equally spaced around the peri-meter of the vessel. The impeller shaft entered through the top mounted bearing

Figure 5.2

The 20 litre Vessel

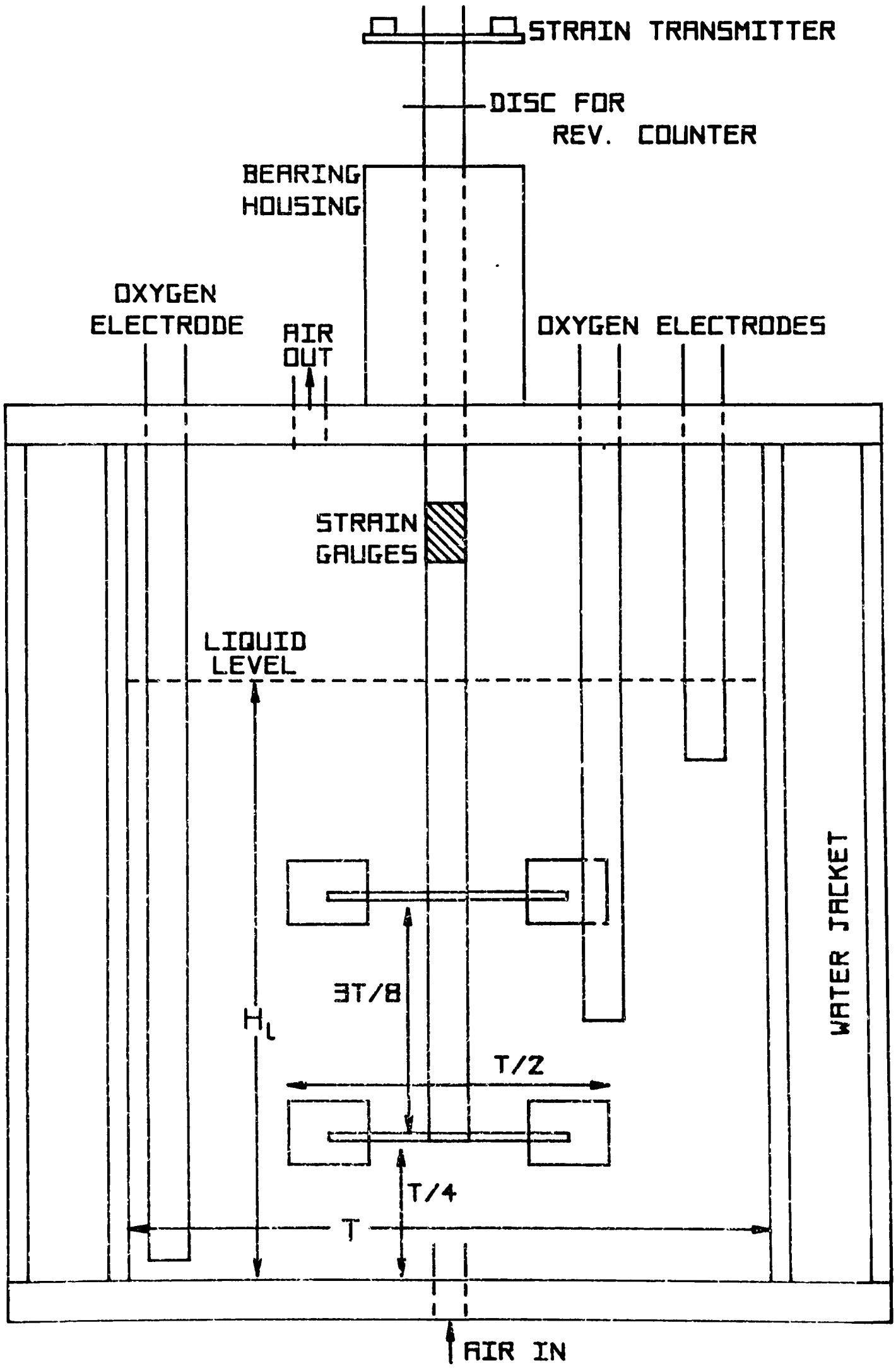

PLATE 1

THE 201 VESSEL

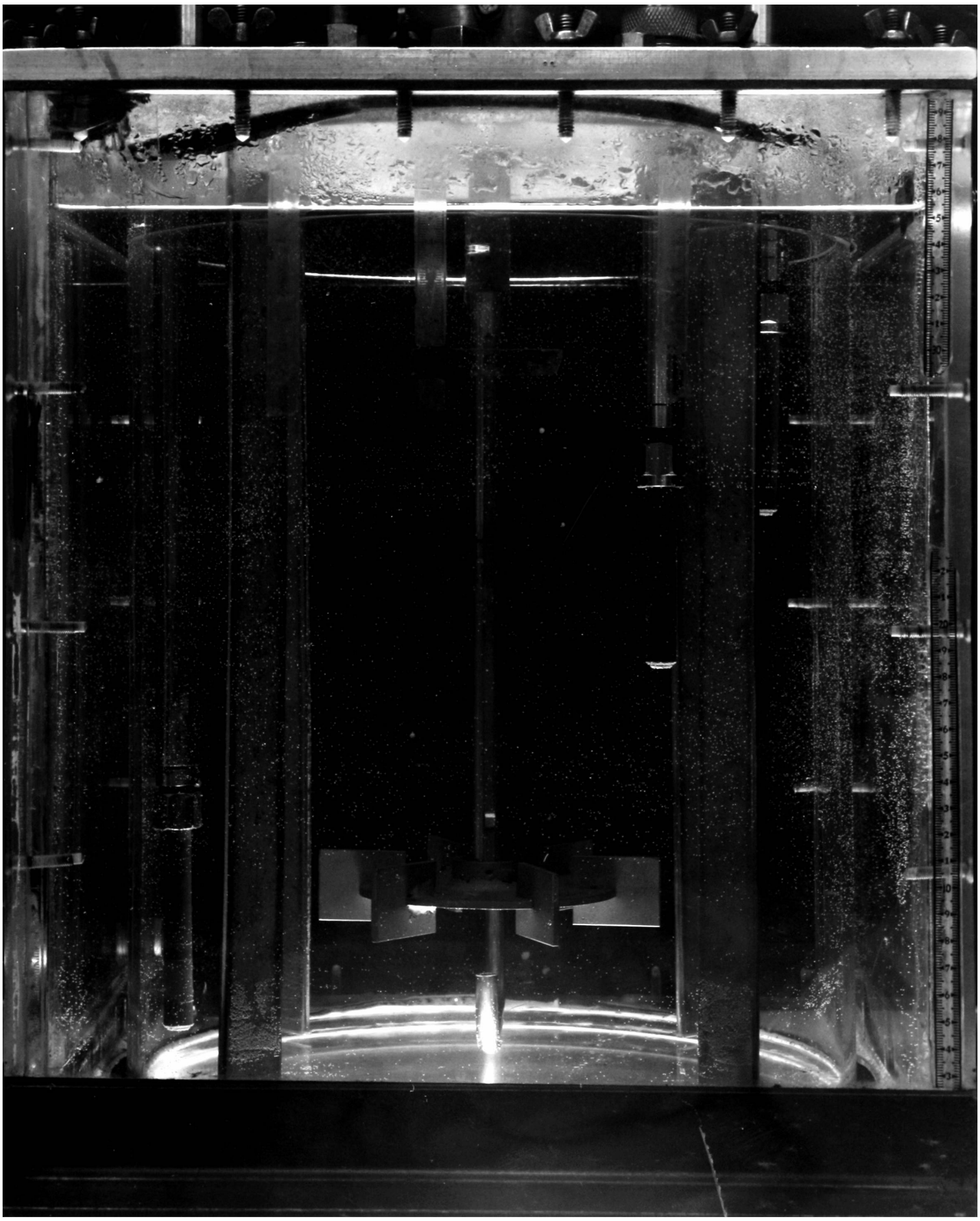

housing and was driven via a flexible coupling by a 1200 W reversible d.c. motor, fitted with a variable speed controller.

The rotational speed of the shaft was measured using a 60 hole disc mounted near the top of the impeller shaft outside the vessel. As it rotated, the holes allowed light to strike an infra-red optical switch. The pulses were electrically counted and displayed as revolutions per minute (digital readout) using a D.M.T2 Digital Modulator Tachometer supplied by Farnell Instruments Ltd. of Yorkshire, England. The range of impellers which were used in this vessel are described in the next section.

The gas was sparged into the vessel at the bottom of the liquid using either a pipe point sparger, i.e. a single hole (diameter 6 mm), centrally located beneath the impeller shaft, or a ring sparger of 0.125 m diameter, containing 16 equally spaced 0.5 mm holes, similarly located. The hold-up of gas within the liquid was measured by visual observation of the liquid height under aerated and unaerated conditions. The unaerated level was generally set at 0.3 m, equivalent to the diameter of the vessel. The aerated level was measured at three points, behind and in front of the baffles and in the centre of the vessel. In practice these three readings were very similar in the more viscous liquids used, except at the highest impeller speeds. Where the levels varied substantially an average value, estimated at the time of observation was used.

Heating and cooling of the vessel contents was achieved by pumping hot or cold water through the water jacket under the control of a T350 temperature control unit supplied by Thermocouple Instruments Ltd. of Cardiff, Wales. This was connected to the thermocouple placed within the inner vessel and could adequately control the temperature to within 1 °C. It was found that more precise and stable temperature control, with less rapid oscillations about a mean value could be obtained by manually controlling the temperature and the flow rate of the water

through the outer jacket. This was particularly the case where mass transfer experiments were being carried out. Under these circumstances different impeller speeds were in use for short periods of time, altering the heat load which had to be removed. This could be anticipated and the outer jacket filled with cold or warm water as required prior to altering the impeller speed.

5.1.2) Impellers Used in the 20 litre Vessel

These are shown in plate 2 and figures 5.3 - 5.5, with the dimensions in table 5.2. Six bladed disc turbines of Rushton dimensions in two diameters were used (D = T/3 and D = T/2) either singly, or in pairs of the same diameter. The lower impeller was always mounted at a clearance of 0.075 m (c = T/4) from the base of the vessel. Where used the second turbine was mounted 0.112 m above the first, a separation of s = 3T/8. When using the larger disc turbine (D= T/2), the upper turbine was replaced in some experiments with a 45° pitched blade turbine of the same diameter and at the same separation. Two Intermig impellers, diameter 0.174 m, (D = 0.58T) were also used. These impellers consisted of two large blades fitted to the central hub at an angle to the vertical, with two pairs of small blades mounted at the end of each large blade at an angle to the large blade, as is shown in figure 5.5. Thus the outer blades tended to pump the liquid in the opposite vertical direction to that achieved by the inner blades. As the motor was reversible both directions of pumping could be easily investigated. The two Intermigs were identical, so they both pumped in the same direction. They were mounted at an angle of 90° to each other, when viewed along the axis of the shaft, at a separation of 0.15 m, s = T/2. The clearance of the lower impeller was as cited above for the turbine impellers. A ring sparger was used in conjunction with the Intermigs in some cases, as the lack of a disc allowed the gas to rise through the liquid without interacting

Table 5.2

Dimensions of Impellers Used in the 20 litre Vessel

Impellers	Diameter D mm	D/T	Blade Dimensions Vertical height mm	Width mm	Thickness mm	Disc Dimensions Diameter	Thickness	Blade Angle to vertical	No. of Blades
Disc Turbine:									
large	150	½	29	38	3	111	3	—	6
small	100	⅓	20	25	3	75	3	—	6
Pitched Blade Turbine	150	½	30	56	3	NO DISC		45°	6
Intermig	174	.58				NO DISC			
inner blades			34	26	2			+55°	2
outer blades			11	48	2			-60°	8

DISC TURBINE

PITCHED BLADE TURBINE

INTERMIG

PLATE 2 IMPELLERS USED IN THE 20 l. VESSEL

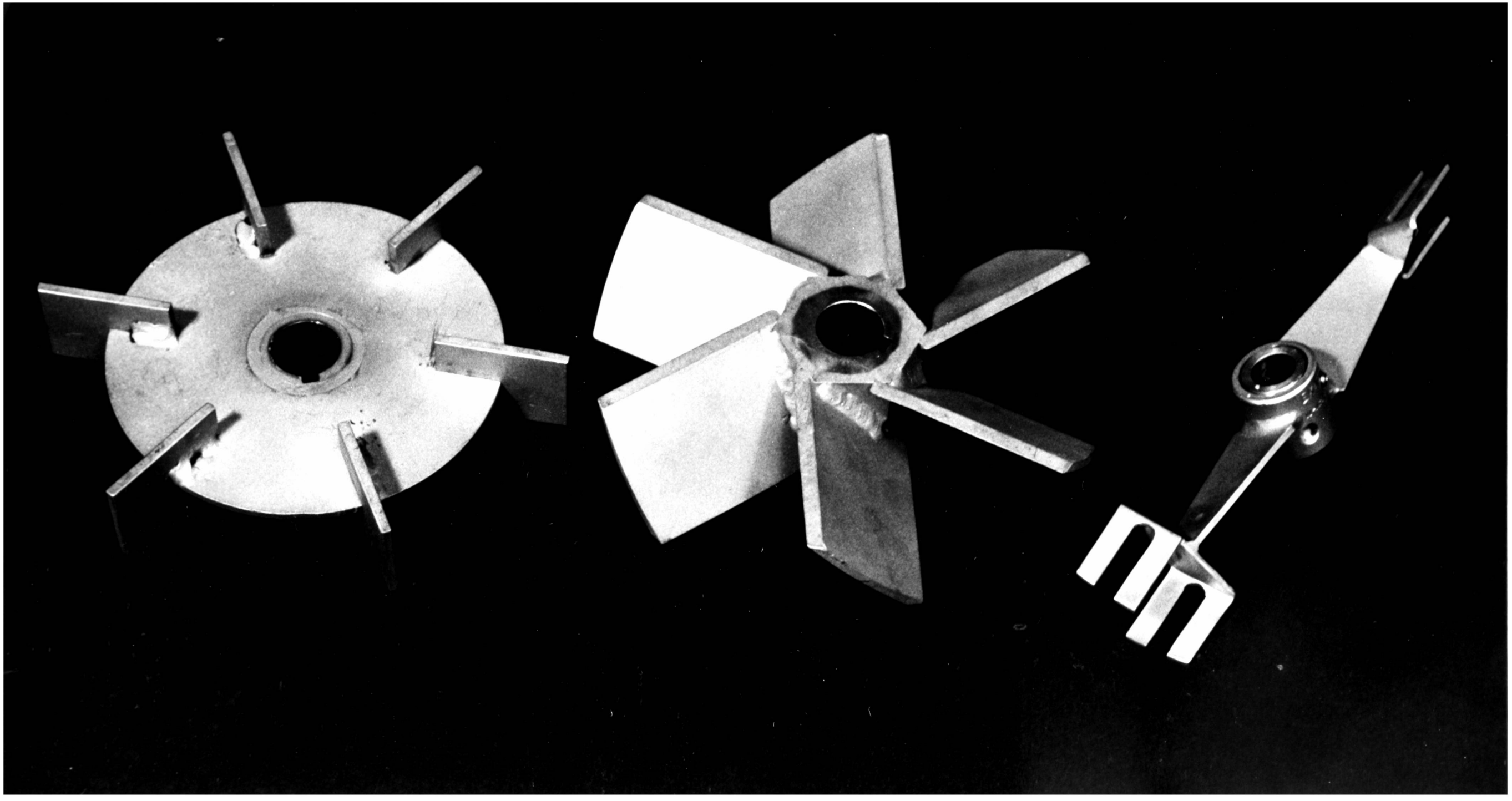

Figure 5.3 Disc Turbine

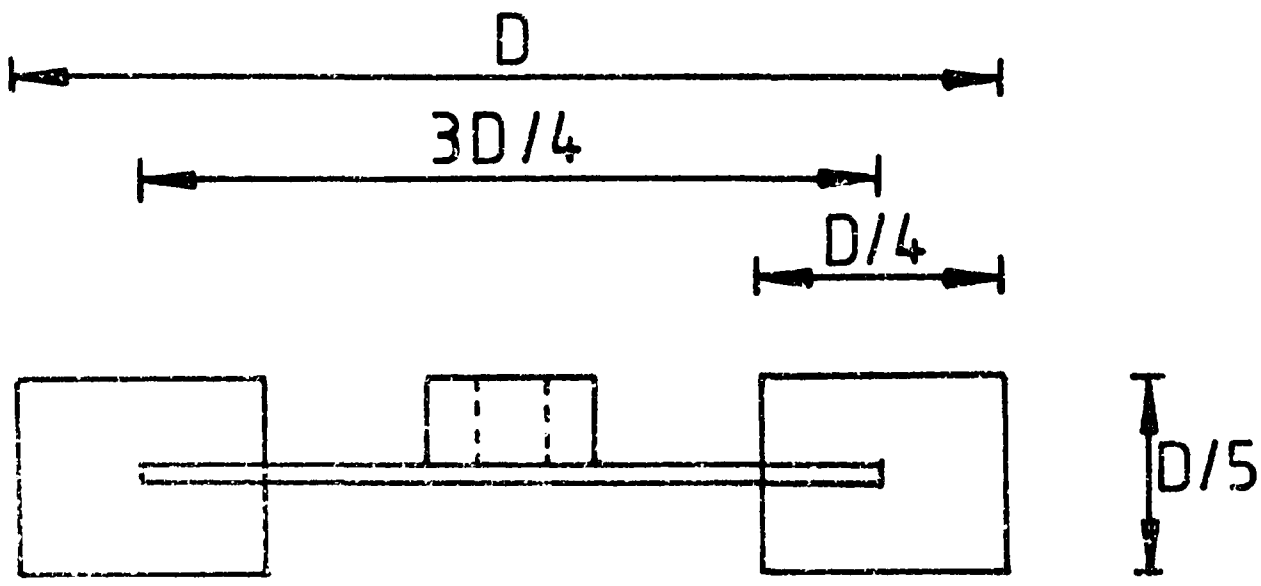

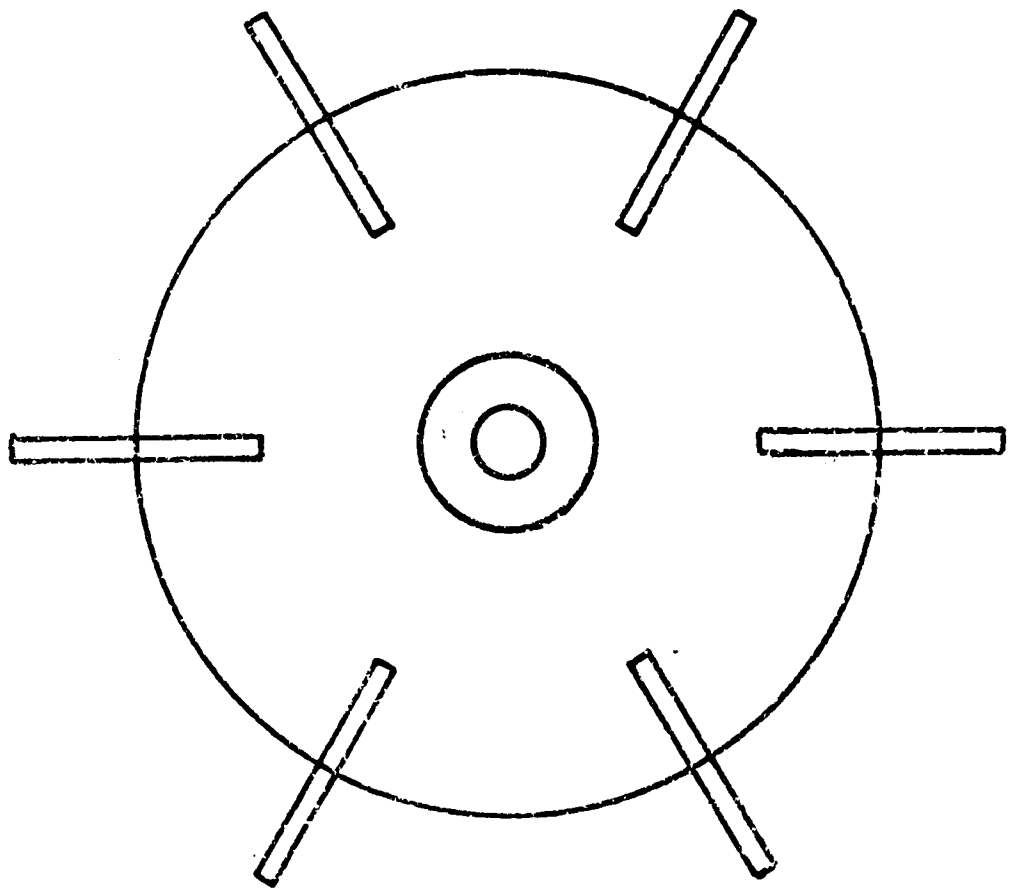

Figure 5.4 Pitched Blade Turbine

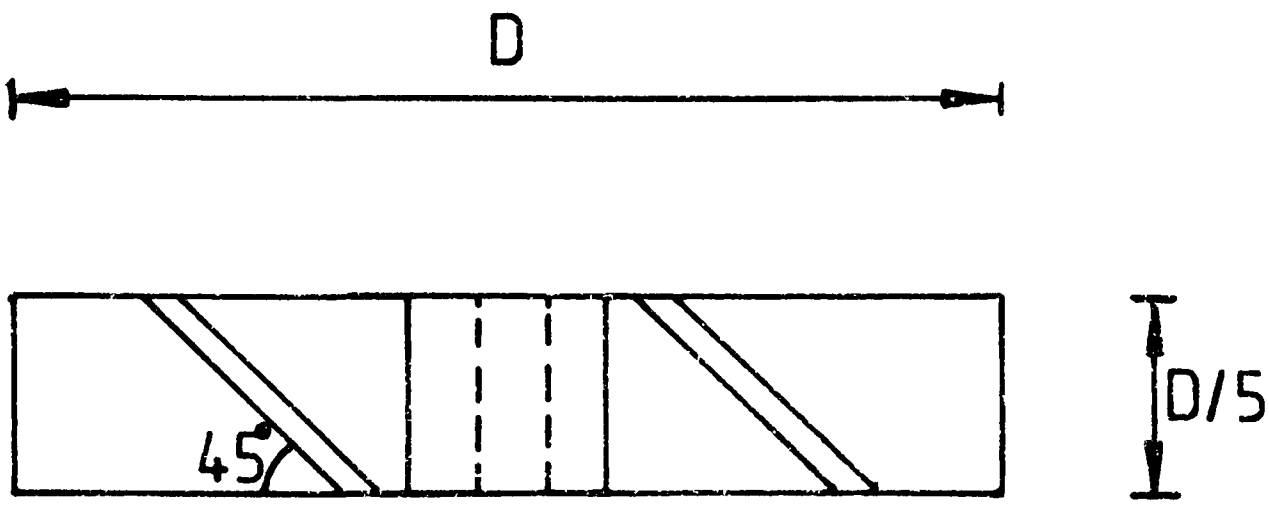

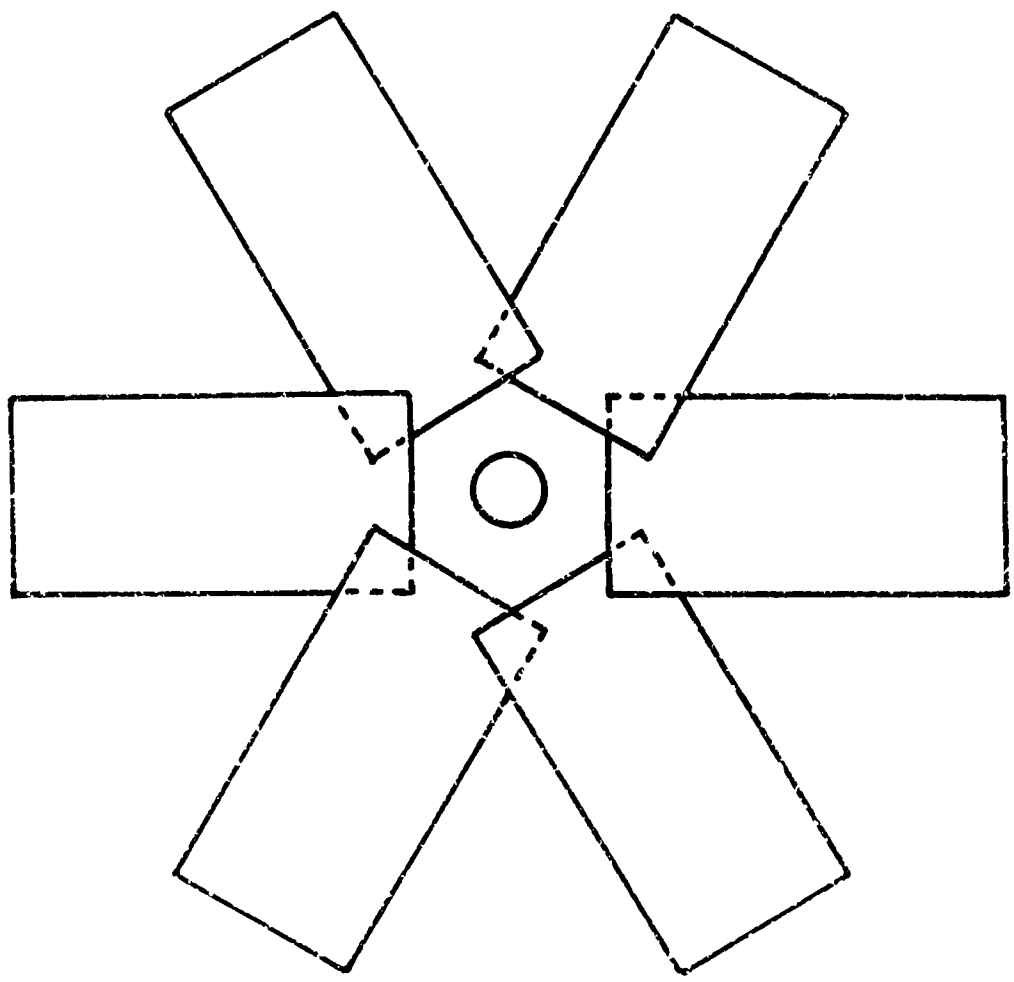

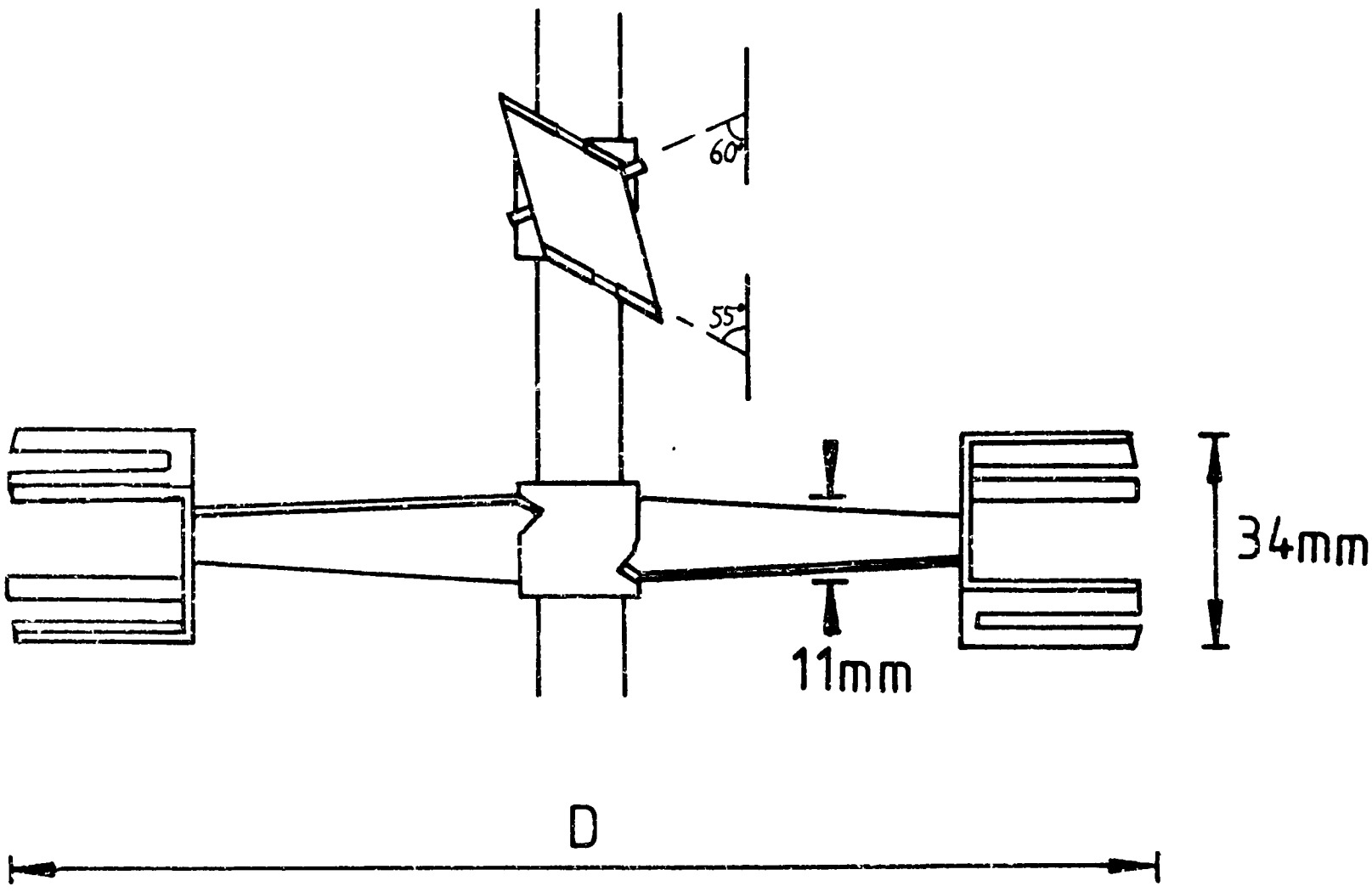

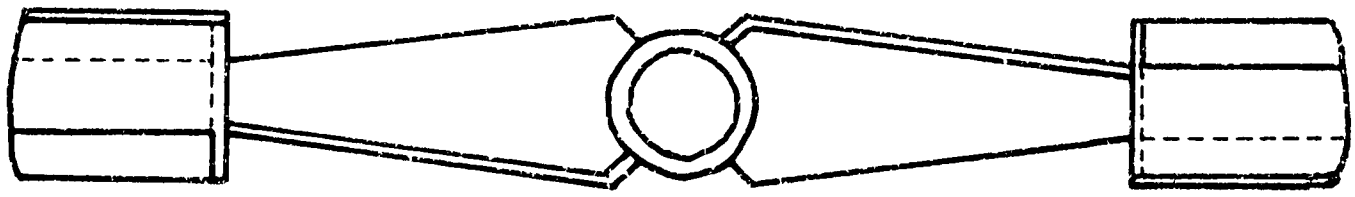

Figure 5.5 Intermig Impeller

with the tips of the blades under some circumstances, as described in Chapter 7.

5.1.3) Measurement of Power Consumption

Fitted to the impeller shaft, above the level of the liquid, were the strain gauges used in the measurement of the torque on the impeller shaft. A full bridge of two pairs of gauges was used, mounted on opposite sides of the shaft. The wires for these ran up the inside of the hollow shaft to the transmitter unit mounted outside the vessel at the top of the impeller shaft. This unit, model TX3A provided a signal which was picked up and fed to a I08B indicator unit, both supplied by Astech Electronics Ltd. of Surrey, England. The output, which was directly proportional to the torque on the shaft, was monitored on a Servoscribe chart recorder. The readings on the recorder, using ranges of 20 mV - 5 V, were calibrated using known weights of 5 g to 10 kg, hung on the tip of an impeller fixed to the shaft, which was in turn held in a horizontal position and prevented from rotating. The torque could be calculated by multiplying the weight by the distance of the impeller tip from the centre of the shaft by the gravitational constant, g. In this way torques, in the range 3.7×10^{-3} - 3.7 N.m could be measured. The power consumed, P, is given by:

$$P = 2\pi tN \qquad (5.1)$$

Where t is the torque and N is the impeller speed in revolutions per second.

5.1.4) Equipment for Gas Stream Flow Measurement and Compositional Analysis

Figure 5.6 shows schematically the layout of the equipment used to measure the volume flow rates and composition of the inlet and exit gas streams. In general the same equipment was used for both the 5 litre and

Figure 5.6

Schematic Diagrams of Gas Streams.

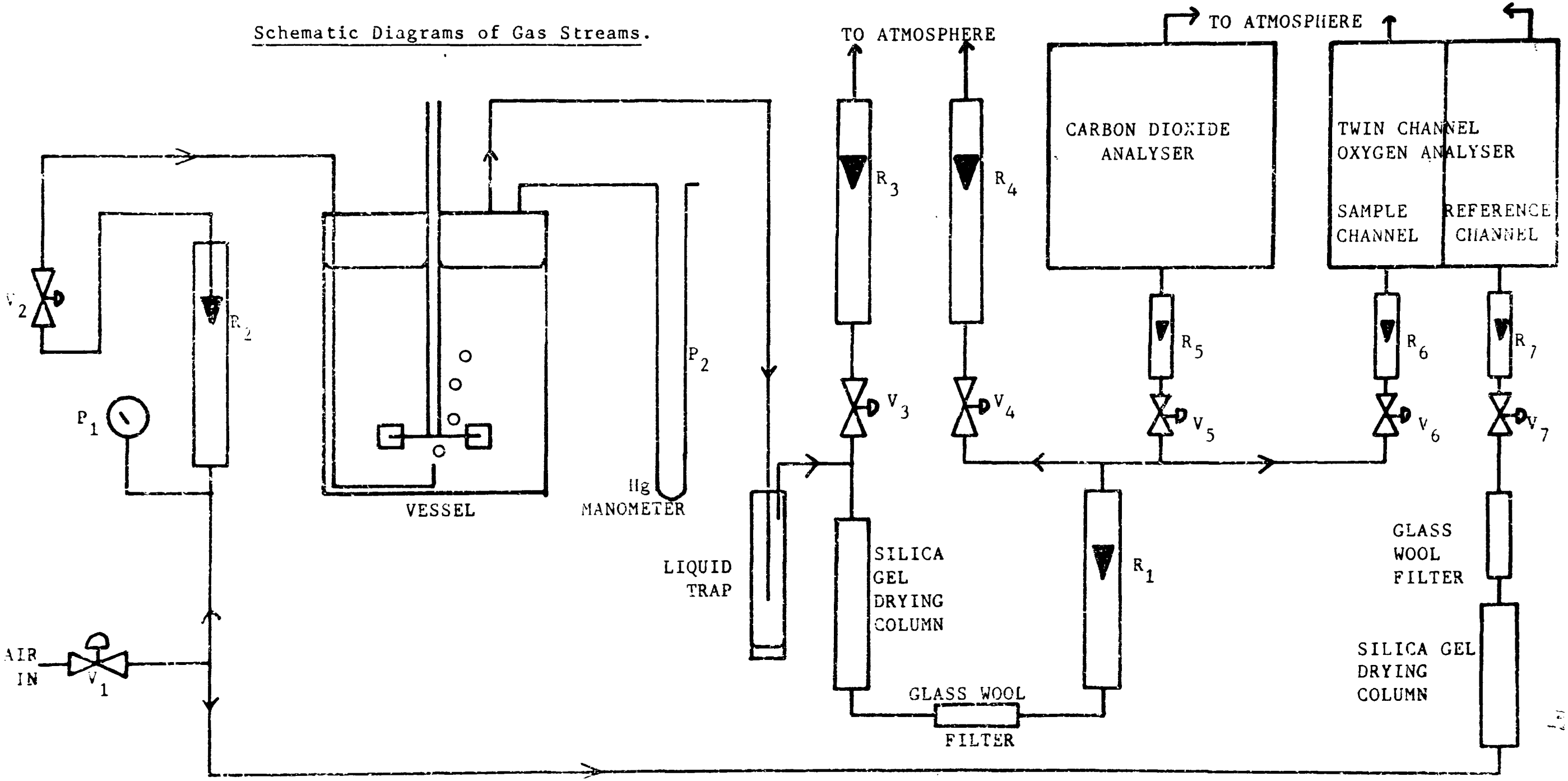

Legend for Figure 5.6

V_1 : Regulating valve used to set pressure on gauge P_1 and in inlet rotameter R_2

V_2 : Regulating valve used to set inlet air flow rate measured by rotameter R_2

V_3 : Regulating valve used to set pressure in the vessel as measured on the mercury manometer P_2

V_4 : Used to regulate flow through the drying column, measured on R_1 and R_4

V_5 : Used to regulate flow through the carbon dioxide analyser, measured on R_5

V_6 : Used to regulate flow through sample channel of the oxygen analyser, measured on R_6

V_7 : Used to regulate flow through the reference channel of the oxygen analyser, measured on R_7

Typical Flow Rates and Pressures Used

P_1 : 10 psi above atmospheric pressure

P_2 : 150 mm Hg above atmospheric pressure

R_2 : 5 - 40 $l.min^{-1}$

R_3 : 3 - 38 $l.min^{-1}$

R_1 : 2 $l.min^{-1}$

R_4 : 1.8 $l.min^{-1}$

R_5, R_6 and R_7 : 100 $ml.min^{-1}$

20 litre vessels. The air supply from the compressor of 70 psig. was regulated to 10 psig. in the inlet rotameter which was calibrated using a dry gas meter. The inlet flow rate was controlled by a valve mounted on the exit from the rotameter before passing through the sparger into the vessel. The exit gas stream from the vessel was passed through a trap to remove any water droplets, before being split into two streams. The first stream of 2 $l.min^{-1}$ was further treated and analysed. The second stream which was the residue, passed through a valve which was used to regulate the pressure in the vessel and a rotameter to measure its flow rate. It then passed into the atmosphere. The first gas stream was dried in a silica gel column, passed through a glass wool filter to remove any particles and then through a rotameter to measure its flow rate. This stream was then split into three separate streams. The first part, flow rate 100 $ml.min^{-1}$, passed through a regulating valve and rotameter, then through the carbon dioxide analyser and into the atmosphere. The second part, flow rate 100 $ml.min^{-1}$, passed via a regulating valve and rotameter through the sample channel of the oxygen analyser and then into the atmosphere. The third part consisting of the remainder of the 2 $l.min^{-1}$ passed via a regulating valve and rotameter straight into the atmosphere.

In addition a sample of the inlet gas stream was split off just before the inlet rotameter. This passed through a silica gel drying column, regulating valve and a rotameter, at a flow rate of 100 $ml.min^{-1}$. Then it was passed through the reference channel of the oxygen analyser into the atmosphere. Provision was also made to switch the gas streams to the analysers, enabling the calibration gases, nitrogen and carbon dioxide/air mixture (5%/95%) to be passed through the analysers whilst the sample gases were diverted into the atmosphere. This was accomplished using zero dead volume 3-way glass valves and is not shown in figure 5.6.

Plate 3 shows the oxygen analyser and the measuring section of the carbon dioxide analyser, in addition to the main 20 litre vessel. The gas analysers used were as follows:

a) Carbon Dioxide Analyser

An Infra-Red Process Stream Analyser, Model PSA401, supplied by Feedback Instruments Ltd. of Crowborough, Sussex, England was used. Its operation relies on the fact that carbon dioxide absorbs energy in the infra-red region of the spectrum. Using narrow bandwidth filters (2%), selected by means of an interference filter, it measures the absorption of the sample flow cell (length 0.012 m) at a sample wavelength (4.28 μm), relative to that at a reference wavelength (3.95 μm). The electronic circuitry extracts a signal which is proportional to $(I_r - I_s)/(I_r + I_s)$. Where I_s and I_r are the measured intensities at the sample and reference wavelengths respectively. This is a good approximation to $\log_e(I_r/I_s)$ which the Beer-Lambert law states is proportional to the concentration of the absorbing species. Further circuits then linearise the output and convert it to read % CO_2 on the instrument meter. The output reading is dependent on temperature variations and pressure variations, as these will alter the absolute concentration in the flow cell. The temperature of the flow cell is controlled to a constant 45°C, but variations in atmospheric pressure alter the output reading of the analyser,requiring frequent recalibration.

A 0 - 10 mA output, for 0 - 10% carbon dioxide, was provided in this instrument. This was used to provide a 0 - 10 mV output for 0 - 5% carbon dioxide by connecting an appropriate resistor across the output. This voltage signal was then fed to one channel of a 3 channel chart recorder, model 320, supplied by Chessel Ltd. of Worthing, Sussex, England.

b) Oxygen Analyser

An oxygen analyser type OA.184 supplied by Taylor Servomex Ltd. of Crowborough, Sussex, England was used. This consisted of two separate

PLATE 3 THE 20 l. VESSEL AND GAS ANALYSIS EQUIPMENT

O_2

ANALYSER

CO_2

ANALYSER

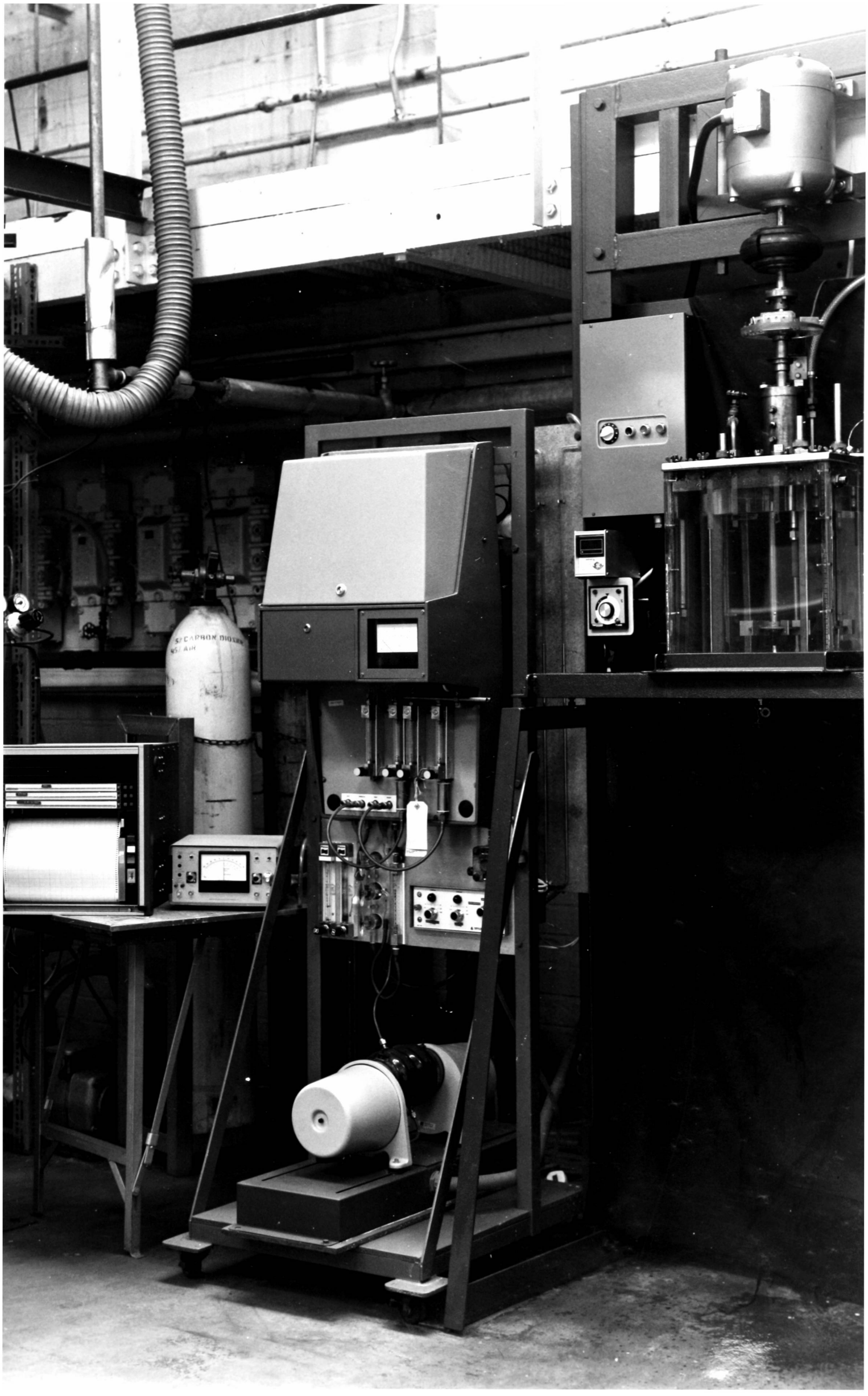
5% CARBON DIOXIDE
95% AIR

oxygen analysers mounted in a common case. Their operation relies upon the paramagnetic properties of oxygen. Oxygen passing through a magnetic field alters that field and affects the position of a diamagnetic dumb-bell supported in the field. The torque acting on the dumb-bell is proportional to the partial pressure of oxygen in the surrounding gas. This torque is measured using a feedback system to restore the position of the dumb-bell, the current required being proportional to the torque. Accurate calibration of the full range of oxygen concentrations is possible using just two point concentrations, in this case 0% and 20% oxygen concentrations provided by nitrogen gas and a carbon dioxide/ air mixture (5%/95%).

As with the carbon dioxide analyser, temperature and pressure variations will affect the reading obtained by altering the partial pressure of oxygen in the flow cells. The temperature within the analyser is regulated to 45°C and because two channels are used, the effect of pressure variations is reduced by using the difference signal between the two. Nevertheless frequent calibration was carried out as the instrument was generally used in its most sensitive range (see below). The difference reading was obtained using a RB276 Difference Unit supplied by Taylor Servomex. This box of electronic circuits subtracted the output of the sample channel from that of the reference channel giving an output which was the difference of tne two. The ranges of outputs available were 0 to 1, 2.5, 5, 25, or 100% enabling oxygen concentration differences to be read on the Chessel chart recorder to accuracies of better than 0.01% for a difference of less than 1%, providing careful calibration was maintained.

5.1.4) Other Equipment Used in Mass Transfer Experiments

a) Dissolved Oxygen Electrodes

Several types of dissolved electrodes were tested for their

suitability for use under the conditions imposed during this work. The requirements were an electrode which could sense the temperature, adjusting its output accordingly, which was also insensitive to changes in the velocity of the liquid around the probe tip. The most suitable electrode found was the Schott Gerate Digital Oxygen Meter and Probe, model number CG867, supplied by Camlab Ltd. of Cambridge, England. These electrodes functioned polarographically, according to the Clark principle[99]; that is they use an electrolytic cell to which a polarising voltage of 800 mV is applied. The cathode is platinum and the anode silver, so oxygen molecules present in the cell are reduced to OH^- ions at the cathode. This produces a current, which is proportional to the oxygen concentration within the cell. The oxygen concentration within the cell is limited by the rate of diffusion across the membrane which separates the electrolyte of the cell from the sample solution. This membrane is made of 25 μm PTFE film and allows only small molecules, such as gases, but not ions to pass across. The rate of diffusion across the membrane is controlled by the dissolved oxygen activity within the sample solution, not the absolute concentration of oxygen in the sample solution (see Chapter 4, section 4). Thus the output of the probe should be independent of the solution characteristics, depending only on the temperature and pressure of the oxygen in the solution. Calibration at zero and full scale deflection was necessary as a residual current always flowed in the electrolytic cell, even when no oxygen was present. For the calibration method used, see Chapter 6.

Three dissolved oxygen electrodes and their associated meters were used. The first or primary electrode, which was connected to the Chessel chart recorder, was placed near to the impeller or impellers to give a high flow of liquid across the tip. This reduced the impeller speed dependency of the electrode and prevented bubbles adhering to the probe tip and altering the reading. The other two electrodes were positioned

in the remote areas of the vessel, in regions of reduced liquid flow. The tip of one was placed in the bottom corner, between two baffles, approximately 1 - 2 cm from the base of the vessel. The other was placed with its tip 3 - 5 cm below the liquid surface near the edge of the vessel between two baffles, figure 5.7 shows these positions. The exact position of the primary electrode in the main body of the tank was determined by the impellers in use. Care was taken to ensure that the electrode was not in the main discharge stream of the impeller, as this would subject it to a high liquid velocity, unrepresentative of the vessel as a whole. When using two impellers the tip was placed just below the mid-point of the two, as can be seen in figure 5.2. For one impeller the probe tip was placed ca. 1 - 2 cm above the impeller, as can be seen in figure 5.7. In both cases the tip was between 30 and 50 mm from the impeller tip in a horizontal direction. It was the output of this middle electrode which was continuously recorded and used to determine $k_L a$ values. The readouts of the other electrodes were used for comparison purposes (see Chapter 7, section 4).

b) Glucose Pump

During the mass transfer experiments, glucose was continuously supplied using a DCL metering pump. This constant displacement pump could be used at flow rates of 0 - 0.16 $l.hr^{-1}$, giving 0 - 80 $g.hr^{-1}$ of glucose for a 500 $g.l^{-1}$ solution. In general the flow rate was maintained at 11 $g.hr^{-1}$ of glucose for the majority of the experiments carried out (see Chapter 6).

c) Chart Recorders

The oxygen analyser, carbon dioxide analyser and dissolved oxygen meter outputs were all connected to a Chessel chart recorder, model 320 supplied by Chessel Ltd. of Worthing, Sussex, England. This utilised three inputs of 0 - 10 mV, recorded by three separate pens, each capable of using the full width of the chart paper. Chart speeds of 6 $cm.min^{-1}$

Figure 5.7

Schematic Representation of the 20 litre Vessel, Showing the Positioning of the Dissolved Oxygen Electrodes, When Using One Disc Turbine.

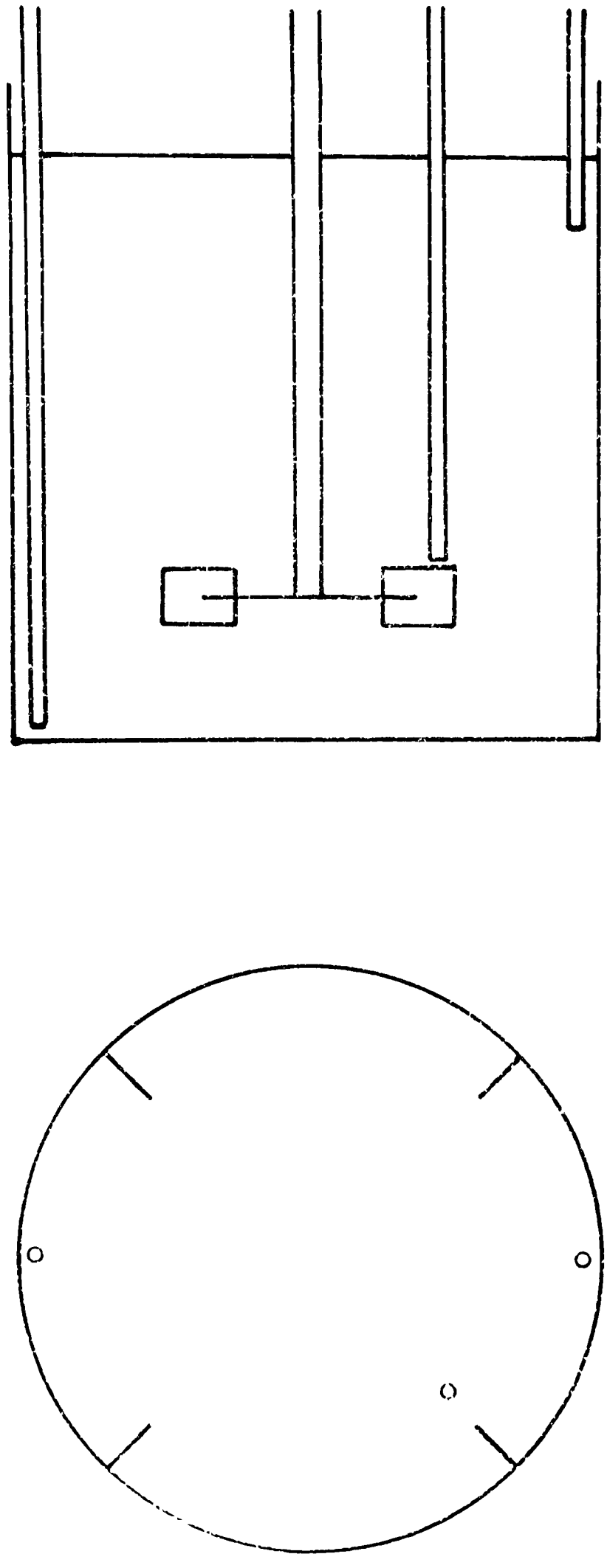

to 1 $cm.hr^{-1}$ were available. With long term experiments (up to three days) monitored at 2 $cm.hr^{-1}$ and shorter term experiments monitored at 6 $cm.hr^{-1}$.

The output of the torque measuring equipment was connected to a Servoscribe single pen recorder using ranges of 20 mV - 5V fsd. and a chart speed of 1 - 12 $cm.hr^{-1}$, depending on the duration of the experiment.

5.2) Equipment Used in the Measurement of Rheological Properties

Each of the three systems used is outlined in table 5.3, with a more complete description given here.

5.2.1) Weissenberg Rheogoniometer

The most sophisticated of the three instruments used, this is a Weissenberg Rheogoniometer, model 19, supplied by Sangano Weston Controls Ltd. of Bognor Regis, Sussex, England. It consists of three main units, a drive unit, the measuring system and an electronic control and readout unit. The drive unit consists of a 25 rps motor and a gear box, providing 60 speed steps, giving rotational speeds of 7.9×10^{-6} to 6.25 rps which is equivalent to 4.96×10^{-5} to 39.27 $radians.s^{-1}$ at the lower platen of the measuring system. A second motor and gearbox drives a sine wave generator which allows oscillatory measurements to be carried out simultaneously with the continuous mode measurement. The measuring unit consists of a robust frame holding the rotating truncated lower cone and the stationary upper plate. A frictionless air bearing torsion head holds the upper plate allowing the torque due to viscous drag to be measured using a torsion bar and transducers. The lower platen is supported by a leaf spring. This allows small movements in the vertical direction due to the presence of a normal force, to be measured using an induction transducer, with the position of the platen restored using a feed-back mechanism. The same transducer provides a measurement of

the gap setting which can be controlled manually or by a servo system to maintain the desired gap of 93 μm. A 50 mm diameter truncated cone, angle 2°, is used in conjunction with a 50 mm plate. Depending on the leaf spring fitted, normal forces in the range 4.8×10^{-2} N - 1×10^{2} N can be measured. The shear rate range available is 7.1×10^{-4} to 9×10^{3} s^{-1} and the measurable shear stress range 9.6×10^{-5} to 1.22×10^{6} Pa. The control and readout section consists of transducers linked to solid state electronics. It provided readouts of gap setting, normal force and torsion measurement. Limited temperature control was obtained by using the instrument in a constant temperature room.

5.2.2) Deer Rheometer

A series III model, Deer Rheometer, supplied by Rheometer Marketing Ltd. of Leeds, Yorkshire, England, was used for the majority of routine shear stress and shear rate analyses carried out. It consists of an electronic control system and a measuring system. Unlike the other rheometers used here it operated by applying a known torque and measuring the produced speed of rotation or displacement. The lower plate is mounted on a glass vessel through which constant temperature water was circulated to provide temperature control. The upper cone is supported in a frictionless air bearing and driven by a variable torque control motor. The gap is set using a micrometer to 26 μm. The rotational speed is displayed on a digital readout as radians.s^{-1} for speeds > 0.01 radians.s^{-1}. There was also a displacement output which measured small movements of the cone, this enables creep measurements to be carried out and monitored using a chart recorder. The torque range available is 10×10^{-7} - 1×10^{-2} N.m and the accurately measured speed range is 0.5 - 50 radians.s^{-1}. The displacement could be measured over a range of 1 radian with an output to the chart recorder of 5 V.radian^{-1}. With the 50 mm cone and plate used this provided a shear stress range of

3×10^{-2} - 3×10^{2} Pa and a shear rate range of 38 - 3820 s^{-1}.

5.2.3) The Contraves Rheometer

This was supplied by Contraves Industrial Products Ltd. of Ruislip, Middlesex, England. It consists of a Rheomat 30 measuring head and control instrument coupled to a Rheoscan 30 programming unit. The Rheomat 30 measuring head and control system provided an applied motor speed, which was accurately controlled using a closed loop feedback system. The torque required to maintain that speed was measured by a torsion bar. The maximum torque measureable was 0.05 N.m. The use of different measuring systems allowed the range of shear stresses which could be measured to vary between 0.6 and 2×10^{5} Pa. This allowed measurement of viscosities between 1×10^{-3} - 17×10^{6} Pa.s. The programming unit enabled the instrument to be used over a wide range of shear rates with automatic stepping between the speeds and output of speed and torque to a X - Y recorder. The range of speeds used was 0.08 - 5.8 s^{-1}, with the instrument controls set to provide a steady increase of speed, providing the maximum speed after one minute followed by holding 5.8s^{-1} for twenty seconds then gradually reducing the speed to zero over a period of one minute. This gave a range of shear rates which depended upon the measuring system used. For the two concentric cylinder measuring systems used here, 'B' and 'C', the maximum shear rate was 157 and 97 s^{-1} respectively.

Table 5.3

Rheometers

Type	Supplier	Measuring System Geometry
Weissenberg Rheogoniometer (Model 19)	Sangano Weston Controls Ltd. Bognor Regis, Sussex	50 mm, 2° Truncated Cone & 50 mm Plate, Gap = 93 μm
Deer Rheometer Series III	Rheometer Marketing Ltd. Leeds, Yorkshire	50 mm, 0.75° Truncated Cone & 50 mm Plate, Gap = 26 μm
Contraves Rheomat 30	Industrial Products Ltd. Ruislip, Middlesex	Coaxial Cylinders of Various Dimensions

5.3) Oxygen Solubility Experimental Equipment

As outlined in Chapter 6, section 4, three methods were used in the determination of the solubility of oxygen in the solutions of interest. The enzymic method was used in the 5 litre vessel described in section 5.1, which was fitted with a dissolved oxygen probe and connected to the gas analysis instruments. The other two methods, which monitored the physical absorption of oxygen from the gas phase, required purpose built apparatus.

This was constructed of glass and is shown in figure 5.8. It consisted of two vessels, mounted in a constant temperature water bath, each of 2 litre capacity. Vessel A acted as a reservoir for the gas and was connected to a cylinder of oxygen. Vessel B contained approximately 1 litre of the liquid of interest and was connected to a vacuum pump which was used to degas the liquid. Each vessel was equipped with a mercury manometer and the vessels were joined by a glass pipe, divided by a three way valve which would allow the reservoir to be purged with oxygen. Between the two vessels was mounted a differential manometer filled with glycerol which allowed accurate measurement of the difference in pressure between the two vessels. Thus once the valve, D, between the vessels had been opened to allow the oxygen from the reservoir into the contacting vessel, closure of valve C, between the two arms of the manometer, enabled pressure differences between the vessels to be measured. A magnetic stirrer was mounted under the contacting vessel, below the constant temperature water bath. This was used to stir the liquid, aiding mass transfer.

In the third method used, the pressure in the vessel was kept constant by altering the volume of the gas phase as the oxygen was absorbed. For this a 50 ml burette attached to a length of PVC tubing was connected to the contacting vessel. Water from the burette could be allowed to fill the tubing until the glycerol manometer indicated that the initial pressure was regained.

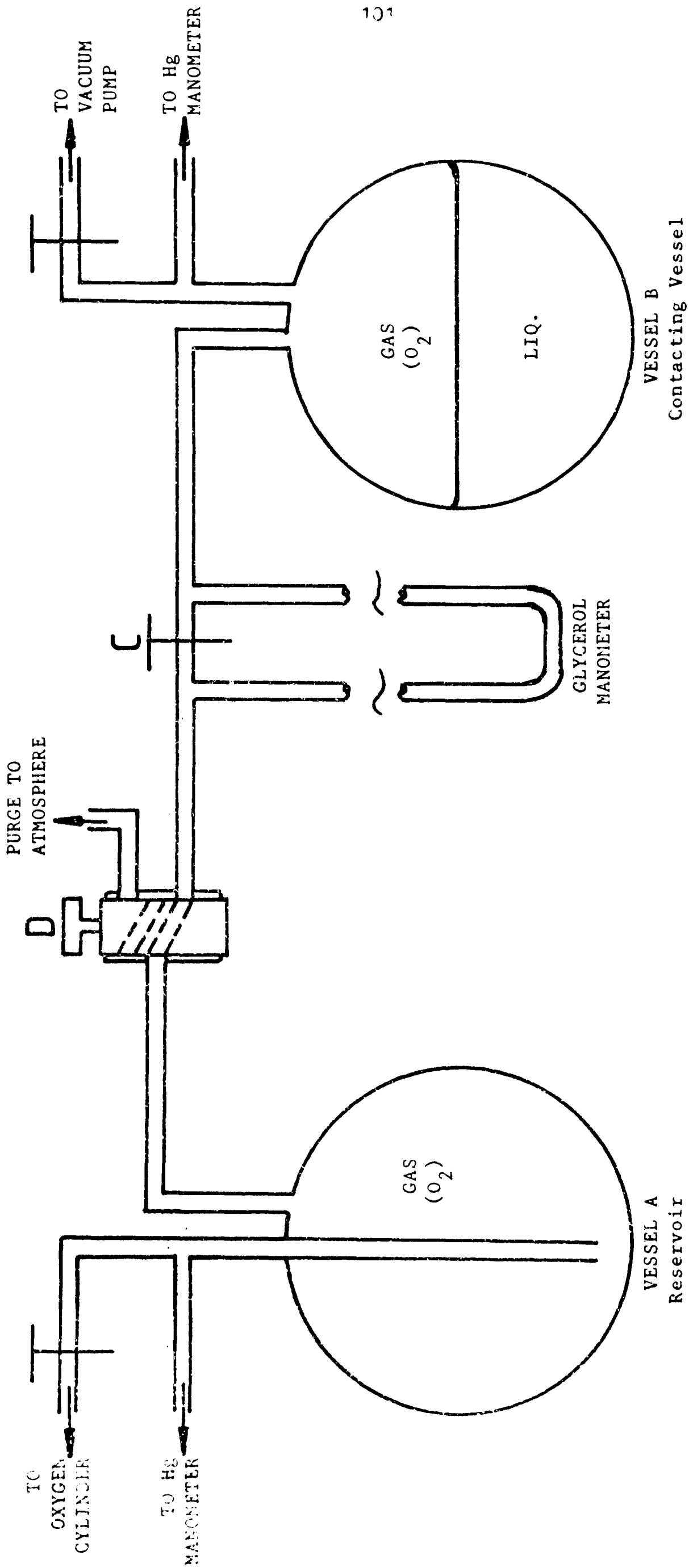

Figure 5.8 All Glass Apparatus Used in Oxygen Solubility Measurements

CHAPTER 6

EXPERIMENTAL METHODS EMPLOYED AND RESULTS OF PRELIMINARY EXPERIMENTS

6.1) Introduction

The various methods in common use for the measurement of volumetric mass transfer coefficients ($k_L a$) were discussed in Chapter 4. It was concluded that a steady state method involving the use of respiring microorganisms would be best suited to $k_L a$ measurement in high viscosity systems. However, information on the use of this method, which was available in the literature and which could be of use in the detailed design of the experimental method was sparse. Therefore some time was spent on preliminary experiments, before the method was perfected. As the early results obtained were important in the development of the final experimental method, they are reported in this chapter. The results obtained once the experimental method was in its final form are reported in the following chapters.

In addition to the main series of mass transfer experiments carried out, some important subsidiary experiments were conducted. These are also reported in this chapter in sections 3 and 4, following the description of the major part of the experimental work and the preliminary results obtained in section 2. These subsidiary experiments are categorised as: a) measurement of oxygen solubility and b) rheological and constitutive analysis of samples taken during the main study.

6.2) Mass Transfer Studies

Initially experiments were carried out in the small vessel (diameter, T = 0.16 m) described in Chapter 5. This had no facility for measurement of the power input; there was room for only one dissolved oxygen probe and temperature control facilities were limited. It was only used as a means of developing and testing the experimental method. The major

part of the work was then carried out in the larger, 20 litre vessel (diameter, T = 0.30 m). Whichever size vessel was in use, it was necessary to prepare the solution being studied and calibrate the measuring instruments prior to carrying out the mass transfer studies.

6.2.1) Preparation of CMC Solutions

CMC solutions were prepared for use in the small vessel by mixing the desired weight of CMC with water in a 5 litre beaker. The water was agitated with a turbine impeller and the CMC powder was shaken onto the surface. Care was needed to avoid clumping of the CMC producing lumps in the final solution which were difficult to dissolve. This could happen if the CMC was added too rapidly, so that it was not wetted thoroughly. It also happened if the CMC was added too slowly, then the CMC which was already in the water would dissolve, raising the viscosity before all the CMC was added.

In the 20 litre vessel the method used was similar. Here the solution was made up directly in the vessel itself, the CMC being added through a 30 mm hole in the top plate using a funnel. The level of water in the vessel was chosen so that the final volume would be 20 litres after the addition of the yeast required for the mass transfer experiments. This meant that if 1 kg of yeast was added, then only 19 litres of water was used in the preparation of the CMC solution. The amount of CMC used was that required to produce 20 litres of solution of the required concentration.

In all cases the CMC solution was stirred overnight to ensure that all the powder dissolved and that a homogenous solution was produced.

6.2.2) Calibration of Instruments Associated with Mass Transfer Studies

i) Carbon Dioxide and Oxygen Analysers

Prior to calibration, dried air was passed through these analysers

for a minimum of several hours. This removed any water vapour which may have accumulated within the analysers, particularly the oxygen analyser which contained filters which may absorb some water vapour. Changes in atmospheric pressure could alter the readings given by these analysers, so calibration checks were carried out before, during and after the mass transfer experiments. Zero readings for oxygen and carbon dioxide were accomplished by passing "oxygen-free" nitrogen gas through the analysers. This gas was used to set the zero for the reference, sample and carbon dioxide measuring channels, it was also used to set the zero difference between the two oxygen channels on the output of the RB276 difference unit, (see Chapter 5 for description of equipment). A special gas mixture, 5% by volume of carbon dioxide in air, was used to set the spans of the analysers, the oxygen channel readings being set to 20% and the carbon dioxide reading set to 5%. The difference reading was again set to zero on its most sensitive setting. Dry air was then passed through the reference channel of the oxygen analyser. This gave a difference reading of between 1 and 1.05%. Some of the exit gas stream from the vessel could then be passed through the carbon dioxide analyser and the sample channel of the oxygen analyser, after first passing through a drying column (see figure 5.6). The analysers required only 100 $ml.min^{-1}$ for each channel, so the residue of the exit gas stream was passed through a regulating valve, to maintain the correct back pressure and a rotameter used to measure its flow rate, before passing into the atmosphere.

ii) Dissolved Oxygen Electrode

The tips of the dissolved oxygen electrodes were first placed in a solution of sodium sulphite until a steady reading was obtained. This gave the zero readings for the electrodes. The electrodes were then placed in their appropriate positions in the vessel containing the previously made up solution. Agitation and aeration commenced and the pressure

within the vessel was regulated to that in use in the mass transfer experiments: 150 mm Hg in the 20 litre vessel and 200 mm Hg in the smaller vessel. These pressures were chosen as the minimum pressure which could be maintained at the highest gas flow rates used in the vessels. A constant pressure in the vessel was desirable, at all the gas flow rates used, to ease evaluation and comparison of the results obtained.

Care was needed in choosing the impeller speed at which calibration of the electrodes was to be carried out, as the readings obtained could be dependent on the agitation rate, particularly in the more viscous solutions used. This is related to the presence of a stagnant liquid film around the probe membrane, which reduces the diffusion rate of oxygen into the electrode[99,100]. The thickness of this film is considered to be highly dependent on the shear rate within the vessels, which is in turn dependent on the agitation rate. Thus higher agitation speeds will give higher dissolved oxygen readings, for the same oxygen concentration. To overcome this the electrodes were calibrated at a high impeller speed, chosen to correspond to the highest impeller speed which would be required in the forthcoming experiment. When the readings had stabilised and the temperature in the liquid had reached 25.0°C, then the full scale reading for each dissolved oxygen meter was set to 100%, equivalent to full scale deflection on the chart recorder. The impeller speed was then varied over the full range which would be used in the following experiment and the dissolved oxygen readings at each speed noted. These readings were used to produce correction factors which were used later in the mass transfer experiment, at the relevant impeller speeds, to remove the impeller speed dependency of the dissolved oxygen electrodes from the readings obtained, prior to evaluating $k_L a$. In practice the main dissolved oxygen probe, that is the probe nearest to the impellers, was hardly affected by changes in impeller speed over the ranges used in the experiments. The other probes, which were situated in areas of lower

liquid flow rate , were affected, particularly in the more viscous solutions. An example of this is shown in table 6.1, for a 0.8% CMC solution agitated using a single disc turbine (D = T/2) in the 20 litre vessel (T = 0.3 m). The precise electrode positions can be found in Chapter 5. Briefly the middle electrode was positioned closest to the impeller in a region of high liquid flow and hence suffered least from impeller speed dependency. The bottom electrode was in a corner of the vessel, well away from the agitation and shows a high impeller speed dependency. The top electrode was in a region where liquid flow was controlled by the movement of gas bubbles through the liquid and showed little dependence on agitation conditions prevalent in the lower half of the vessel.

Table 6.1 Dependence of Dissolved Oxygen Readings in Agitation Conditions

[For a single disc turbine (D = T/2) in 0.8% CMC (n = 0.455, K = 3.7 $Pa.s^n$)]

IMPELLER SPEED	POWER INPUT	DISSOLVED OXYGEN % READINGS		
N rpm	P W	Bottom electrode	Middle electrode	Top electrode
860	298	100	100	100
697	165	96	98	98
643	130	95	97.5	97
592	95.5	93	97.5	97
503	57.3	89	97	96

The relationship between the dissolved oxygen reading and the concentration of oxygen within the vessel is discussed later in this chapter, in section 3.

Once the dissolved oxygen probes and gas analysers had been calibrated, the equipment was left operating in the manner in which it would be

used in the mass transfer study to follow. This helped to ensure that the readings were stable and accurate. One or two hours later, the mass transfer study was commenced. The derivation of $k_L a$ from the readings obtained is described in Appendix 1, the errors associated with the method are described in Appendix 2.

6.2.3) Experimental Methods Used in Determination of $k_L a$

i) Methods Used Initially

Once the instruments were calibrated, the yeast and glucose could be added. No additional materials, such as salts were added, as there was no need to promote the growth of the yeast. The sole object of supplying glucose was to give the yeast a substrate which it could oxidise for their energy requirements, using up oxygen in the process. Yeast was chosen for use in these experiments because of its ready availability in bulk, removing the need to grow, harvest and store large quantities of other microorganisms. Yeast has an advantage over some other microorganisms in that it can live in aerobic and anaerobic conditions without damage. In the absence of oxygen, yeast produces alcohol and carbon dioxide when utilising glucose for energy. Carbon dioxide is also produced when oxygen is available for respiration, but in lower amounts. This affects the respiratory quotient, RQ, which is the ratio of the amount of carbon dioxide produced to the amount of oxygen used up. Measurement of RQ gives an indication of the conditions which the yeast are subject to. A high RQ (RQ > 1) indicates some degree of anaerobic fermentation. This may be due to the presence of regions of low or zero oxygen concentration or due to a high glucose concentration (0.02 - 0.1% w/v) within the solution[137]. Use can be made of this variation in RQ, as described in Chapter 7, section 4.2.

Dried yeast, manufactured by Distillers Company Ltd. (DCL) was used and the glucose was added as a powder. The amounts chosen were

initially arbitrary, with 4 - 25 $g.l^{-1}$ of yeast and 10 - 30 $g.l^{-1}$ of glucose being used. The yeast and glucose levels affect the range of k_La values which can be accurately measured. The higher the yeast and glucose levels are, the higher is the demand for oxygen. This produces large oxygen uptake rates and large driving forces for mass transfer, which are accurately measurable. However if the k_La value is low and the oxygen demand is high, then the dissolved oxygen concentration falls to zero. This may lead to production of alcohol within the liquid, through anaerobic fermentation, which is undesirable because it may affect the value of k_La.[93,94] If too little yeast or glucose is present, then the demand for oxygen will be low, and the driving force will be low as well. This makes accurate measurement of k_La more difficult.

After adding the yeast and glucose, agitation and aeration were commenced. As the gas leaving the vessel had to flow through the analysers, it was necessary to maintain a pressure slightly above atmospheric pressure in the vessel. This was 200mm Hg pressure for the small vessel and 150 mm Hg pressure for the 20 litre vessel. This higher pressure may be expected to alter the k_La values within the system, particularly through alteration of the bubble size. This has however been found to be negligible for small pressure increases[64,113]. Monitoring of the gas analyser readings and dissolved oxygen concentration was commenced immediately, whilst the impeller speed and air flow rate were kept constant. The results obtained from a typical experiment are shown in figure 6.1, here 0.2% CMC was used in the small vessel. In general it was found that the oxygen uptake rate (OUR) and carbon dioxide production rate (CPR) were very high initially, as was the respiratory quotient (RQ). This was accompanied by very low or zero dissolved oxygen concentrations. This was followed by a period of one to two hours in which the OUR and CPR fell and the dissolved oxygen concentration rose. Steady values for the OUR, CPR and dissolved oxygen concentration were usually noted

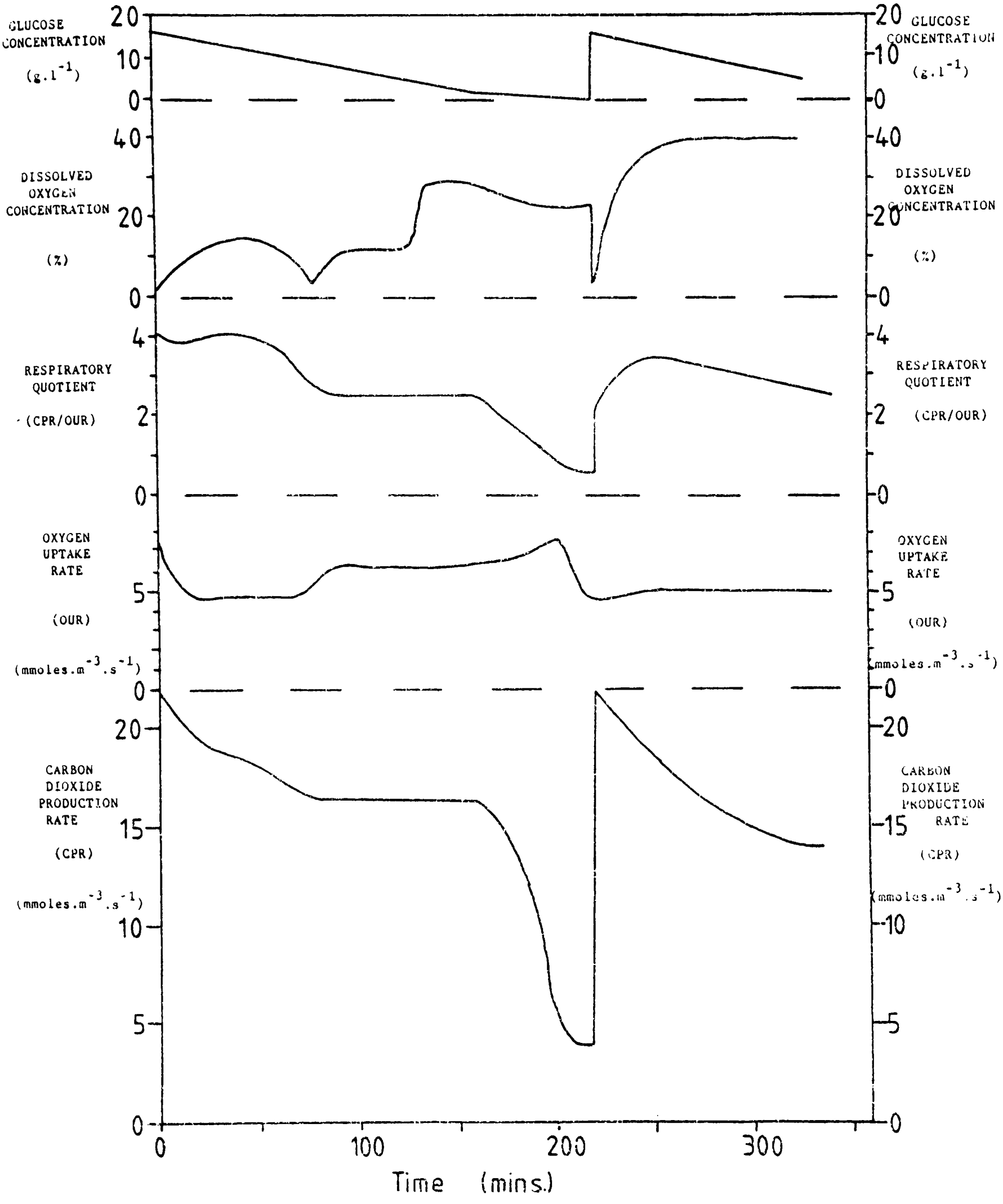

Figure 6.1

Variations in Culture Variables with Time

Small Vessel, 0.2% CMC

after this period of time and k_La measurements could be made. Variations of impeller speed or air flow rate produced new steady states and new k_La values. After a further period of time, which varied from experiment to experiment, the OUR and CPR declined to low values and the dissolved oxygen concentration rose as the glucose in the solution was exhausted. At this point RQ fell below 1 for the first time in the experiment. Addition of further amounts of glucose at this point caused the whole cycle to be repeated. During the course of the experiment, samples were taken for rheological analysis. The frequency of this varied, upwards from two per day.

ii) Refinements and Adjustments Made to the Initial Method

In order to remove the large fluctuations in OUR and CPR it was decided that the glucose would be added continuously, at a slow rate. It was hoped that this would also maintain a very low concentration (< 0.02% w/v) of glucose in the solution and prevent the high RQ values seen. Glucose addition was carried out using a positive displacement pump,to pump a concentrated glucose solution (500 $g.l^{-1}$) into the vessel through a long hypodermic needle. This greatly improved the stability of the oxygen and carbon dioxide readings, extending the length of time of the steady states and increasing the time over which readings could be taken. For example, an experiment was conducted using 0.4% CMC in the small vessel (V = 3 litre) at a glucose flow rate of 3 $g.hr^{-1}$ and an initial yeast concentration of 17 $g.l^{-1}$. This glucose addition rate represents a much lower rate of substrate usage than was seen in the experiment portrayed in figure 6.1. Consequently the OUR and CPR values were lower, particularly the CPR value. They were also stable over a period of 30 hours, giving OUR = 4.5 $\pm$ 0.2 mmoles $O_2.m^{-3}.s^{-1}$ and CPR = 3.15 $\pm$ 0.1 mmoles $CO_2.m^{-3}.s^{-1}$. Thus RQ was reduced to 0.7, reducing the possibility of alcohol being produced within the solution. As the reduction in OUR was slight and the time period over which a steady state was maintained increased, k_La values

could still be measured with the same if not better degree of accuracy.

Continuous addition of glucose also gave a degree of control over the demand for oxygen, by controlling the supply of substrate for respiration. Using this method the time of the experiments was extended from several hours to up to three days continuous monitoring of $k_L a$. Experiments were then conducted in the 20 litre vesselenabling measurement of power input to be linked to the $k_L a$ measurements. This also afforded the opportunity to measure the variation in dissolved oxygen concentration within the liquid, as all three electrodes could be fitted to the vessel.

Excessive foaming of the solutions containing yeast was noted in several experiments particularly where the CMC concentration was low (< 0.8%). Examination of the yeast under a microscope using a Methylene Blue staining method to colour the dead yeast[138], showed that only 50% of the yeast were alive. Samples of fresh block yeast supplied by DCL showed over 90% viability and when used in the 20 litre vessel, the solutions showed a much lower tendency to foam. For this reason a change was made in the experimental method: fresh block yeast was used instead of dried yeast. A greater weight of yeast was required, because of its high water content. It was found that the block yeast had a 25% dry solids content when dried at 105°C overnight. Using this yeast, experiments were carried out in the 20 litre vessel using CMC solutions of 0 - 1.4% concentrations at yeast levels of 10 - 150 $g.l^{-1}$, where the weight of yeast is the fresh wet weight as supplied by DCL Ltd.

The results obtained using this method in the 20 litre vessel were found to vary slightly depending on the yeast concentration, the glucose feed rate and the duration of the experiment. Figure 6.2 shows the results of several mass transfer experiments carried out using solutions of 0.8% CMC. All the experiments were carried out using two Rushton turbines (D= T/2) at heights T/4 and 5T/8 above the bottom of the vessel. A range of speeds and two air flow rates were used, 1 and ½ vvm. The

results of 5 experiments each lasting up to three days are shown, with k_La plotted as a function of the power input per unit volume (P/V). The yeast and glucose levels used are given in table 6.2. The scatter obtained in the results cannot be explained by recourse to the minor variations in rheology for the different experiments, nor is it an indicator of error in the experimental measurement of k_La, which is analysed in Appendix 2. Figure 6.3 and table 6.3 show similar data to that contained in figure 6.2 and table 6.2 for studies carried out in the same equipment using water instead of CMC solutions. The results of 9 experiments using an air flow rate of 1 vvm are shown. The variation in k_La values with yeast concentration and time is much greater than in 0.8% CMC. This suggests that the presence of CMC in the solution suppresses or masks to some extent the effects seen in water. The mechanism for this is not clear, but it may be linked to the decreased tendency towards foaming observed in viscous CMC solutions.

Examination of the results obtained in water showed that the duration of the experiment had a marked effect on the k_La values obtained. Separation of the results according to the day on which they were collected showed that k_La increased with time, as is shown in figure 6.4, for 0.5 kg yeast in 20 litre of water at a glucose feed rate of 24 $g.hr^{-1}$. In addition the dependence of k_La on P/V increases slightly and the dependence of k_La on Q is reduced for results obtained later. This can be seen in figure 6.5, for data collected at two air flow rates on day 1 and day 3 of the same experiment, with additional data added from a similar experiment. Figure 6.5 also shows the two correlation equations produced by Van't Riet[71] for k_La values in water, obtained from the results of several workers. Although complete agreement with the results presented here is not obtained, the same general trend can be seen between the results obtained here on day 1 and Van't Riet's first equation, i.e. low dependence of k_La on P/V, high dependence on Q. Similarly the day 3

Table 6.2

Experimental Conditions and Legend for Data shown in Figure 6.2

Solution : 0.8% CMC

Experiment	1	2	3	4	5
Legend	▲	△	●	○	■

Yeast Type	DRIED YEAST			FRESH YEAST	
Amount of Yeast $g.l^{-1}$	6.2	8.6	10	10	24
g/20 l	123	172	200	200	480
Glucose Flow Rate $g.hr^{-1}$	15 - 20	15	16	8	24

Table 6.3

Experimental Conditions and Legend for Data shown in Figure 6.3

Solution : Water

Experiment	1 - 3	4	5	6 - 7	8 - 9
Legend	▲	△	●	○	■

Yeast Type	FRESH YEAST IN ALL EXPERIMENTS				
Amount of Yeast $g.l^{-1}$	25	35	50	150	150
Glucose Flow Rate $g.hr^{-1}$	24 - 32	24	24 - 32	24	56 - 72

Figure 6.2

$k_L a$ versus P/V in 0.8% CMC, Two Disc Turbines (D=T/2)
Results of 5 Experiments, see table 6.2 for legend.

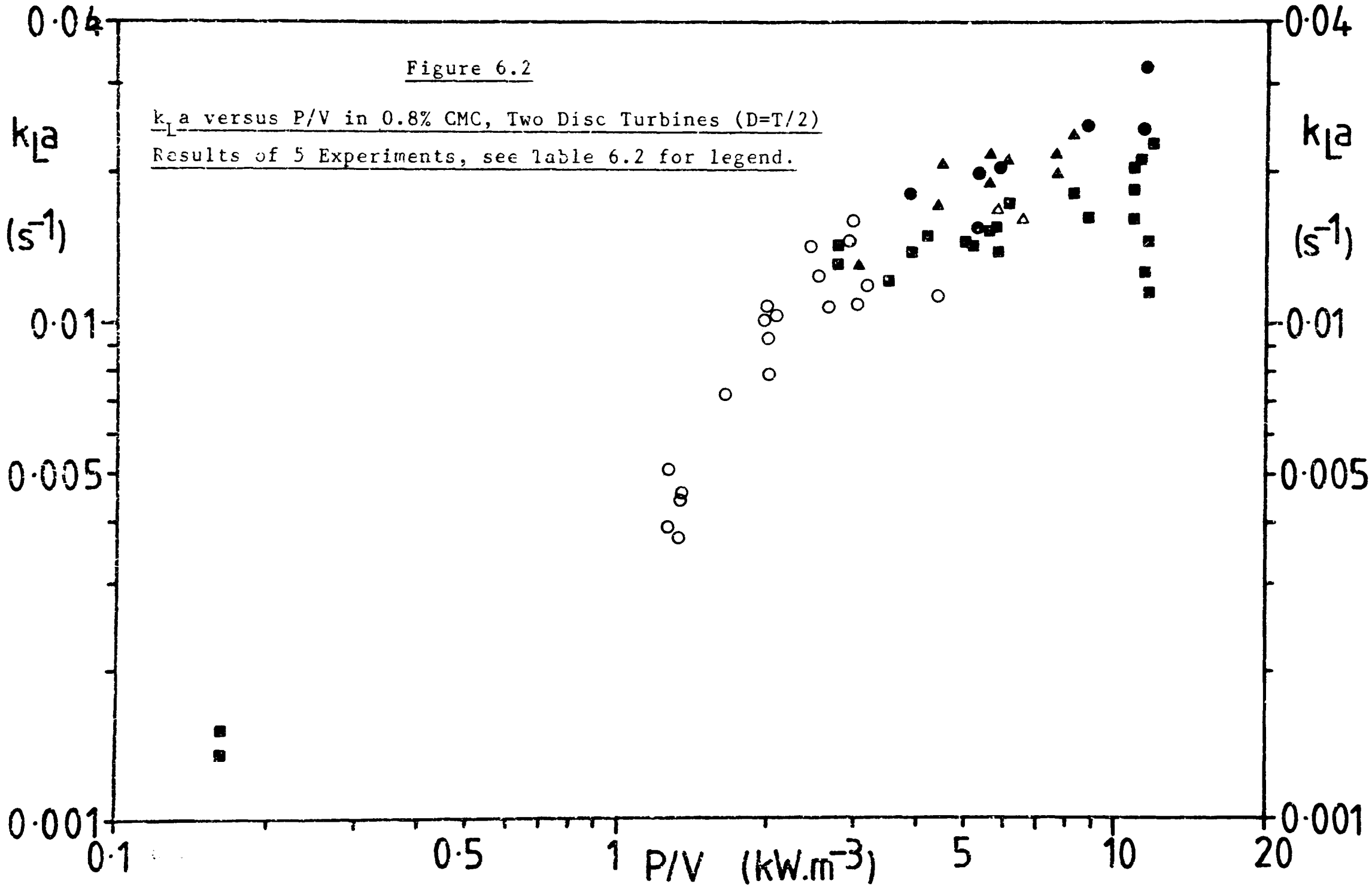

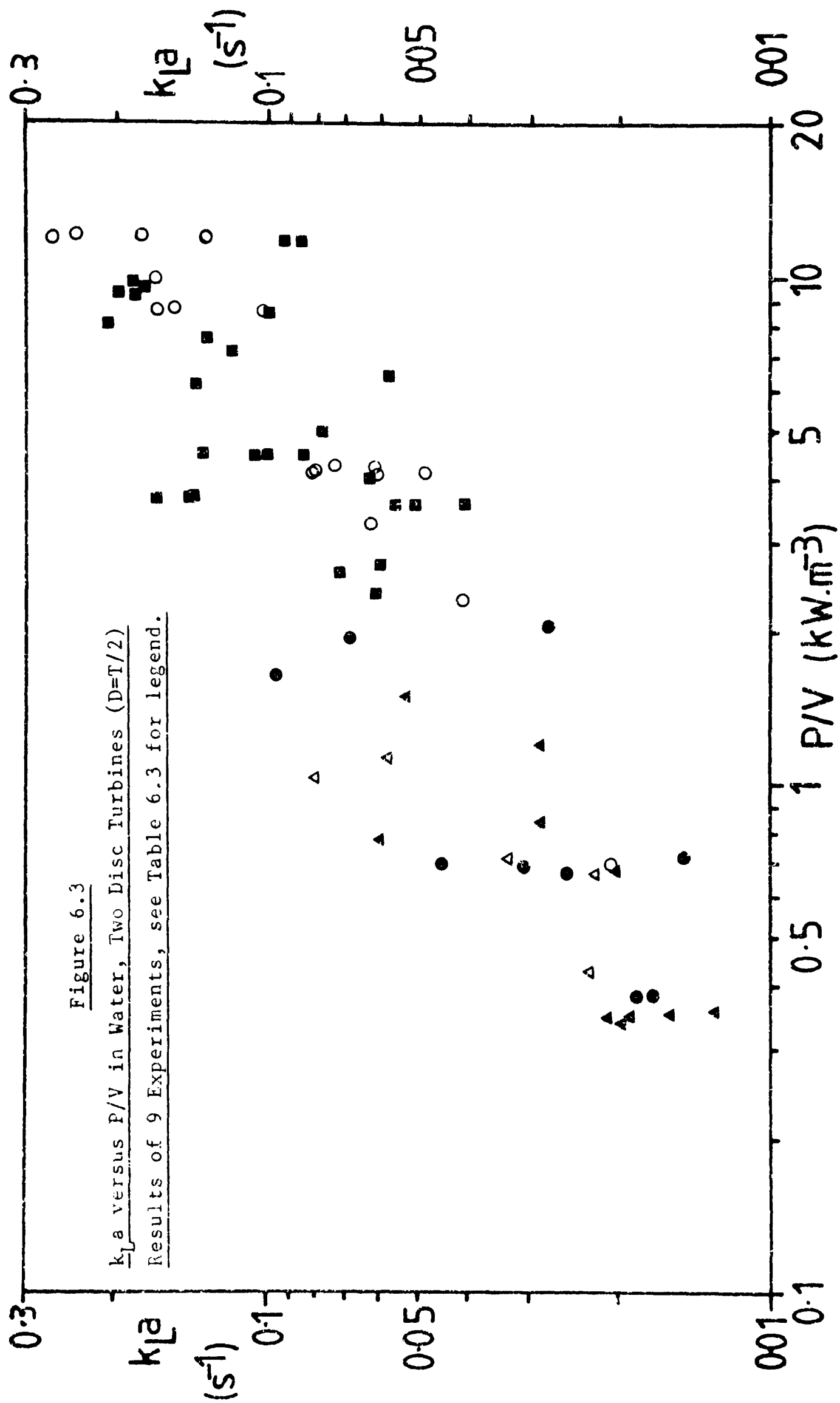

Figure 6.3

k_La versus P/V in Water, Two Disc Turbines (D=T/2)

Results of 9 Experiments, see Table 6.3 for legend.

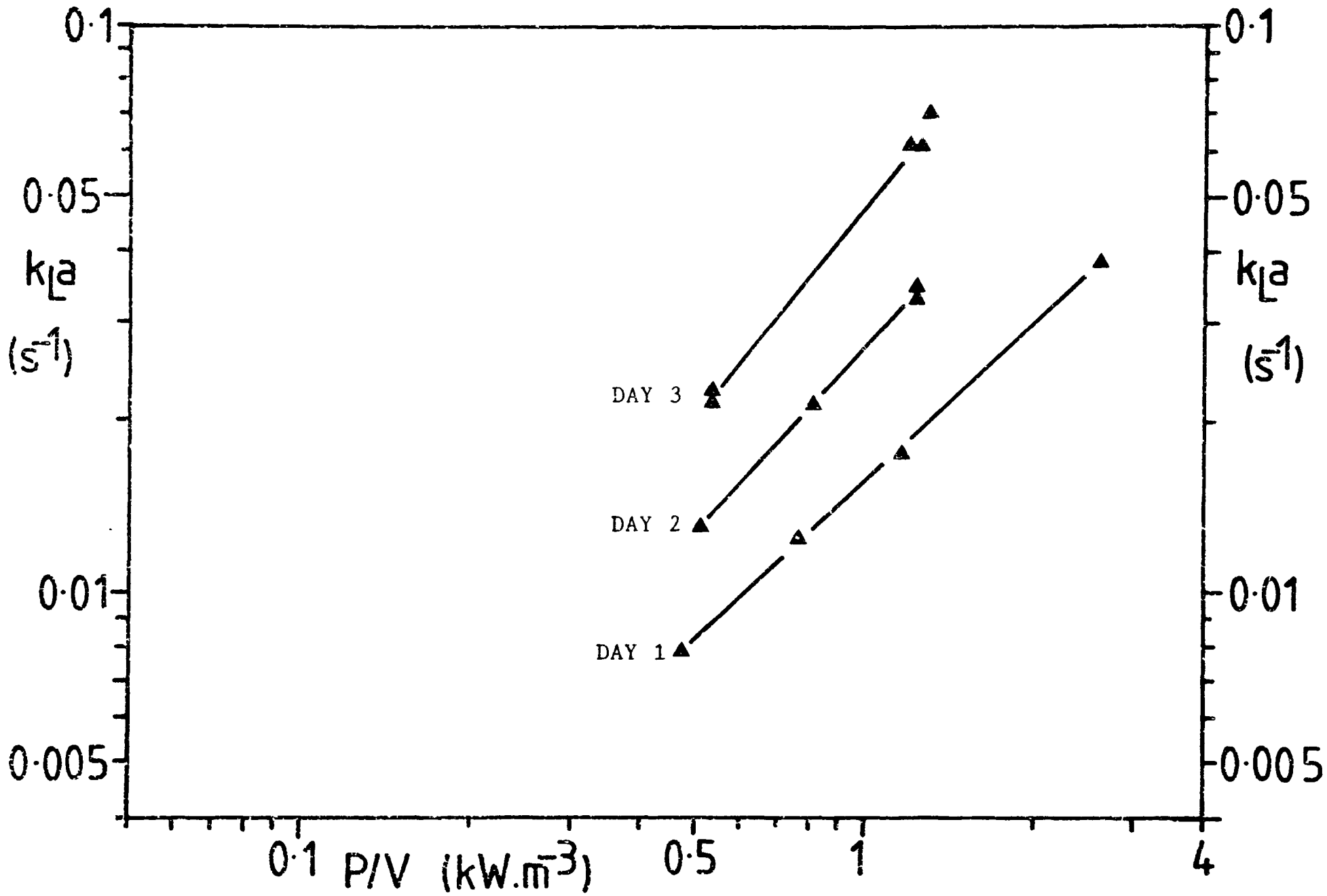

Figure 6.4 $k_L a$ versus P/V, for Two Disc Turbines in Water. Q= ½ vvm

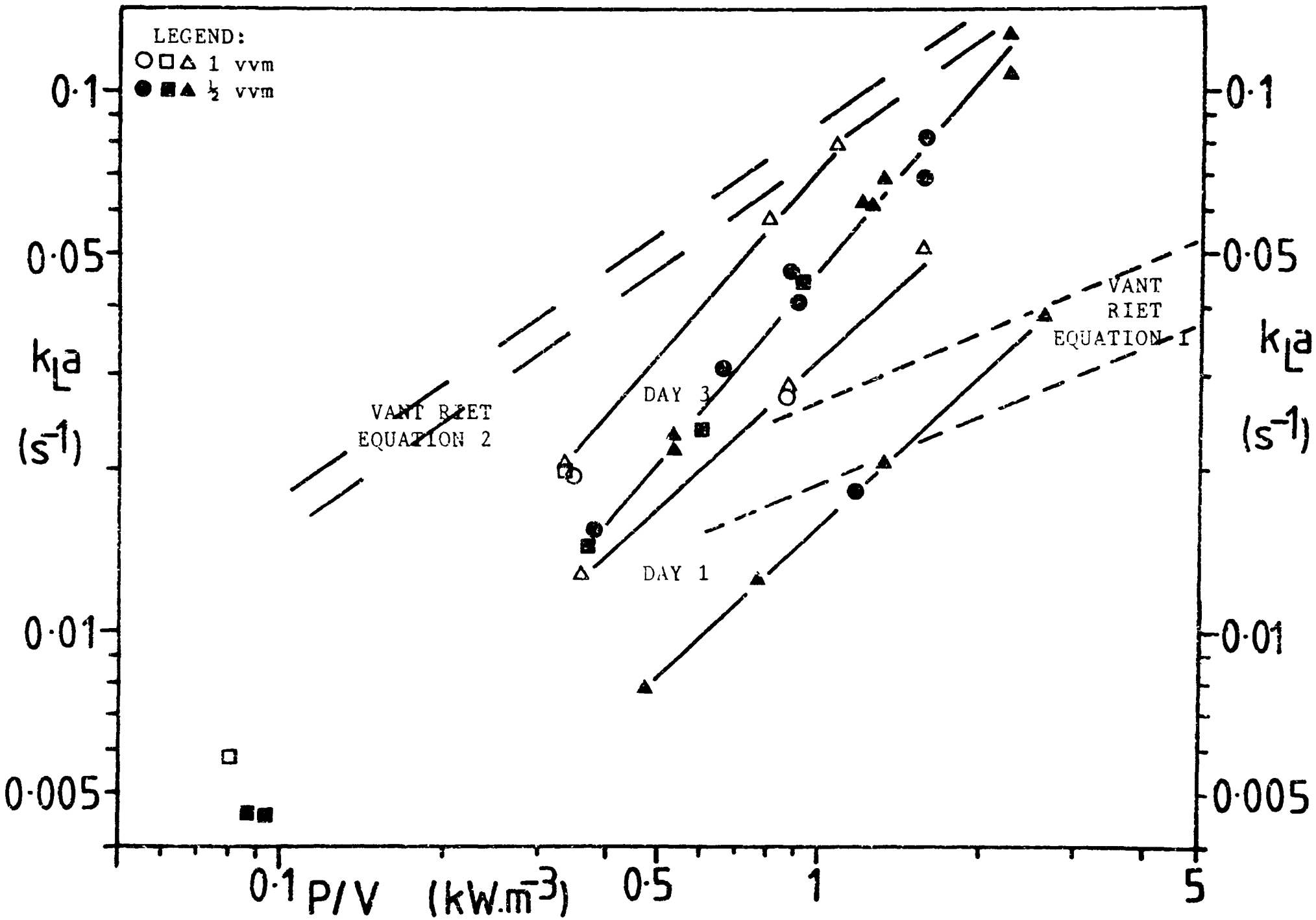

Figure 6.5 k_La versus P/V, for Two Disc Turbines in Water. Q= ½ & 1 vvm

results and Van't Riet's second equation both show a higher dependence on P/V and a lower dependence on Q.

Van't Riet's first equation is for k_La values in coalescent systems, which he defines as pure water or water with a low salt concentration (< 0.02 M). It was obtained from the results of experiments carried out using the dynamic gassing out method, taking the form:

$$k_La = 2.6 \times 10^{-2} (P/V)^{0.4} . v_s^{0.5} \qquad (s^{-1}) \quad (6.1)$$

Where v_s is the superficial gas velocity, i.e. the volumetric gas flow rate divided by the cross-sectional area of the vessel. The second equation is for k_La values in non-coalescent systems, defined as having salt concentrations in excess of 0.1 M. This gives:

$$k_La = 2.0 \times 10^{-3} (P/V)^{0.7} . v_s^{0.2} \qquad (s^{-1}) \quad (6.2)$$

Here the majority of results were obtained using chemical methods to determine k_La (see Chapter 4).

This would suggest that the solutions used here are altering from coalescent to non-coalescent systems over the course of the experiments.

A series of experiments was carried out to investigate some of these effects, as set out below.

iii) Experiments Used to Determine the Variation of k_La with Parameters Intrinsic in the Method

As the variations due to yeast concentration, glucose feed rate and duration of experiments were more apparent in water alone, it was decided that this series of experiments would be carried out in the absence of CMC. This had the advantage of removing any effects associated with high viscosity or variations in rheology and enabled a comparison with data available in the literature for k_La in water, as described above. Analysis of samples taken from the solutions using the methods outlined in section 6.4 was also made easier if CMC was absent.

The experiments were carried out in the 20 litre vessel using fresh yeast. The only difference between these experiments and the main series of experiments designed to look at $k_L a$ variation with air flow rate, rheology and impeller speed, was that the air flow rate and impeller speed were kept constant. Samples were taken frequently and analysed for glucose, ethanol, yeast concentration and residual material concentration. In addition a CO_2 / acetone cold trap was installed in the exit gas line and the condensate which collected was analysed for ethanol. In all cases no ethanol was detected in this condensate. Ethanol was detected at very low levels, less than $1 g.l^{-1}$, in some samples taken from earlier experiments conducted at high glucose feed rates ($45 g.hr^{-1}$) into a 20 litre solution containing 3 kg fresh yeast. The presence of alcohol was linked to periods of high carbon dioxide production rate (17.1 mmoles $CO_2.m^{-3}.s^{-1}$) compared to low oxygen uptake rate (7.6 mmoles $O_2.m^{-3}.s^{-1}$) at zero dissolved oxygen levels. This gave a high respiratory quotient (RQ = 2.2) which is indicative of anaerobic fermentation and production of alcohol. In order to avoid alcohol production, this present series of experiments was conducted at a relatively high impeller speed, 5.3 rps, giving a power input of approximately 4 $kW.m^{-3}$. This ensured that the $k_L a$ values and dissolved oxygen concentrations obtained were relatively high, as expected no ethanol was found in the samples. This had the disadvantage of making the $k_L a$ values obtained very sensitive to any error in the dissolved oxygen reading so calibration checks were carefully carried out on the dissolved oxygen probe before and after the experiments. This heightened sensitivity of $k_L a$ to the dissolved oxygen reading at high dissolved concentrations can be explained by an examination of the denominator in equation 4.12. The driving force is expressed as the difference between the bulk liquid phase and the interfacial region oxygen concentrations. The gas phase concentration is then related to the interfacial region oxygen concentration by Henry's coefficient. As

the difference between these two measurements is reduced at high dissolved oxygen concentrations, a small error in measurement of either can produce a large error in their difference. Thus if the dissolved oxygen concentration is 80% of the saturation value, a 1% error in the reading will produce a 5% error in $k_L a$.

The caution required in interpreting results at high dissolved oxygen levels and a desire to determine whether the high shear rate at 5.3 rps was having an effect on $k_L a$ stability through shear destruction of the yeast prompted a further two experiments conducted at a lower impeller speed, 3.0 rps. Again the air flow rate was 1 vvm and two yeast concentrations were used. The results of these and the previous experiments at 5.3 rps are shown in figure 6.6. Table 6.4 gives the experimental conditions for each experiment. It can be seen from the figure that yeast concentration and glucose feed rate do affect the $k_L a$ values obtained. At a glucose feed rate of 16 g glucose.hr^{-1} per kg yeast or greater, $k_L a$ is not stable for any period of time, but rises steadily. Even at low glucose feed rates, if the yeast concentration is high (150 g.l^{-1}) then the steady state produced does not last particularly long. At low glucose feed rates and at a yeast concentration of 50 and 100 g.l^{-1} long steady states were achieved. These show that increasing yeast concentration increases the $k_L a$ value. Even at these levels the steady state values of $k_L a$ were not achieved until 10 - 14 hours had passed after the addition of the yeast. The length of these steady states may indicate that the reduced shear rate at the lower impeller speed is an influencing factor, reducing the degree of shear induced damage to the yeast. This would concur with the reduction in scatter of $k_L a$ results seen in viscous CMC solutions (figure 6.2), where the high viscosity will ensure the rapid decay of the turbulent eddies, which might damage the yeast.

Figure 6.7 shows the results of analysis of the samples removed

Table 6.4

Experimental Conditions and Legend for Results shown in Figures 6.6 and 6.7

Experiment	1	2	3	4	5	6
Legend	○	●	□	■	△	▲
Yeast Conc. $g.l^{-1}$	150	50	150	150	50	100
Glucose Feed Rate $g.hr^{-1}$	48	24	24	24	11	22
Impeller Speed rps	5.3	5.3	5.3	5.3	3.0	3.0

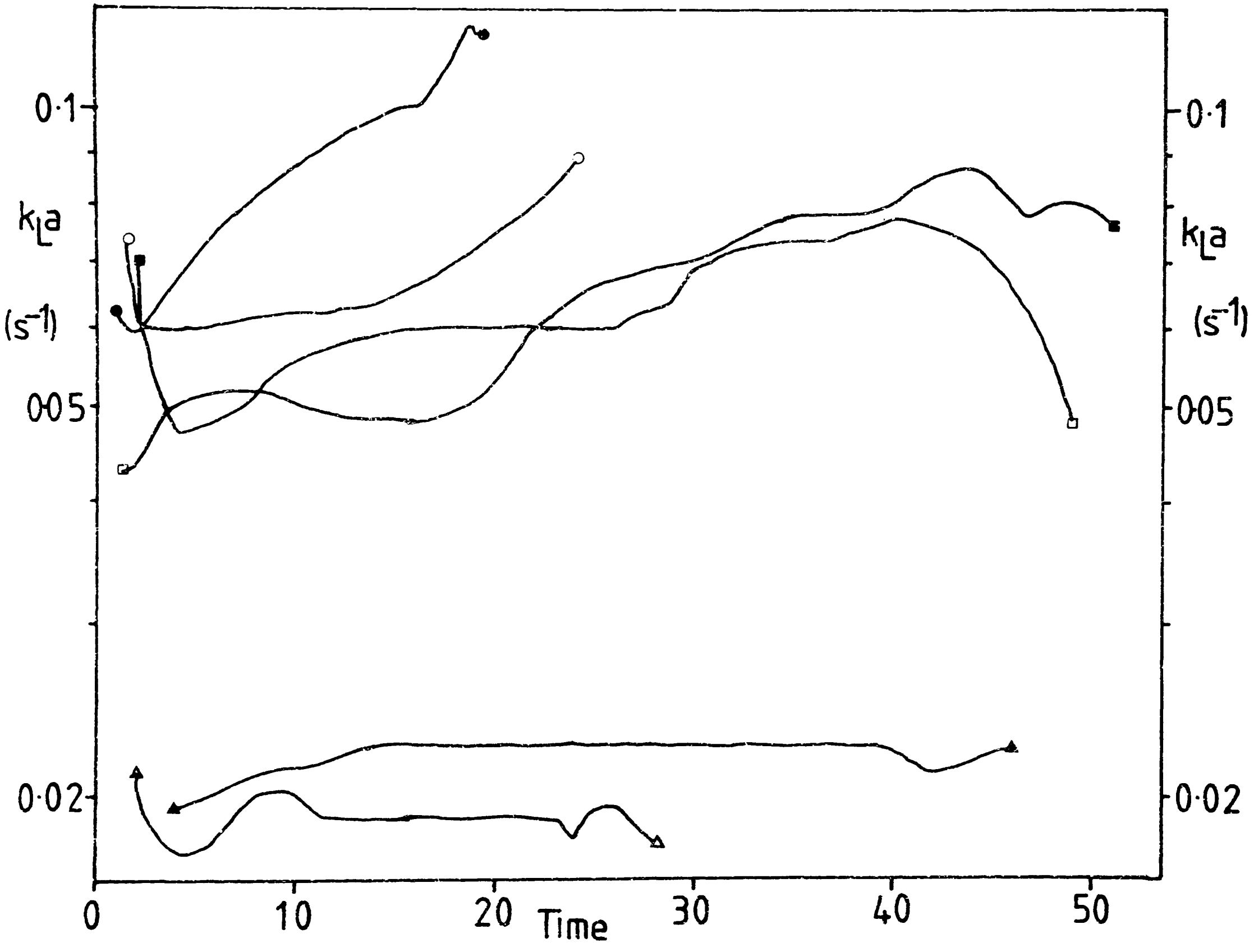

Figure 6.6

$k_L a$ versus Time at Various Yeast Concentrations and Glucose Feed Rates. Two Disc Turbines (D=T/2), Q = 1 vvm Twenty Litre Vessel

[See Table 6.4 for Legend]

Figure 6.7

Variation of Yeast Concentration and Concentration of Residual Material with Time, in the Mass Transfer Experiments shown in Figure 6.6

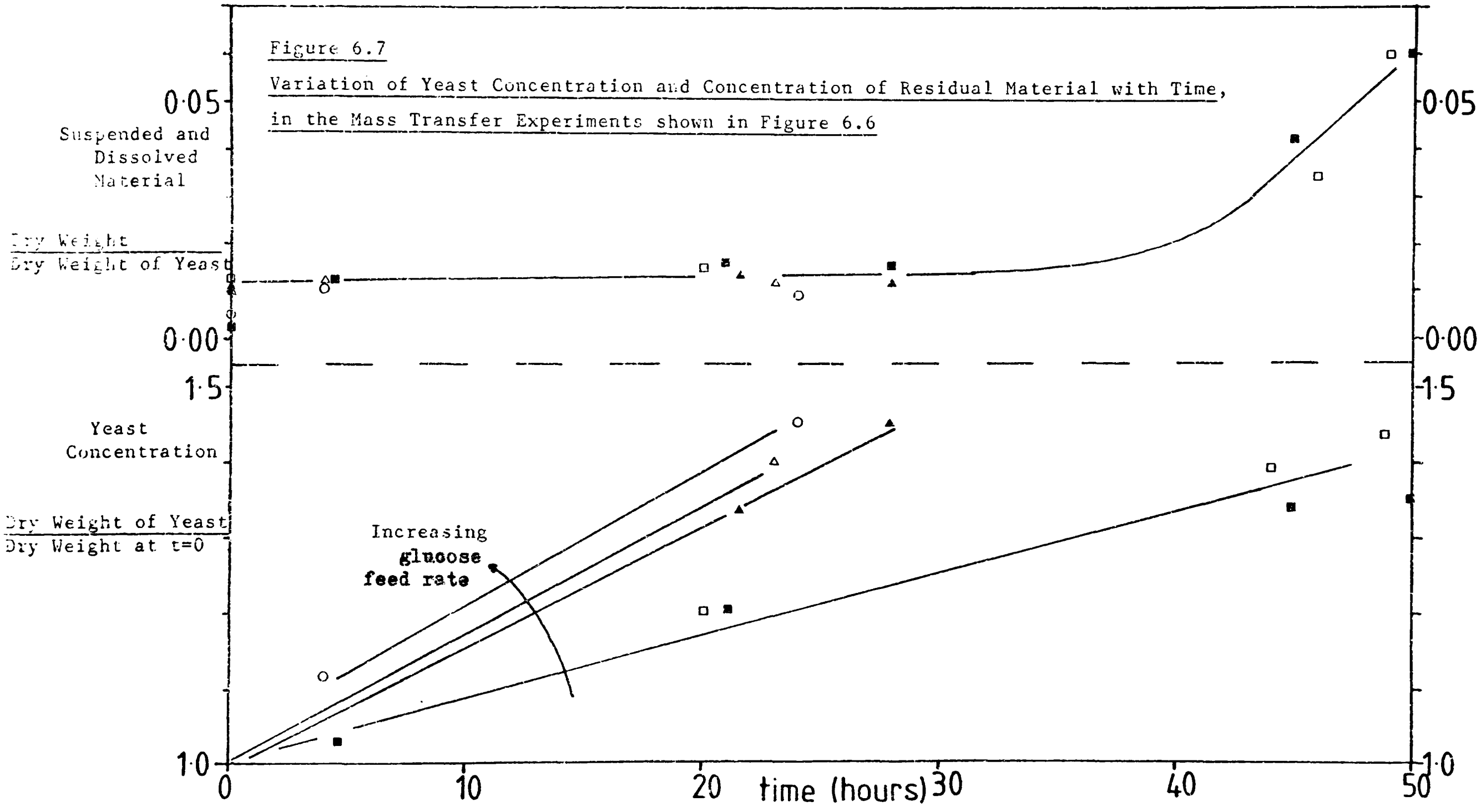

from the experiments just discussed. Again table 6.4 gives the experimental conditions. As would be expected, increasing yeast growth rates occur with increasing glucose feed rate. The interesting results are the residual material levels, which are a measure of the amount of material dissolved in the solution and small particles suspended in the solution after the yeast cells have been centrifuged out. Expressed in the figure as dry weight per dry weight of cells, it can be seen that for all the experiments the level remains reasonably constant for the first 20 - 30 hours. In the last period of the experiments, between 40 and 50 hours, this level rises substantially. This corresponds to the reduction in $k_L a$ values seen after 40 hours of experiment and these two factors may be linked. The constancy of the residual material level over the time of the experiments would indicate that the yeast is not being damaged by shear within the vessel. It would be expected that cell damage would be apparent through increases in dissolved material due to cell wall leakage, or increases in suspended fragments due to cell break up[139]. Samples of supernatant were subjected to ultraviolet and visible spectral analysis, in an effort to determine the nature of the dissolved and suspended material. Over the full range measured a high reading was obtained, which is indicative of a high level of suspended material. Peaks were obtained at 260 - 280 nm, which is indicative of the presence of deoxyribose nucleic acid derivatives dissolved in the solution.

Measurement of the conductance of the supernatant solutions for the experiment at 50 g yeast.litre^{-1} at times 0 and 23 hours gave results of 115 and 90 μmho respectively. This indicates that there is little change in ionic strength over the initial part of the experiment and if any change occurs at all then it is a slight reduction in ionic strength. Over the same period the pH dropped from 4.5 to 4.2, for all the experiments the pH of samples was found to be between 4 - 4.5.

Quantitative analysis of the solutions of yeast were not carried

out. It is assumed that the solutions are complex mixtures containing many different biological compounds and particulate matter. From the results obtained in this series of experiments, it was decided that mass transfer experiments in CMC solutions would proceed with the experimental conditions more closely defined. A single yeast concentration and glucose flow rate would be used, chosen for the stability of the steady state values obtained. Bearing in mind the requirement that as large a range as possible of $k_L a$ values would need to be measured.

iv) Final Format of Experimental Method

The level of yeast chosen was 50 $g.l^{-1}$ and the glucose feed rate 11 $g.hr^{-1}$. Otherwise the experiments were carried out as outlined previously. After addition of the yeast, $k_L a$ was monitored for up to 30 hours. During the period prior to 12 - 15 hours when $k_L a$ was not steady no changes in impeller speed or air flow rate were made. Over the course of the rest of the experiment, the stability of $k_L a$ with time was monitored by periodic use of a set air flow rate and impeller speed. All the results discussed in the following chapters were obtained using this method during periods in which $k_L a$ was not varying with time.

The levels of yeast and glucose chosen limited slightly the range of $k_L a$ values which could be measured accurately. In particular the accurate measurement of high $k_L a$ values, such as are found at high power inputs in low viscosity solutions, was prevented. In the presence of a medium or high dissolved oxygen concentration, where the glucose feed rate limited respiration, the oxygen uptake rate obtained was approximately 2.6×10^{-3} moles $O_2.m^{-3}.s^{-1}$. This corresponds to an oxygen difference of ca. 0.35% between the inlet and exit air streams at 1vvm, this is taken into account when determining the gas phase concentration in the vessel (see Appendix 1 for the calculation of $k_L a$, OUR, $C^* - C_L$, etc.). The oxygen analyser is capable of measuring accurately smaller differences than this, which is necessary when the dissolved oxygen concentration fell to low or zero values; when this occurs the mass transfer coefficient

limits the supply of oxygen from the gas phase, reducing the oxygen used and hence the oxygen difference measured by the analyser. k_La values were still measured under these circumstances. When oxygen is limiting and the OUR falls then glucose can accumulate in the solution. This may allow anaerobic fermentation to take place and alcohol formation may occur. As alcohol can affect k_La[93,94], the dissolved oxygen level was not allowed to remain at zero for long periods of time. The impeller speed was increased to a previously used high value and k_La measured under these conditions to ensure that it had not been affected by the low dissolved oxygen concentration. Any glucose accumulated in the solution was then rapidly used up and the OUR returned to normal.

6.3) Measurement of Oxygen Solubility and Results Obtained

To measure the solubility of oxygen in solutions of CMC, several methods were used. Each was tested in water to determine its suitability and accuracy, before using in CMC solutions. The first method described was also tested in solutions of glucose and sodium chloride.

Method 1 : Enzymic Method

This method was adapted from that of Kappeli and Fiechter[130]. The 5 litre vessel, which was used for mass transfer experiments, was also used here. The principle behind the method is simple. A known amount of oxygen is released into the solution of interest. This alters the reading of a previously calibrated dissolved oxygen probe and the change in percentage saturation is used to determine the amount of oxygen which would give a reading of 100%. This is the required solubility measurement.

The dissolved oxygen probe was first calibrated in a known volume of the solution of interest within the 5 litre vessel at a low impeller speed. The impeller speed was kept low to ensure that surface aeration and surface movement were kept to a minimum. Nitrogen gas and air were

used to determine the zero and span of the oxygen meter, at atmospheric pressure and at the chosen temperature. The oxygen was then stripped from the liquid using nitrogen gas before the gas supply was switched off. Agitation was halted until all the gas bubbles had left the solution. This was aided in the viscous CMC solutions by reducing the pressure in the headspace above the liquid using a vacuum pump. Then agitation was restarted and a solution of catalase (1 ml) supplied by Sigma Ltd. of London, England was added to the vessel. A small stream of nitrogen gas was passed through the headspace of the vessel at 20 - 100 $ml.min^{-1}$. This prevented the absorption of oxygen through the surface of the liquid. Analysis of this nitrogen stream using the oxygen analyser was used to determine whether oxygen was being removed from the liquid over the time scale of the experiment. With the equipment set up in this manner, the dissolved oxygen reading which was at or near zero was noted. Then some hydrogen peroxide solution (0.2 molar, 2 - 10 ml) was added to the liquid. This caused an immediate rise in the dissolved oxygen reading of approximately $10\%.ml^{-1}$ and note was made of the steady reading obtained after less than one minute. In this time it was shown by the oxygen analyser that negligible oxygen escaped into the headspace through the liquid surface. In the worst case 3% of the oxygen produced was removed after 1 minute, which was longer than the time taken for a steady state dissolved oxygen reading to be registered.

The hydrogen peroxide solution used was analysed according to the method given by Vogel[140]. This gave a measure of the amount of oxygen which was released by the enzyme and could be equated to the change in dissolved oxygen reading to give the solubility of oxygen within the liquid. Table 6.5 gives a summary of the results obtained and a comparison with literature values.

Table 6.5 The Solubility of Oxygen in Various Solutions

Solution	Temperature °C	Oxygen solubility at 1 atmosphere air pressure (0.21 atmospheres oxygen pressure) moles $O_2.m^{-3} \times 10^{-1}$		
		Literature[126]	Experimental	Error
Distilled Water	25	2.663	2.58 - 2.75	± 3%
Glucose solution (6 moles per 1000g water)	20	1.30	1.26 - 1.33	± 3%
Sodium Chloride solution (1.93 molar)	25	1.41	1.58	+ 12%
CMC (0.8%)	25	—	2.55 - 2.65	—

It can be seen that the results obtained for distilled water and glucose solutions agree well with the literature, unlike the result obtained for sodium chloride solution. This may be due to inaccuracies in making up the solution: if the solid salt contained water, or was impure, then the actual concentration of salt in the final solution would have been lower than expected. As the solubility of oxygen in salt solutions is very sensitive to concentration variations, this may have caused this spurious result. It is also a possibility that the measuring method was affected, in some manner, by the ions in the solution. As CMC solutions contain quantities of sodium ions, it was decided that further corroboration of the results obtained in the CMC solutions was necessary. For this reason, a purely physical absorption method was tried.

Method 2 : Physical Absorption at Constant Volume, Noting the Change in Pressure Produced

The method of Quicker et al.[129] was used, which relies on the Gas

Law: (PV = nRT). A known volume of oxygen at a known pressure is contacted with a known volume of liquid which is devoid of oxygen. The resulting pressure change, at constant temperature and volume, gives the number of moles of oxygen absorbed.

The apparatus, described in Chapter 5 and shown in figure 5.8, consisting of a gas reservoir, a contacting vessel and several manometers was housed in a thermostatted water bath at 25°C. The samples of water and 1.4% CMC solution being tested were degassed under vacuum overnight. This caused a slight change in volume due to evaporation which was noted and taken into account. With the contacting vessel still under vacuum, pure oxygen gas from a cylinder was allowed into the reservoir at 3 psig. The reservoir was then sealed and the vacuum removed. Opening the valve between the reservoir and the contacting vessel allowed the oxygen into contact with the liquid. The valve between the vessels and the two manometer tappings was then closed and the reduction in pressure caused by the absorption of the oxygen in the liquid was noted on the manometer containing glycerol. Stirring and shaking of the liquid were employed to speed up the absorption process. For the 1.4% CMC solutions used, it could take hours to reach equilibrium.

The errors inherent in the method meant that reasonable results could not be obtained, even for water. It was necessary to know precisely the volume of the vessel headspace, which varied due to changes in liquid volume during degassing and movement of the manometer fluids. For this reason the method was adapted slightly.

Method 3 : Physical Absorption at Constant Pressure, Noting the Change in Volume Produced

This method, adapted from method 2, used the same principle and apparatus as method 2. Instead of measuring the small change in pressure of a large volume of gas during oxygen absorption, it was decided that

measurement of a change in volume of the gas at constant pressure would involve less inherent error. The method was adopted from that of Hitaka et al.[128]

The experiment was carried out in the same manner as in method 2, until the pressure in the contacting vessel started to change due to oxygen absorption. When this happened the pressure was returned to its initial value by allowing water from a burette to flow into a flexible pipe connected to the contacting vessel. When no further pressure change was noted on the glycerol manometer, the volume of water which had been added to maintain the initial pressure was noted and assumed to be equal to the volume of oxygen absorbed. By noting the volume of the liquid of interest and the absolute pressure within the vessel, the solubility of oxygen could be determined.

For water results of $\pm$ 5% of the literature value were obtained, whilst for 1% CMC an average of 2.56×10^{-1} moles $O_2.m^{-3}.Atm^{-1}$ Air was obtained with similar scatter of results. This is 4% below the literature value for water and agrees well with the results obtained in method 1. Wasan et al.[141] measured the solubility of oxygen in CMC solutions, finding that little reduction occurs below a concentration of 2% CMC. which supports the results found here. It may seem at first sight that a viscous liquid, such as a 1% solution of CMC in water, should have a much lower oxygen solubility than that found. However it should be noted that the solution is still 99% water and for low molecular weight solutes, such as glucose and salts, much higher concentrations of solute are required to reduce the solubility of oxygen to a significant extent.

The slight reduction of solubility found in the CMC solutions appears to be negligible, particularly when compared to the probable reduction caused by the addition of yeast to the solution. It would not be an easy task to measure the solubility of oxygen in solutions of

live yeast. For this reason, the value of the solubility of oxygen in all the solutions used in this work has been taken to be that obtained in water, i.e. 2.663×10^{-1} moles $O_2.m^{-3}.Atm^{-1}$ Air at 25°C.

6.4) Analysis of Samples from Mass Transfer and Mixing Studies

6.4.1) Rheological Analysis

As the CMC solutions used were slightly thixotropic (see Chapter 3), all rheological measurements were made after the solution had been agitated for at least 30 minutes. Samples taken after periods of aerated agitation contained gas bubbles, which were removed by centrifugation prior to measurement of the rheological properties. Shear stress - shear rate data were obtained for all the experiments carried out with CMC solutions. In addition a proportion of the samples were analysed to determine their viscoelastic properties. A description of the instruments and their use is contained in Chapter 5.

The Contraves rheometer was used for routine measurement of shear stress - shear rate relationships in all the early mass transfer experiments. Its ease of use allowed frequent measurements to take place. This enabled the determination of the effects of the experimental conditions on the rheology. Of particular interest was whether the presence of yeast accelerated the breakdown of the CMC, reducing the apparent viscosity.

The Deer rheometer was used for more exacting measurements of the shear stress - shear rate relationships in all the later experiments. A larger range of shear stresses and shear rates could be measured accurately, making it particularly useful for measurements in the more dilute CMC solutions. It could also be used to carry out creep compliance measurements. Some creep compliance experiments were carried out, but the results were erratic, possibly due to the presence of fermenting yeast in the samples. They are not reported here.

The Weissenberg Rheogoniometer was used for shear stress - shear rate measurements and measurement of the 1st normal stress difference in selected experiments. Of particular interest was the possible effects of bubbles present in the samples on the viscoelasticity of the solutions. Fermenting yeast solutions were used to investigate this, by measuring their viscoelastic properties with gas bubbles present and after centrifugation. An estimate of the bubble size and number was obtained by measuring the volume change of a sample as it fermented and microscopically examining the bubbles to measure their diameter.

Results Obtained from Rheological Studies

The range of impeller speeds used during mass transfer studies was between 3 and 17 rps which according to equation 3.2 gives a range of shear rates which are of interest of 35 - 200 s^{-1}, for $k_s = 11.5$. In order to compare the three rheometers, several samples were analysed on two instruments at once. Figures 6.8 to 6.10 show selected results of comparisons of the instruments, with experimental conditions shown in the figures. It can be seen that at high shear rates ($\dot{\gamma} > 30\ s^{-1}$), reasonable agreement between the instruments is obtained. The range of shear rates on the Contraves is slightly limited though, particularly when using system C, ($\dot{\gamma}_{max} = 95\ s^{-1}$), which was necessary for analysis of concentrated CMC solutions (> 1%). At lower shear rates, some deviation of the results obtained in the Contraves occurs. However for the range of shear rates which are of interest in the mass tranfer experiments (i.e. 30+ s^{-1}) adequate results are obtained in each instrument.

Figure 6.11 shows the power law parameters n versus K, plotted with CMC concentrations as a parameter. The scatter of results obtained shows that it is not possible to reproduce these parameters exactly when making up the CMC solutions. It should be noted that these results

Figure 6.8

Comparison of Shear Stress versus Shear Rate Data for 0.8% CMC Produced Using the Deer,□, and Contraves,O, Rheometers

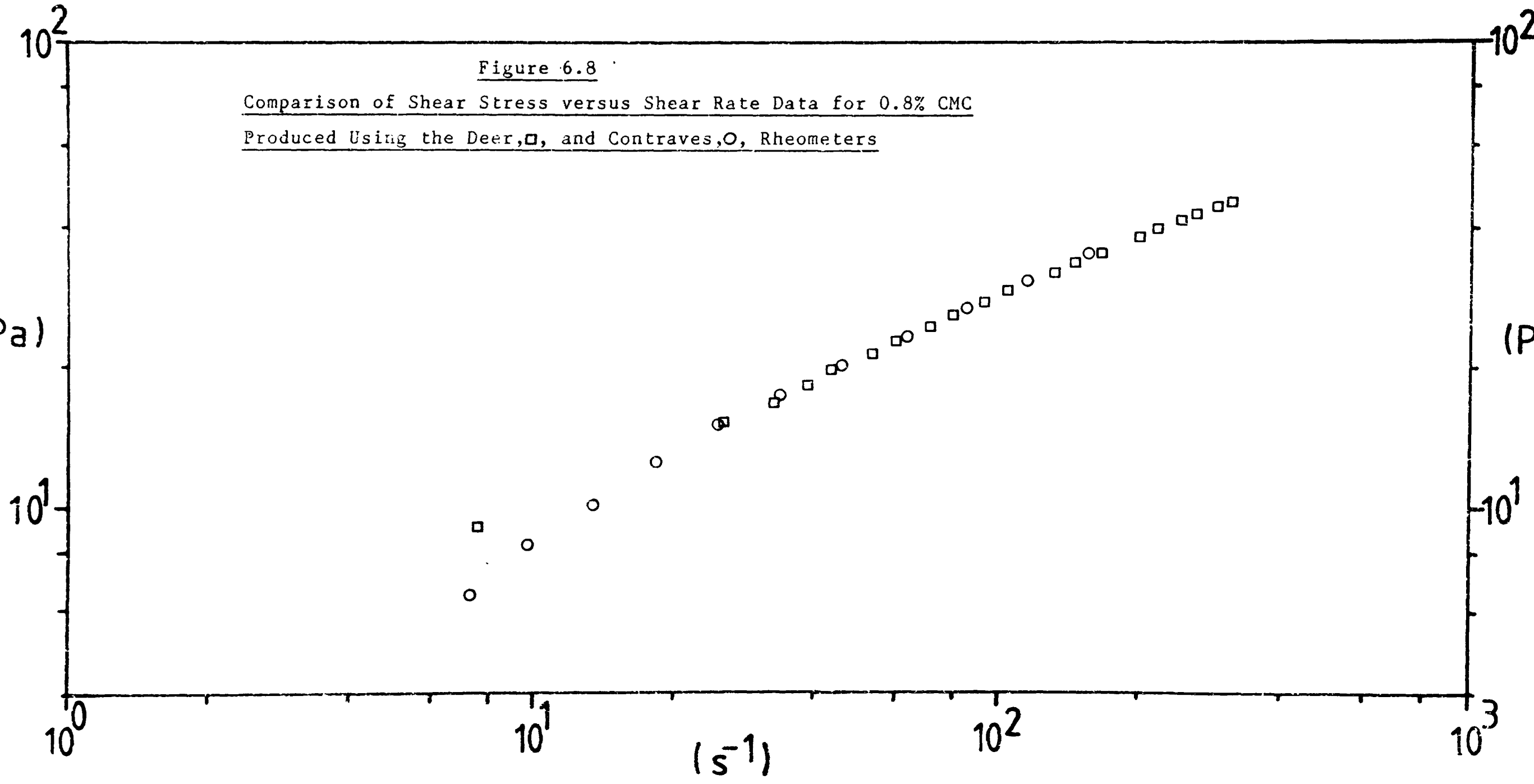

Figure 6.9

Comparison of Shear Stress versus Shear Rate Data for 1.4% CMC Produced Using the Contraves,O, and Weissenberg,Δ, Rheometers

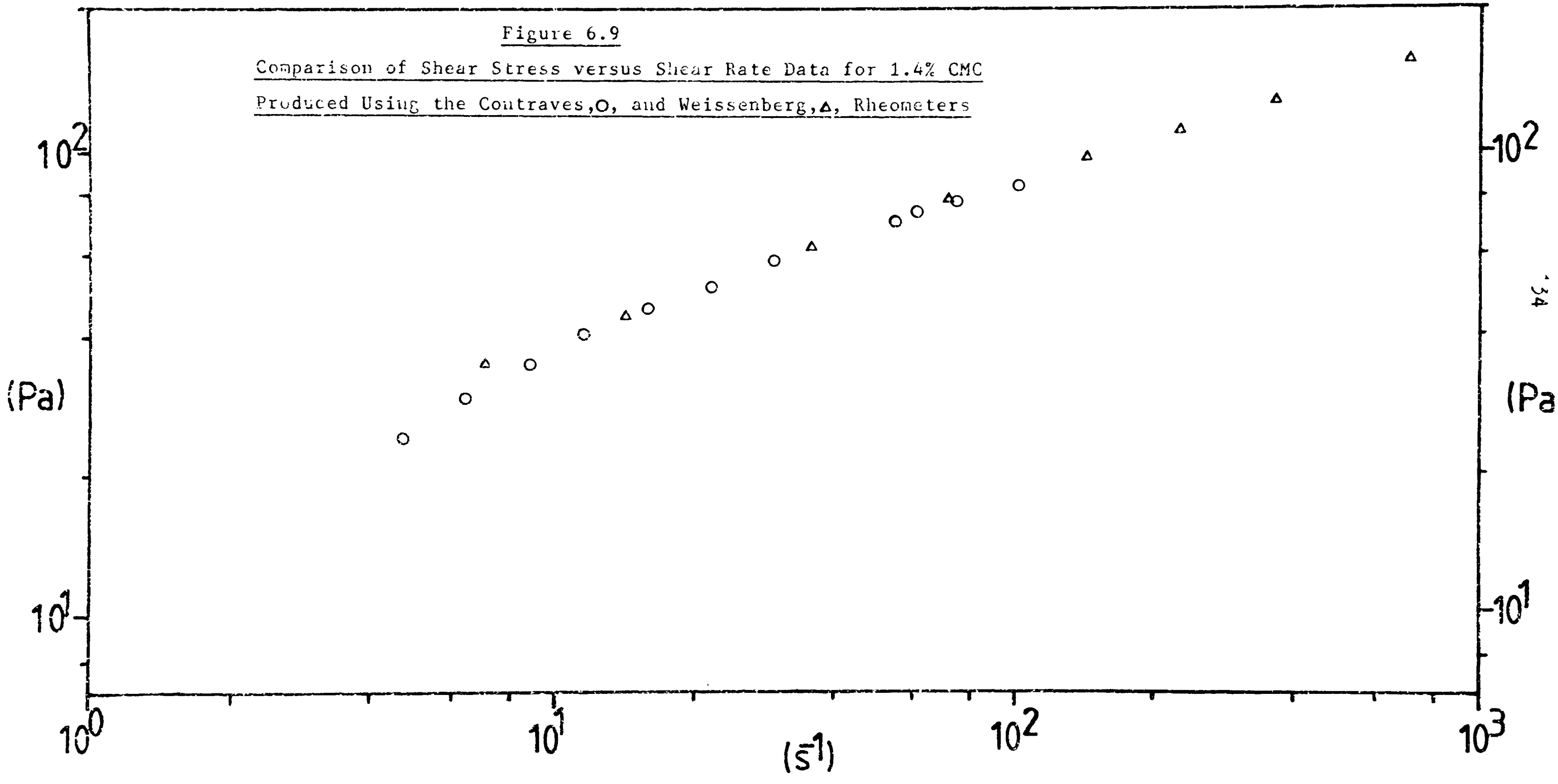

Figure 6.10

Comparison of Shear Stress versus Shear Rate Data for 1.1% CMC Produced Using the Deer,□, and Weissenberg,△, Rheometers

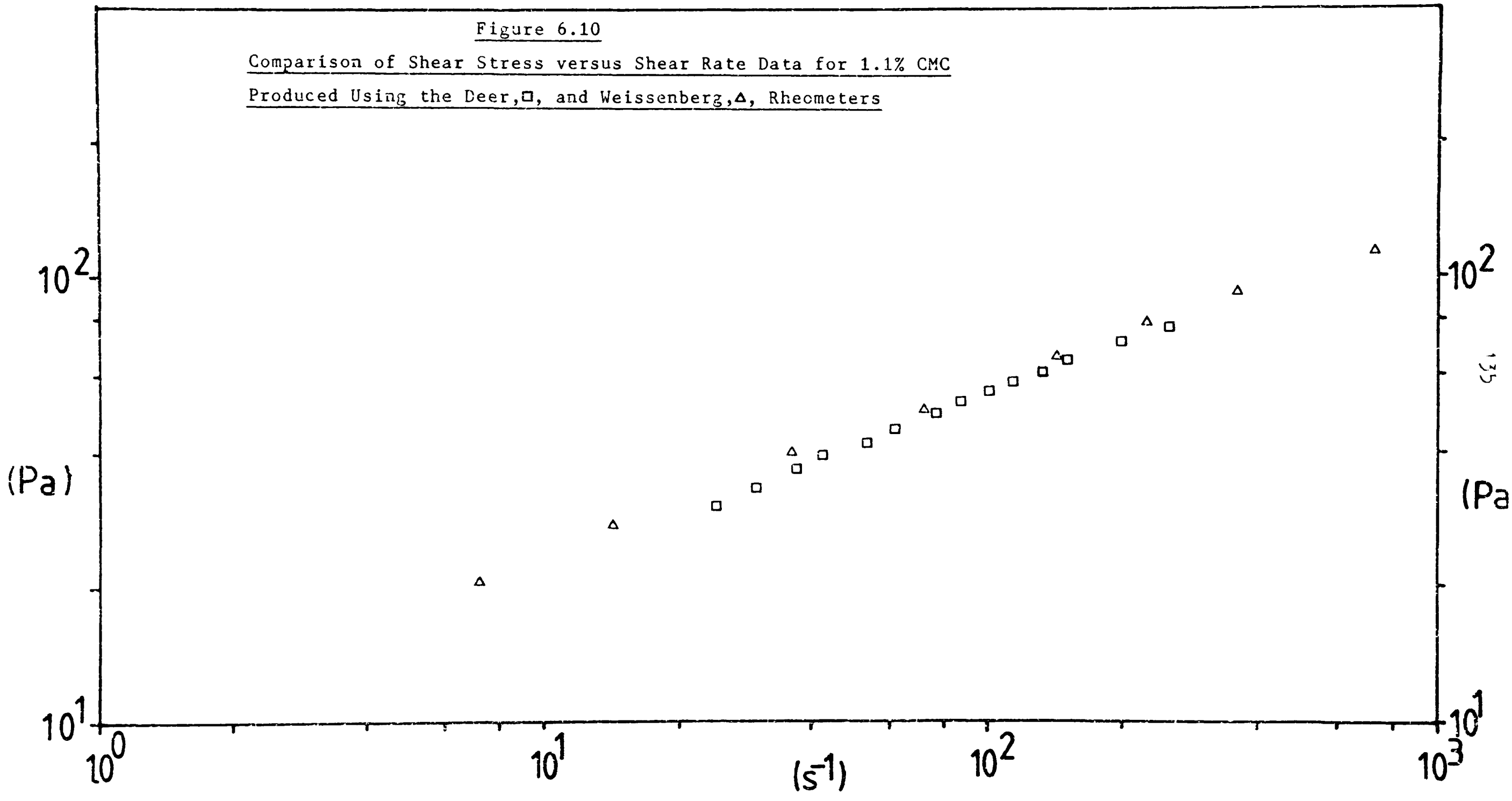

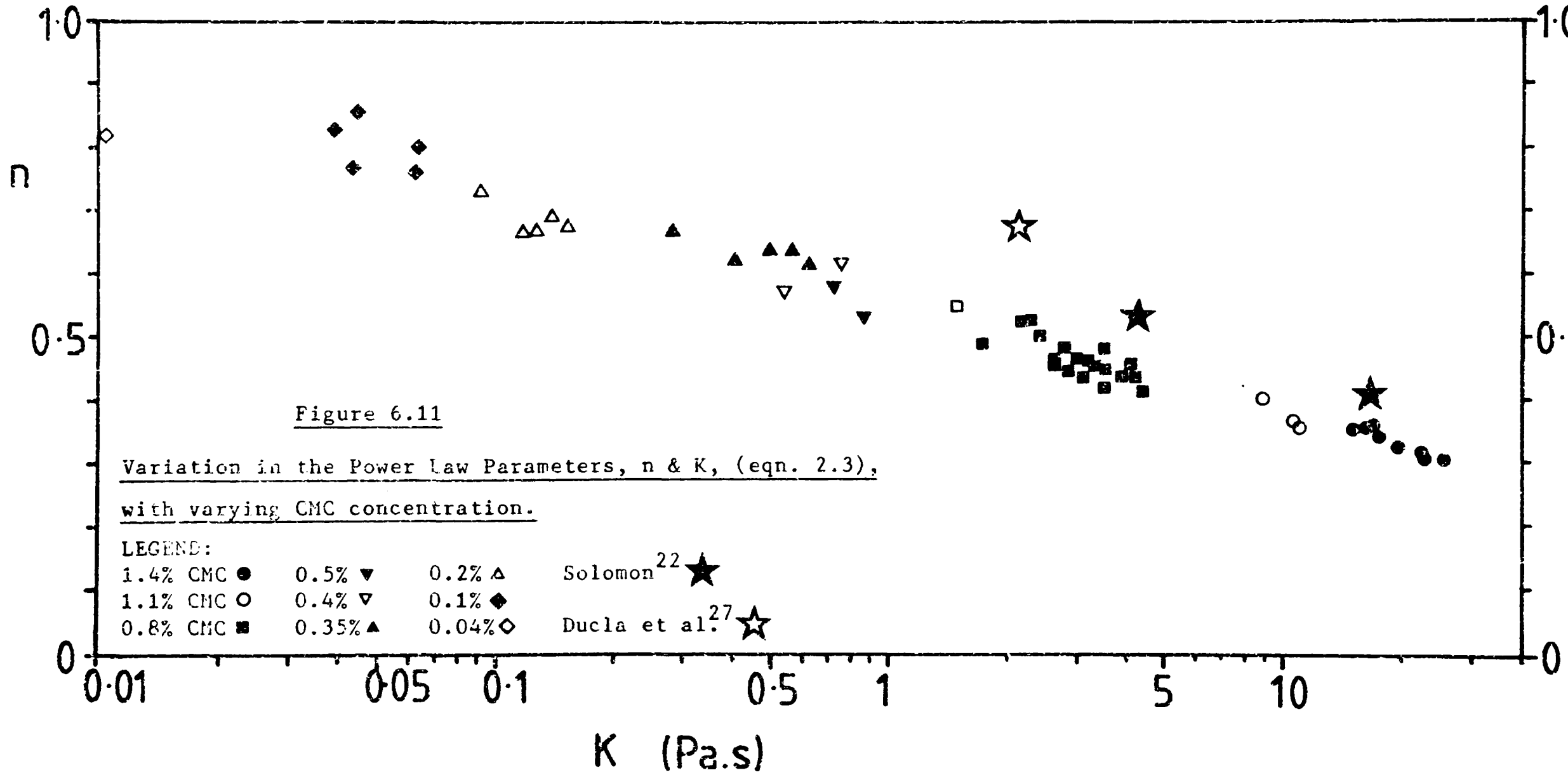

Figure 6.11

Variation in the Power Law Parameters, n & K, (eqn. 2.3), with varying CMC concentration.

were obtained with solutions of different ages and with various levels of yeast in them. It has been found that solution age is an important factor in determining the rheological properties of the CMC solutions. A fresh 0.8% CMC solution containing no yeast had power law parameter values of n = 0.423, K = 4.6 $Pa.s^n$. After 70 hours standing in the 20 litre vessel used for the mass transfer studies, at room temperature, these parameters had altered to n = 0.465 and K = 3.3 $Pa.s^n$. At a representative shear rate of 115 s^{-1}, this gives a reduction in representative viscosity from 0.297 Pa.s to 0.260 Pa.s over a 70 hour period. For a similar 0.8% CMC solution containing yeast, the same representative viscosity was reduced from 0.275 Pa.s (n = 0.458, K = 0.492 $Pa.s^n$) to 0.233 Pa.s (n = 0.492, K = 2.6 $Pa.s^n$) over a 48 hour period. Thus the presence of yeast may accelerate the decomposition of the CMC slightly. The actual addition of the yeast to the CMC solution can also cause the rheological properties to alter. In general slight reductions in apparent viscosity was found when large volumes of yeast were added (50 - 150 gl^{-1}), which may be expected, as the yeast can be considered to be diluting the CMC solution. In some cases slight increases in μ_a were noted, which may be explained as experimental error, as at the concentration used (< 38 g dry $wt.l^{-1}$) the yeast was not expected to enhance the viscosity. This may not be the case, as work carried out within the department, using the same rheological instruments and the same yeast as used here, has shown that a concentration of yeast of 180 g dry $wt.l^{-1}$ has a viscosity of 0.1 - 0.12 Pa.s over the shear rate range of interest here[142]. Thus smaller quantities of yeast may enhance the viscosity slightly.

The results obtained when using the Weissenberg Rheogoniometer to measure the viscoelastic properties of the CMC solutions are shown in table 6.6. It can be seen that no substantial variation in the 1st normal stress difference can be linked to the presence of yeast. The presence of gas bubbles in the 1.1% CMC solution has increased the viscoelasticity.

These bubbles were produced by adding a drop of glucose solution to the CMC and yeast solution. After a short period of time the amount of gas in the liquid was approximately 4% by volume. Microscopic examination showed that the gas bubbles were ca. 0.50 mm in diameter. Samples of this solution were subjected to rheological analysis with the gas bubbles present and then with the gas bubbles centrifuged out.

Table 6.6 Viscous and Viscoelastic Data for CMC Solutions

CMC Concentration	Viscous Parameters Equation 2.3		Viscoelastic Parameters Equation 2.12		Comments
%	n	K	b	A	
1.4	0.325	19.12	0.403	53.7	No yeast
1.4	0.320	19.25	0.410	49.6	No yeast
1.4	0.320	22.80	0.440	49.6	Yeast present
0.8	0.414	4.52	0.662	4.88	No yeast
1.1	0.360	10.74	0.430	29.6	Yeast present
1.1	0.350	11.15	0.400	38.6	Yeast and gas bubbles (4%)

A comparison of these results with those of Solomon[22] (see table 2.1), obtained in similar CMC solutions, show that much higher 1st normal stress differences were obtained here. Similarly inspection of the n and K values show that solutions exhibiting increased shear thinning were produced here for the same concentration of CMC. Data obtained by Ducla et al.[27] for the same type of CMC show much reduced K and increased n values, with their data for 1% CMC solutions near to that obtained here for much more dilute solutions. This data has been included for comparison in figure 6.11. This serves to illustrate the marked effect that the means used to prepare the solutions can have on the rheological behaviour of a liquid.

6.4.2) Physical and Chemical Analysis

Selected samples removed from the vessel during mass transfer experiments were analysed to determine the concentration of yeast, glucose, alcohol and dissolved and suspended material. A known volume of sample was centrifuged to deposit the yeast cells. The supernatant was then removed and the yeast washed with distilled water and then centrifuged again. Samples of yeast and supernatant were dried overnight at 105°C then cooled and weighed.

Further quantities of supernatant were filtered through 0.22 μm millipore filters to remove any suspended particles prior to analysis for glucose and ethanol. Ethanol analysis was carried out using gas liquid chromatography, whilst glucose analysis was carried out using a method developed by Miller[143], using 3,5 dinitro salicylic acid, which reacts with the glucose present producing an orange solution which can be analysed using an UV-visible spectrometer at a wavelength of 540 nm.

CHAPTER 7

POWER AND MIXING IN VISCOUS CMC SOLUTIONS

7.1) Introduction

The principal aim of this work is to determine the volumetric mass transfer coefficient (k_La) and its variation with power consumption, rheological properties and gas flow rate, when using a variety of impeller types and combinations. A greater understanding of the reasons for the variations in k_La, as described in Chapter 8, may be obtained from a study of the manner in which power consumption and gas-liquid mixing are also affected by variations in gas flow rate, rheological properties, impeller speed and impeller type. Such studies are generally presented using the dimensionless numbers described in Chapter 3, section 1. The majority of the studies carried out using viscous liquids show the variation in the gassed and ungassed power numbers, Po_g and Po, with changing Reynolds number, Re. There are two reasons for this use of Re. Firstly, the viscosity is now an important variable where high viscosity liquids are being studied, which is not the case with low viscosity ones. Secondly it has been found that the variation in Po_g with varying gas flow rate is much reduced by increasing viscosity, as described in Chapter 3. This reduces the usefulness of plots of Po_g versus the gas flow or aeration number, Fl_g. Thus the format generally used here is to present Po_g and Po as functions of Re.

In addition to this, some variations in gas hold-up, ε , and bulk mixing patterns are reported here in conjunction with the variations in Po_g. The hold-up can play a major role in the determination of the gas-liquid mass transfer. Generally the variation in the mass transfer coefficient k_L, is limited in a given system, with the major changes in the volumetric mass transfer coefficient, k_La, being effected through changes in the interfacial area, a[144]. This in turn is dependent on the

gas hold-up, as increasing ε increases a, for a fixed bubble size. In viscous liquids this may be a gross over simplification[13], with bubble diameter, shape and residence time affecting both k_L and a. However ε is still a useful indicator by which agitation efficiency may be considered. The bulk mixing is important as it can affect both $k_L a$ and the accuracy with which $k_L a$ can be measured. It is necessary for the viscous liquid to be reasonably well mixed, with no large stagnant zones, to ensure that the whole volume of the liquid is being utilised effectively. It is also desirable to achieve a uniform level of dissolved oxygen, as this allows the mass transfer process to be more easily modelled. For these reasons some of the work reported here has been carried out using two impellers mounted on the shaft. This has been found to be advantageous in promoting adequate liquid mixing in viscous solutions[22].

The following impeller systems, which are described in Chapter 5 and shown in figures 5.3 - 5.5 and plate 2, were investigated:

a) Single disc turbine : diameter = T/2 & T/3
at a height from the base of the vessel of c = T/4

b) Two disc turbines : diameter = T/2 & T/3
with c = T/4 and a separation, s = 3T/8

c) A single disc turbine in combination with a 45° pitched blade turbine : diameter = T/2
c = T/4, s = 3T/8

d) Two Intermig impellers : diameter = 0.58T
c = T/4, s = T/2

Initially the results obtained for unaerated mixing are presented for all the impeller systems in viscous CMC solutions. This is followed by the results obtained using disc turbines for aerated mixing, then the results of aerated mixing using the other impeller combinations are presented. In most of the figures the independent variable used is the Reynolds number. From Chapter 3, section 1, it can be seen that this relies upon the use of a mixer shear rate constant, k_s, in the determination of the apparent viscosity when shear thinning liquids are used. Following

Metzner and Otto [23], the value chosen for k_s is 11.5, which has often been used in the literature, allowing a comparison of this work with that of others (see Chapter 3). The shear thinning nature of the solutions used makes it impossible to quote the apparent viscosity, μ_a, when describing the differences between the results obtained. In order to help visualise the relative viscosities of the solutions used, a representative shear rate of $\gamma_r = 100\ s^{-1}$ has been used to determine a representative viscosity, μ_r. This corresponds to μ_a at an impeller speed of N = 8.7 s^{-1} when $k_s = 11.5$. It shoud be emphasised that the values of μ_r quoted do not correspond to μ_a within the vessel, except when N = 8.7 s^{-1}, and μ_r values have not been used in the determination of any of the data quoted in this thesis.

Finally, in section 7.4, the overall performance of the various agitation systems used is compared by looking at their overall effect on the fermentation variables, dissolved oxygen concentration and respiratory quotient. These provide an additional means of judging the usefulness of the impellers in the viscous solutions.

Conclusions regarding the agitator performance are discussed at the end of each section where relevant. The overall conclusions which can be drawn from the studies discussed in this chapter and the next are detailed in Chapter 9, with some suggestions for further work which can usefully be carried out.

7.2) Unaerated Mixing

The results obtained for unaerated mixing of various CMC solutions (0.4 - 1.4% w/w) using one disc turbine are shown in figures 7.1a, (D = T/3) and 7.1b, (D = T/2). The most comprehensive of the literature data have been included for comparison. These cover Newtonian liquids[39], shear thinning inelastic liquids[24,25] and shear thiuning viscoelastic liquids[42]. It can be seen that the two impeller sizes give very similar

Po - Re curves, which is in keeping with the results found by other workers[22]. However both impeller sizes show higher Po values in the laminar regime (Re < 10) than are given by inelastic liquids. This enhancement of Po at Re < 10 occurs to the same degree (ca.40%) for the more viscous CMC solutions (0.8 and 1.4%), which are the only solutions used here which show moderate viscoelastic properties, as described in Chapter 6. This enhancement of Po in the laminar regime is clearly related to the viscoelastic properties of the solutions used. It is the same as that shown in figure 7.1a for viscoelastic liquids[42], and does not occur when less concentrated CMC solutions are used which show no measurable viscoelasticity. This can be seen in figure 7.1b for 0.4% CMC agitated using one disc turbine (D = T/2), in the laminar regime this data is lower than that seen for more concentrated solutions and is similar to the literature data for inelastic liquids.

It is possible to make the results seen in the laminar regime, when agitating viscoelastic liquids, coincident with those of inelastic liquids, by reducing the value of k_s. This would reduce the average shear rate at a given impeller speed, increasing the apparent viscosity and hence reducing Re (see Chapter 3, section 1). The data collected here are insufficient for a precise value of k_s to be determined, but k_s is approximately 9.5 for a 1.4% CMC solution and 10 for a 0.8% CMC solution. These compare with a value of k_s = 11.5 which has been used in the preparation of the figures shown. Thus only a slight reduction in k_s is required. In comparison, Ducla et al.[27] used very similar CMC solutions to those used here and found much lower values for k_s. They obtained k_s = 7.1 for turbines and k_s = 6.1 for pitched blade turbines in 1% and 1.25% CMC solutions.

This alteration of k_s to make the Po - Re curves coincident in the laminar regime, rests on the assumption that the viscoelastic properties

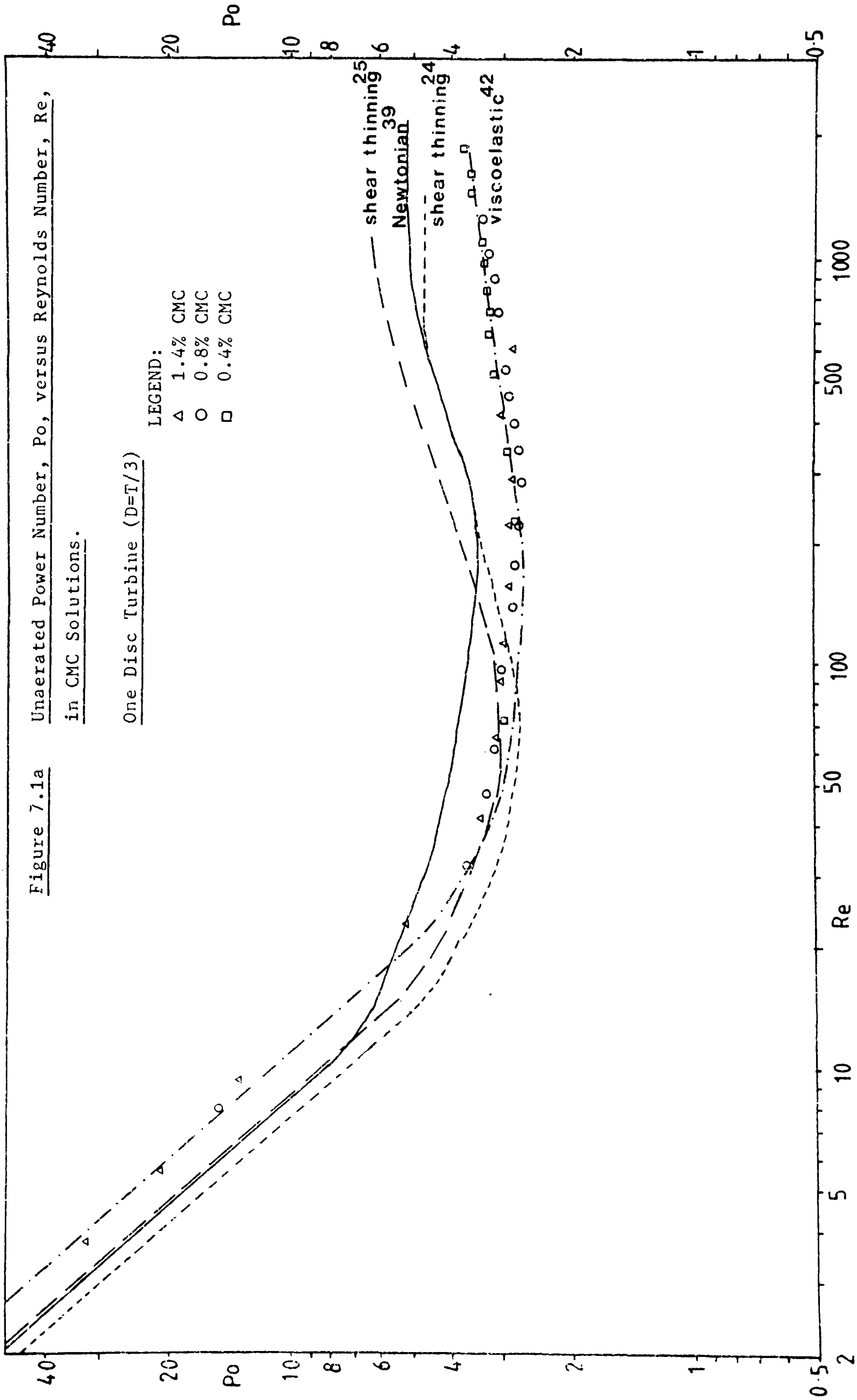
Unaerated Power Number, Po, versus Reynolds Number, Re,
in CMC Solutions.
One Disc Turbine (D=T/3)
LEGEND:
Δ 1.4% CMC
O 0.8% CMC
□ 0.4% CMC
shear thinning 25
Newtonian 39
shear thinning 24
viscoelastic 42
Po
Re
40
20
10
8
6
4
2
1
0·5
100
500
1000
50
10
5
2

Figure 7.1a

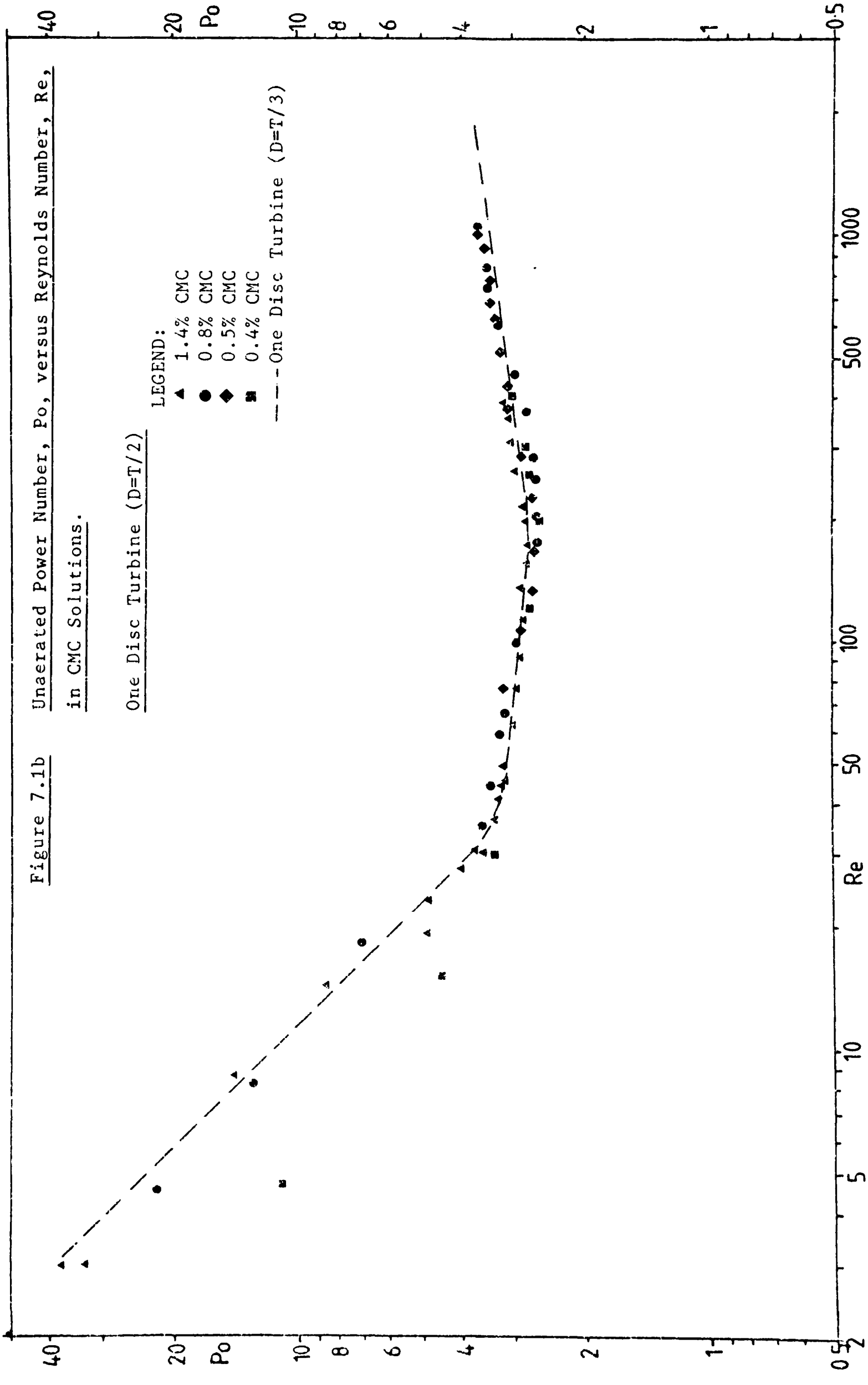
Unaerated Power Number, Po, versus Reynolds Number, Re,
in CMC Solutions.
One Disc Turbine (D=T/2)
LEGEND:
1.4% CMC
0.8% CMC
0.5% CMC
0.4% CMC
---One Disc Turbine (D=T/3)
Po
Re
40
20
10
8
6
4
2
1
0.5
100
500
1000
5
10
50

Figure 7.1b

of the liquid are reducing the average shear rate found within the vessel, compared to that found for an inelastic liquid. An alternative explanation is that the viscoelastic properties of the liquid do not affect the average shear rate, in which case the determination of Re is correct and a higher power consumption and hence increased Po are found at a given Re. Whichever view is correct, the resultant effect is highly dependent on the rheological properties of the solution and the geometry of the agitator. Solomon[22] found that solutions of 1.4% CMC showed the same degree of enhancement when agitated by single disc turbines (D = 0.25 - 0.6T), or a pitched blade turbine (D = T/2), or by a combination of a disc turbine and a pitched blade turbine (D = T/2). However, when using a 4.5% Xanthan gum solution, which had very similar viscoelastic properties to the 1.4% CMC solution, enhancement was not found when using a single disc turbine, although it did occur when using the impeller combination or when using a pitched blade turbine alone.

The solution of Xanthan gum used by Solomon[22] did exhibit a yield stress, which may have affected the results obtained. Separation of the effects due to the viscoelastic properties from effects due to the viscous and shear thinning behaviour of the solutions used is not easily done. Prud'Homme and Shaqfeh[44] measured the torque required to agitate Boger fluids in the laminar regime using a disc turbine (D = 0.44T). Boger fluids have the advantage of being highly viscoelastic, yet with a viscosity which is virtually independent of the shear rate, as described in Chapter 2, section 1. They found that increasing the viscoelasticity of the solution, by increasing the concentration of polyacrylamide in the solution, increased the enhancement of the torque, although the viscosity remained the same. They explained these effects in terms of the additional energy required to produce the secondary flows which result from competition of the elastic forces with the inertial forces.

In the transition region ($10 < Re < 10^3$) it can be seen that

shear thinning liquids show a considerably reduced Po value when compared to Newtonian liquids. Inelastic shear thinning liquids show a relatively sharp minimum at Re = 50. The liquids used here show a shallow minimum at Re = 70 to 200. This extends the region of reduced power consumption to higher Re, delaying the onset of fully turbulent mixing. This has been attributed to the drag reducing tendency of viscoelastic liquids[42], which is supported by the results presented by Hocker et al.[145] and also by Schugerl[13], for polyacrylamide solutions. These highly viscoelastic solutions do not exhibit a minimum in the Po - Re curve; with increasing Re, Po falls to a low value and does not increase again at high Re.

Solomon[22] found that the impeller diameter and type had a marked effect on whether fluids which exhibited low levels of viscoelasticity followed the curve for inelastic fluids or viscoelastic fluids in this region. For 1.4% CMC and 4.5% Xanthan gum solutions, impeller size had no effect and the data follows the curve for viscoelastic fluids. In 2% Xanthan gum using small (D < 0.34T) impellers the data follows the viscoelastic curve, but for large impellers (D = 0.5 & 0.6T) the data follows the inelastic line. Further results were obtained using Carbopol solutions. These had lower levels of viscoelasticity than Xanthan gum or CMC solutions, however anomalous results were obtained, with a 0.17% Carbopol solution following the curve for viscoelastic data when using small impellers whilst the more viscoelastic and viscous 0.3% Carbopol solution followed the curve for inelastic fluids at all impeller sizes.

At Re > 10^3 there is considerable variation in the level of Po obtained by different workers. Here the fully turbulent regime is developed and the Po - Re curve levels out. It is possible that these variations in the value of Po which are found in this region can be attributed to minor variations in geometry, particularly on the small scale[42]. Rushton et al.[38] and Bates et al.[39] found that the degree of

baffling of the vessel had a marked effect in this region, with wider baffles increasing the constant value of Po seen at Re > 10^4 for Newtonian fluids.

Figures 7.2a and 7.2b show similar Po - Re curves to those shown in figure 7.1, but for two disc turbines mounted at a separation of 3T/8. The general shape of the curves is similar to that found for one disc turbine, but at higher Po values. In general, good agreement is obtained in the laminar regime with the literature data for two disc turbines in Newtonian[24,39] and inelastic shear thinning liquids[24], the exception being agitation of 0.8% CMC using two small disc turbines (D = T/3), which shows enhanced Po values, similar to those seen when agitating viscoelastic liquids with a single disc turbine. This enhancement is also observed under gassed conditions (see next section), but is not shown by the other liquids used. That little enhancement is seen in the laminar regime when agitating with two disc turbines can be attributed to the interaction of the two impellers, which alters the power consumption. Two impellers at a high enough separation would be expected to give Po values of twice that of one impeller. As the impellers are brought closer together the flow patterns produced by each interact, altering the power consumed. Bates et al.[39], working with Newtonian liquids, found that at an impeller separation greater than one impeller diameter (s > D), two disc turbines gave slightly less than twice the power consumption of one disc turbine. At s = D the power consumed rose to just over twice that of one disc turbine and for s < D the relative power consumption varied, rising to a peak then falling sharply as s approached zero. Metzner et al.[24] varied the impeller diameter, and hence s/D, for two disc turbines in Newtonian and shear thinning liquids. They found that the variation in Po as s/D varied was reduced in the non-Newtonian liquids, which they linked to the rapid increase in viscosity due to the fall in shear rate away from the impellers. Allsford[146] has determined the power consumed by two small disc turbines in viscoelastic CMC solutions.

Figure 7.2a Unaerated Power Number, Po, versus Reynolds Number, Re in CMC Solutions.

Two Disc Turbines (D=T/3)

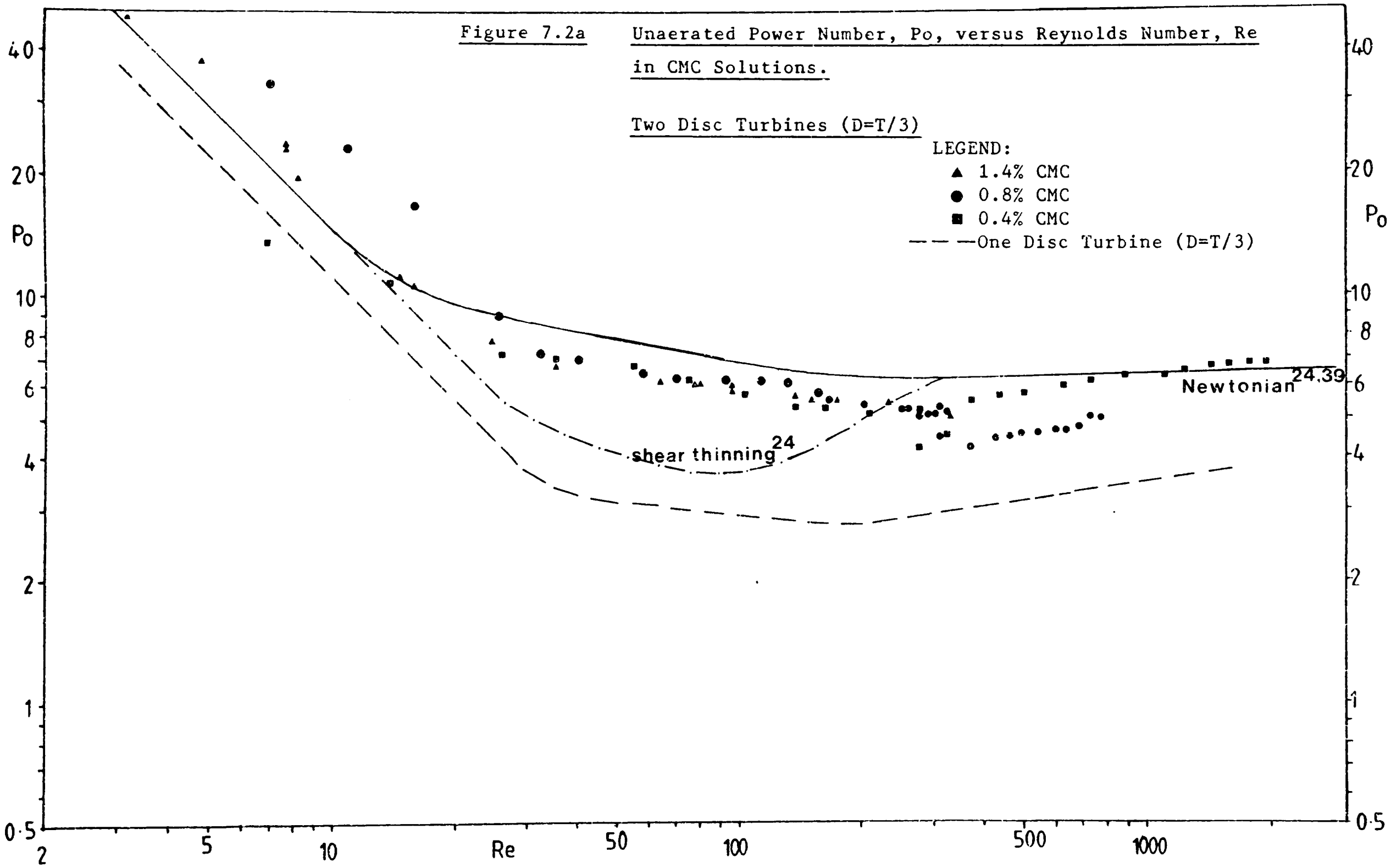

Figure 7.2b Unaerated Power Number, Po, versus Reynolds Number, Re, in CMC Solutions.

Two Disc Turbines (D=T/2)

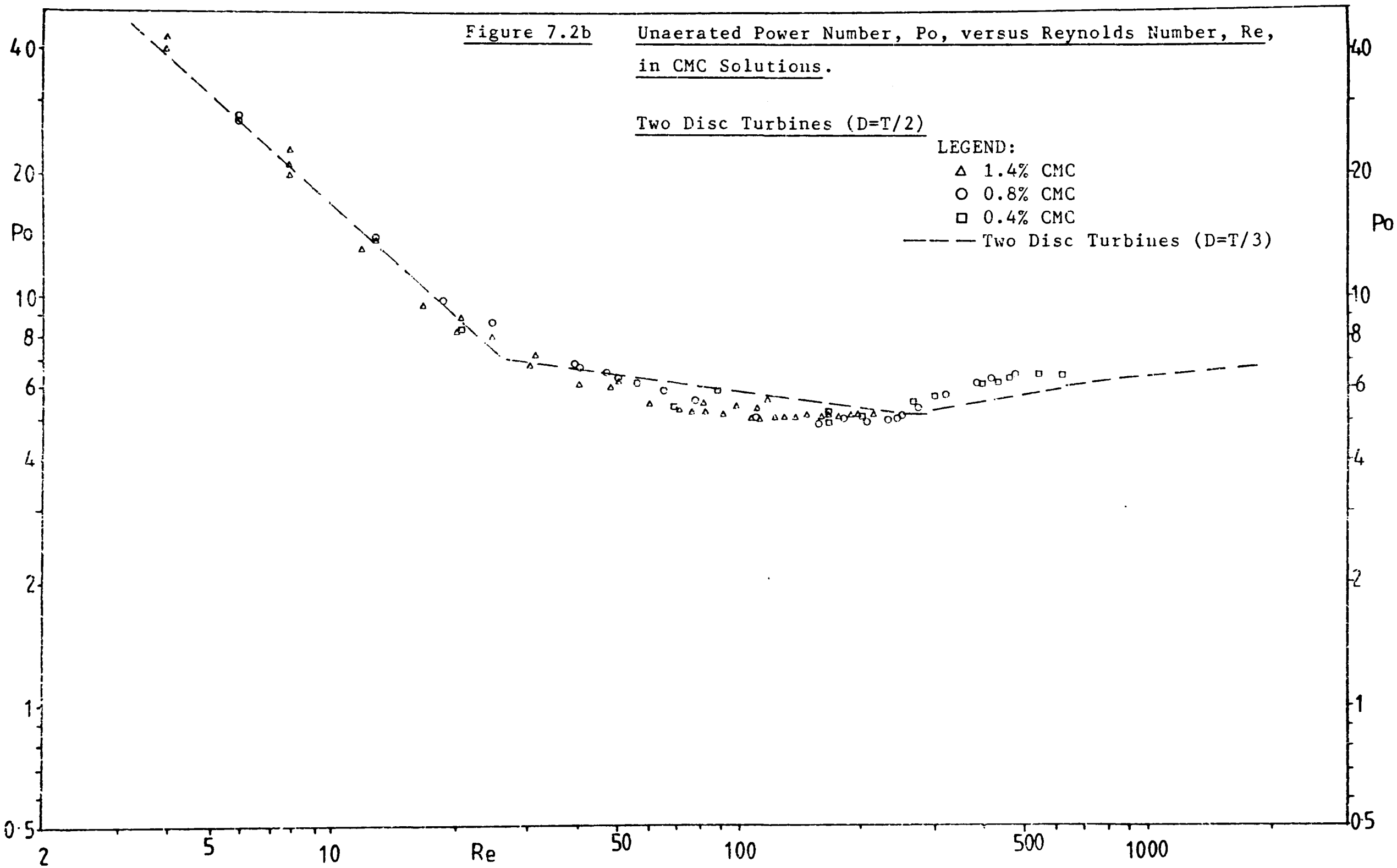

He measured the torque for each impeller separately, using strain gauges mounted above each impeller, similar to those used here (see Chapter 5). This showed that a complex interaction does take place between the impellers even if s > D. Clearly the s/D ratio is of importance in determining the power consumed by dual impeller systems, as are the rheological properties of the liquid. Here two small disc turbines (D = T/3) were used at a separation of s = 3T/8 = 1.12D. The power consumed in the laminar region was 1.6 times that consumed by one disc turbine, except in 0.8% CMC where: Po_{2DT}/Po_{1DT} = 2.3. For two large disc turbines (D = T/2) in all the liquids used, s = 3T/8 = 0.75D and Po_{2DT}/Po_{1DT} = 1.6.

The interaction of the impellers again produces a deviation from the behaviour expected (from consideration of the results obtained using one disc turbine) at higher Reynolds numbers. When using two small disc turbines (D = T/3), two different levels of Po can be encountered at Re > 300. This was linked to the formation of two types of mixing pattern, as shown in figure 7.3. Mixing pattern A, in which liquid circulates between the two impellers gave a lower power consumption than mixing pattern B. Mixing pattern B, in which two distinct zones of mixing located around each impeller were visible, was found to be more stable at high Re in the lower viscosity (0.4% CMC) solution, whilst mixing pattern A was preferred at high Re in the more viscous solutions. Similar behaviour was noted under gassed conditions (see next section) and has been seen in water agitated by two disc turbines (D = T/3)[147]. The transition between the two mixing patterns occurred at Re = 300, with either mixing pattern occurring at or around this Re depending on the means used to reach this level of agitation. Gradually increasing the impeller speed from a lower value led to mixing pattern A. Whilst a rapid increase in impeller speed led to mixing pattern B.

When using two larger disc turbines (D = T/2) only mixing pattern B was observed in this region. It is assumed that the reduced gap

Figure 7.3

Mixing Patterns Obtained in CMC Solutions at Re > 300 When Agitating with Twin Disc Turbines (D=T/3). [See Figure 7.2a for Associated Po Values]

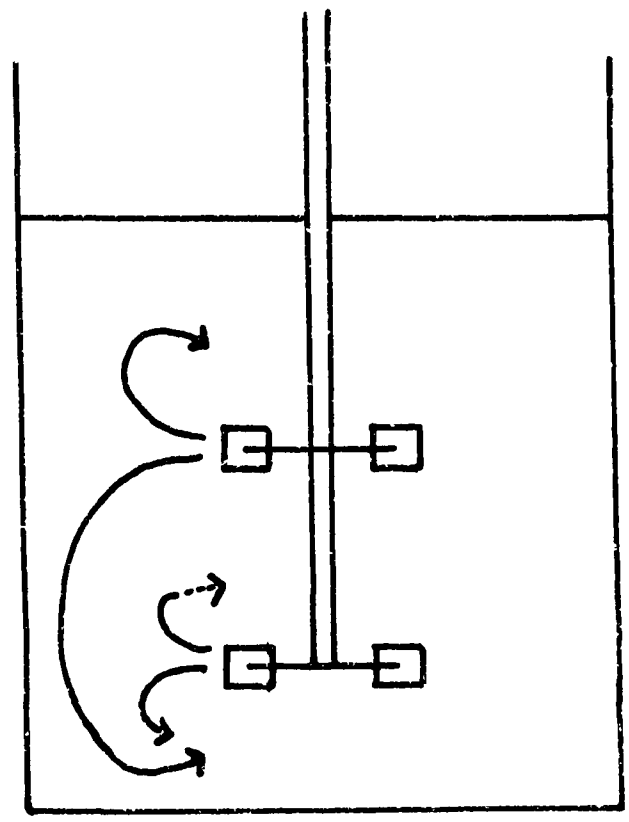

A

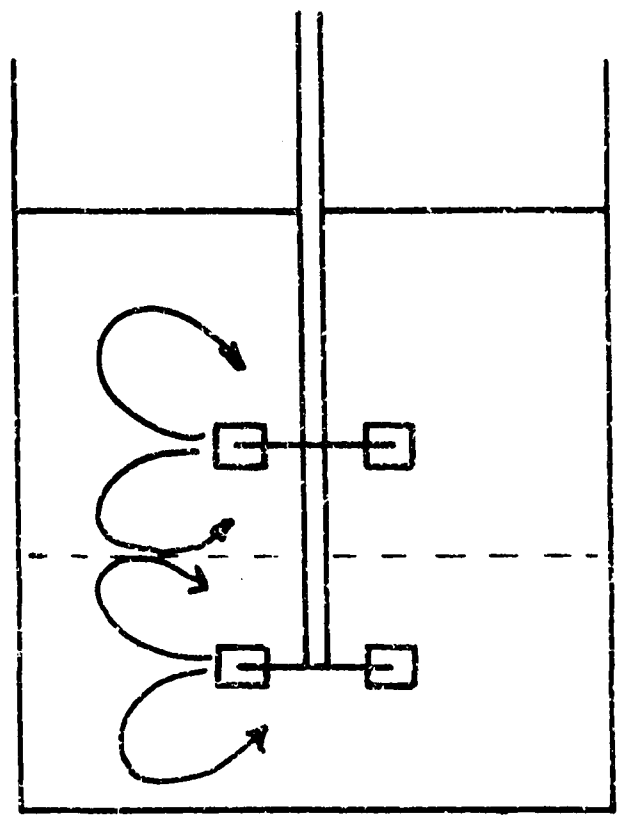

B

between the impeller tip and the vessel wall was instrumental in preventing pattern A from forming.

Figure 7.4 shows the results of ungassed power consumption studies using the two Intermig impellers (D = 0.58T) and when using the 45° pitched blade turbine in combination with a disc turbine (D = T/2). For these impeller combinations the direction of rotation determines the direction in which the liquid is pumped around the vessel. The pitched blade turbine can pump upwards or downwards. The Intermig pump in both directions at once. For descriptive purposes the label " upward pumping " will be used to denote the state in which the central blades of the Intermig are pumping upwards and the outer blades are pumping downwards. For the opposite case, " downward pumping " will be used.

For the pitched blade turbine combination, similar power consumption was noted at Re < 100 to that obtained using two disc turbines of the same diameter. Above Re = 100 the power number continued to fall to lower values than those obtained with two disc turbines, levelling out at Re = 200 - 300, Po = 4.6. For 1.4% CMC upward pumping at high Re required more power than downward pumping. The reverse was found in 0.8% CMC. These variations in Po at high Re were accompanied by large distortions in the surface of the liquid, which presumably causes the variations seen in the power consumption.

Bates et al.[39] studied various impeller types in Newtonian liquids. They found that the Po values in the laminar regime were dependent only on the blade height, with taller blades showing high Po. The pitch of the blades, the presence of a disc and whether the blades were curved or not, did not affect Po in the laminar regime, although it did affect Po in the turbulent regime, with pitched blade turbines showing much lower Po values than disc turbines. Thus the shape of the curve found here for a pitched blade turbine in combination with a disc turbine is as would be

Figure 7.4 Unaerated Power Number, Po, versus Reynolds Number, Re, in CMC Solutions.

a) Pitched Blade/Disc Turbine Combination (D=T/2)

b) Two Intermigs (D=0.58T)

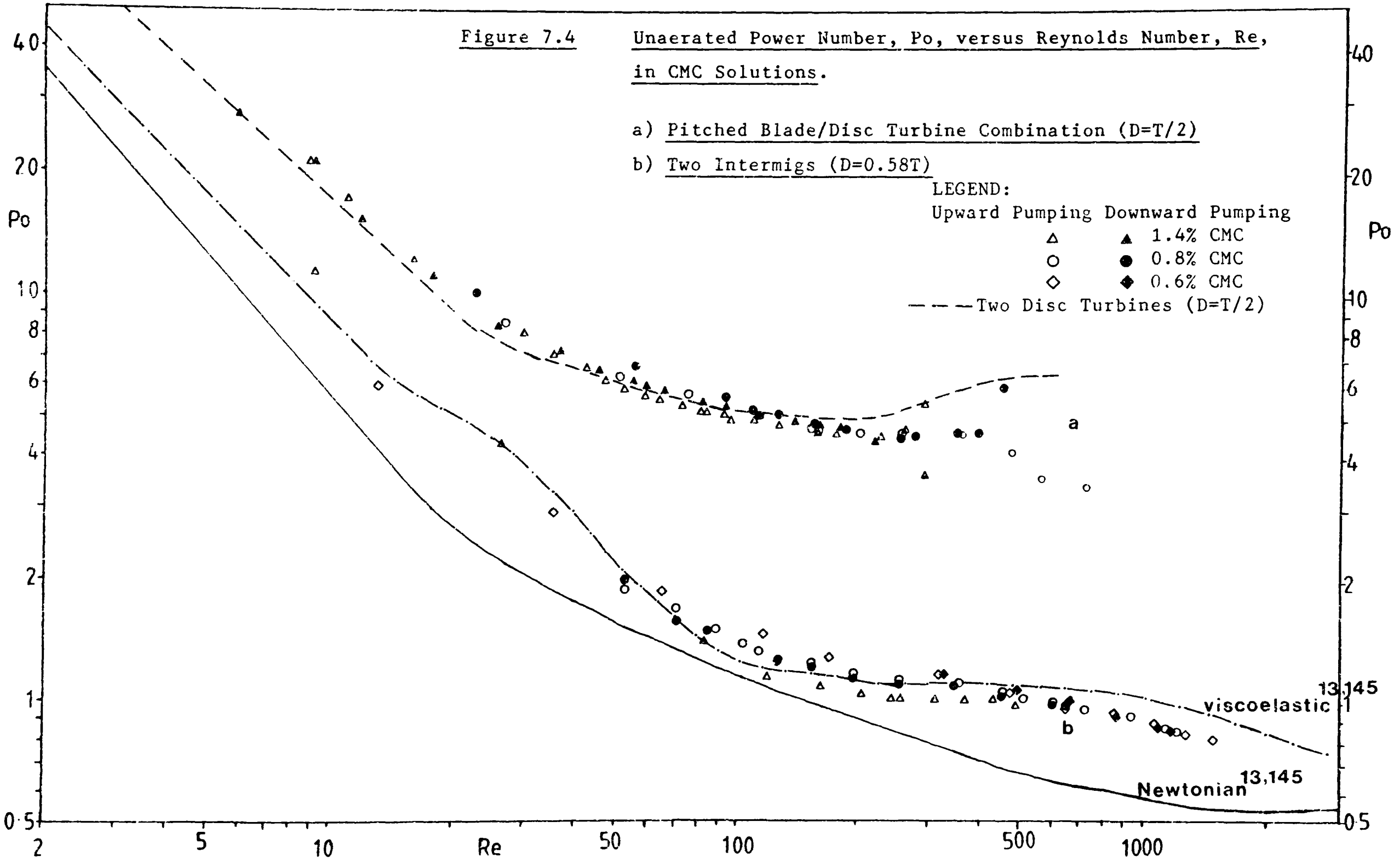

expected from a consideration of the literature results cited in Chapter 3.

For the Intermig impellers, direction of rotation made no difference to the power consumed for the range of impeller speeds and solutions studied. These impellers showed a much lower power consumption than the other impeller combinations at all Reynolds numbers. In addition, no minimum in the Po - Re curve was found in the transitional regime. Po fell with increasing Re up to the maximum impeller speeds attained before surface aeration occurred. The bold line in figure 7.4 is for Newtonian liquids and the dashed line is for highly viscoelastic PAA solutions in a similar system[13,145]. It can be seen that in the solutions used here the data deviate markedly from the Newtonian line at high and low Reynolds numbers. This is very similar to the results presented by Hocker et al.[145] and Schugerl[13], for agitation of highly viscoelastic polyacrylamide solutions using Intermigs. This behaviour is presumably linked to the rheological complexities of the solutions used, in a similar manner to that found for disc turbines.

7.3) Aerated Mixing

7.3.1) Disc Turbine

Figure 7.5 shows the data collected at a flow rate of ½ vvm, for one disc turbine (D = T/2), in a range of CMC solutions. For comparison the solid line shows the data presented in figure 7.1b, that is for the same solutions and impeller under unaerated conditions. For the less concentrated CMC solutions ($\leqslant$ 0.8%), the gassed power number Po_g begins to fall below Po at a point where stable gas filled cavities can be seen forming behind the blades of the impeller. For these solutions this occurs in the transition region between laminar and turbulent flow. At lower Re the gas rises straight through the impeller region, although small bubbles can be seen trapped in the liquid behind the impeller blades, which moves with the impeller. In 1.4% CMC small cavities become attached to the impeller blades at lower Re in the laminar regime. The cavities and the small bubbles in the liquid do not appear to affect Po_g, which closely follows Po in the laminar regime and beyond, up to the point at which large stable cavities appear and Po_g is reduced compared to Po. With increasing solution concentration this point is reached at higher impeller speeds, although the increasing viscosity reduces Re, until for 1.4% CMC the straight line found in the laminar regime for Po and Po_g virtually continues at higher Re in the transitional region under gassed conditions. This may suggest that the presence of the gas filled cavities reduces the turbulence generated by the impeller and extends the region of laminar flow.

The relationship between the point at which Po_g and Po deviate and the impeller speed, diameter and number is shown for disc turbines in table 7.1. It can be seen that increasing impeller diameter reduces the speed at which this point occurs, but no single dependence on N,D and μ_a is apparent. For the larger impellers used, (D = T/2), the speed rises with increasing number of impellers, but when smaller impellers are

Figure 7.5 Aerated Power Number, Po_g, versus Reynolds Number, Re, in CMC Solutions.

One Disc Turbine (D=T/2), ½ vvm

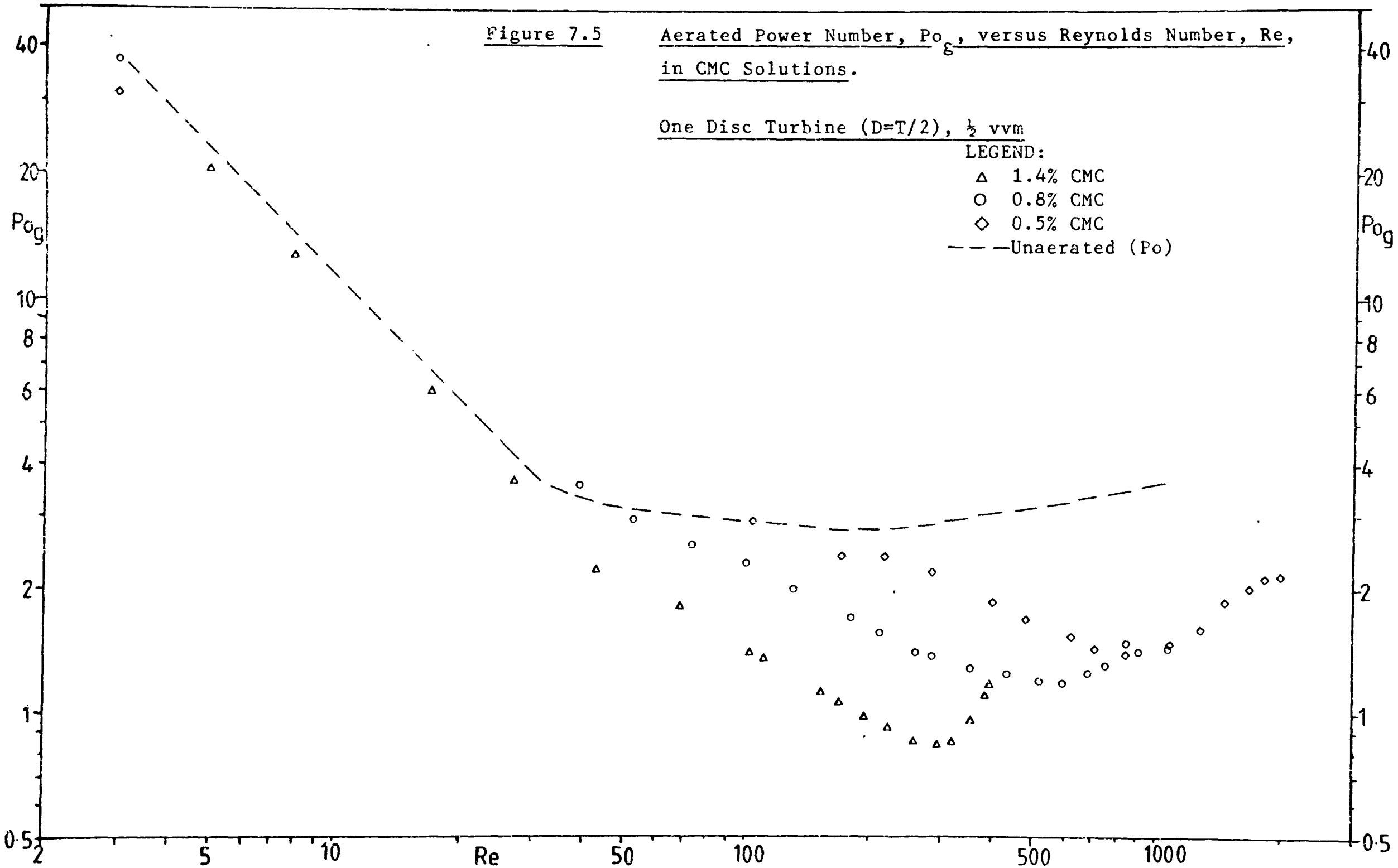

Table 7.1

Criteria for Onset of Stable Cavity Formation and Divergence of Po_g from Po

Solution Concentration	μ_r ($\dot{\gamma}_r = 100\ s^{-1}$)	Small Impeller (D = T/3) N	Re	Po_g	Fr	ND	Large Impeller (D = T/2) N	Re	Po_g	Fr	ND	
1.4%	0.858	4.5	35	3.4	0.206	0.45	2.4	27	3.64	0.088	0.36	Single
0.8%	0.347	3.2	60	3.0	0.104	0.32	1.8	53	3.00	0.050	0.27	Disc
0.4%	0.071	2.2	124	2.6	0.089	0.22	1.75	200	2.70	0.047	0.26	Turbines
1.4%	0.858	4.4	30	7.0	0.197	0.44	2.8	38	5.40	0.120	0.42	Dual
0.8%	0.347	2.5	43	6.7	0.064	0.25	2.1	84	5.00	0.067	0.32	Disc
0.4%	0.071	1.7	79	6.0	0.029	0.17	2.3	250	5.00	0.081	0.35	Turbines

used (D = T/3), the speed required falls with increasing number of impellers. It seems likely that this is linked with the variation in interaction of the impellers seen with varying s/D ratios, as discussed in the previous section for unaerated mixing.

As the impeller speed is further increased, Po_g continues to fall whilst the cavities grow larger. In the more viscous solutions (1.4 & 0.8% CMC) the amount of gas held within the impeller increases until a stage is reached where the impeller is almost completely enveloped in gas, similar to the doughnut described by Yagi and Yoshida[49] (see Chapter 3). Here gas is not being dispersed, but coalesces with the gas in the impeller region before being released as large bubbles which rise vertically through the liquid in the region of the impeller shaft. This build up and release of gas is periodic particularly with more viscous solutions. This causes a slight variation in torque reading, which is most noticeable when using a small diameter disc turbine (D = T/3), as described below.

Further increases in impeller speed lead to the onset of gas dispersion. This occurs as a cloud of bubbles which enter the well mixed liquid cavern around the impeller. In 0.8% CMC agitated with a disc turbine (D = T/2) the size of this cavern is such that it reaches to the vessel walls, when the impeller speed required to produce a bubble cloud is reached. The bubbles recirculate through the impeller and at the walls are free to rise through the liquid. Thus in 0.8% the impeller speed required to form a bubble cloud, N_{BC}, is the same as that required to produce complete distribution of the gas, N_{CD}. At this point the gas and liquid circulation within the lower half of the vessel is controlled by the impeller, whereas circulation in the upper half of the vessel is controlled by the action of the gas rising through the liquid, so N_{CD} cannot be assumed to give complete or full mixing of the vessel contents. For agitation with one disc turbine (D = T/2) in 0.8% CMC, $N_{BC} = N_{CD} = 4.5\ s^{-1}$ ($P/V = 0.53\ kW.m^{-3}$). For 1.4% CMC the cavern size is smaller

and gas bubbles are retained more effectively within the cavern, here N_{BC} = 7.9 s^{-1} and even at this speed the majority of the gas still escaped the impeller region as large bubbles. Complete distribution of the gas over the whole vessel area was achieved at N = 13 s^{-1}, P/V = 7.6 $kW.m^{-3}$ in 1.4% CMC when using a single large disc turbine (D = T/2), although large regions in the upper part of the liquid remained virtually stagnant, even at the highest speed used (N = 17 s^{-1}, P/V = 24.2 $kW.m^{-3}$). Here the passage of the gas through the upper half of the liquid did little to increase the circulation of the liquid.

In solutions of lower apparent viscosity, with μ_r = 0.17 Pa.s or less, corresponding to a CMC solution of 0.5% or less, gas distribution occurs in a similar manner to that in water, but at higher impeller speeds as the viscosity increases. This can be seen from the data contained in table 7.2. This type of distribution is described in full elsewhere[42,48]. No bubble cloud is produced and the onset of adequate gas and liquid mixing can be considered to occur at the impeller speed which produces complete dispersion of the gas throughout the liquid, N_{CD}. When agitating with a single disc turbine (D = T/2), N_{CD} for 0.5% CMC (μ_r = 0.167 Pa.s) is 4.6 s^{-1}. This is similar to N_{CD} for 0.8 % CMC (μ_r = 0.347 Pa.s), although the large difference in apparent viscosity alters the manner in which gas is dispersed, and particularly the degree of liquid movement achieved away from the impeller region.

When using two disc turbines (D = T/2), as shown in figure 7.6, similar behaviour was found as for one disc turbine. The impeller speed required for the formation of a bubble cloud rose slightly in all the solutions. In the 0.5% and 1.4% CMC solutions N_{CD} was reduced slightly when two impellers were used, although N_{CD} rose slightly in the 0.8% CMC solution, due to the rise in N_{BC} in this solution. These variations were accompanied by an increase in the power consumed, when two impellers are used, as can be seen in table 7.2. It was now possible to achieve

Figure 7.6 Aerated Power Number, Po_g, versus Reynolds Number, Re, in CMC Solutions.

Two Disc Turbines (D=T/2), ½ vvm

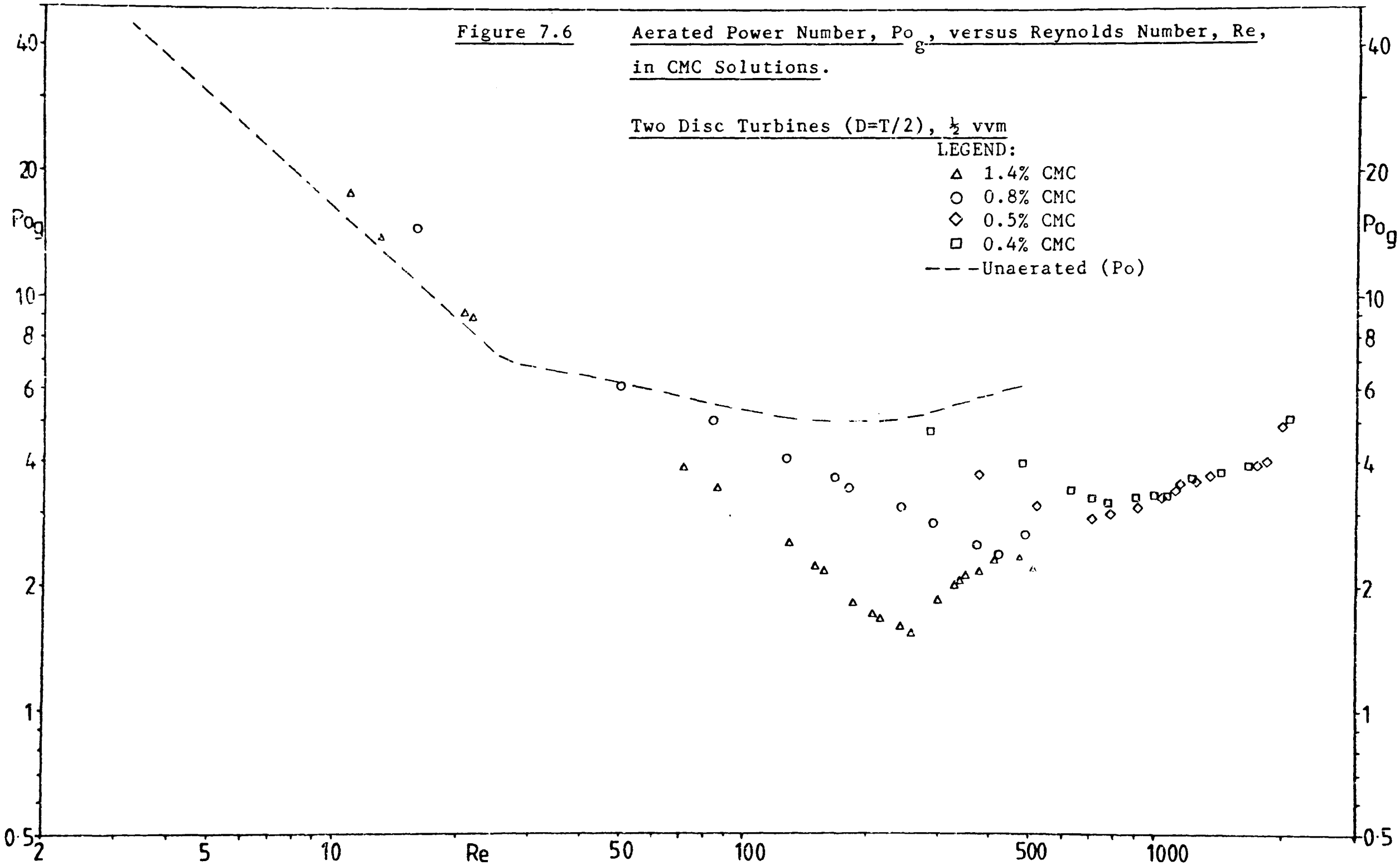

Table 7.2

Operating Variables for Bubble Cloud Formation and Complete Gas Distribution, at an Air Flow Rate of ½ vvm.

		Bubble Cloud Formation (B.C.)		Complete Gas Distribution (C.D.)				
CMC Concentration (%)		1.4	0.8	1.4	0.8	0.5	0.4	0
μ_r (Pa.s)		0.858	0.347	0.858	0.347	0.167	0.071	0.001
Impeller Configuration	Operating Variable							
One Disc	N (s^{-1})	8.0	4.5	13	4.5	4.6	3.3	1.9
Turbine	Re (-)	196	222	500	222	705	750	4.4×10^4
(D=T/2)	P/V ($kW.m^{-3}$)	1.88	0.53	7.6	0.53	0.57	0.51	0.10
Two Disc	N	8.3	5.0	11	5.0	4.1	-	-
Turbines	Re	202	270	326	270	419	-	-
(D=T/2)	P/V	3.7	1.4	10.1	1.4	0.85	-	-
One Disc	N	16	7.0	26	11	-	6.7	3.6
Turbine	Re	288	234	667	474	-	635	3.6×10^4
(D=T/3)	P/V	1.06	0.29	10.4	0.83	-	0.21	0.07
Two Disc	N	15	7.0	24.5	11	-	7.0	3.9
Turbines	Re	231	219	528	445	-	637	3.9×10^4
(D=T/3)	P/V	2.35	0.53	15.9	1.5	-	0.44	0.15
Pitched Blade/	N	7.0	5.0	cf. two disc				
Disc Turbine	Re	168	274	turbines				
Combination	P/V	2.8	1.2	(D=T/2)				
(D=T/2)								
Two Intermigs	N	11	6.0	not	9.5			
(D=0.58T)	Re	434	500	achi-	1000			
Point sparger	P/V	5.5	1.3	eved	3.6			
Two Intermigs	N				8.5			
(D=0.58T)	Re				950			
Ring sparger	P/V				2.7			

adequate gas-liquid mixing of the most viscous solutions used (1.4% CMC, μ_r = 0.858 Pa.s) although precise definition of the impeller speed at which this is achieved is made difficult due to the persistence of stagnant regions in the lower corners and behind the baffles. These regions persisted until N = 12 s^{-1}, P/V = 15.1 $kW.m^{-3}$, although a reasonable estimate of N_{CD} is 11 s^{-1}, P/V = 10.1 $kW.m^{-3}$.

The results obtained using small disc turbines (D = T/3) are shown in figures 7.7 and 7.8. The impeller speeds required for bubble cloud formation and complete gas dispersion are higher than when using the large disc turbines. In 0.8% CMC N_{BC} and N_{CD} are no longer coincident, with N_{CD} raised to 11 s^{-1}, whilst N_{BC} = 7 s^{-1} for both one and two small disc turbines. These differences are accompanied by a decrease in the power required to produce a bubble cloud in 0.8% and 1.4% CMC, although the power required for complete gas dispersion in these more viscous solutions rises as the impeller diameter is decreased. This is the reverse of the effect seen at lower viscosities (μ_r < 0.1 Pa.s), as is shown in table 7.2. In addition the 1.4% CMC solution showed regions of slow liquid movement existing near the bottom and top corners of the vessel, similar to those seen when using a single large disc turbine, (D = T/2), even when agitating with two small disc turbines (D = T/3) at the highest impeller speed achieved of N = 27 s^{-1}, which corresponds to a power consumption of 20.6 $kW.m^{-3}$.

All the values of N, P/V and Po_g quoted above have been for a gas flow rate of ½ vvm. In general little effect was noted of varying gas flow rate on the impeller speed required for gas distribution, although slight reductions in the power required to achieve complete gas distribution were noted at the higher gas flow rate of 1 vvm. This is mainly due to variation in Po_g seen in the solutions, as can be seen in the figures.

Figure 7.7 Aerated Power Number, Po_g, versus Reynolds Number, Re, in CMC Solutions.

One Disc Turbine (D=T/3)

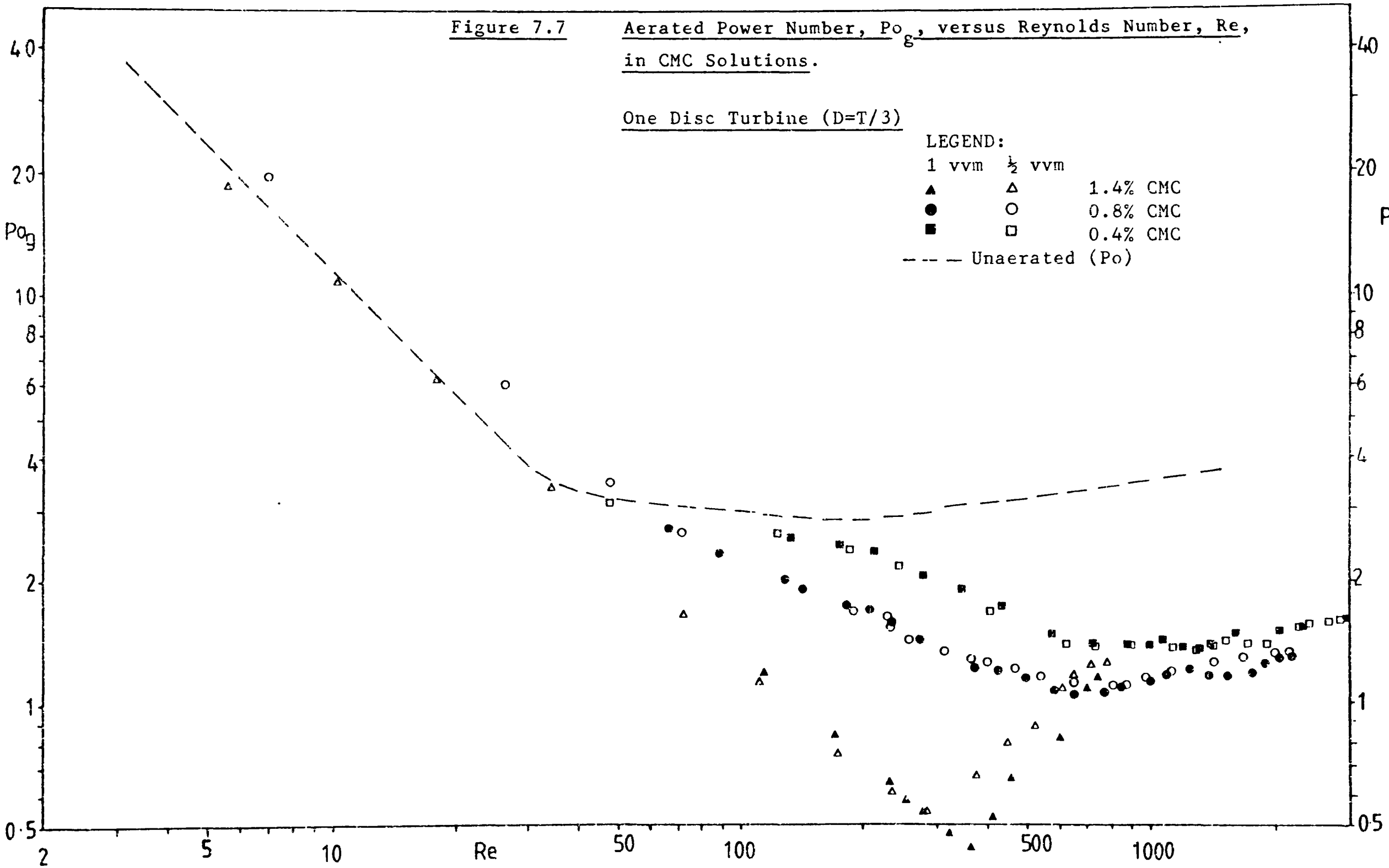

Figure 7.8 Aerated Power Number, Po_g, versus Reynolds Number, Re, in CMC Solutions.

Two Disc Turbines (D=T/3)

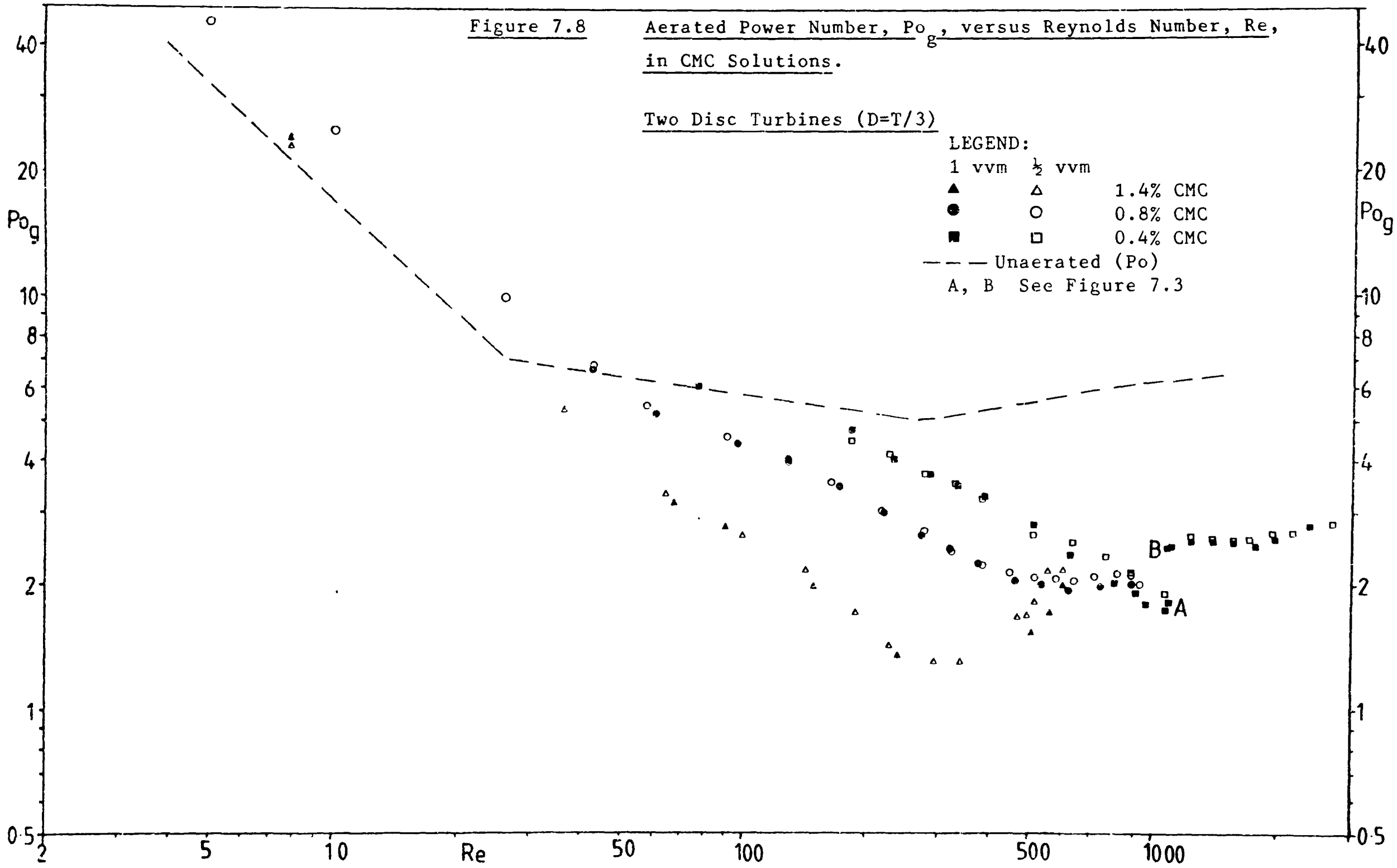

Overall, of the disc turbine agitator systems used, only the two large disc turbines (D = T/2) produced adequate gas and liquid movement throughout the vessel in 1.4% CMC, at the power inputs and impeller speeds available. Requiring an impeller speed greater than 12 s^{-1} with a consequent power consumption of greater than 15 $kW.m^{-3}$. This concurs with the results found by Solomon[22], who studied the liquid mixing under gassed and ungassed conditions in similar viscous liquids. There is a problem in defining when an adequate level of liquid mixing is achieved in viscous shear thinning liquids, in that virtually stagnant regions can persist even when the majority of the vessel contents are well mixed, making visual observation of full liquid mixing highly subjective. Allsford[146] attempted to overcome this problem by studying mixing times for the different agitators in similar solutions. In this work the mass transfer studies require that the dissolved oxygen concentration in the liquid is measured. Advantage has been taken of this to determine the variation in dissolved oxygen concentration found in different parts of the vessel, which can be a suitable criterion by which the liquid mixing can be judged. This is discussed in detail for all the impellers used in section 4 of this chapter.

As mentioned before, the interaction of the gas and the impeller can produce slight periodic variations in the torque required at a given impeller speed. These variations are most noticeable when using a single small disc turbine (D = T/3), as shown in figure 7.7a. This is probably linked to the lower torque found when using this impeller at a given Re or impeller speed, when compared to dual disc turbines or a single large disc turbine. This means that the same amplitude of variation in torque will be a large proportion of the total torque required when using this impeller. In addition these variations were most noticeable in the more viscous CMC solutions (1.4%), this may be entirely due to

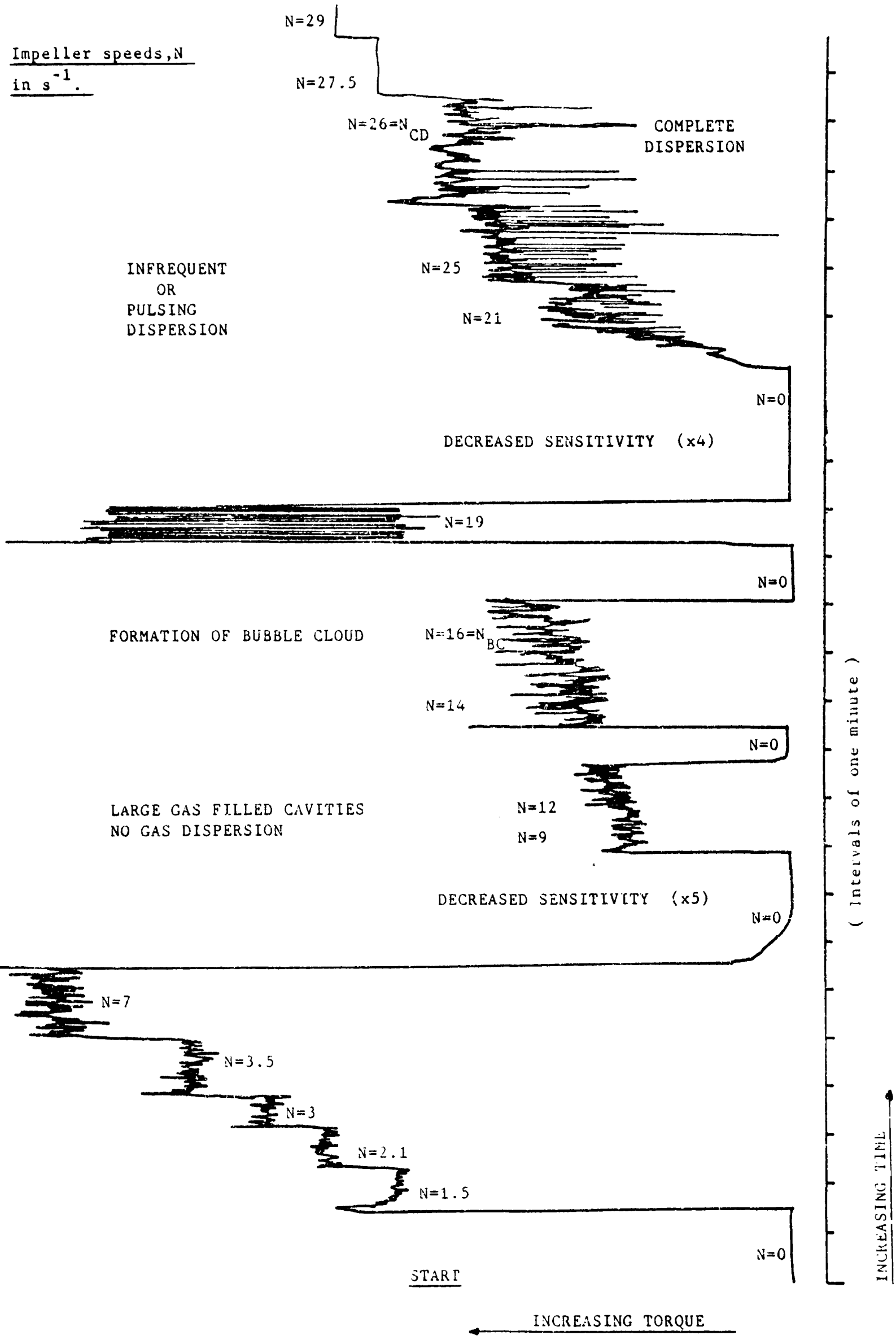

Figure 7.7a Variations in Torque on the Impeller Shaft when Agitating 1.4% CMC with a Single Disc Turbine (D=T/3)

the effect of the higher viscosity, however the increased viscoelasticity of this solution may also be important, particularly as this effect is related to the action of the gas bubbles, which can be altered by altering viscoelasticity[30,50], as discussed in greater detail below. Again any effect due to viscoelasticity would be more prevalent at smaller impeller diameters due to the increased impeller speeds required for given conditions of Re, Fr, etc.

At low impeller speeds, prior to the onset of bubble cloud formation, but after gas filled cavities have formed, the torque required oscillates slightly. In 1.4% CMC, whenusing a single small disc turbine (D = T/3), at Q = ½ vvm, this results in a frequency of approximately 0.5 Hz with an amplitude of 2½% of the required torque at N = 4.5 s^{-1}. This rises to a frequency of 0.8 Hz with an amplitude of 15% at N = 15.6 s^{-1}, just prior to bubble cloud formation. When a large disc turbine (D = T/2) is used under similar conditions, the frequency is 0.4 Hz and the amplitude 1.5% at N = 4.5 s^{-1}. This rises to 0.5 Hz and 10% at N = 7.9 s^{-1}, i.e. just prior to bubble cloud formation. Altering air flow rate had little effect on these observed phenomena, with a slight reduction in the amplitude of the variation in torque occurring at Q = 1 vvm.

When using the small disc turbine (D = T/3) at impeller speeds above N_{BC} but below N_{CD}, large fluctuations in the torque required were produced. These fluctuations became less frequent as the impeller speed increased, disappearing entirely above N = 25 s^{-1}, which was close to the impeller speed required for complete gas distribution. This variation in torque was much larger than that seen at low impeller speeds, with an amplitude of 25% of the mean torque required. The frequency varied from 0.4 Hz at N = 19 s^{-1} to 0.2 Hz at N = 25 s^{-1}. Visual observation showed that this was linked to the pulsating manner in which the gas dispersion occurred at these impeller speeds, with periods of gas dispersion interspersed with periods of low torque in which the impeller was flooded with

gas and no dispersion took place. This also occurred when using two small disc turbines (D = T/3) in 1.4% CMC, but was virtually absent when the large impellers were used. At high impeller speeds, where the agitator was able to disperse all the gas stream, the torque remained stable.

For all the impeller systems used, once gas dispersion had begun, increasing the impeller speed increased the rate of gas and liquid circulation. With increasing N , Po_g continues to fall, reaching a minimum in the transition region for the disc turbines. In solutions of intermediate concentration (0.4 - 0.8% CMC), the minimum in the Po_g - Re curve is very shallow, with Po_g rising slowly at higher Re. In the more viscous 1.4% CMC solutions the minimum is sharp and Po_g rises rapidly at higher Re. The value of Po_g(min) and the Re at which it occurs is dependent on the solution concentration. The more viscous solutions exhibited a lower Po_g(min) value at lower Re. All the values obtained are collected in table 7.3. From this it can be seen that the ratio of Po_g(min) to Po at the same Re , is as low as 0.28, 0.36 and 0.4 for 1.4, 0.8 and 0.5% CMC solutions agitated by one disc turbine (D = T/2) at an air flow rate of ½ vvm. When using two disc turbines (D = T/2), Po_g(min)/ Po is 0.34, 0.39 and 0.43 for the same solutions of CMC. Thus the power consumption is not reduced by gassing to such a great extent, when using two disc turbines as when using one disc turbine.

When using one or two smaller disc turbines (D = T/3) in 0.8 and 0.4% CMC solutions, similar values for Po_g(min) are obtained to those just described. The presence of two alternative mixing patterns, as described in section 7.2, affects the power consumption at high Re when two small disc turbines are used. Whilst mixing pattern A occurs (see figure 7.3), Po_g is reduced compared to the values obtained when using the larger disc turbines (D = T/2). The increase in Po_g seen above

Table 7.3

Minimum Values of Po_g and the Associated Po and Re Values for Various Agitation Conditions and CMC Concentrations

Air Flow Rate		1 VVM				½ VVM			
CMC Concentration (%)		1.4	0.8	0.5	0.4	1.4	0.8	0.5	0.4
Impeller Configuration									
One Disc Turbine (D=T/2)	Re	-	532	-	888	295	590	840	827
	Po	-	2.9	-	3.3	3.0	3.25	3.45	3.25
	Po_g(min)	-	1.22	-	1.55	0.85	1.2	1.4	1.59
Two Disc Turbines (D=T/2)	Re	280	430	670	-	240	430	670	760
	Po	5.2	6.2	6.4	-	5.2	6.2	6.4	6.4
	Po_g(min)	1.6	2.35	2.8	-	1.7	2.4	2.75	3.2
One Disc Turbine (D=T/3)	Re	365	650	-	1300	290	650	-	1300
	Po	2.85	3.0	-	3.4	2.75	3.0	-	3.4
	Po_g(min)	0.44	1.05	-	1.35	0.54	1.10	-	1.33
Two Disc Turbines (D=T/3)	Re	-	630	-	1100	345	650	-	1100
	Po	-	4.7	-	6.3	5.0	4.7	-	6.3
	Po_g(min)	-	1.95	-	1.75	1.3	2.05	-	1.9
Pitched Blade /Disc Turbine Combination (D=T/2)									
Downward Pumping	Re	315	450	-	-	290	-	-	-
	Po	4.5	4.6	-	-	4.5	-	-	-
	Po_g(min)	1.3	1.78	-	-	1.5	-	-	-
Upward Pumping	Re	290	390	-	-	245	390	-	-
	Po	4.5	4.6	-	-	4.5	4.6	-	-
	Po_g(min)	1.73	2.35	-	-	1.97	2.55	-	-
Intermigs		no minimum values of Po_g found							

Po_g(min) is delayed until mixing pattern B dominates. This is shown as a step change in the Po_g - Re curve for the 0.4% CMC solution in figure 7.8, occurring at Re = 1000 which is much higher than in the unaerated system. When agitating 1.4% CMC solutions using one or two small disc turbines (D = T/3), the Po_g values obtained are much lower than those obtained using the larger turbines, at a given Re. This results in much lower values of Po_g(min), and is accompanied by a marked reduction in the ability of the impellers to cope with the gas flow; some of the gas was seen to pass through the impeller region as large bubbles, even at high impeller speeds. Solomon[22] found that this change in position of the Po_g - Re curve when agitating 1.4% CMC with single disc turbines of various diameters (D = 0.6 - 0.25T), occurred as a single step between the T/2 and T/3 diameter impellers, with the data obtained for T/2 and 0.6T diameter impellers virtually coincident, as was that of the 0.25T and T/3 diameter impellers. A possible explanation for these occurrences is that the viscoelastic properties of the solution are affecting the gas distribution and hence reducing the power consumption. For a given Re the smaller impellers operate at higher impeller speeds than the large impellers. In the 1.4% CMC solution, this gives rise to a greater effect due to the viscoelasticity of the solution, as the Deborah number will be higher, producing more " solid-like " behaviour, see Chapter 3, section 1 and Walters[8], which may well occur as a step change once a critical diameter is reached.

The effect of altering gassing rate on the power consumption is generally very small in the viscous solutions used here although the reduction in Po_g compared with Po can be large, especially when compared with the effects seen at lower viscosities, as shown in figure 8.23. Figures 7.9 - 7.11 show Po_g - Re curves for two air flow rates, ½ and 1 vvm, when using two large disc turbines (D = T/2) to agitate 1.4, 0.8 and 0.5% CMC solutions. One area where a marked effect is seen, is around

Figure 7.9

Hold-Up, ε, and Po_g versus Re, in 1.4% CMC. Two Disc Turbines (D=T/2)

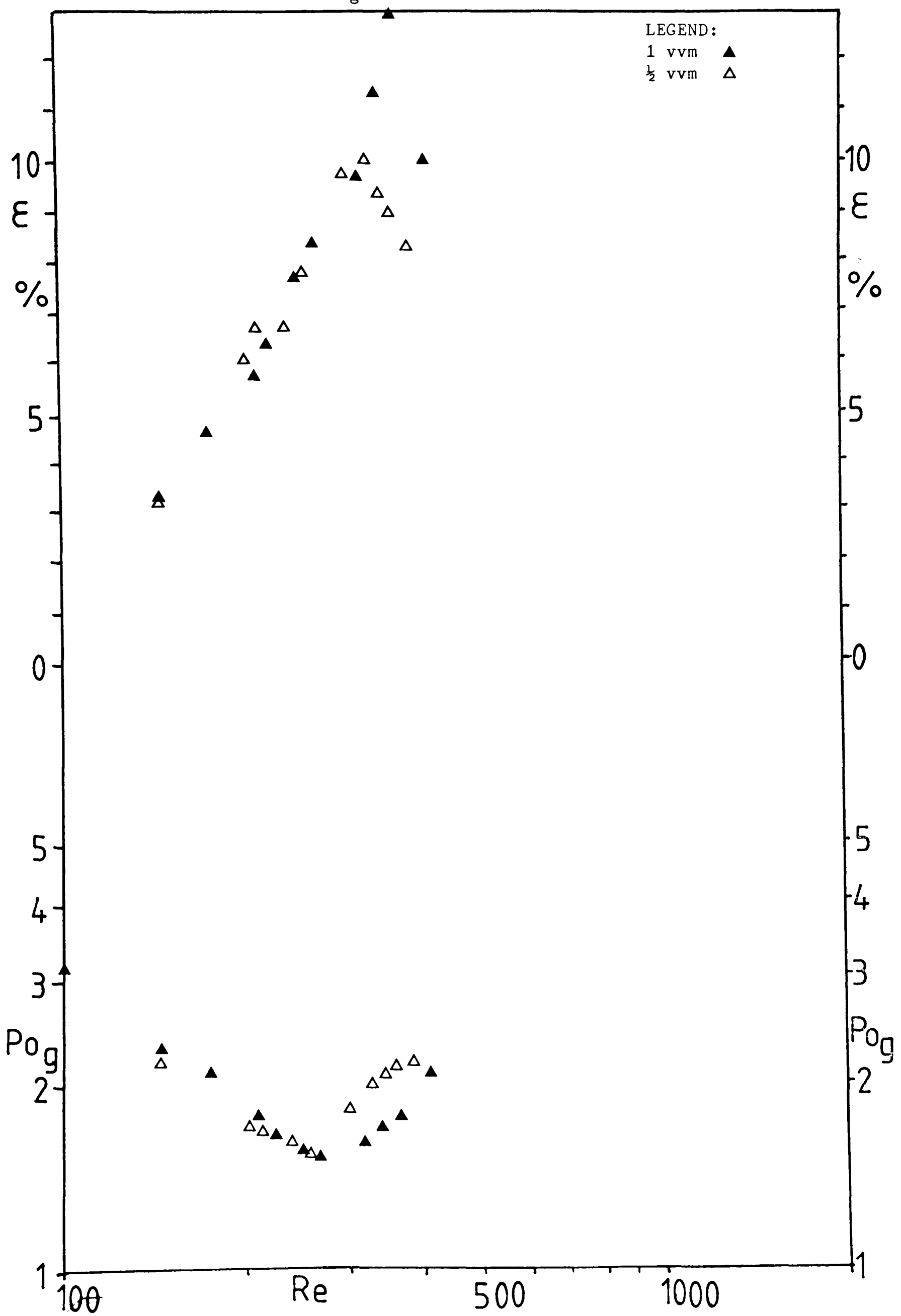

Figure 7.10

Hold-Up, ε, and Po_g versus Re, in 0.8% CMC. Two Disc Turbines (D=T/2)

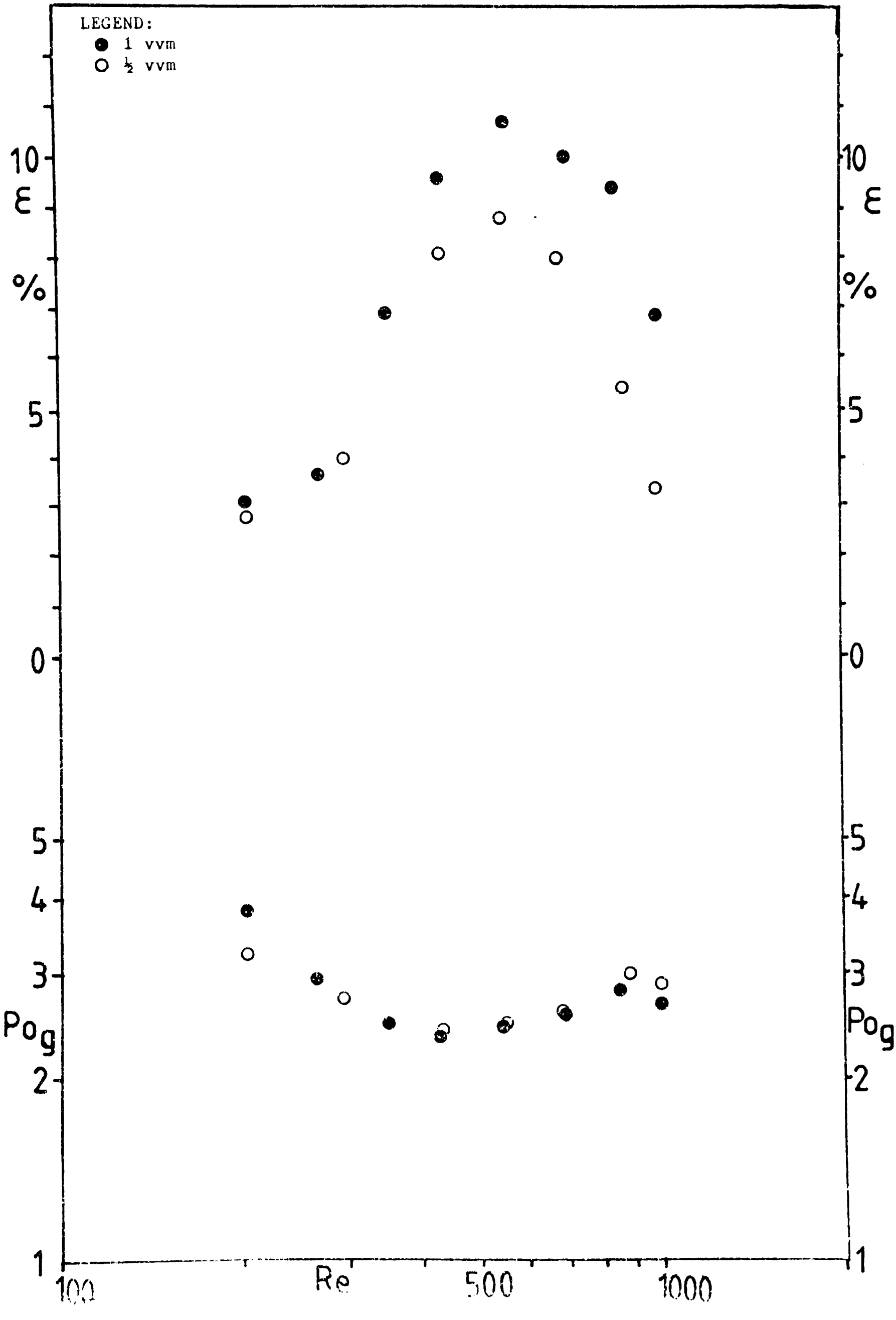

Figure 7.11

Hold-Up, ε_g, and Po_g versus Re, in 0.5% CMC. Two Disc Turbines (D=T/2)

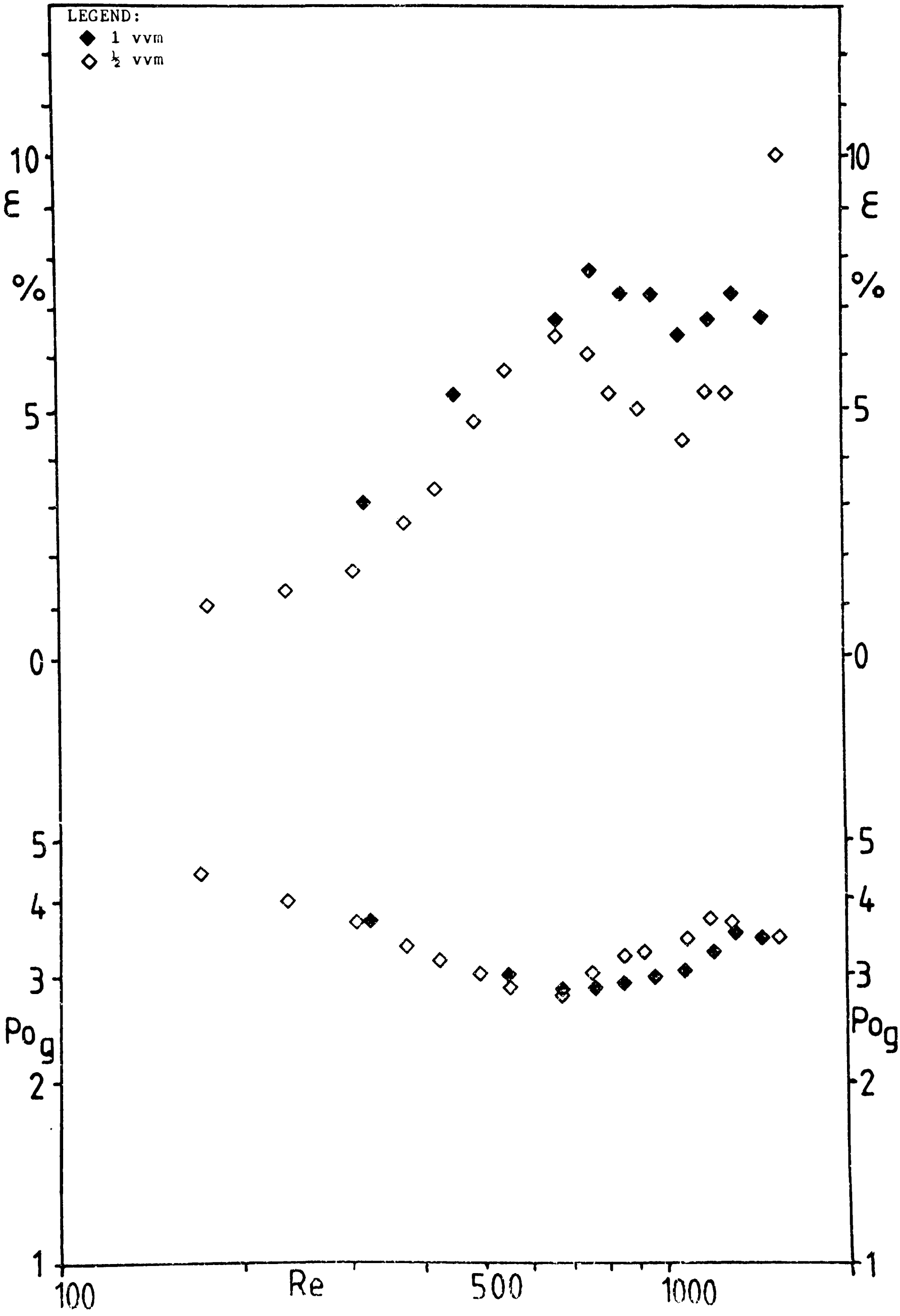

the minimum in the curve for the 1.4% CMC solution. This area is shown in greater detail in figure 7.9a for Q = ½, 1 & 2 vvm using the same impellers but in a different solution of 1.4% CMC, so slightly different values were obtained for Po_g due to a slight difference in rheological properties. As the gas flow rate is increased, the upturn in the Po_g - Re curve is delayed to higher Re, with a lower value of Po_g(min) occurring. The separate curves rejoin at higher Re and a downturn in Po_g is noticed. This is probably associated with the gross recirculation of gas which renders Po_g independent of the actual gassing rate. A similar downturn in Po_g is seen in lower viscosity solutions (figure 7.10 and 7.11). Similar results were found for the small disc turbines (figures 7.7 and 7.8) and when using a single disc turbine. Again it is thought that the marked viscoelastic nature of the 1.4% CMC solution may be the cause of this, as discussed below, however the precise reason is uncertain, as the bubbles within the solution prevent any observation of the impeller region. Figures 7.9 - 7.11 also show the variation in hold-up obtained for the 1.4, 0.8 and 0.5% CMC solutions. It can be seen in all the figures that the hold-up reaches a maximum at a slightly higher Re than that which gives the minimum in Po_g, then falls quite sharply. For the 0.5% CMC solution, the hold-up rises again at higher Re, which can be associated with the downturn in Po_g seen at high Re. Again similar behaviour is shown when using small disc turbines (D = T/3) and when using a single impeller, or when using the pitched blade turbine/disc turbine combination. These are reported fully in Chapter 8, where the implications which this has for mass transfer are detailed. One explanation for this general behaviour is that the gas filled cavities may begin to reduce in size as the impeller speed increases and the distribution of the gas becomes more efficient. This would increase the drag on the impeller blades and reduce the gas hold-up in the impeller region. The increased drag leads to higher Po_g values, whilst the reduction in hold-

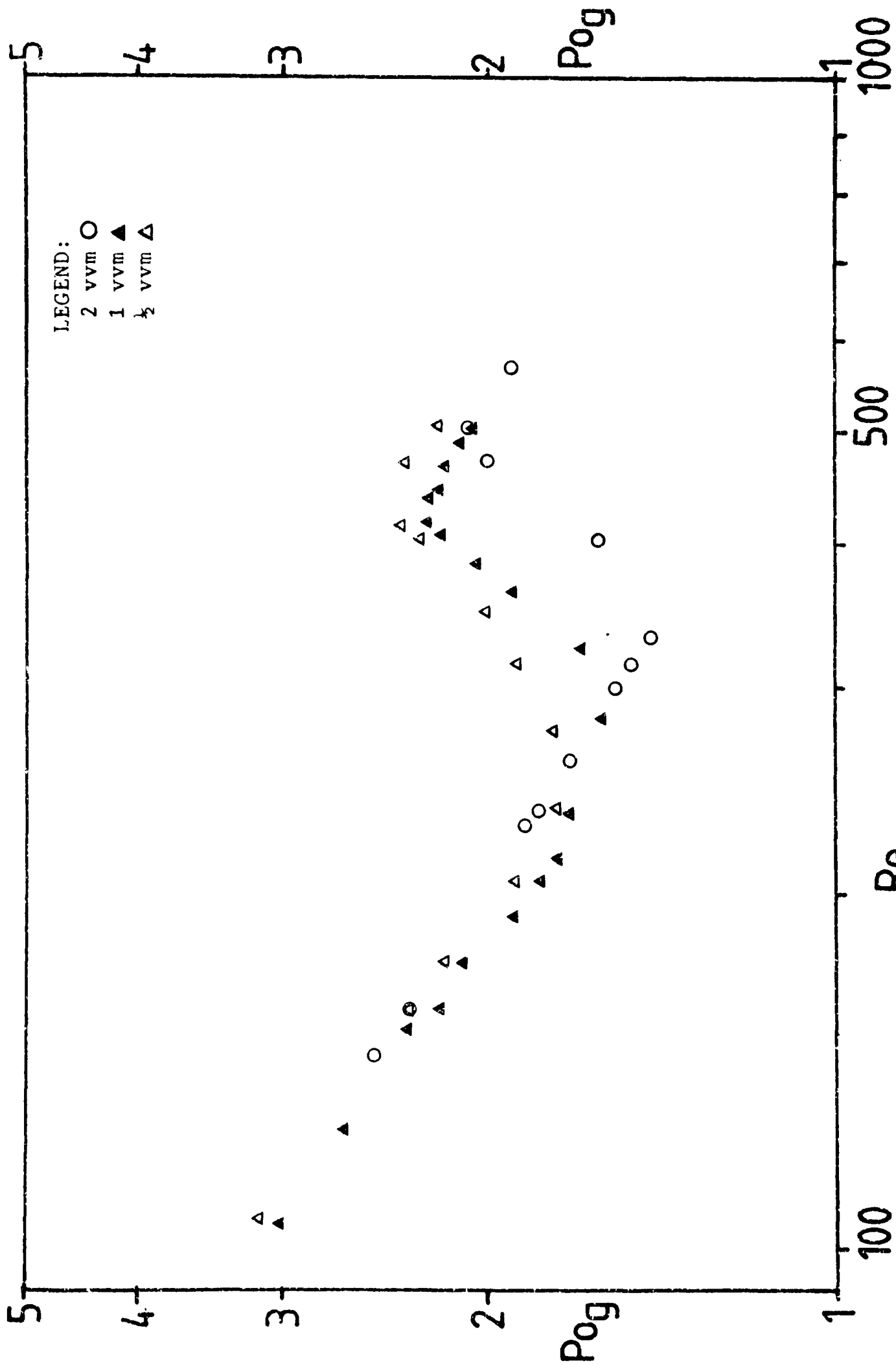

Figure 7.9a P_{o_g} versus Re, in 1.4% CMC. Two Disc Turbines (D=T/2)

up in the impeller region reduces the overall hold-up. Solomon[22] observed that the hold-up levelled off at high power inputs in Xanthan Gum solutions, with a slight downturn noted at the highest impeller speeds available when agitating with a single disc turbine of large diameter (D=0.5 - 0.6T). He also reports that the hold-up increases with increasing impeller diameter for a given power input in solutions of CMC and Xanthan Gum. Bruijn et al.[46] and Ranade and Ulbrecht[28] describe large cavities in viscous Newtonian and non-Newtonian solutions which are seen to extend beyond the circumference of the impeller, holding a large volume of gas, possibly equal to or greater than the volume swept by the impeller. Ranade and Ulbrecht[28] report that the size of these cavities increases with increasing impeller speed. It is postulated here that these cavities continue to grow with increasing impeller speed, even though gas dispersion is occurring, until at high speeds their size is reduced. This reduction may be due to the increased flow of liquid through the impeller region, sweeping the gas away from the blades, coupled with the increase in shear rate in the vicinity of the impeller as the blades move more rapidly through the liquid. This reduces the viscosity in the impeller region, which in turn leads to smaller cavities similar in size to those found in low viscosity systems[28,46,47].

The maximum reduction in hold-up noted here is found when agitating 0.8% CMC using two large disc turbines (D=T/2), as shown in figure 7.10. The overall hold-up falls from 9% to 3% at an air flow rate of ½ vvm. This is equivalent to a reduction in volume of gas of 1.3 litres. The volume swept by both impellers is 0.7 litres. This implies that the cavities must extend beyond the tips of the impeller blades by 20-30 millimetres (0.13 - 0.2 D), to hold such a large volume of gas. The maximum size of cavities observed, before bubbles in the solution prevented observation of the impeller region, was at Re = 270, just prior to the onset of gas dispersion. At this point the impellers appear to be enveloped in gas, as described by

Yagi and Yoshida[49], with the cavities extending beyond the area swept by the impeller. Here the hold-up is equal to 4% (0.86 litres), which is already larger than the volume swept by the impellers, although some of this hold-up will be due to the passage of large gas bubbles through the impeller regions and around the impeller shaft. Increasing impeller speed leads to a more rapid increase in hold-up, due to increasing cavity size and the onset of gas hold-up away from the impeller region. It is assumed that the hold-up away from the impellers continues to increase with increasing speed even when the hold-up in the impeller regions decreases at high speeds. This will explain the upturn in hold-up seen in 0.5% CMC at high Re, as shown in figure 7.11. This analysis suggests that maximum hold-up seen outside the impeller region is of the order of 3 - 5% in 0.8% CMC, depending on the air flow rate. Thus the overall hold-up is not a good indicator of the hold-up of small bubbles, which is presumed to be a significant measure for mass transfer purposes[144] particularly in low viscosity systems.

The variations in Po_g with varying gassing rate described above for agitation of 1.4% CMC, could be due to the effects which viscoelastic properties have on bubble break up[66] and coalescence behaviour[40], as increasing elasticity increases the resistance to liquid stretching in the vicinity of the bubbles[30] and reduces the turbulence in the wake of a bubble[50]. In the impeller region this would reduce the frequency of separation of small gas bubbles from the tips of the cavities, which occurs through a turbulent closure mechanism[45], thus reducing the gas handling capability of the impeller, at a given impeller speed. At Re below the minimum in Po_g, the impeller is incapable of handling all the gas flow and the size of the cavities remains large. Above the minimum in Po_g all the gas flow is dispersed radially, through the cavities behind the blades, the size of which is determined by the elastic properties and the gas flow rate, a higher gas flow rate producing larger cavities, which lead to less drag and lower Po_g values.

7.3.2) Intermig Impellers

As when using disc turbines, the power consumption when aerating is reduced compared to the unaerated case when using these impellers. Po and Po_g are shown for a range of solutions in figure 7.12, gas dispersion begins between Re = 300 - 500 (see table 7.1), but complete gas distribution and good liquid mixing do not occur at Re < 1000. This means that good gas and liquid mixing was not obtained at all in the 1.4% CMC solution, even though a ring sparger was used to promote dispersion. Ring spargers are thought to aid gas dispersion when using Intermig impellers because they supply the gas directly to the tips of these impellers. This is the part of the impeller which is moving fastest, thus producing the highest shear rate, in addition the design of the outer blade tips would increase the turbulence in the liquid flowing over the blades, aiding the

Figure 7.12

Po_g versus Re for Two Intermigs (D=0.58T)

Upward Pumping only. Air Flow Rate; ½ vvm

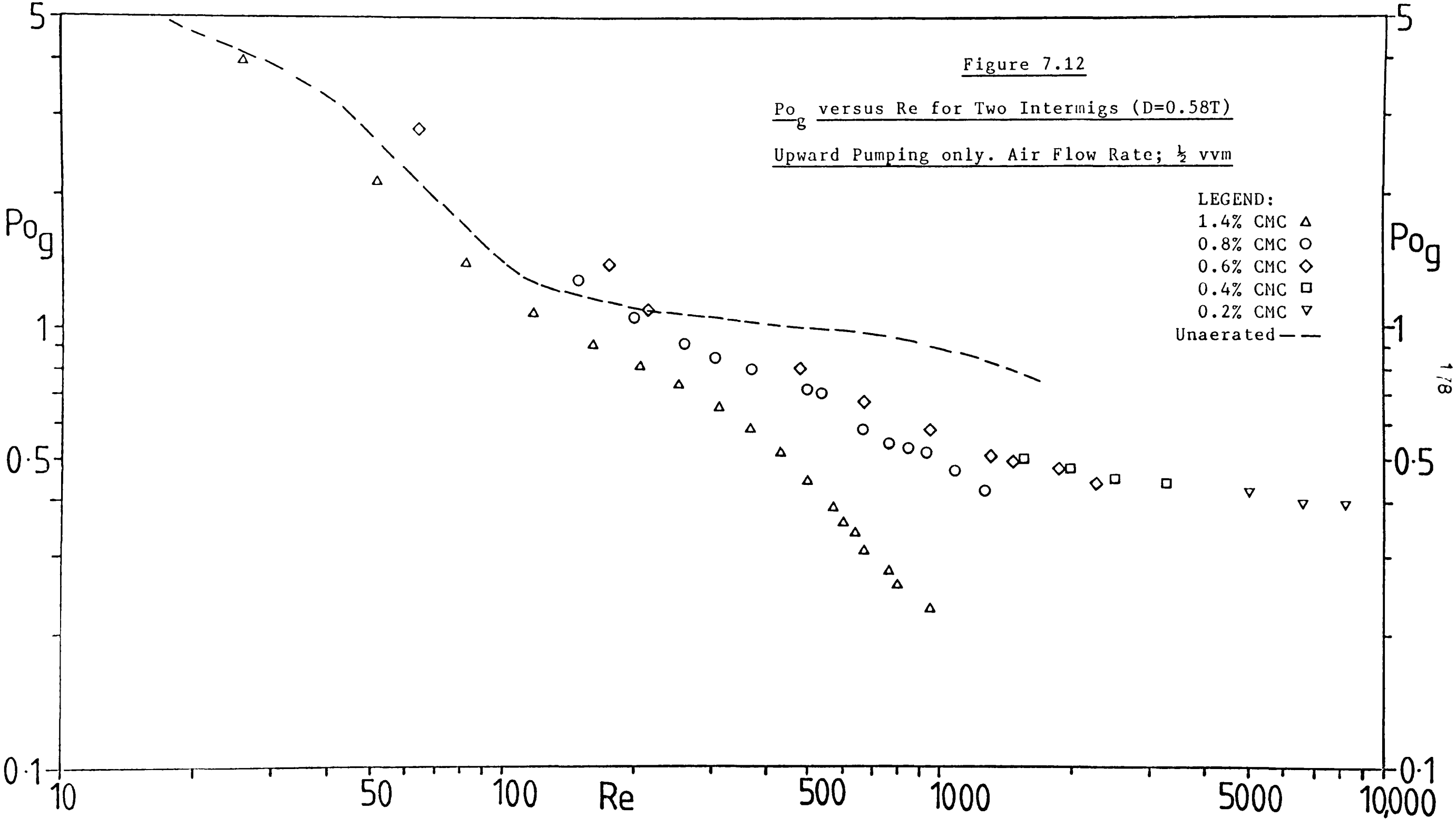

break up of the gas bubbles. When using disc turbines the choice of sparger type is less critical, as the disc forces the liquid into the region of the blade tips. Tests in a 0.8% CMC solution showed that reasonable gas and liquid mixing was obtained at N = 9.5 s^{-1}, when using a point sparger, which reduced to 8.5 s^{-1} when using a ring sparger. This did not affect the power consumed. Unlike the disc turbines, no Po_g(min) is found using these impellers to agitate viscous solutions. As Re increases Po_g continues to fall until the maximum impeller speed available is reached. It should be noted that the Po_g values are very low compared to those given by disc turbines. Thus very high impeller speeds are required to consume a moderate amount of power. Po_g/Po also decreases with increasing Re, as Po does not fall as steeply with increasing Re as Po_g does. This compares with rising Po_g/Po at high Re when using disc turbines.

Figure 7.13 shows the dependence of Po_g on direction of rotation and gassing rate in a 0.6% CMC solution. At high Re, Po_g is slightly lower for Q = 1 than for Q = ½, otherwise there is no effect of gassing rate. The direction of rotation does affect Po_g with " downward pumping " giving a larger power consumption. Figure 7.13a shows the hold-up and Po_g for two gassing rates, for a range of CMC solutions, when pumping upwards. The same hold-up values were obtained when pumping downwards and it can be seen that the hold-up is hardly affected by the gassing rate. A comparison with the results obtained for disc turbines and the implications this has for mass transfer can be made from the figures contained in Chapter 8. Under gassed conditions, in all the solutions, severe vibrations were encountered at higher impeller speeds. This has been noted by the manufacturers[148], and others[149], who propose that it is a resonance effect determined by the natural frequency of the vessel and its contents. As it is only apparent under gassed conditions, it is possible that it is associated with gas being trapped by the impeller blades, as seen when

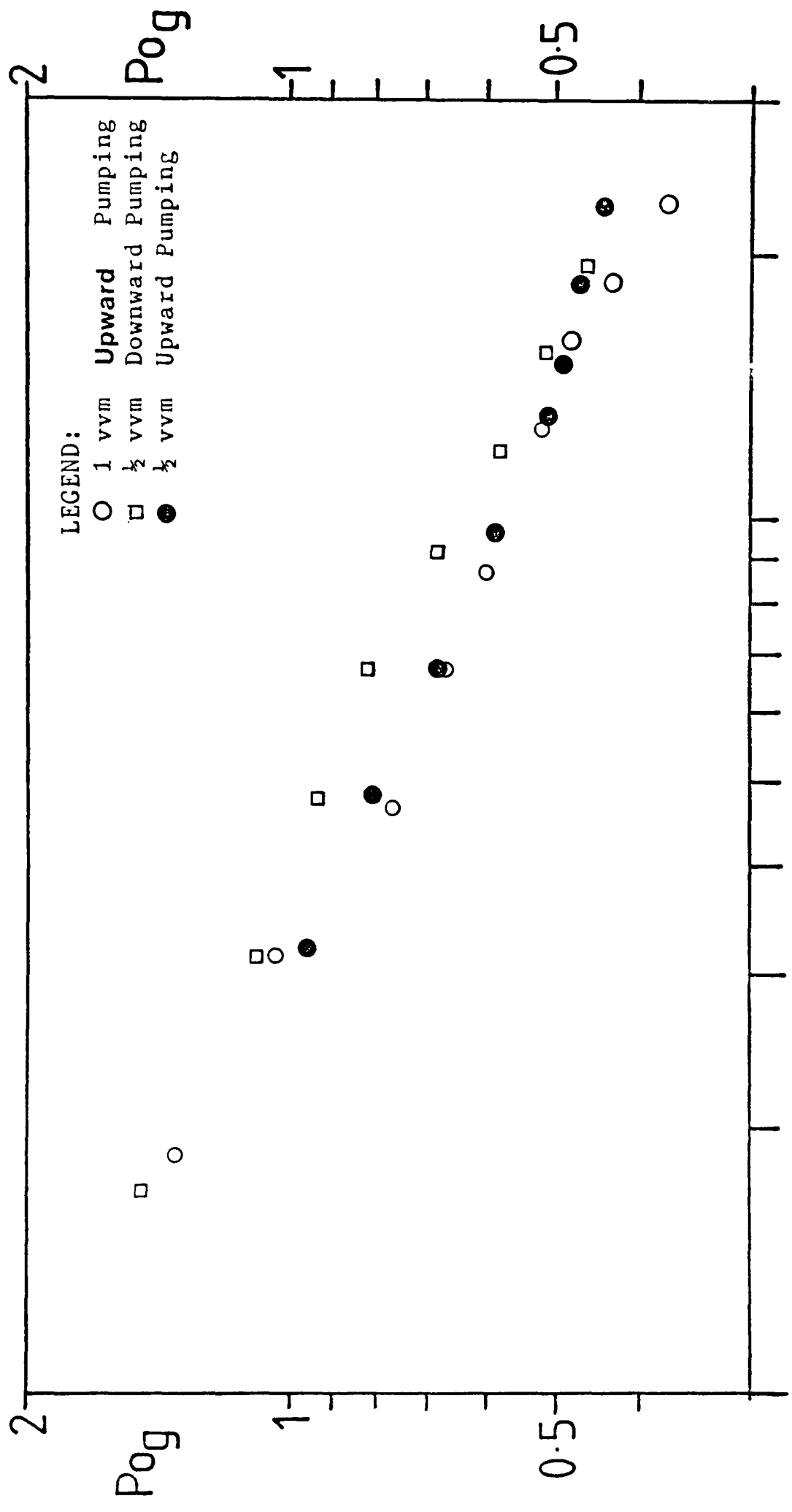

Figure 7.13

$\frac{Po}{g}$ versus Re in 0.6% CMC, Two Intermigs (D=0.58T)

Figure 7.13a

Hold-Up, ε_g, and Po_g versus Re [Intermig Impellers (D=0.58T)]

Q = 1 & ½ vvm; CMC concentrations: 1.4% ▲△, 0.8% ●○, 0.4% ■□, 0.2% ▼▽

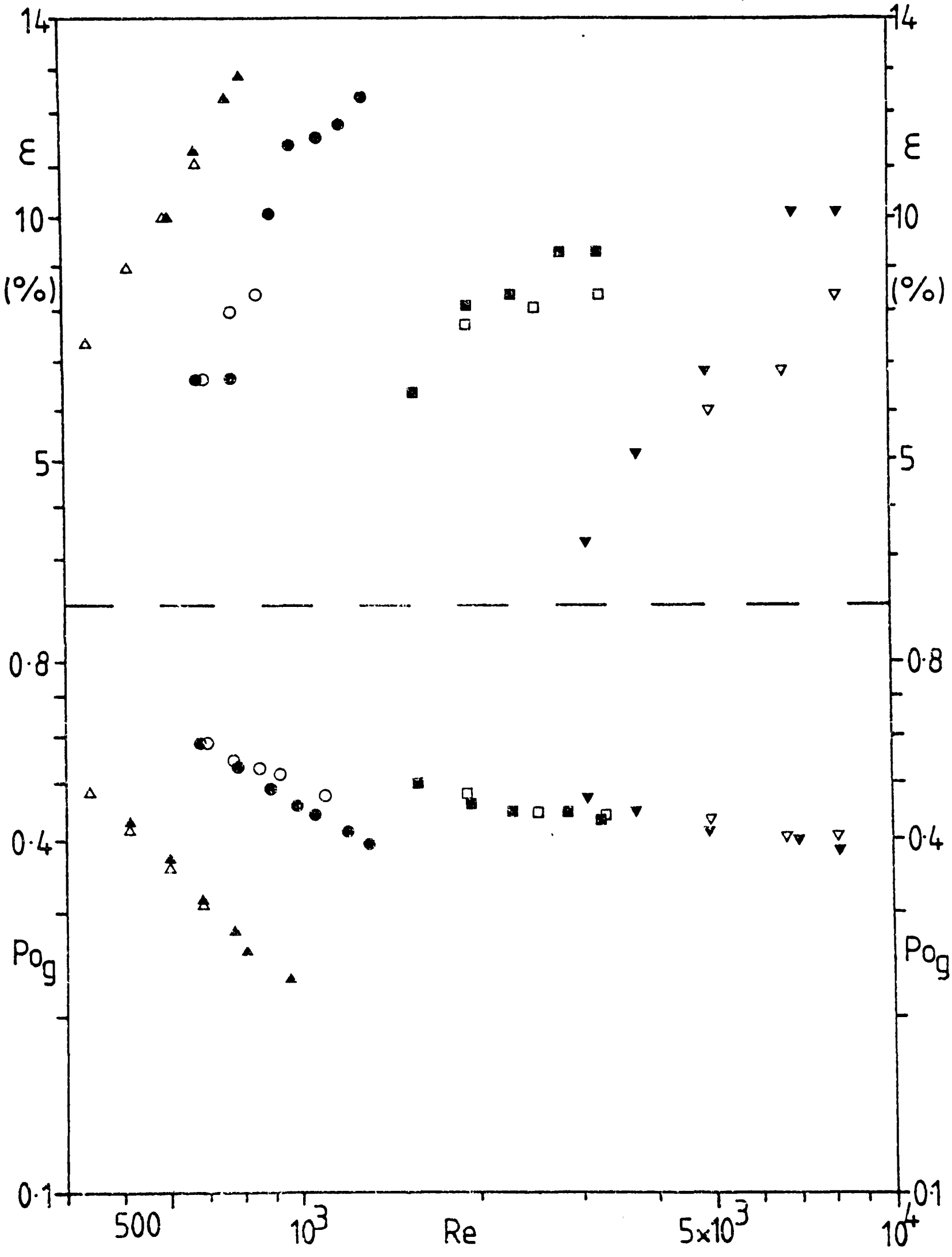

using pitched blade turbines, which are described in the next section.

7.3.3) The Pitched Blade Turbine in Combination with a Disc Turbine

At Re below that which gave Po_g(min) for two disc turbines, this impeller combination gave very similar Po_g values to those obtained using two disc turbines of the same diameter (D = T/2). Bubble cloud formation and gas distribution begins at slightly lower Re, and its onset is dependent on the pumping direction. In 1.4% CMC, shown in figure 7.14, gas distribution begins at Re = 160 when upward pumping and at Re = 180 when downward pumping. At higher Re, Po_g continues to fall. For downward pumping Po_g reaches a minimum at Re = 300 for Q = ½ vvm which compares with Re = 240 for two disc turbines. For upward pumping Po_g reaches a minimum earlier at Re = 240 and the Po_g values are higher once gas is being distributed. Thus depending on the pumping direction, the Po_g values obtained fall either side of those found for two disc turbines at Re > 150 with a higher ratio of gassed to ungassed power consumption (P_g/P), as Po for these impellers in this region is lower than for two disc turbines. The hold-up obtained is also shown in figure 7.14. It is increased at higher gassing rates at higher Re and is dependent on the pumping direction with downward pumping giving lower $\mathcal{E}$ values. At the highest Re (440) in 1.4% CMC marked fluctuations in the torque were observed when downward pumping. The mean torque required was much higher than expected giving a sharp increase in Po_g when compared to that obtained at slightly lower Re and N for this combination. Figure 7.15 shows that similar variations in torque were obtained at intermediate impeller speeds in 0.8% CMC over the range: Re = 430 - 820. At higher and lower Re, the torque readings were relatively stable in 0.8% CMC and Po_g was much lower. Visual observation showed that these fluctuations in the torque were matched by a variation in the hold-up, which is also shown in figure 7.15. As the hold-up rose, the torque fell. This was followed by the sudden release

Figure 7.14

Po_g and Hold-Up, ε, versus Re for 1.4% CMC. One Disc Turbine and One 45° Pitched Blade Turbine (D=T/2).

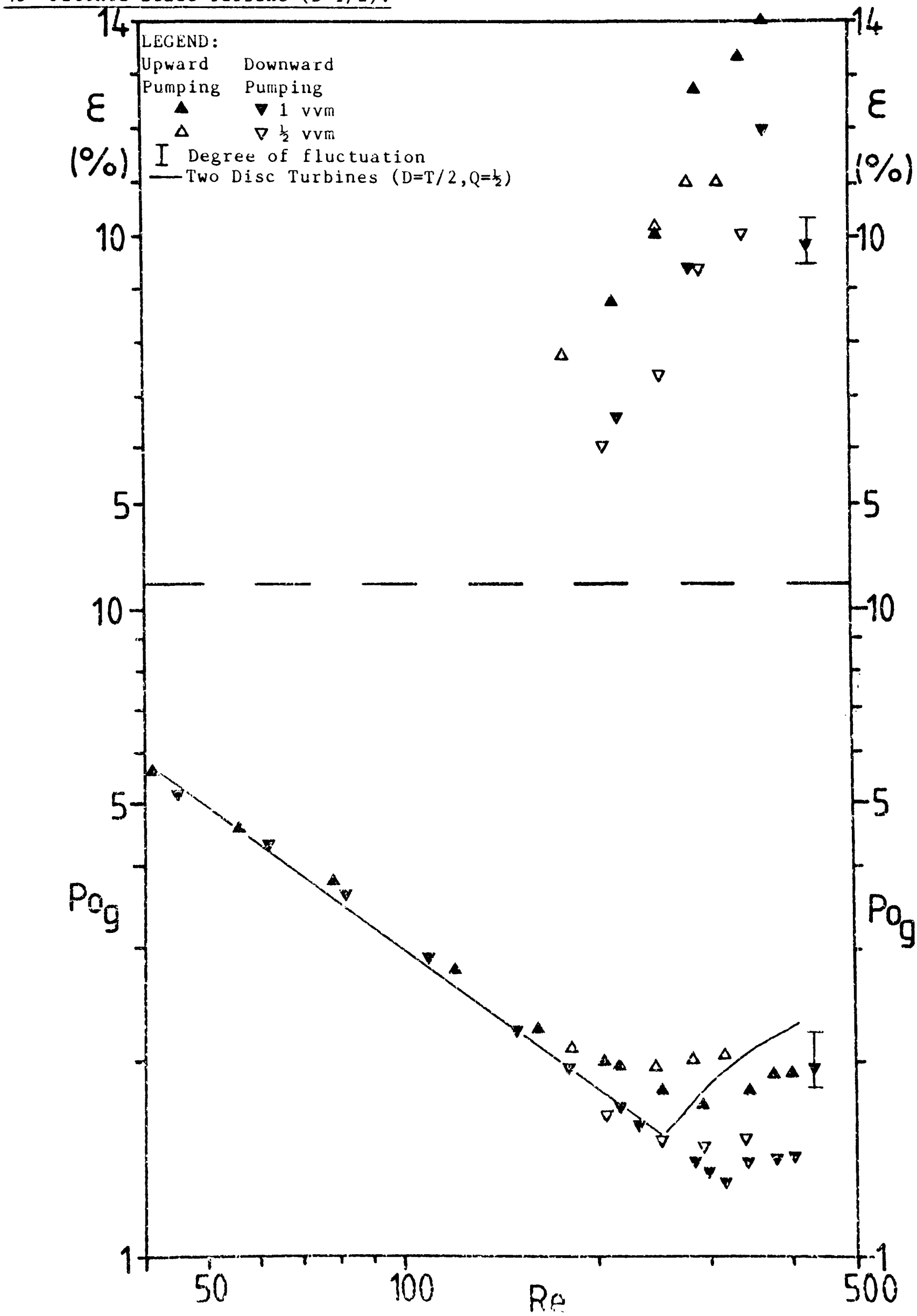

Figure 7.15

Po_g and Hold-Up, ε, versus Re for 0.8% CMC. One Disc Turbine and One 45° Pitched Blade (D=T/2).

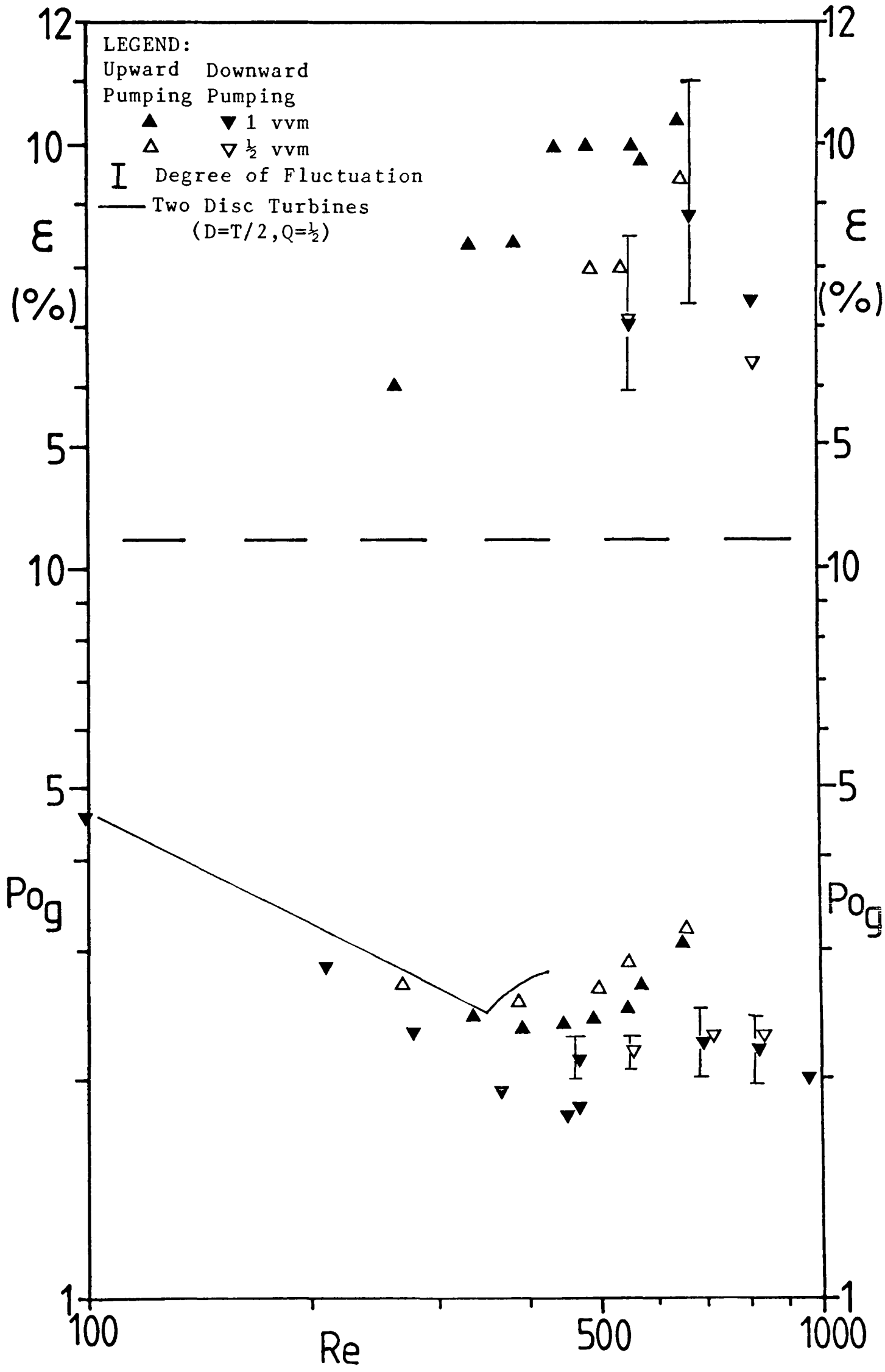

of a large gas bubble in the middle of the liquid surface, accompanied by a sharp fall in hold-up and increase in torque. This was associated with the trapping of gas below the upper impeller. At these impeller speeds the buoyancy or upwards velocity of the gas is matched by the downwards force of the liquid being pumped out of the impeller. This results in gas being trapped under the impeller around the shaft. As the amount of gas increases, its buoyancy also increases until it overcomes the downward flow of liquid and is suddenly expelled from the solution. The cycle is then repeated. At impeller speeds outside this region the forces involved are unevenly matched with downward liquid flow dominating the gas flow at higher impeller speeds. At lower impeller speeds the downward liquid flow from the impeller is overcome by the buoyancy of the gas, allowing the gas to enter the impeller and be distributed radially. No similar variations were seen in the upward pumping mode, where liquid flow and gas buoyancy reinforce each other.

In 0.8% CMC this impeller combination requires a similar Re for the formation of a bubble cloud as is seen when using two disc turbines (D = T/2). In addition the Po_g values obtained are slightly lower at Re > 200, than those found for two disc turbines of the same diameter, giving a lower power consumption at N_{BC} particularly in the downward pumping mode.

For both the 1.4% and 0.8% CMC solutions, complete gas distribution occurred at similar impeller speeds in the upward pumping mode as seen for two large disc turbines (D = T/2). A more precise comparison would be inappropiate, as this subjective test relies upon visual observation of the vessel contents.

7.3.4) Conclusions and Comments on Aerated Mixing

From the results presented and discussed in this section, it can be seen that the power consumption and degree of mixing achieved by the

different impeller systems in the viscous solutions used, is varied. This is in part due to the effects which the viscoelasticity of the solutions have on mixing performances and power consumption, which alters with changing impeller diameter. In addition the shear thinning nature of the solutions reduces the mixing efficiency away from the impeller region. For adequate mixing of the most viscous solutions used, under gassed conditions, dual impeller systems of large diameter are required, although the high rotational speeds and low power consumption of the Intermig impellers does not produce the same level of gas-liquid mixing as is produced by the turbine combinations, with the additional problem of vibration occurring at certain impeller speeds.

The reduction in power consumption when gassing, compared with the ungassed liquid, can be much higher in these liquids than is generally seen in low viscosity systems. This is shown by the difference in Po and Po_g values which are shown in figure 8.23, although much higher power consumption is required to produce adequate gas-liquid mixing as the apparent viscosity of the solutions is increased.

Overall the differences noted here in the performance of the different impellers lead to or are accompanied by differences in mass transfer performance. As has been seen in the preceding sections large differences in Po_g and Re values are obtained when using different numbers of or types of impellers in the different solutions. This makes a comparison of mass transfer performance using Re as an independent variable impossible. For this reason, most of the results in the next chapter are presented in terms of power consumption in order to compare different impellers. This is a generally used criteria, principally because it is related to the cost of installation and running of agitation equipment. Where relevant, data presented in this chapter is represented in Chapter 8, using the different format. This will aid an understanding of the variations seen in mass transfer performance. To obtain a complete description of the

results presented in Chapter 8, requires some reference to the results presented and discussed in this chapter.

7.4) Additional Information Regarding Liquid Mixing Under Fermentation Conditions in the More Viscous Solutions

It can be seen from the preceding section, that the point at which adequate gas and liquid mixing occurs in the more viscous solutions is difficult to define from visual observation alone. It does however require very high power inputs of the order of 150 - 300 W depending on the agitator system used to achieve complete distribution of the gas throughout the liquid, when the liquid is very viscous (1.4% CMC, μ_r = 0.86 Pa.s). This corresponds to a power input per unit volume, P/V, of 7.5 - 15 $kW.m^{-3}$ which is prohibitive, in terms of energy costs and the heat load produced. An alternative point of view is to look at the minimum power inputs required to achieve an efficient system for aerobic fermentation to occur throughout the vessel. At this point it can be assumed that the vessel contents are being utilised effectively, providing maximum yield for minimum cost. This depends in part on the amount of yeast present and the substrate feed rate, as these parameters determine the oxygen uptake rate and hence the level of dissolved oxygen within the solution that is available for respiration by the yeast. These factors were maintained at virtually constant levels in all the experiments carried out, which enables a comparison of the different agitation systems to be made. Two criteria have been identified which can be applied to the system used here. These are described below.

7.4.1) Variation in Concentration of Oxygen in Different Parts of the Vessel

In an aerobic fermentation, if regions exist within the vessel where the concentration of dissolved oxygen is very low, or zero, then this results in a reduction of the effective volume which is being utilised

and can be harmful to the microorganisms or may cause unwanted by-products to be formed[54,150 - 152]. Thus even if the rest of the vessel contents have an adequate supply of oxygen, the existence of these regions will reduce the overall growth rate, product yield etc. In a given part of the vessel the oxygen can be supplied by local mass transfer from the gas phase and by transfer from regions of higher dissolved oxygen concentration through mixing of the liquid or by diffusion of oxygen through the liquid. If these processes are ineffective then marked variations in dissolved oxygen concentration can occur, which may be measured using dissolved oxygen electrodes.

A description of the electrodes and their positioning is contained in Chapter 5, with the means used to calibrate them at all the impeller speeds encountered in the viscous fluids is contained in Chapter 6. The principal probe, used in the estimation of mass transfer coefficients, was located near to the impeller when a single impeller was used, or in between the impellers when dual impellers were used. A second electrode was located with its probe tip in the upper regions of the liquid close to the wall. The third electrode was located with its tip close to the bottom corner of the vessel, between the two baffles. During each mass transfer experiment carried out, note was made of the dissolved oxygen readings at each impeller speed and air flow rate used. Clearly, as $k_L a$ varies with varying impeller speed (see Chapter 8), then the dissolved oxygen concentration varies also. Here we are only concerned with the relative readings of the three electrodes, so for simplicity the readings of the electrodes located in the top and bottom of the vessel have been divided by the reading for the centrally located electrode for presentation in the figures. For agitation of solutions of 0.8% CMC or less (μ_r = 0.35 Pa.s) it was found that the three probes gave virtually identical readings over the whole range of power inputs studied, regardless of impeller type. This included agitation with a single disc turbine, where the liquid

movement in the upper regions of the vessel is controlled by the movement of the gas through the liquid, as in a bubble column, making liquid movement slow. In 1.4% CMC (μ_r = 0.86 Pa.s) only dual agitator systems were used, as the use of single disc turbines in this solution did not provide sufficient liquid movement in the upper half of the vessel to ensure accurate measurement of the dissolved oxygen concentration, due to gas bubbles lodging on the tip of the electrode for long periods of time.

The results shown in figure 7.16 were obtained in a 1.4% CMC solution agitated using two disc turbines (D = T/2). It can be seen that a power input of greater than 8 $kW.m^{-3}$, corresponding to an impeller speed of 11 s^{-1} (Re = 340) for Q = 1 vvm, or 10.5 s^{-1} (Re = 313) at Q = ½ vvm, is required for reasonably even dissolved oxygen concentration throughout the vessel. However the dissolved oxygen concentration is not reduced to zero in the bottom corner until the impeller speed is reduced to 9 s^{-1} (Re = 240), corresponding to less than 5 $kW.m^{-3}$. When using Intermig impellers (figure 7.17) in the same concentration CMC solution, the results obtained show that the dissolved oxygen concentration in the lower corner of the vessel remains at zero at the highest impeller speed used, N = 16 s^{-1} (Re = 960), P = 7.6 $kW.m^{-3}$. The upper electrode indicates a wide variation in oxygen concentration at power inputs of up to 6.2 $kW.m^{-3}$ corresponding to an impeller speed of 14 s^{-1} (Re = 770). Thus the performance of the Intermig impellers is considerably worse than that of the disc turbines, despite the larger impeller diameter. The use of a pitched blade turbine in combination with a disc turbine (D = T/2) results in the upper half of the liquid undergoing a wide variety of liquid flows and varying dissolved oxygen concentrations, as can be seen in figure 7.18. When pumping upward the dissolved oxygen concentration in this region is higher than that found in lower impeller regions, particularly at intermediate power inputs, P/V = 7 - 9 $kW.m^{-3}$.

Figure 7.16

Two Disc Turbines (D=T/2)

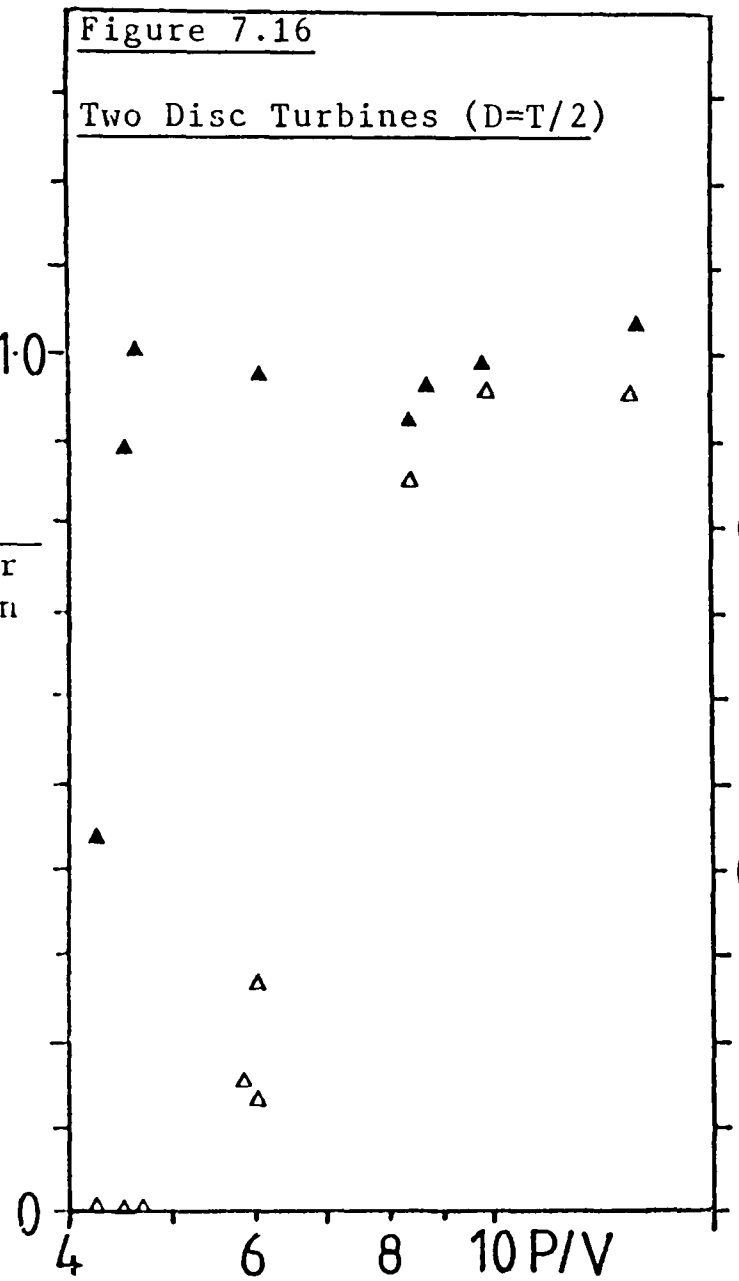

D.O. / D.O. Impeller Region

Figure 7.17

Intermigs

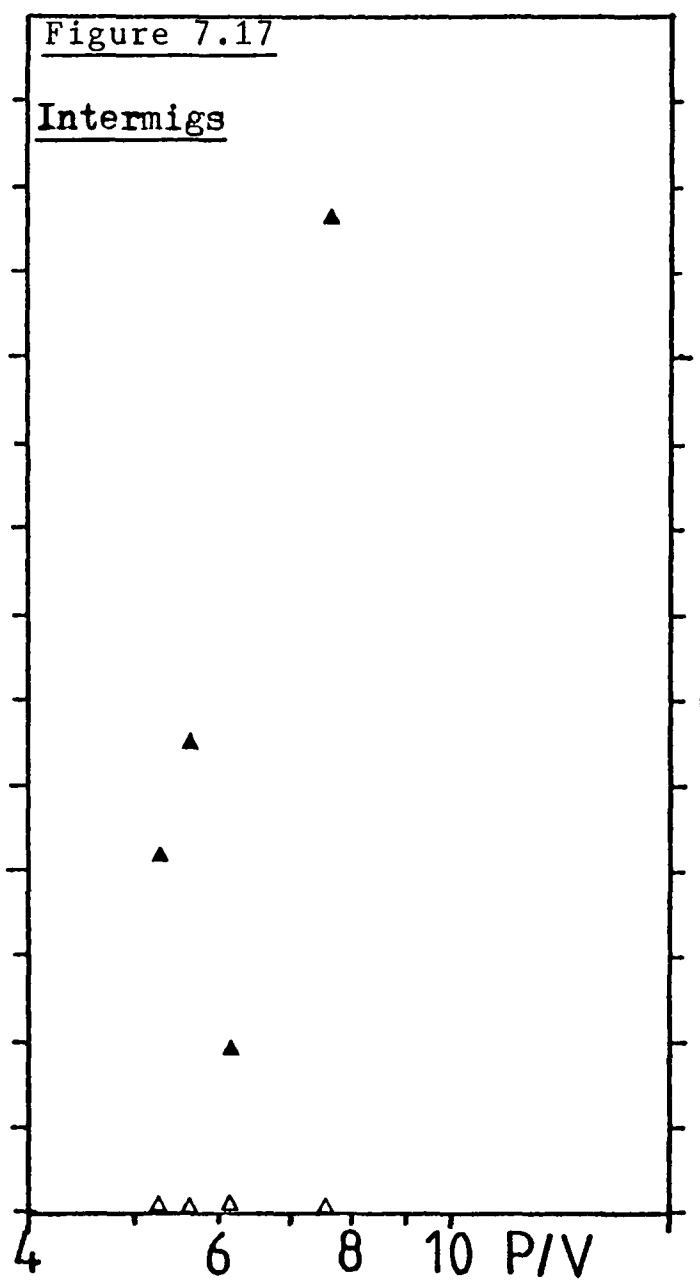

Figure 7.18

Pitched Blade/ Disc Turbine

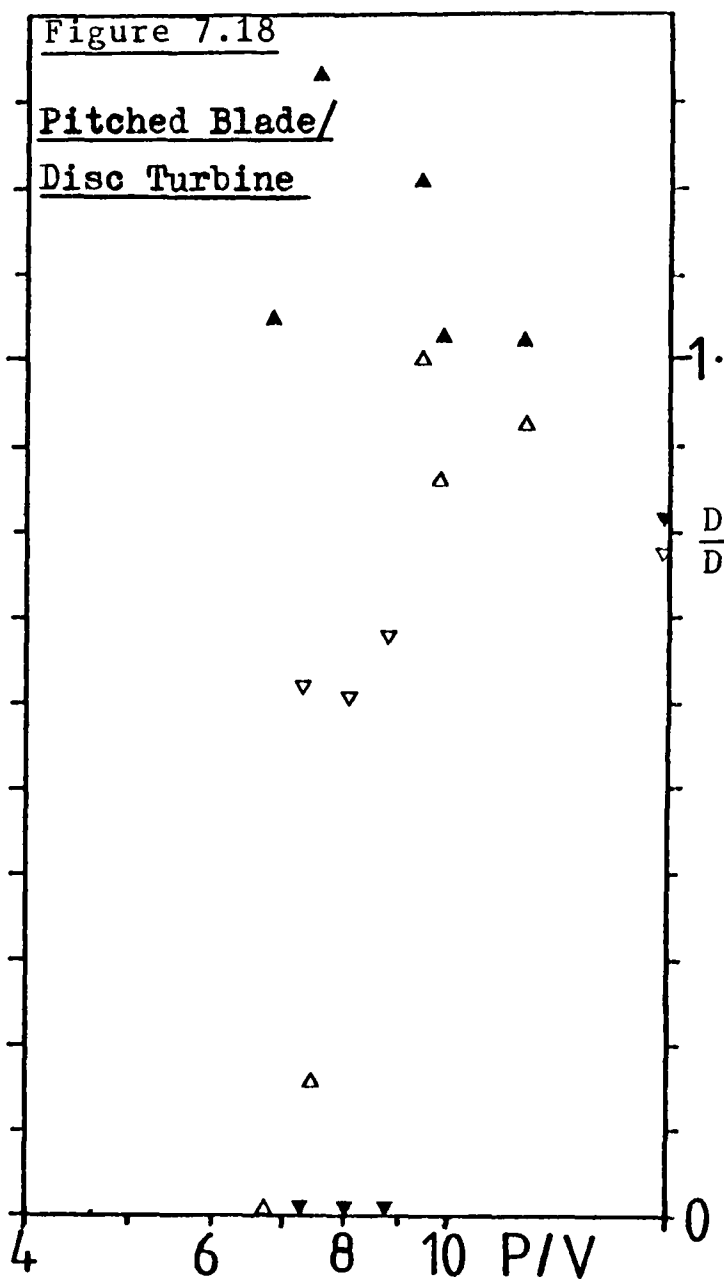

D.O. / D.O. Impeller Region

Variation in Point Dissolved Oxygen Readings in 1.4% CMC

Bottom electrode: ▽△ . Top electrode: ▼▲ . Upward Pumping: ▲ △ . Downward Pumping: ▼ ▽ .

The lowest electrode indicates similar behaviour to that found when using two disc turbines, with non-zero oxygen concentration registered at N = 10 s^{-1} (Re = 281), P/V = 7.5 $kW.m^{-3}$ and a reasonably even oxygen concentration available at N = 10.5 s^{-1} (Re = 307), P/V = 9.4 $kW.m^{-3}$, both at Q = ½ vvm, which are similar speeds to that shown by two disc turbines, although the power input is higher.

When pumping downwards the lower electrode indicates virtually the same behaviour as when pumping upwards, with the possibility that non-zero oxygen concentration occurs at lower P/V, due to the higher impeller speeds at lower power consumptions, giving rise to lower Po_g values (see figure 7.14). In the upper regions of the vessel downward pumping has a catastrophic effect on liquid mixing, rendering the liquid near to the wall virtually stagnant. This is shown by the very low oxygen concentrations seen using the upper electrode at P/V = 7 - 9 $kW.m^{-3}$. At higher power inputs, P/V = 15.6, N = 13 s^{-1}, (Re = 434), the presence of a large gas bubble underneath the upper impeller increases the average torque, and hence P/V is increased, although the torque fluctuates wildly. This reduces the dissolved oxygen readings for both the upper and lower electrodes when compared to upward pumping, indicating that the liquid flow is reduced.

Overall the use of the dissolved oxygen electrode readings provides an indication of the degree of liquid mixing within the vessel. Here it has been found that the two disc turbines (D = T/2) provide the most even oxygen concentration at the lowest power input. The use of more than three electrodes would enable further useful results to be gained in this area. However the results must be treated with caution where the general level of oxygen is low within the liquid, as is caused by low k_La, making a small effect look more significant. In addition low k_La values may reduce the dissolved oxygen concentration to zero throughout the liquid. This prevents an estimation of the mixing ability of the agitator using this technique, although the mixing within the

vessel will still affect the performance of the fermentation, as outlined in the next section.

The variation in dissolved oxygen concentration may affect the k_La values measured, in that a value for the concentration is required to determine the driving force applicable for the mass transfer rate measured. Fortunately major variations were only seen at low oxygen concentrations where the driving force is near to the maximum attainable, so a small error in the estimation of C_L does not introduce significant error in the estimation of k_La. See Appendix 2 for further details. One exception was when using the disc turbine and pitched blade turbine combination in the downward pumping mode. Here large areas in the top of the vessel became virtually stagnant with very low dissolved oxygen concentrations. Here it was necessary to estimate a mean value of C_L, which may introduce a slight error into the k_La values determined.

7.4.2) Indicators of Mixing Efficiency Provided by the Culture

The mass transfer experiments carried out here have utilised a growing culture of Bakers Yeast within the viscous solutions. Yeast was chosen as it has the advantage of being able to continue to grow under conditions of low or zero dissolved oxygen concentration, such as may occur here, by producing alcohol. When sufficient oxygen is supplied, the glucose substrate present is oxidised to carbon dioxide and water according to the overall reaction:[151]

$$C_6H_{12}O_6 + 6O_2 \longrightarrow 6CO_2 + 6H_2O$$

Thus for each molecule of oxygen used, one molecule of carbon dioxide is produced. The ratio of the carbon dioxide produced to the oxygen used is termed the Respiratory Quotient, RQ and for totally aerobic fermentation of glucose RQ = 1. In the anaerobic situation where no oxygen is available, glucose is utilised to produce energy by forming

alcohol:[151,153]

$$C_6H_{12}O_6 \longrightarrow 2C_2H_5OH + 2CO_2$$

Here RQ is infinity as no oxygen is utilised. Thus measurement of RQ gives an indication of the state of the culture and the availability of oxygen for aerobic respiration. An RQ of greater than one indicating that some degree of anaerobic fermentation is taking place.

In practice this ideal picture can be altered by several factors:

a) In the presence of a high sugar concentration (> 0.02 - 0.1% w/v) anaerobic respiration can be induced, even if the supply of oxygen is such that the solution is saturated[137]. Known as the Crabtree effect, or the reverse Pasteur effect, this raises RQ.

b) If alcohol is present, in the liquid or within the yeast, it can be utilised to provide energy when oxygen is available, according to:[151,154]

$$3O_2 + C_2H_5OH \longrightarrow 2CO_2 + 3H_2O$$

This will lower RQ.

c) Carbon dioxide produced during respiration can be utilised by the yeast[153,154]. This may occur if the substrate levels are very low. This reduces RQ.

d) Carbon dioxide may remain dissolved in the liquid or undergo reaction to form other soluble species reducing its concentration and hence reducing mass transfer to the gas phase. In addition it may be held within the yeast in quantity prior to transfer to the liquid[154]. This will also reduce RQ.

The respiratory quotient can be measured by analysis of the inlet and exit gas phases of the vessel, which is already carried out here for the determination of mass transfer coefficients as described in Chapter 6. The results obtained for agitation of 0.8% CMC (μ_r = 0.35 Pa.s) at an air flow rate of ½ vvm are shown in Figure 7.19 for all the impeller

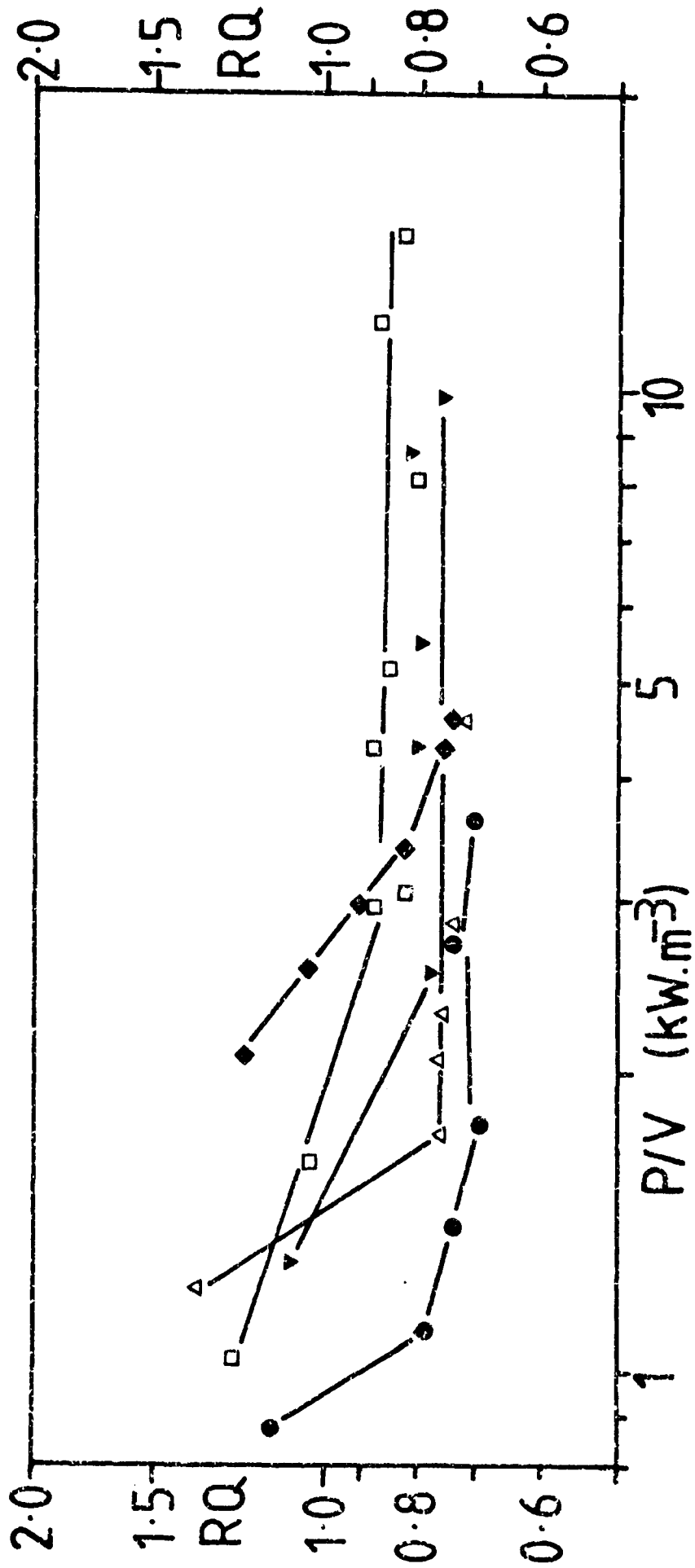

Figure 7.19

Variation in the Respiratory Quotient, RQ, with Power Input, in 0.8% CMC

One Disc Turbine (D=T/2), □; Two Disc Turbines (D=T/2), Δ; Two Disc Turbines (D=T/3), ●; Two Intermigs (D=0.58T), ◆; Pitched Blade/Disc Turbine Combination (D=T/2), ▼.

systems used. Similar results were obtained at Q = 1 vvm. At high P/V (> 5kW.m^{-3}) it can be seen that RQ is between 0.7 and 0.8, which is below the level required for totally aerobic respiration of glucose. As this level seems to be the general base level found in all experiments at all viscosities , it is postulated that some of the carbon dioxide is being removed through mechanisms c) and/or d) outlined above, in this way between 20 - 30% of the carbon dioxide is removed. Barford and Hall[154] found that a similar level of CO_2 was unaccounted for in their yeast cultivations, not appearing as cell mass or in the exit gas stream. They determined that it was removed from the cells or the solution, during heating which was required to determine the dry weight of the samples. Some results can be seen at low RQ values (< 0.7). These occur when the impeller speed is raised after a period with the dissolved oxygen level equal to zero in the liquid. They are likely to be caused by the oxidation of alcohol which has accumulated during these periods. These low RQ values only exist for short periods of time, generally less than 20 - 30 minutes, which indicates that little alcohol has been formed. At the lower power inputs shown,RQ rises,exceeding 1 for each agitator system studied, indicating an excess of CO_2 production due to insufficient oxygen for aerobic respiration to occur throughout the vessel. Each of the impeller systems can be judged from the minimum power at which it produces RQ values between 0.7 and 0.8. It can be seen that the Intermigs require 4.3 kW.m^{-3} (N = 10.5 s^{-1}, Re = 1100) to achieve this,whereas the dual turbines require much less power, even though they move more slowly and have a smaller diameter. The results for turbines are 1.1 kW.m^{-3} (N = 10.0 s^{-1}, Re = 390), 1.7 kW.m^{-3} (N = 5.7 s^{-1}, Re = 300) and 2.5 kW.m^{-3} (N = 6.2 s^{-1}, Re = 383) for two disc turbines (D = T/ 3), two disc turbines (D = T/2) and one disc turbine in combination with a 45° pitched bladeturbine respectively. Interestingly for the turbine impeller systems, the smallest impeller achieves the

best results in terms of lowest RQ values, at low power inputs. This may be expected from the ability of the small fast impellers to begin to disperse gas at lower impeller speeds, even though they cannot easily mix all the liquid (see section 7.3). The single disc turbine (D = T/2) shows higher RQ values over the whole range, never falling below RQ = 0.8. This would suggest that parts of the liquid are always starved of oxygen, these are probably located in the upper half of the vessel. A similar rise in RQ is seen below a power input of 3 $kW.m^{-3}$ (N = 8.5 s^{-1}, Re = 620) to that seen when using the dual impeller systems, although the slope is much shallower.

In 1.4% CMC solutions (μ_r = 0.86 Pa.s) similar results were obtained for the agitator systems used. The point at which RQ rose above 0.8 was moved to higher power inputs as is shown in figure 7.20. Here the impeller combination of a disc turbine and a pitched blade turbine produced the poorest result, requiring N = 10 s^{-1} (Re = 280), P/V = 7.5 $kW.m^{-3}$ for RQ < 0.8. This was followed by the Intermigs at N = 13 s^{-1} (Re = 680), P/V = 5.5 $kW.m^{-3}$, with the dual disc turbine (D = T/2) giving the best result at N = 9 s^{-1} (Re = 240), P/V = 4.5 $kW.m^{-3}$. At lower P/V the RQ value rose sharply for all the impeller systems indicating a rapid drop in mixing efficiency. It should be noted that the Intermigs were only just capable of achieving a RQ value less than 0.8, as higher power inputs were not available due to the heavy vibration encountered in the system at such high impeller speeds.

As a general comment, achieving a low RQ value is necessary to ensure proper utilisation of the carbon source, rather than wasting it as CO_2 and alcohol. In particular alcohol is particularly relevant here, because of the adverse effect which it may have on k_La values within the system, as mentioned in Chapter 4, section 2.3. In practise high RQ's at low dissolved oxygen concentrations could not be avoided, as it was

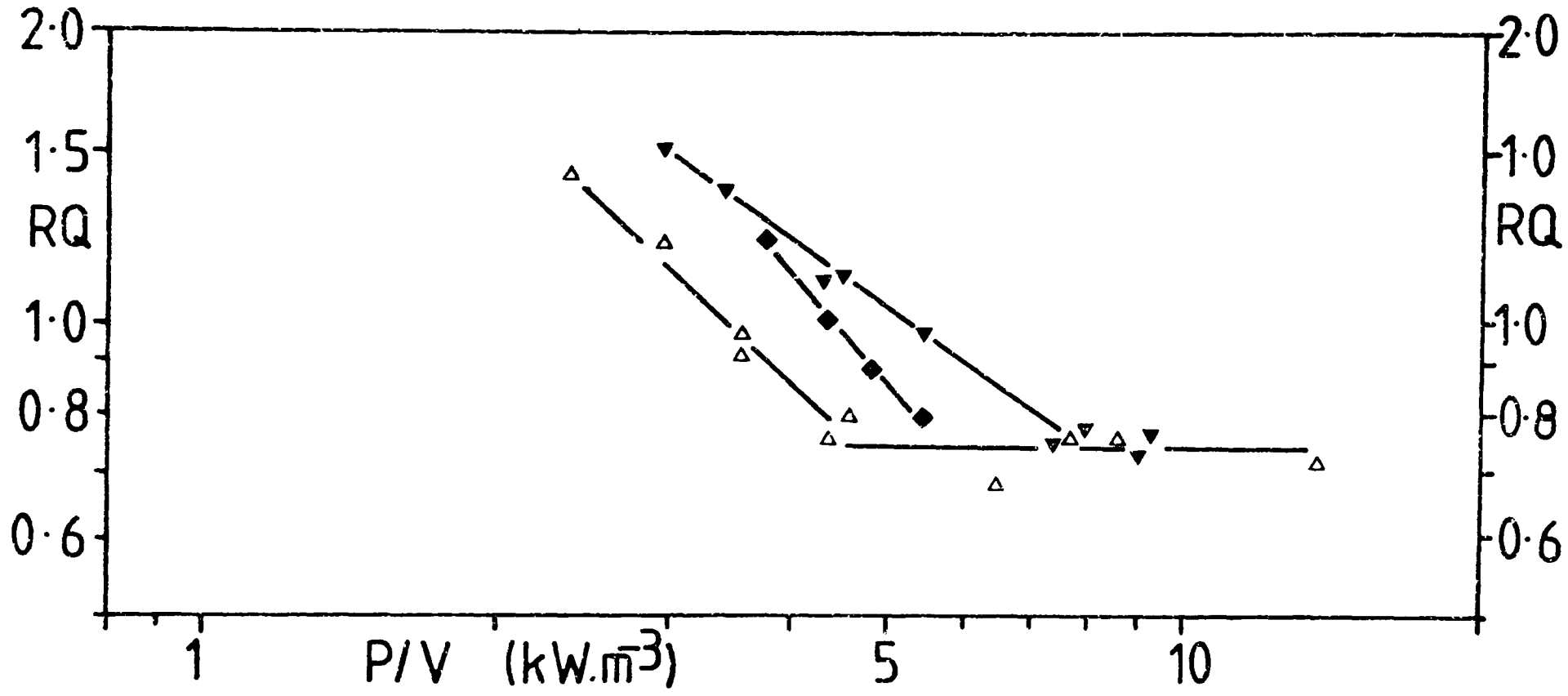

Figure 7.20

Variation in the Respiratory Quotient, RQ, with Power Input, in 1.4% CMC Two Disc Turbines (D=T/2), △, Pitched Blade/Disc Turbine Combination (D=T/2), ▼, and Two Intermigs (D=0.58T), ◆.

necessary to measure $k_L a$ values over as wide a range as is possible. In all cases the periods of time spent at lower agitation speeds were kept to a minimum, and the system was allowed to achieve full stability at higher agitation speeds, before $k_L a$ measurements were recommenced after a period of low dissolved oxygen concentrations. With this done, all hysteresis of the $k_L a$ values was removed and confidence was maintained in the results and method.

7.4.3) Conclusions Regarding Dissolved Oxygen Concentration and RQ Measurements

Clearly the two procedures just described are interdependent, with high RQ values only occurring at low or zero dissolved oxygen concentrations. They both provide a means of estimating the efficiency of a fermentation and comparing different agitator systems. They are in fact capable of more than this in that the measurement of RQ values provides information relevant to the overall process in terms of yield, by-product formation and efficiency, whilst the measurement of point dissolved oxygen values can pinpoint areas in which the vessel contents are not being efficiently utilised. In a fuller study this could lead to a better understanding of relevant variables in fermentation design, in that full gas and liquid mixing are not necessarily required for an efficient process.

Overall the Intermigs showed a poorer performance than their large diameter and high speed at low power inputs would suggest in terms of mixing efficiency. They may of course be better in other geometries, such as in tall vessels where their ability to pump liquid up and down the vessel would be more fully utilised. The same could apply to the pitched blade turbine/disc turbine combination. As in the visually observed mixing, the combination of two large disc turbines (D = T/2) showed the best results overall, although at low power inputs in intermediate viscosity solutions, the higher speed of the small disc turbine and the single disc

turbine favoured these designs.

These conclusions are not at variance with those which can be drawn from the mass transfer results discussed in the next chapter.

CHAPTER 8

MASS TRANSFER RESULTS IN CMC SOLUTIONS

8.1) Introduction

From a study of the literature reported in Chapter 4, section 5, it can be seen that the volumetric mass transfer coefficient, k_La, is often presented as a function of the agitator power consumption, or the power input per unit volume, P/V. This has the advantage of being independent of the geometry used, enabling a comparison of different impeller sizes and types in different vessels. Here it is desired to show how k_La varies with variations in viscosity, as well as P/V and air flow rate, Q. This has necessitated the measurement of k_La in a wide range of CMC solutions, 0 - 1.4%, giving variations in apparent viscosity from 0.001 - 1 Pa.s.

Initially the results obtained in water will be presented, this gives the opportunity to compare results with the data available from the literature for water and discuss some of the factors which can affect k_La. This is followed by the presentation and discussion of the results obtained in the more viscous CMC solutions (0.8 & 1.4% CMC), where the effects of impeller type and number can be seen. Next the results obtained at intermediate CMC concentrations are presented, followed by a discussion of the effects of altering viscosity in these systems.

The effects of variations in solution composition on k_La have been described in Chapter 6 for the systems used here. It should be noted that the results reported in this chapter were all obtained under identical experimental conditions, as far as is possible. Thus the variations in k_La which are discussed are independent of ionic concentrations, solution age etc., unless stated otherwise.

8.2) Mass Transfer Results in Water

There are many results reported in the literature of studies made of k_La values measured in low viscosity aqueous systems. These have been reviewed adequately by Van't Riet[71] and Judat[155] among others. It was not considered necessary to duplicate a lot of that work here, so only sufficient data have been presented to enable a comparison with the literature and with the data collected in more viscous systems.

Figure 8.1 shows the results obtained in water agitated with one disc turbine (D = T/2), at two air flow rates (Q = 1 & ½ vvm). In addition to k_La, the gas hold-up, ε , and the gassed power number, PO_g, are shown as a function of P/V. It can be seen that k_La increases linearly as a function of P/V and is also dependent on the gas flow rate. As the hold-up is increasing with P/V and Q also, then it seems reasonable to assume that the major part of the increase in k_La is due to an increase in interfacial area, brought about by the increasing impeller speed.

It can be seen by comparison with figure 6.5, that the data obtained here lie close to the "pure water" or coalescent correlation of Van't Riet[71], equation 6.1, although the measured values extend to lower P/V. This agreement is reasonable, as the concentration of ions in the solution used here is low, even though it contains yeast. Ionic concentration measurements, reported in Chapter 6, indicate a salt concentration equivalent to a 0.017M NaCl solution, which is close to the salt concentration found in tap water (0.02M). It should be noted that other workers[155] have obtained different correlations in coalescent systems which predict higher k_La values than those of Van't Riet[71]. These discrepancies would suggest that there is further work to be done in this area, although it is not of principal interest here.

Figure 8.2 shows similar data to 8.1, which was obtained using two disc turbines (D = T/3). For comparisons the k_La data shown in figure 8.1 is included as broken lines. The good agreement obtained between these

Figure 8.1

$k_L a$, Hold-Up (ε) and the Gassed Power Number (Po_g), versus P/V.
One Disc Turbine (D=T/2) in Water.

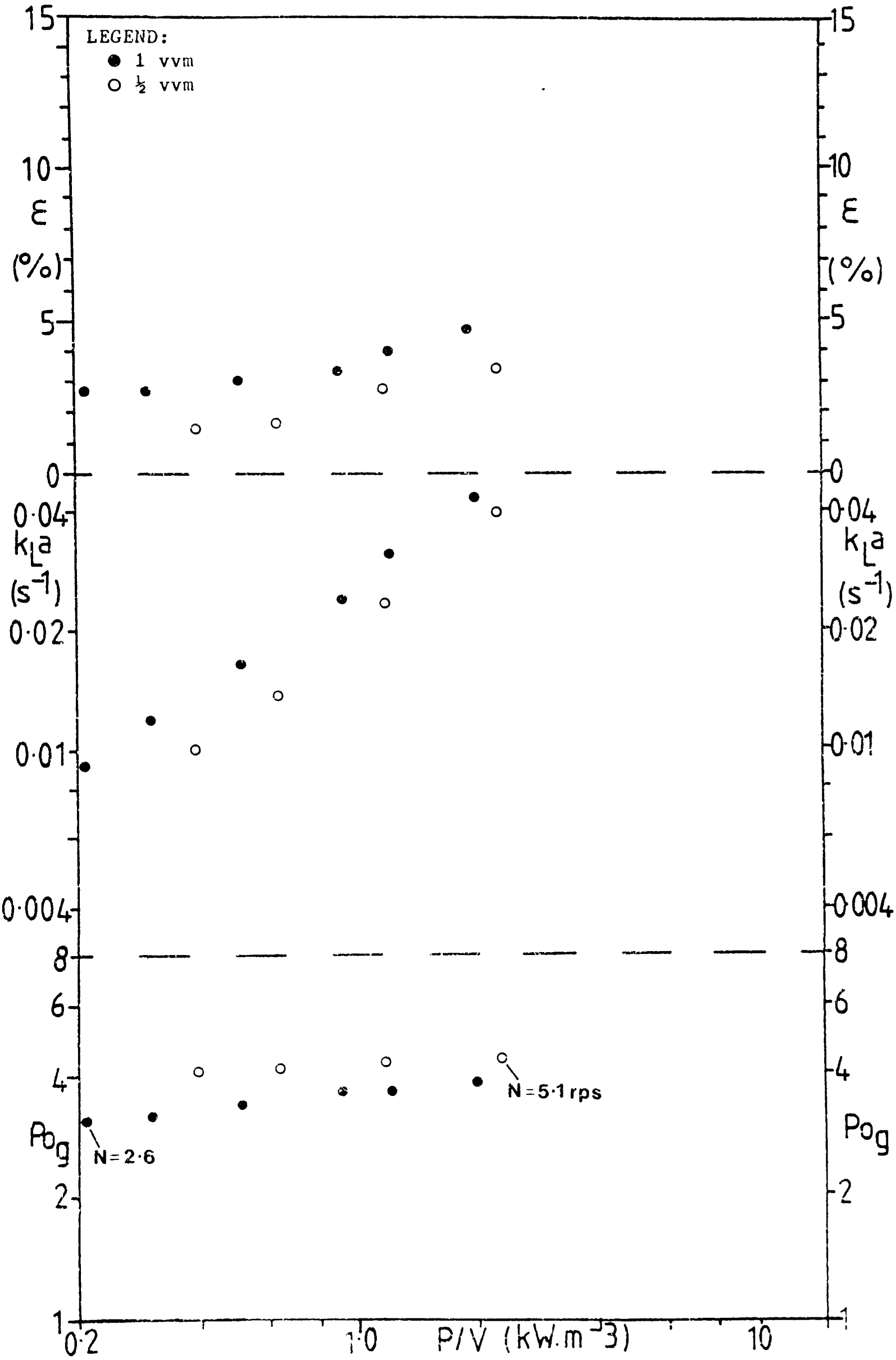

Figure 8.2

$k_L a$, Hold-Up (ε) and the Gassed Power Number (Po_g), versus P/V.
Two Disc Turbines (D=T/3), in Water.

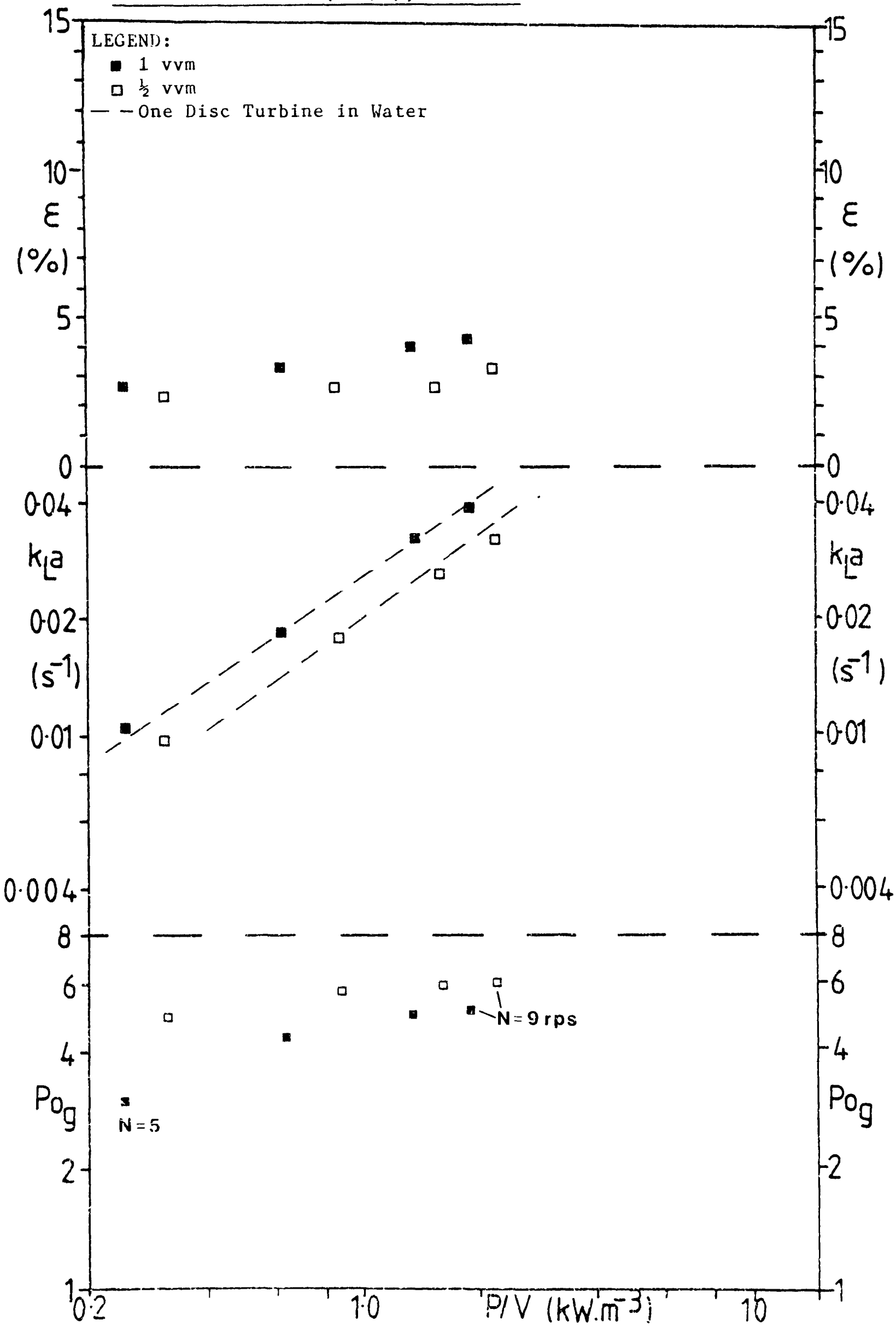

different sets of data indicates that there is little to choose between these impeller systems when agitating water, although the impeller speeds for a given P/V are different, as indicated in the figures.

Figure 8.3 shows data obtained when using two Intermig impellers (D = 0.58T). These give higher $k_L a$ values than when using disc turbines, particularly at the higher P/V. In addition $k_L a$ is less dependent on the air flow rate and the hold-up values obtained are greater. Overall the different directions of rotation available with these impellers had little effect on $k_L a$, although it did affect the hold-up at Q = ½.

From the limited data obtained in water, it can be concluded that the measuring method for $k_L a$ used here yields similar results to those presented in the literature, with the yeast solution behaving as a coalescent medium. In general the size and number of disc turbines used has no effect on $k_L a$ although a moderate increase was found when using Intermig impellers. In the next section the various impeller types and number are compared in viscous CMC solutions.

Figure 8.3

$k_L a$, Hold-Up (ε) and the Gassed Power Number (Po_g), versus P/V.
Two Intermigs (D=0.58T), in Water.

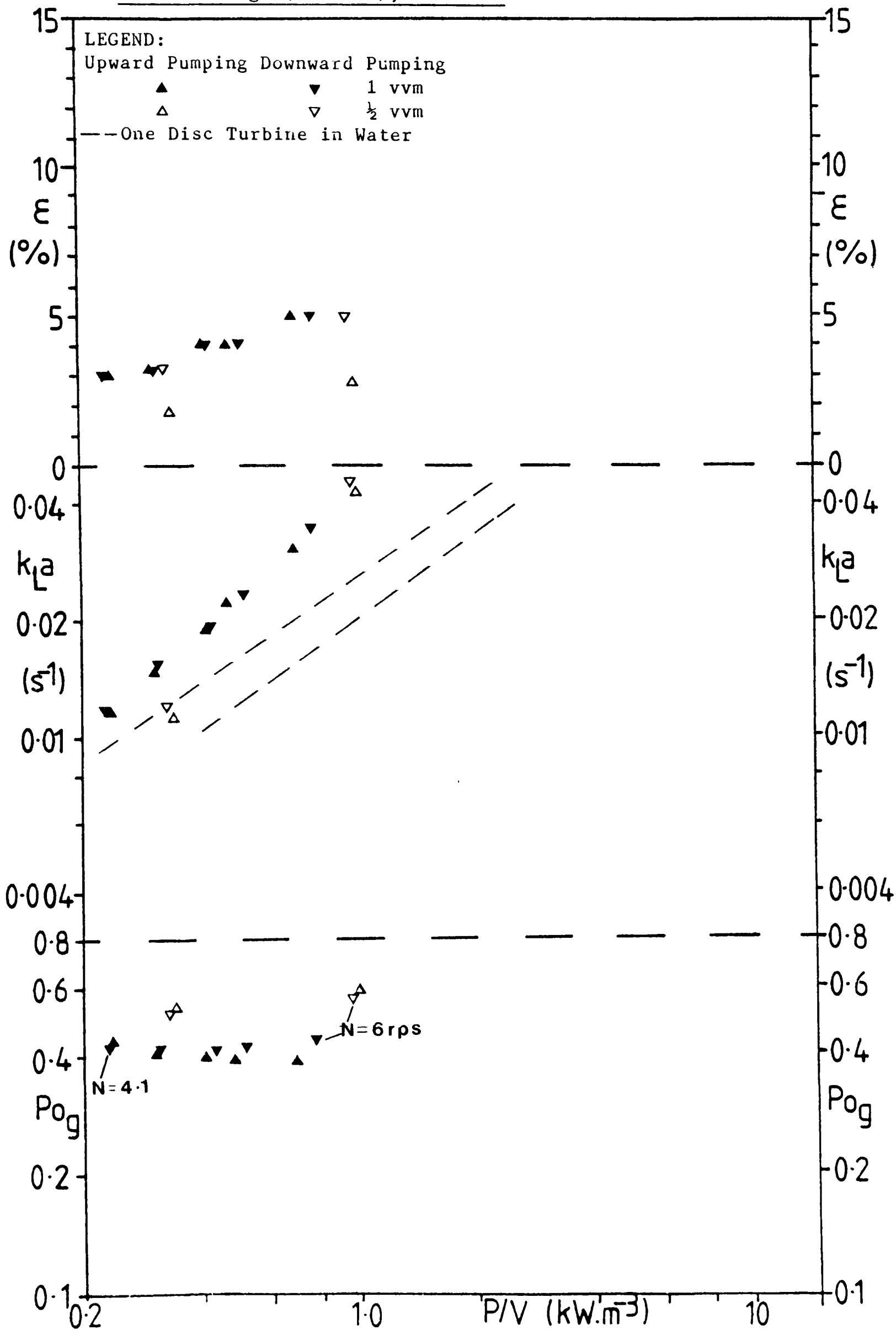

8.3) $k_L a$ Values in Viscous CMC Solutions

All the impeller combinations described in Chapter 5 were tested in the viscous CMC solutions (0.8 & 1.4% CMC) to determine whether any one design gave superior mass transfer performance to the others. The results obtained using two large disc turbines will be discussed first, as these were used in a broad range of solutions and were capable of fully mixing the most viscous CMC solutions used, which some of the other impeller systems could not (see Chapter 7). For the purposes of comparison the results obtained using two large disc turbines are reproduced in each of the figures relating to the other impeller systems, acting as a benchmark by which the other impellers can be judged.

8.3.1) Two Large Disc Turbines (D = T/2)

Figure 8.4 shows $k_L a$, ε and Po_g as a function of P/V with Q as a parameter for a 0.8% CMC solution. A comparison with the figures in the last section shows that $k_L a$ is drastically reduced compared with the values found in water. In addition the effect of air flow rate on $k_L a$ is reduced to virtually nothing, although Q still affects the hold-up obtained. At low power inputs ($P/V < 3\ kW.m^{-3}$), $k_L a$ is highly dependent upon P/V, much higher than the dependence found in water. In this same region ε rises rapidly with increasing P/V. Above $3\ kW.m^{-3}$ the $k_L a$ - P/V curve flattens. This coincides with the maximum ε being reached. At higher P/V, ε falls and $k_L a$ rises with increasing P/V, although the rise is less steep than that at low P/V. This change in slope of the $k_L a$ - P/V curve occurs at a slightly higher impeller speed than that which gives the minimum value of Po_g. As discussed in Chapter 7, this is probably related to the size of the gas filled cavities in the impeller region, and it is at this point that all the gas is being dispersed. That $k_L a$ continues to increase at higher P/V, even though ε is falling indicates that the type of hold-up is changing qualitatively. At high impeller

Figure 8.4

$k_L a$, Hold-Up (ε) and the Gassed Power Number (Po_g), versus P/V.

Two Disc Turbines (D=T/2) in 0.8% CMC.

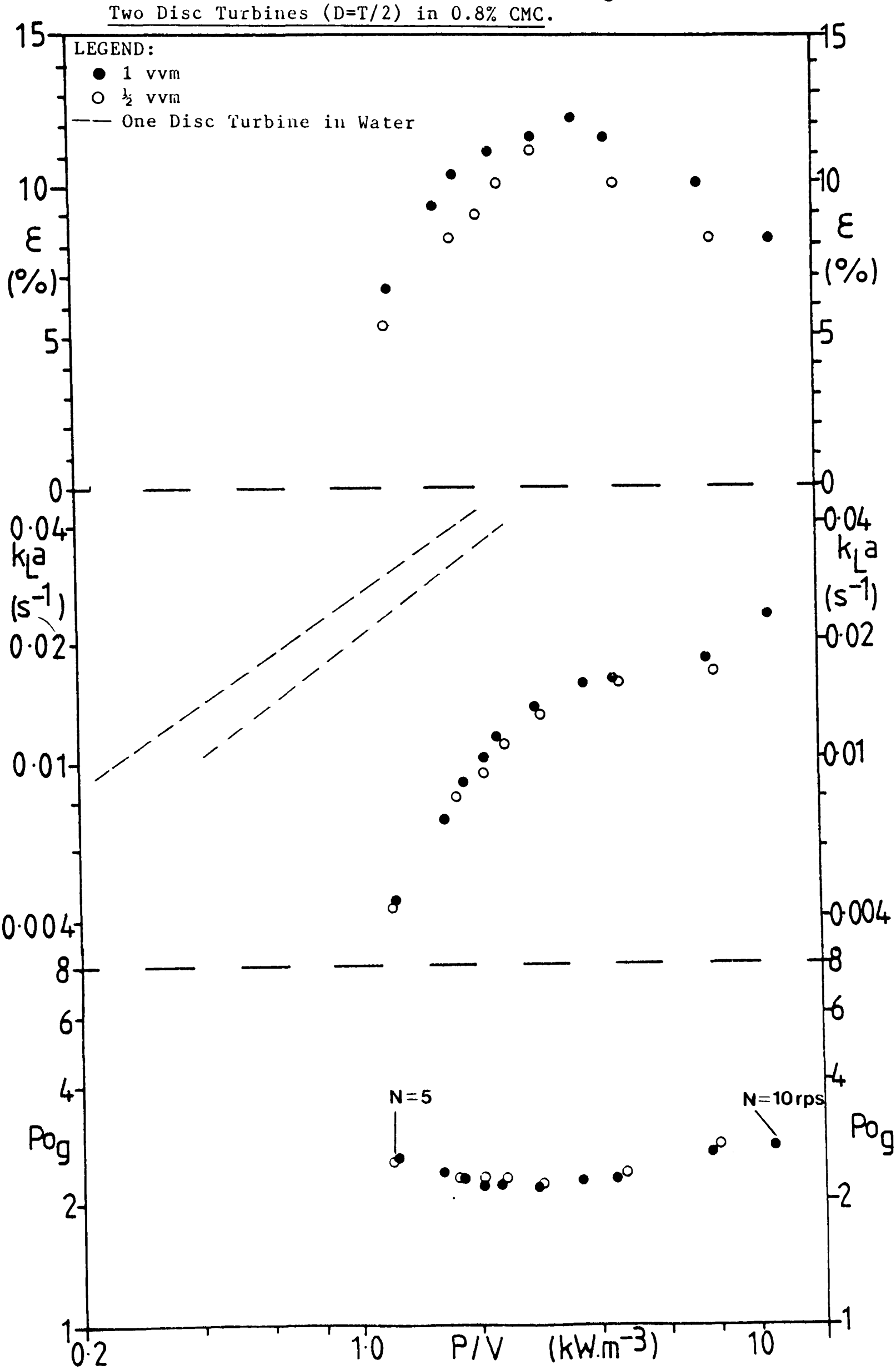

speeds the deviation found in the bubble sizes is reduced, and increased recirculation through the impeller region leads to a more even higher concentration of oxygen in the bubbles that remains in solution. Thus the surface area available for mass transfer is probably increased, even though ϵ falls, and the proportion of the area over which a high driving force is maintained also increases.

By contrast at very low impeller speeds, the hold-up is divided between very large and very small bubbles. The large bubbles are rich in oxygen, but have a low surface area to volume ratio and they leave the solution quickly. The very small bubbles, which have a high surface area to volume ratio, rapidly become depleted of oxygen, yet stay in solution for a long time.

An alternative view of the manner in which k_La varies is this: At high P/V, k_La is at an acceptable level. As P/V falls, k_La declines due to a reduction in turbulence and mixing intensity. This is offset slightly by the rise in ϵ and the fall in Po_g. At lower P/V, ϵ begins to fall and Po_g begins to rise. A large reduction in N reduces turbulence and mixing intensity for only a small reduction in P/V. This causes a large drop in ϵ and k_La falls dramatically.

Figure 8.5 shows similar data to figure 8.4, obtained using a 1.4% CMC solution. k_La is reduced compared to that found in 0.8% CMC, particularly at low P/V. This reduction in k_La compared with 0.8% CMC which is itself greatly reduced compared with water is to be expected from a consideration of the effects which increasing viscosity has on the factors which affect k_La, as discussed in Chapter 4, section 5. At high P/V, ϵ is greater in 1.4% CMC than it is in 0.8% CMC. This is reflected in the different shapes of the k_La - P/V curves obtained, with k_La values in 1.4% CMC only slightly below those in 0.8% CMC at high P/V. In a similar manner to that found in 0.8% CMC, there is a transition in the k_La - P/V curve which

Figure 8.5

$k_L a$, Hold-Up (ε) and the Gassed Power Number (Po_g) versus P/V.

Two Disc Turbines (D=T/2) in 1.4% CMC.

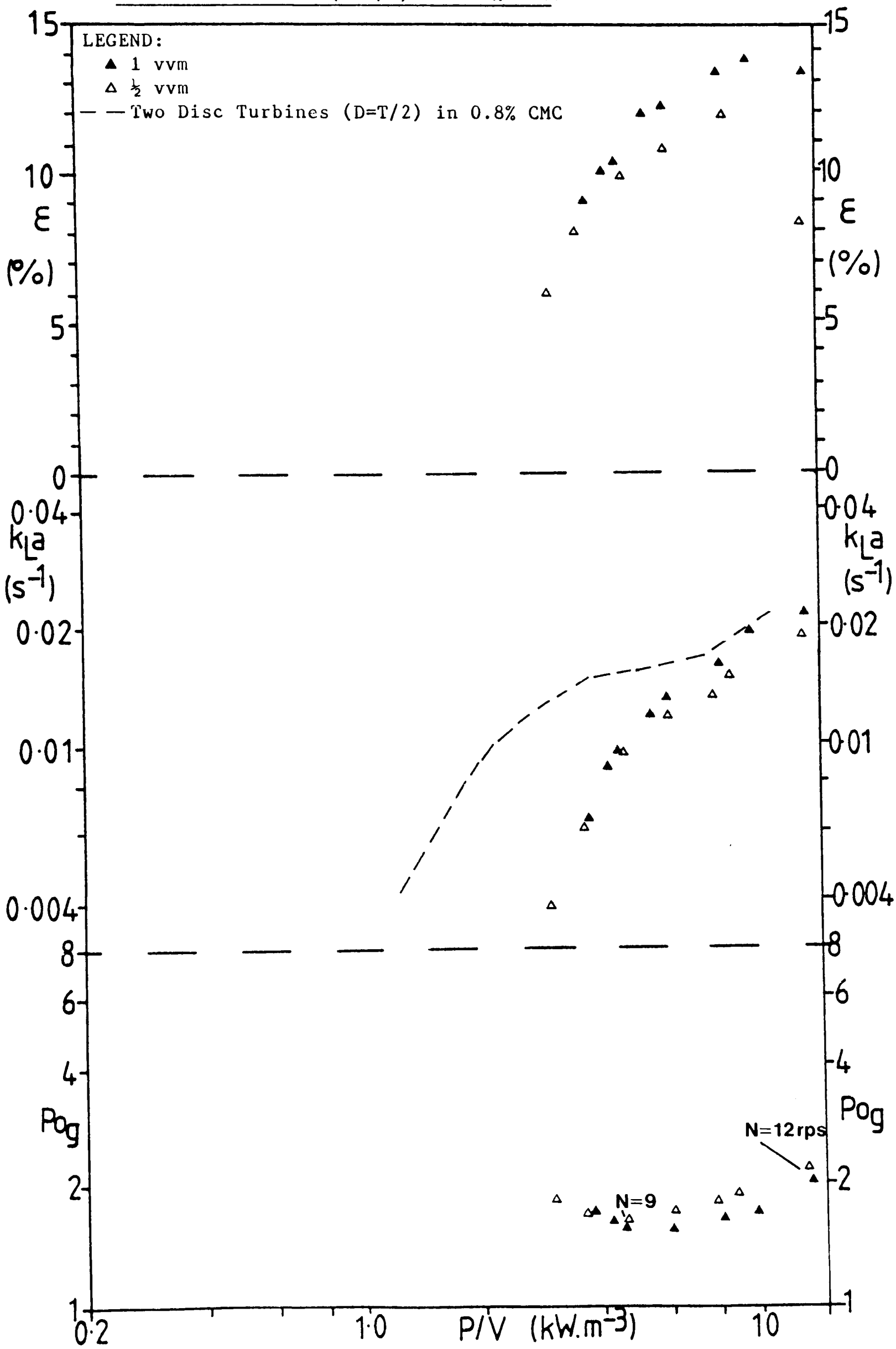

occurs at around 6 $kW.m^{-3}$. Above this power input the dependence of k_La on P/V falls compared with that found at lower P/V. Again this can be linked to variations in ϵ and Po_g, but the transitions are not so clear. One interesting effect is that of Q upon k_La in 1.4% CMC. It would appear that above 6 $kW.m^{-3}$, k_La is dependent upon Q. However if the data is presented as a function of impeller speed (or Re) rather than P/V, as shown in figure 8.5a, then any dependence on Q or ϵ disappears. This indicates that in this most concentrated CMC solution, k_La is totally dependent upon the impeller speed, N, whilst Q and N determine Po_g and P/V. As the minimum Po_g attained and the Re at which it occurs are dependent upon Q, this effects P/V for a given impeller speed at high impeller speeds, producing the apparent effect of Q upon k_La and the change in slope of the k_La - P/V curve.

8.3.2) Two Small Disc Turbines (D = T/3)

The results obtained when agitating 0.8% CMC with these impellers are shown in figure 8.6. For a given P/V the impeller speed required is much higher when using these small disc turbines than when using the larger ones. This is reflected in the results, which show better k_La values at low P/V, which is probably linked to the onset of gas-liquid mixing being achieved at lower P/V, as shown in table 7.2. For intermediate power inputs, P/V = 2 - 4 $kW.m^{-3}$, the k_La values obtained for the two sizes of impeller are very similar. As before no significant effect of air flow rate is noticeable and ϵ values for the two air flow rates are similar to each other, although lower than those obtained using the large turbines. No results were obtained at high P/V levels, because the very high impeller speeds required were not desirable for long periods of time, with severe vibrations apparent in the apparatus. Similarly no k_La results were obtained in 1.4% CMC. This was partly due to the lack of adequate gas-liquid mixing; even at N = 25 s^{-1} (P/V =

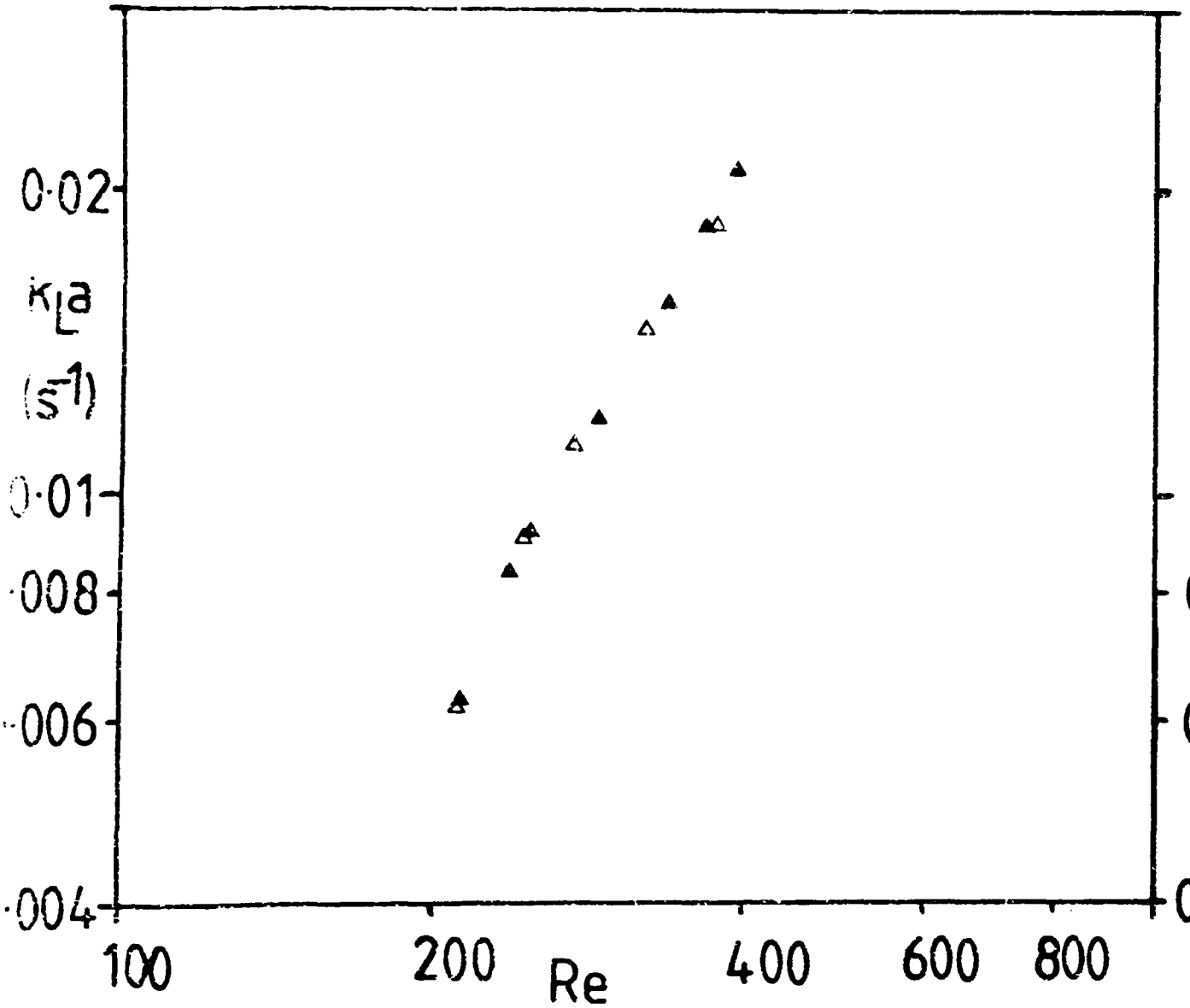

Figure 8.5a k_La versus Reynolds Number in 1.4% CMC Agitated with Two Disc Turbines (D=T/2)

[Legend as in figure 8.5]

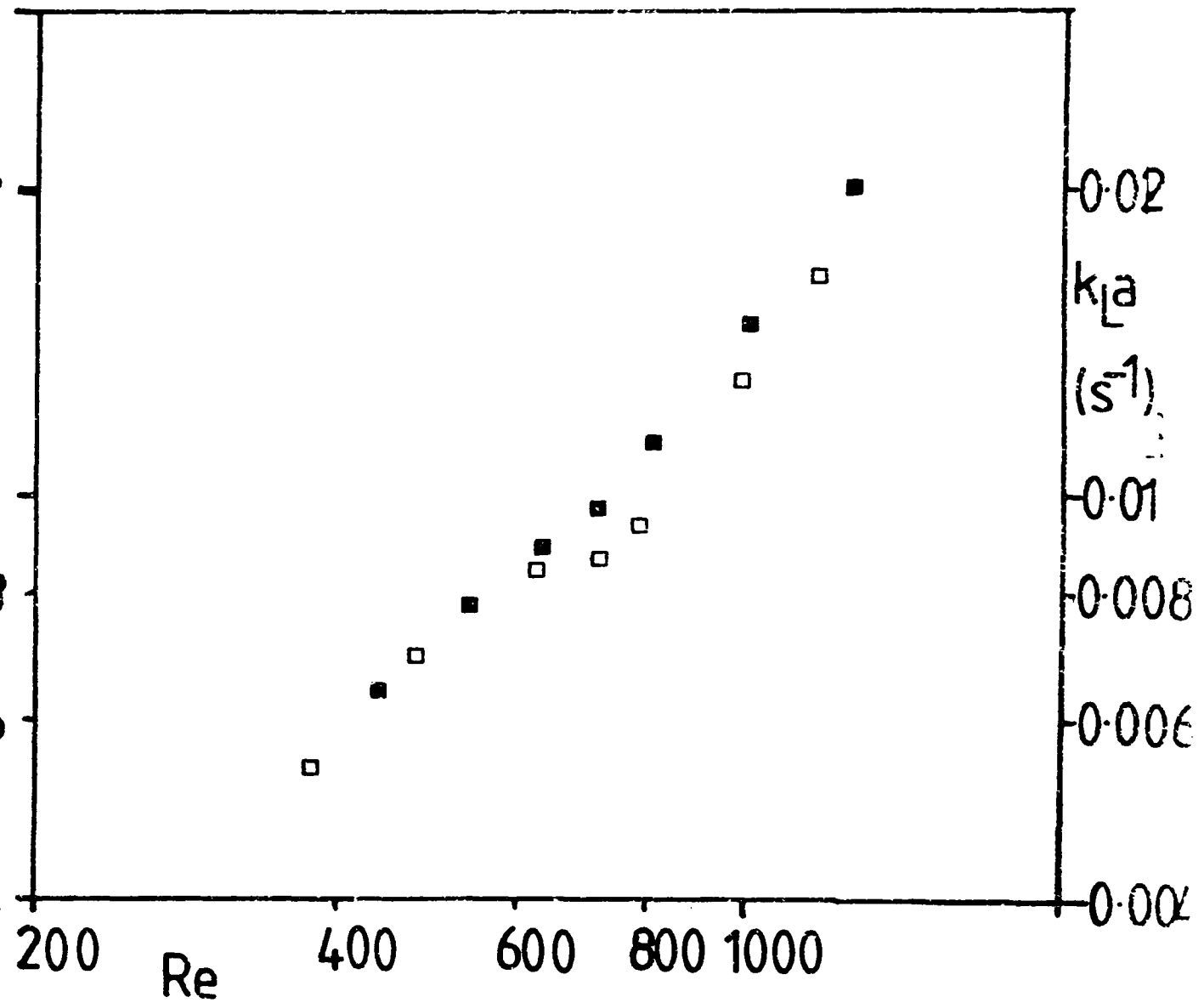

Figure 8.7a k_La versus Reynolds Number in 0.8% CMC Agitated with One Disc Turbine (D=T/2)

[Legend as in figure 8.7]

Figure 8.6

$k_L a$, Hold-Up (ε) and the Gassed Power Number (Po_g) versus P/V.
Two Disc Turbines (D=T/3) in 0.8% CMC.

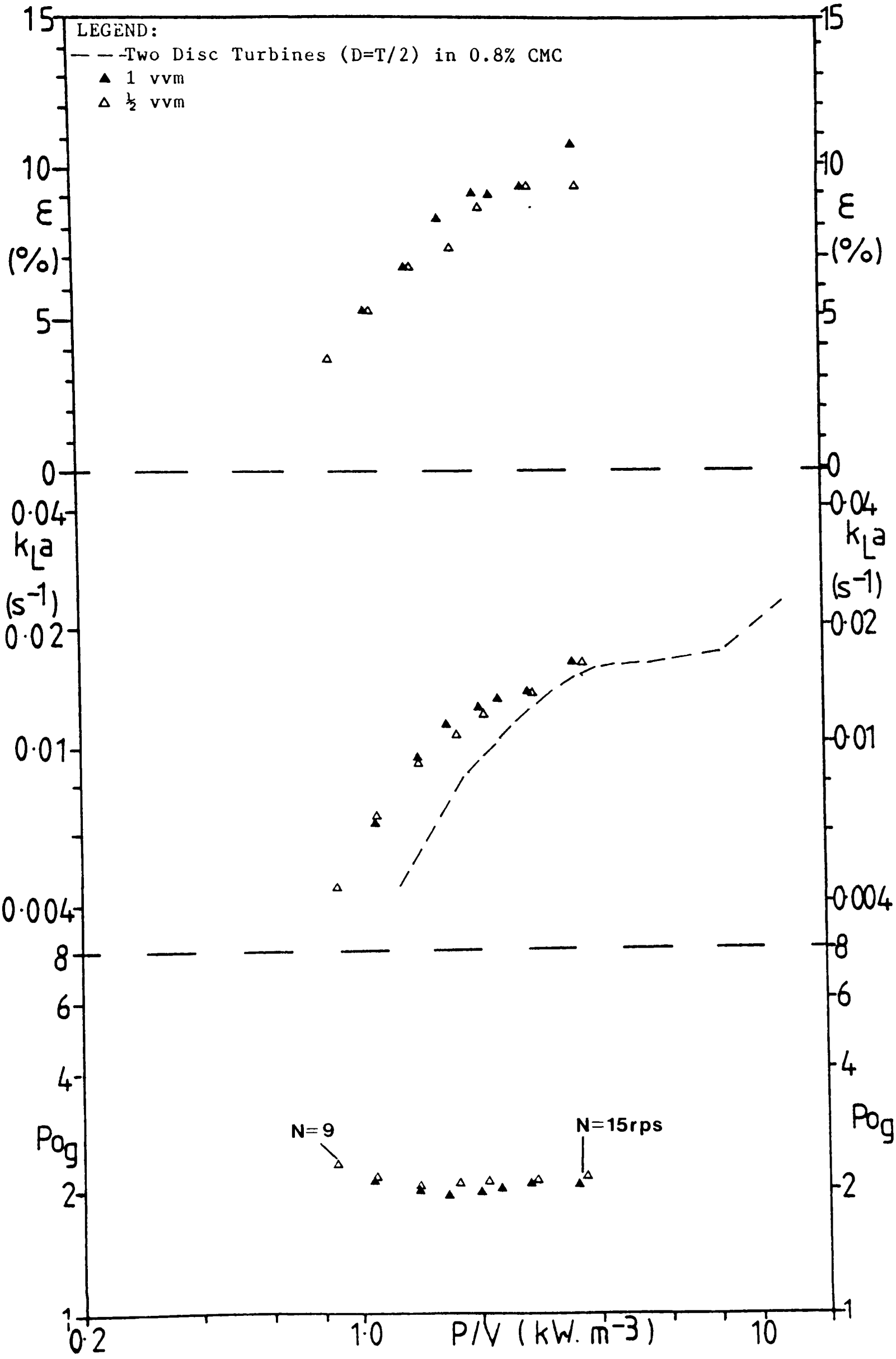

15 $kW.m^{-3}$), large areas in the top 50 mm of the vessel and in the bottom corners remained stagnant. This indicates that the use of small impellers in very viscous systems is not to be recommended.

One interesting effect noted when using these impellers in 0.8% CMC is that the two distinct mixing patterns which could occur at intermediate impeller speeds gave different power consumptions for the same impeller speed (see Chapter 7, section 3.1). The lower data points presented in figure 8.6 were obtained when mixing pattern A was dominant in the solution at N = 9 s^{-1}. The slightly higher data was also obtained at N = 9 s^{-1} but when mixing pattern B occurred. This resulted in a higher P/V and a higher k_La value. Thus neither mixing pattern is preferred, in that they gave similar k_La / P/V performance.

8.3.3) Single Disc Turbine (D = T/2)

As when using two small disc turbines (D = T/3) this impeller was incapable of completely mixing 1.4% CMC adequately at the maximum speed available (N = 17 s^{-1}, P/V = 24 $kW.m^{-3}$). The results of mixing 0.8% CMC using this impeller are shown in figure 8.7. Again at low P/V this impeller gives better k_La data than when using two large disc turbines, presumeably due to the higher impeller speed available for a given P/V. At high P/V the reverse occurs with lower k_La shown by this impeller. This is linked to a reduction in the quality of the mixing in the upper half of the vessel and a reduction in the ϵ values obtained at intermediate P/V, which is particularly marked for Q = ½vvm. This gives a level plateau of the k_La - P/V curve over the range P/V = 4 - 5 $kW.m^{-3}$. Above this P/V, k_La rises again with rising ϵ . For P/V >4 $kW.m^{-3}$ there is a genuine effect of Q on k_La and Po_g, which is shown in figure 8.7a, where k_La is plotted against Re. At ½ vvm the level plateau of k_La at intermediate P/V causes the results for the two air flow rates to deviate at higher N and Re. The difference in the Po_g values for the two air flow rates serves to increase this separation.

Figure 8.7

$k_L a$, Hold-Up (ε) and the Gassed Power Number (Po_g), versus P/V.

One Disc Turbine (D=T/2) in 0.8% CMC.

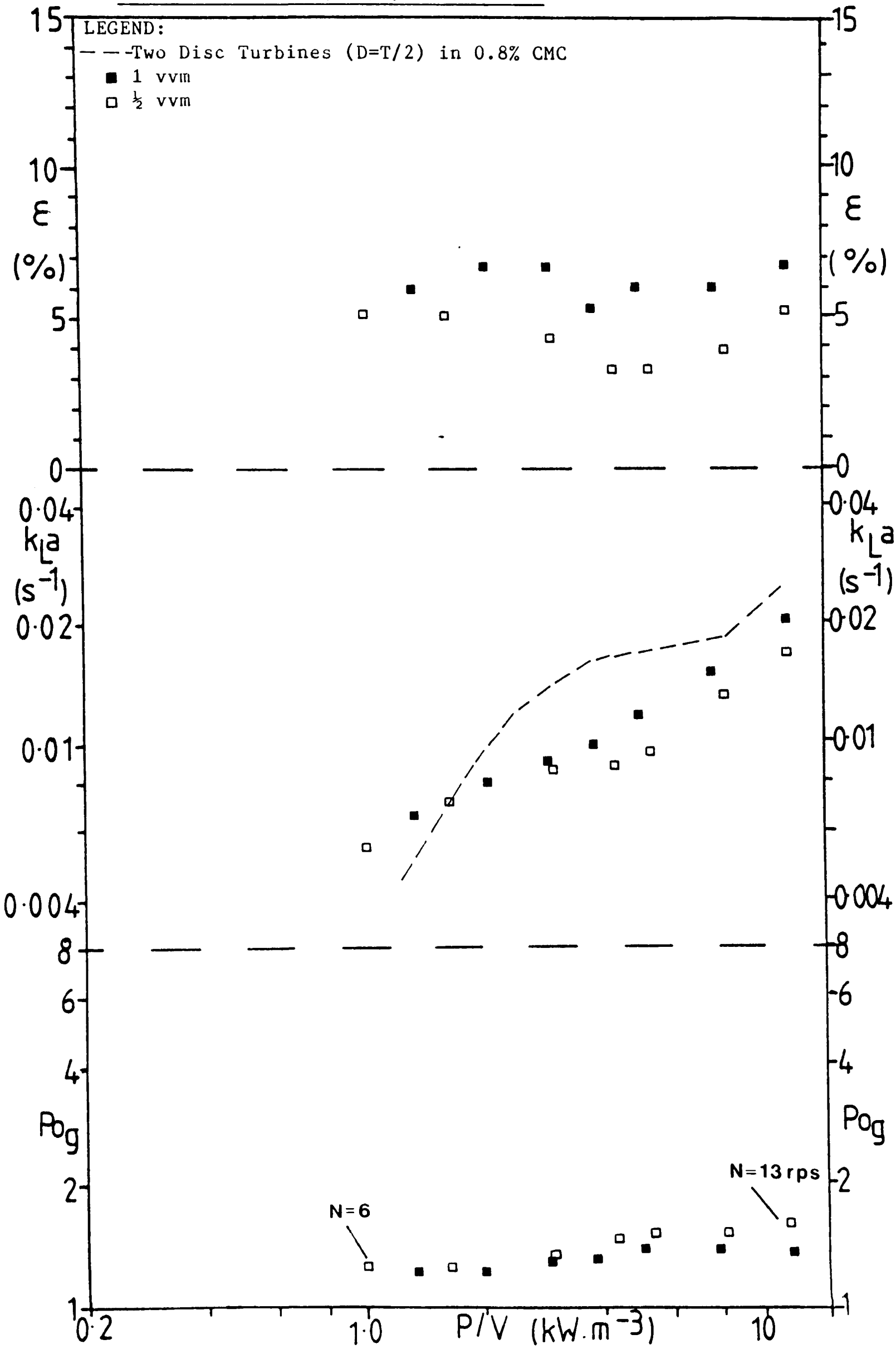

From the results presented in section 8.3 and figures 8.4 - 8.7, it can be seen that the use of a single disc turbine or a pair of small disc turbines (D = T/3) is advantageous for mass transfer at intermediate viscosities, if the k_La values required are very low ($k_La < 0.01\ s^{-1}$) or if the power available is low ($P/V < 1\ kW.m^{-3}$). Under other conditions, two large turbines give better k_La values for a given P/V, especially if the liquid is very viscous as is the case in 1.4% CMC.

The use of the pitched blade turbine in combination with a disc turbine is described in the next section. After that the results obtained using Intermig impellers are described.

8.3.4) 45° Pitched Blade Turbine in Combination with a Disc Turbine (D = T/2)

Figure 8.8 shows the results obtained when using this impeller combination in 0.8% CMC. In the upward pumping direction of rotation, the k_La values show a similar trend to those obtained using two disc turbines, but at lower values. This difference may in part be due to the reduced impeller speed seen for a given P/V when using this combination, as shown by the higher Po_g values. At high and low P/V k_La rises steeply with increasing P/V. In the intermediate range ($P/V = 3 - 6\ kW.m^{-3}$), k_La is virtually independent of P/V, but is highly dependent on Q, with increasing air flow rate giving higher k_La values. In addition, the hold-up shows a shallow maximum at $P/V = 4 - 5\ kW.m^{-3}$ falling at slightly higher P/V. This is followed by a rise in hold-up at high P/V.

In the downward pumping mode lower k_La values are found at intermediate P/V. This is linked to the cyclic variations in hold-up and torque seen at these impeller speeds, which is due to the trapping of gas below the upper impeller (see Chapter 7, section 3.3). At high P/V hold-up and torque are steady and k_La is on a par with that seen in the upward pumping mode, although the hold-up is much lower.

In 1.4% CMC erratic hold-up and torque readings are only seen at

Figure 8.8

$k_L a$, Hold-Up (ε) and the Gassed Power Number (Po_g), versus P/V.
Pitched Blade/Disc Turbine Combination (D=T/2) in 0.8% CMC

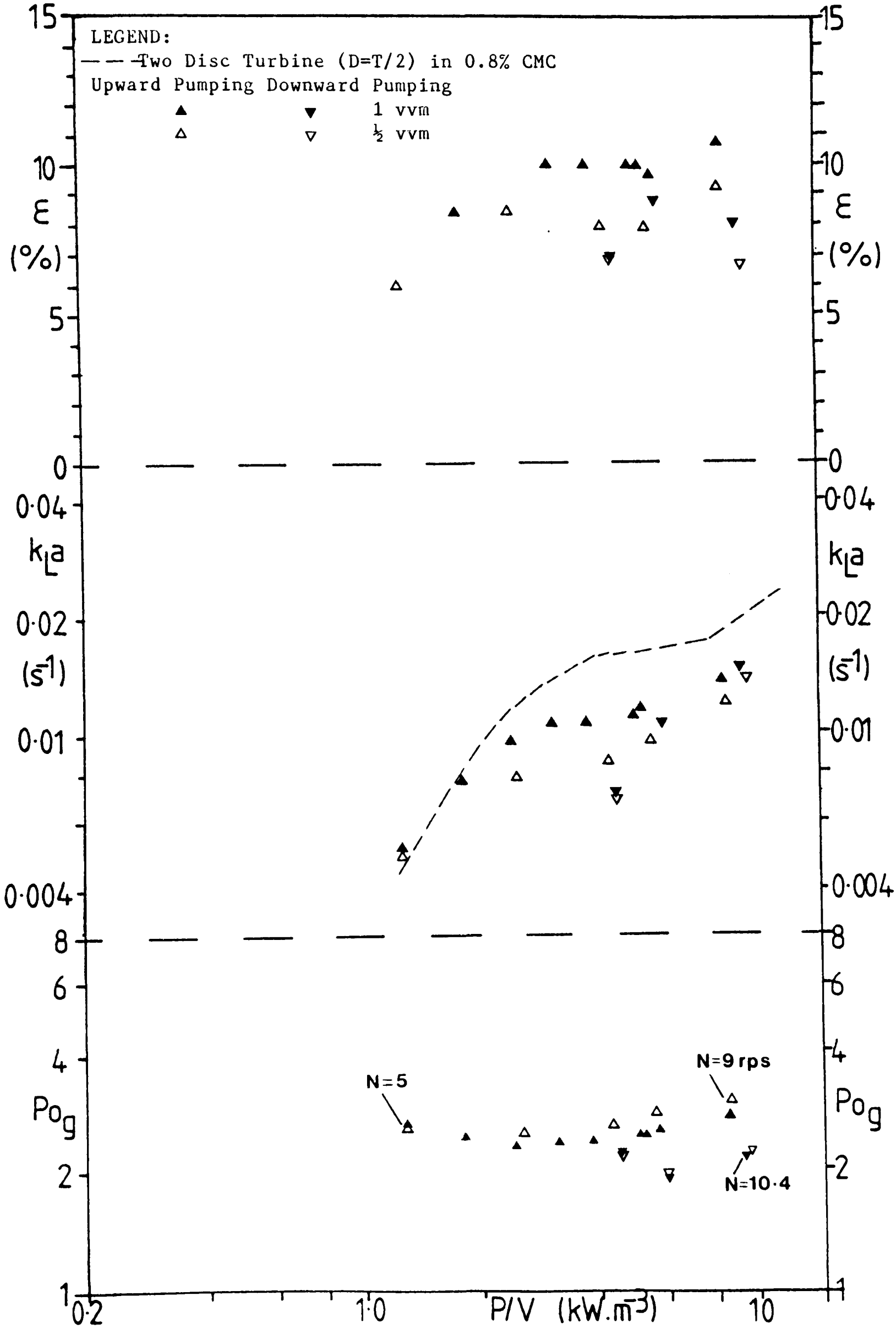

the highest impeller speed when in the downward pumping direction of rotation. This results in an increase in P/V and a reduction in k_La, as is shown in figure 8.9. At lower P/V, the pumping direction has little effect on k_La, although the slightly higher impeller speeds for a given P/V when downward pumping does enhance the k_La values slightly. No effect of Q on k_La is seen, although Q = 1 vvm does give a slightly higher hold-up than Q = ½ vvm, with the same hold-up obtained for both pumping directions. Compared to the results obtained for two disc turbines, k_La values are slightly lower at all P/V and there is much less curvature in the k_La - P/V curve. This contrasts with the results obtained in 0.8% CMC where a large difference in k_La values was seen between this impeller configuration and the use of two disc turbines.

8.3.5) Intermigs (D = 0.58T)

Although the use of a ring sparger did not give different Po_g values when compared to a point sparger in 0.8% CMC solutions, it was found that reasonable gas-liquid mixing could be achieved at lower impeller speeds when a ring sparger was used (see Chapter 7, section 3.2). In order to compare the mass transfer performance of the two sparger types, experiments were conducted using each of them in 0.8% CMC. From the results, shown in figures 8.10 and 8.11, it can be seen that the use of a ring sparger increases the k_La values found by a small amount, particularly at low P/V. This can be attributed to the better gas-liquid mixing at low P/V. The small difference at higher P/V is probably due to a slight variation in rheological properties of the sclutions used; as the solution used in conjunction with the point sparger gave a slightly higher apparent viscosity, which was sufficient to lower the k_La value slightly (see section 8.4), for a given impeller speed.

It can be seen from figures 8.10 and 8.11 that the hold-up increases rapidly with increasing P/V, which is matched by the increase in k_La.

Figure 8.9

$k_L a$, Hold-Up (ε) and the Gassed Power Number (Po_g), versus P/V.
Pitched Blade/Disc Turbine Combination (D=T/2) in 1.4% CMC.

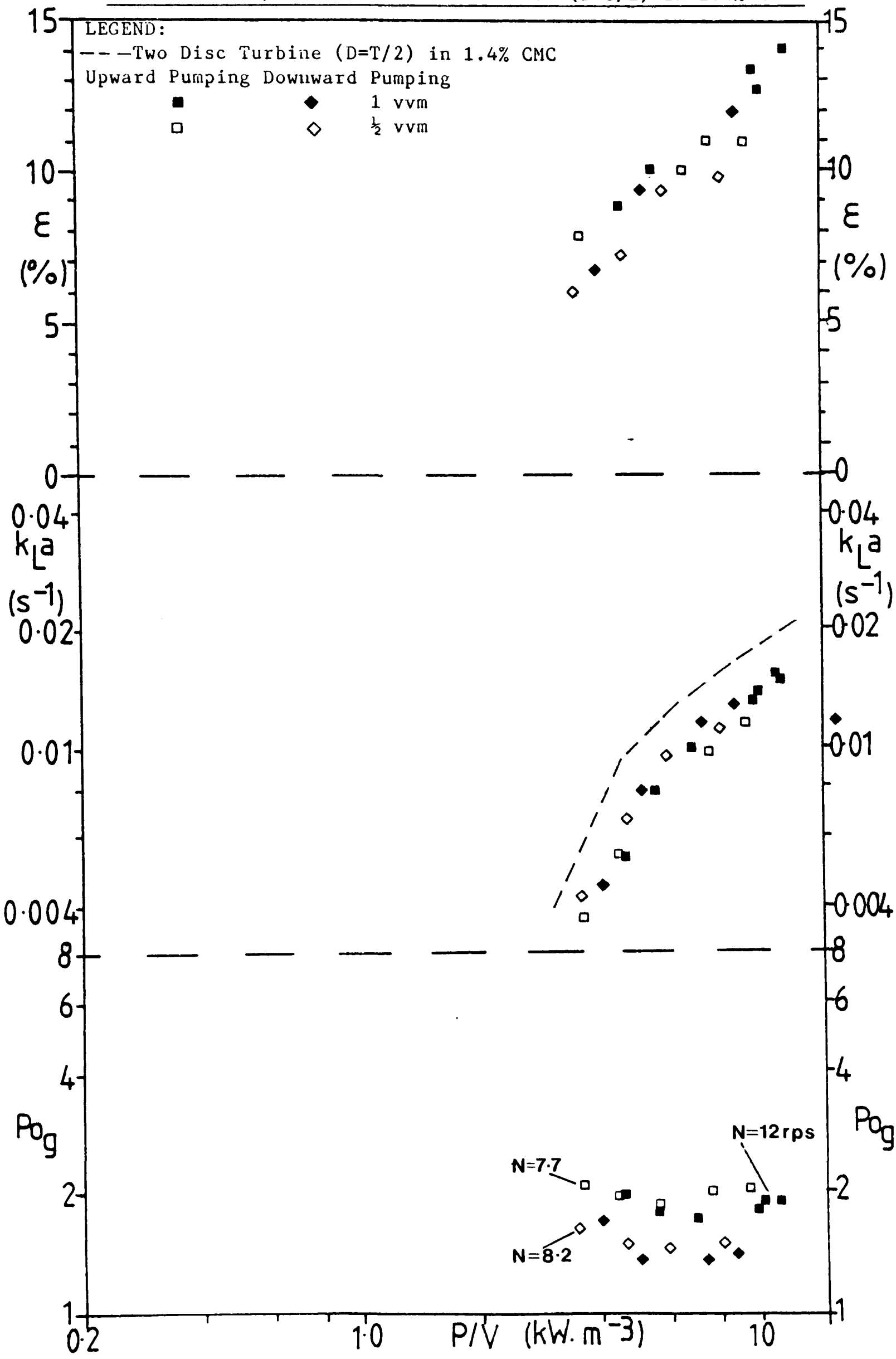

Figure 8.10

$k_L a$, Hold-Up (ε) and the Gassed Power Number (Po_g), versus P/V.

Two Intermigs (D=0.58T) in 0.8% CMC, Ring Sparger

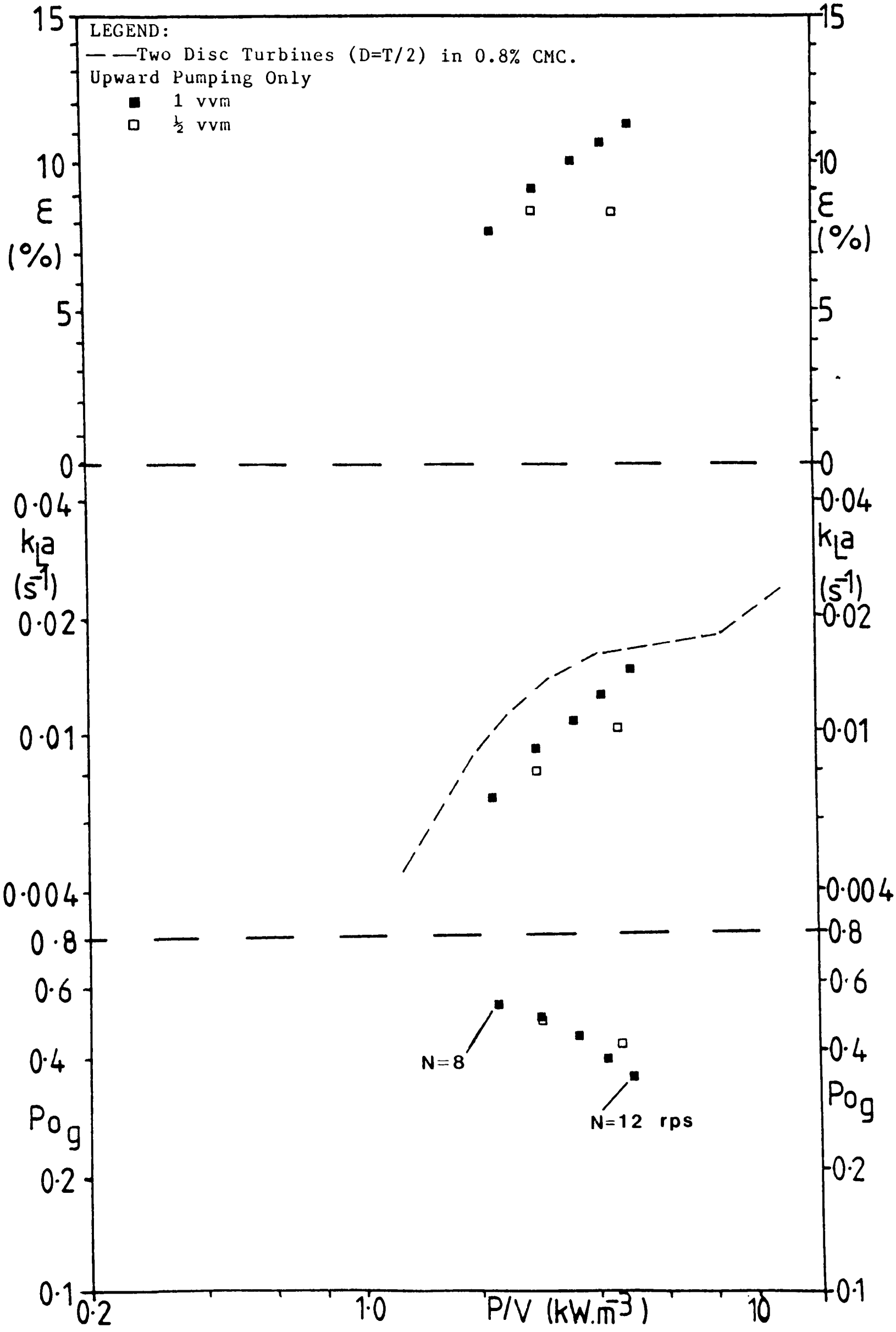

Figure 8.11

$k_L a$, Hold-Up (ε) and the Gassed Power Number (Po_g), versus P/V.

Two Intermigs (D=0.58T) in 0.8% CMC, Point Sparger.

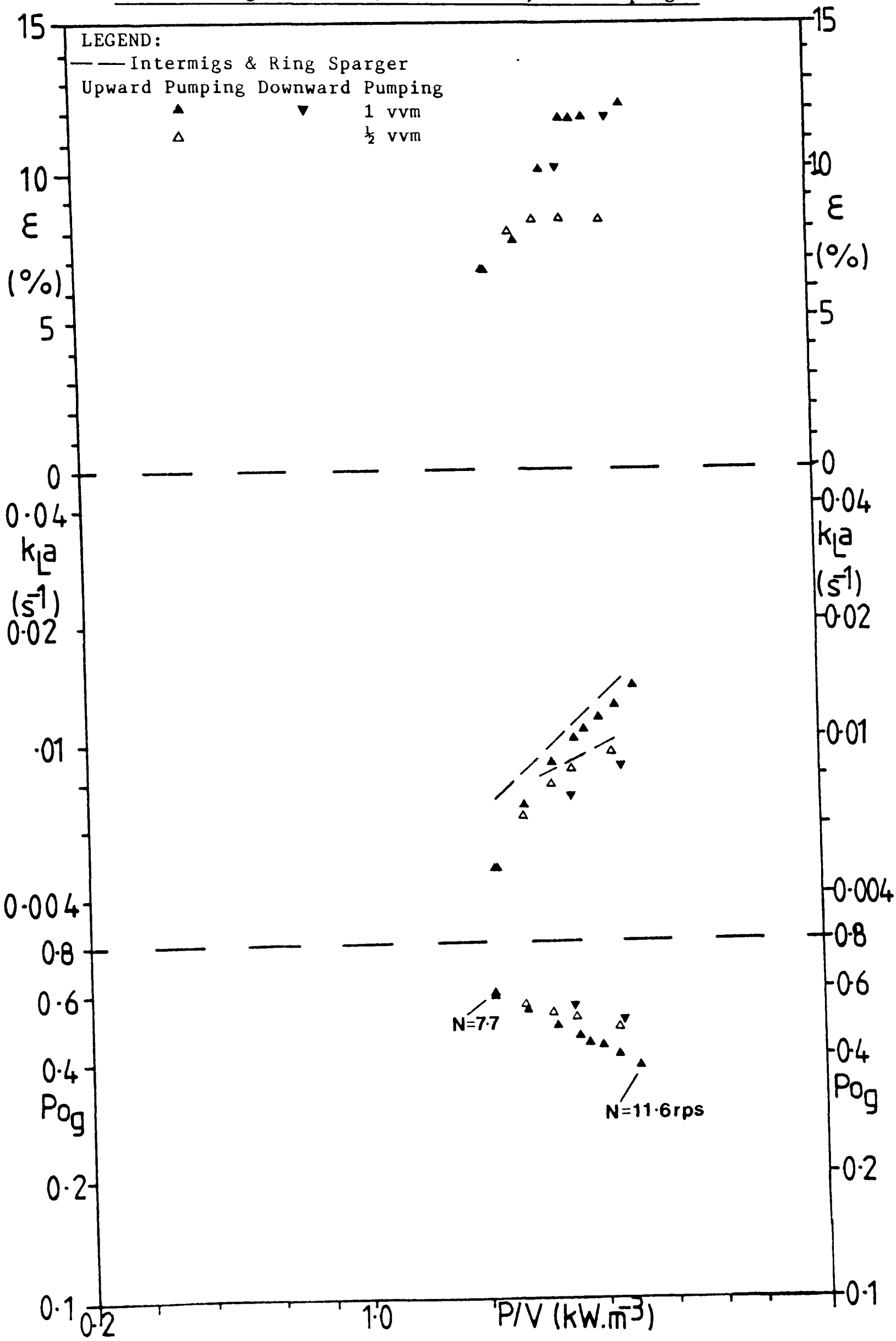

When Q = ½ vvm, the hold-up levels out at approximately 8% for high power consumption, at the same point the Po_g values become dependent upon the gas flow rate with Po_g for Q = ½ higher than Po_g for Q = 1. This variation in behaviour is matched by a difference in k_La values for the two air flow rates which is seen at high P/V. That this is not just an effect due to the change in Q on the value of Po_g can be seen in figure 8.12, where the power consumption has been removed and k_La is plotted against Re. The results at Q = ½ vvm are lower for the same impeller speed, indicating that air flow rate is affecting k_La, separately to the effects due to altering P/V. Figure 11 also shows the results gained when the central blades of the Intermig impellers were pumping downwards. k_La is reduced, although the hold-up remains the same as that found when rotating in the opposite direction.

In 0.8% CMC, these impellers give lower k_La values than those found for two disc turbines particularly at low P/V. This is matched by lower hold-up values in the range measured, although the range was not extended to high P/V, where the hold-up for two disc turbines falls. Measurements were not made at high P/V because of severe vibration which occurred at higher speeds (see Chapter 7, section 3.2). When agitating a 1.4% CMC solution using Intermig impellers shown in figure 8.13, no effect on k_La due to changing Q is seen. In addition the hold-up at both air flow rates is the same for a given P/V. k_La rises rapidly with increasing P/V, giving similar values to those found for two disc turbines at the highest power input. At lower power inputs the Intermigs give slightly lower k_La values when compared to the disc turbines which is matched by slightly lower hold-up values, attained using these impellers. The range of power input available for mass transfer measurements is very small in this solution, which is due to the steepness of the Po_g - Re curves (see figure 7.12) and the very low Po_g values attained. In addition Po_g does not rise again at higher Re, as is found with disc turbines. This all combines to

Figure 8.12

$k_L a$ and Po_g versus Re, for 0.8% CMC

Two Intermigs (D=0.58T) (Legend as figure 8.11)

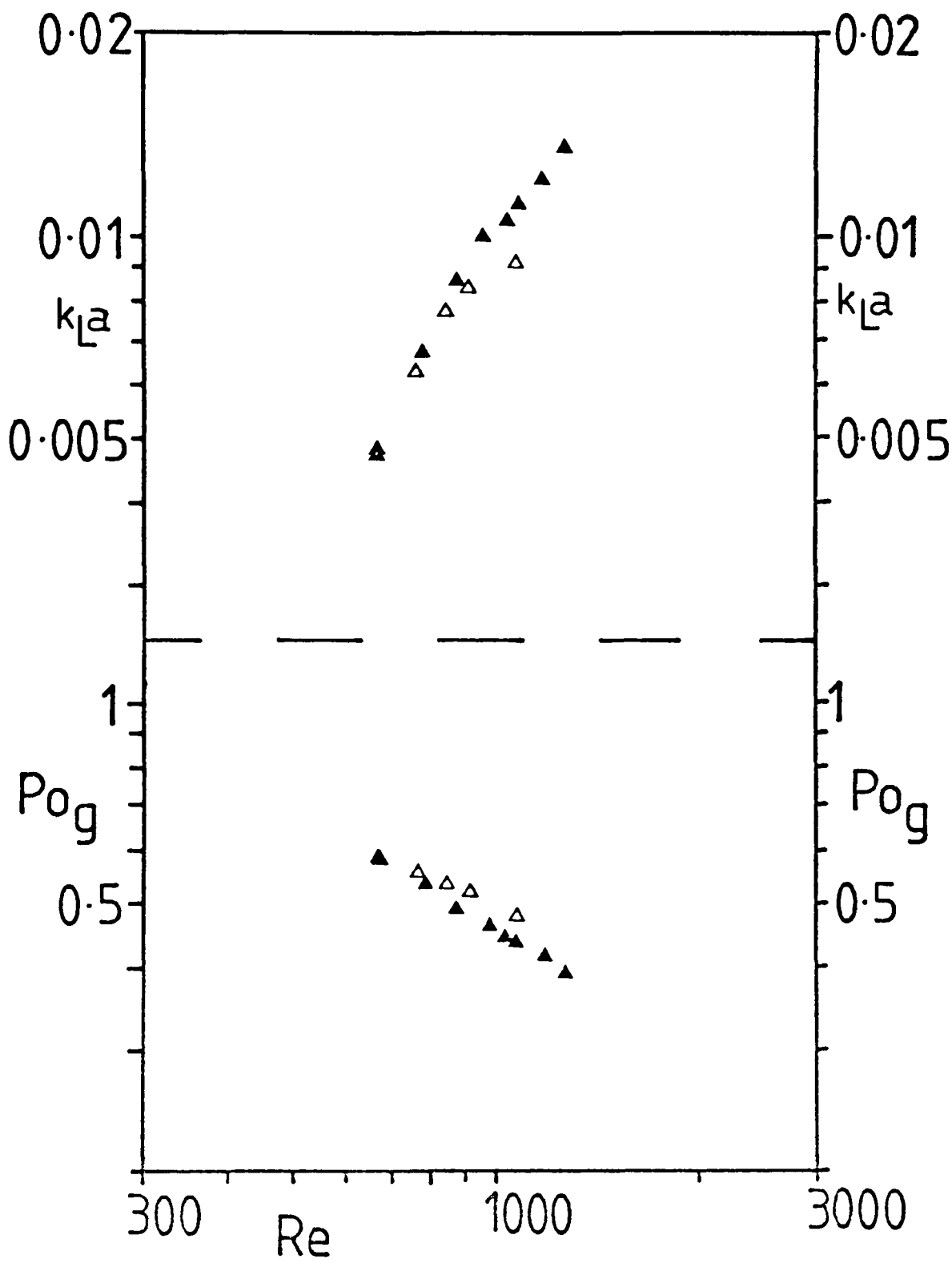

Figure 8.13

$k_L a$, Hold-Up (ε) and the Gassed Power Number (Po_g), versus P/V.
Two Intermigs (D=0.58T) in 1.4% CMC, Ring Sparger.

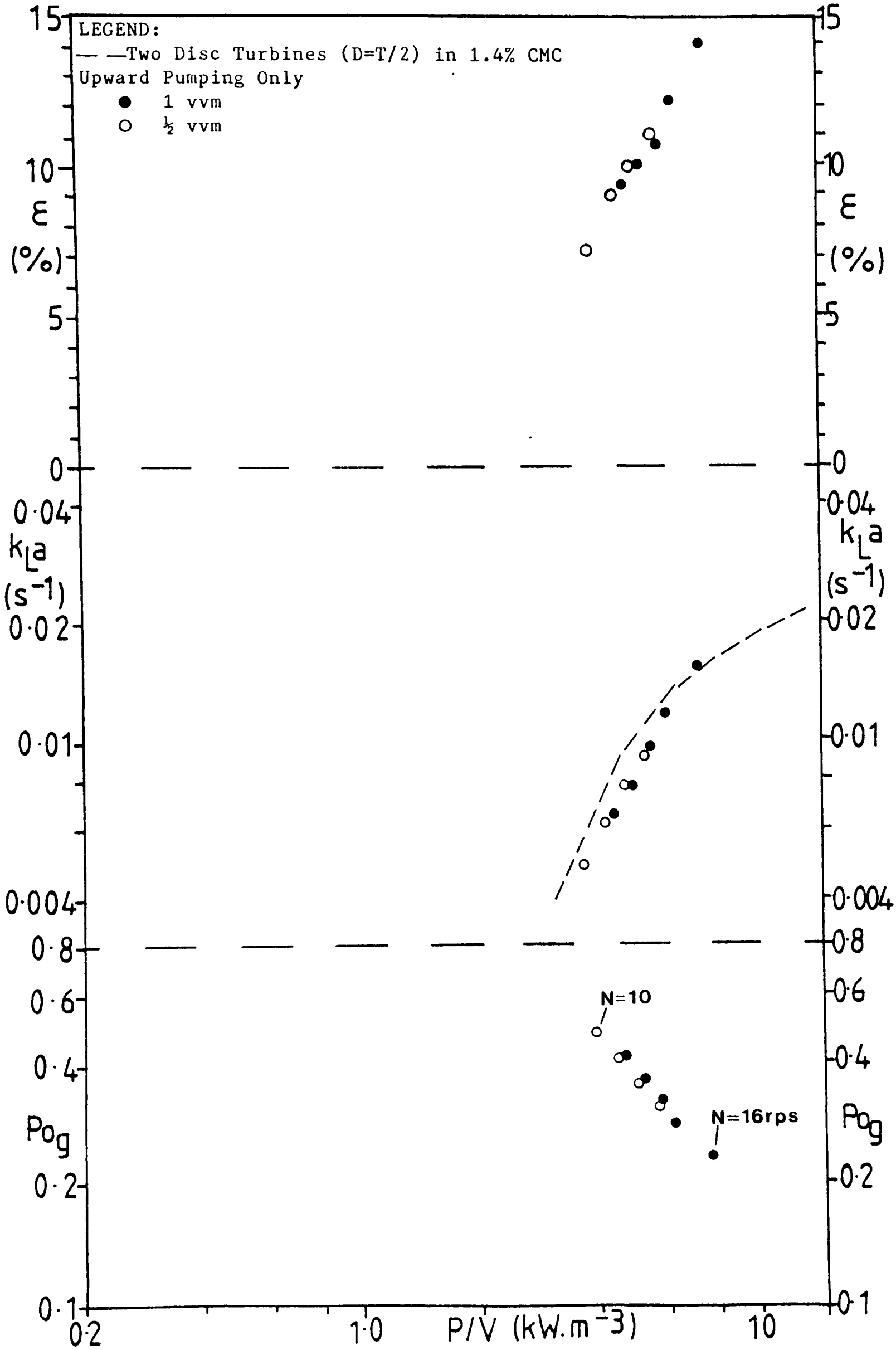

give a large variation in impeller speed for a small variation in P/V, with very high impeller speeds required for high power inputs. This corresponds to low torque values, which could be an advantage, in terms of the cost of installing the motor, etc. required to drive the impellers. The low torque may in part be linked to the number of cavities, as in this case only two blades are fitted to each impeller, so only two main cavities are produced, through which power is dissipated in breaking up the gas stream and producing turbulent eddies. This may also be linked to the severe vibrations found when using these impellers at high speeds under gassed conditions, where the use of multiple bladed impellers smooths out any individual interactions which may lead to vibration.

8.3.6) Conclusions Regarding Mass Transfer in Viscous Solutions

In low viscosity systems $k_L a$ is correlated reasonably well using the power input per unit volume and the air flow rate, with the impeller speed, type and number being of minor importance. In addition the variations in $k_L a$ follow closely the variations in the gas hold-up, with the two variables heavily dependent on the ionic strength of the solution and other dissolved materials, such as surfactants and antifoams[144]. In the viscous solutions used here $k_L a$ is drastically reduced compared with the values in water, for the same P/V. In addition the effects of altering air flow rate are reduced or even disappear and the measured gas hold-up no longer gives a good indication of the interfacial area, especially for disc turbine systems, where the hold-up can be made up of several different types of gas bubbles, i.e. large oxygen rich bubbles, small bubbles depleted of oxygen and the gas filled cavities behind the impeller blades and in regions of reduced pressure behind baffles etc. In the viscous solutions good mixing requires higher power inputs and large diameter impellers. This is in part due to the shear thinning nature of the solutions, which reduces liquid velocity rapidly away from the impeller

region. This makes k_La dependent upon the impeller type, particularly at low power inputs. At high power inputs, the development of more turbulent flow, with its high transport rates on a bulk level renders the type of impeller less important, in addition the solution properties become less important (see next section). At low and intermediate power inputs, i.e. 1 - 6 $kW.m^{-3}$, which may be considered too high in comparison with industrial scale practise, careful thought is required in choice of impeller type/size. Poor performance is given by large impellers at low power inputs (P/V < 2 $kW.m^{-3}$), as they are not capable of dispersing the gas at the low speeds which these P/V require. Smaller impellers will operate at higher speeds for the same power input, so whilst they may not mix the whole vessel contents effectively in the viscous solutions, they do give a reasonable mass transfer capability. At intermediate power inputs (2 - 6 $kW.m^{-3}$), large impellers provide the good gas-liquid mixing required at moderate impeller speeds. When using turbines there is an optimum impeller speed which gives a reasonable k_La value at the lowest P/V. This is due to the shape of the Po_g - Re curve, (see Chapter 7), which increases at high impeller speeds, raising P/V without raising k_La effectively. Operation at the minimum Po_g available ensures a high hold-up and reasonable gas-liquid mixing, giving an optimum k_La, in terms of mass transfer coefficient per kiloWatt per cubic metre. In the very viscous 1.4% CMC solutions altering the air flow rate can alter Po_g(min). Here a higher gas flow rate gives better k_La values, by reducing Po_g(min) and moving it to higher Re. This effect is probably related to the viscoelastic nature of the solution, which is not seen at lower CMC concentrations.

Where the motor size limits the torque available, without limiting the power available, the Intermig impellers may be useful. Their low Po_g at high N means that they require low torque values, whilst still sweeping large volumes of the vessel. At high power inputs they compare well in mass transfer performance with two large disc turbines, although

the severe vibration noted at very high impeller speeds (see Chapter 7) does reduce the range of P/V over which they can operate.

The use of a pitched blade turbine in combination with a disc turbine appeared to offer no advantage over the use of two disc turbines. This may be linked to the proximity of the two impellers, ($s = 3T/8 = 0.75D$), affecting the power consumption. The power consumption for this impeller combination was similar to that found for two disc turbines, whereas the power consumption of a pitched blade impeller alone is much less than that of a single disc turbine in similar solutions, at high Re (> 100)[22]. This would suggest that the interaction of these impellers is producing a higher power consumption than the sum of the two impellers acting independently. In order to determine whether a greater impeller separation would produce lower Po_g values without reducing k_La significantly, experiments would need to be carried out in vessels with $H_l > T$. Under these conditions, the ability to pump liquid vertically within the vessel would be advantageous for mixing and possibly k_La.

In applications relevant to the fermentation industry, the choice of agitator type will depend not only on its ability to provide a reasonable k_La value for a minimum power consumption at high viscosities, but also on its performance at low and intermediate viscosities. This is because in batch fermentation a whole range of viscosities can be encountered over the time span of the process. For this reason it is important to examine the effect which increasing viscosity has on k_La over the full range of viscosities. This is presented in the following section.

8.4) The Effect of Varying Viscosity on $k_L a$

The results presented in section 8.2 for water and in section 8.3 for viscous CMC solutions show that $k_L a$ is reduced at a given P/V in concentrated CMC solutions, compared to $k_L a$ values obtained in water at the same P/V, with the results obtained in 1.4% CMC lower than those in 0.8% CMC. This section focusses on the overall effects of increasing viscosity using a range of solutions from 0 - 1.4% CMC, giving a range of apparent viscosities of 0.001 - 1 Pa.s. As all the solutions (except water) were shear thinning, a shear rate is required from which the apparent viscosity can be determined. In the text a shear rate of 100 s^{-1} has been chosen to enable the apparent viscosities of the solutions to be compared. This is between the highest and lowest average shear rate prevalent in the vessel, providing an indication of the actual viscosities used. For the figures where μ_a is shown, the average shear rate, $\bar{\gamma}_{AV}$, in the vessel will be used. This is determined from the impeller speed according to equation 3.2 using a value of k_s = 11.5; which enables the apparent viscosity to be determined from equation 3.5. Both Intermigs and disc turbines were used in a wide range of CMC solutions, to compare their performance. The results obtained for each will be presented, followed by a comparison of their overall performance.

8.4.1) Disc Turbines

Eight CMC solutions of varying concentrations were used in conjunction with two large disc turbines (D = T/2) to examine the variation in $k_L a$ with altering viscosity. The solutions were 0.04, 0.1, 0.2, 0.35, 0.5, 0.8, 1.1 & 1.4% CMC which had viscosities of 0.005, 0.015, 0.033, 0.071, 0.167, 0.347, 0.561 & 0.858 Pa.s respectively, at a reference shear rate of 100 s^{-1}. These viscosities give an indication of the range used, although the actual values which occur in the vessel will vary with the impeller speed used.

The results obtained in 0.8% and 1.4% CMC have been presented and discussed in section 8.3 (figures 8.4 and 8.5). They show much lower $k_L a$ values than those obtained in water with those in 1.4% CMC lower than those in 0.8% CMC. In addition they show little variation with changing air flow rate but are highly dependent on the power consumption. Figure 8.14 shows the results obtained in the 0.04% CMC solution. In comparison with water, shown in figures 8.1 and 8.2, the modest increase in viscosity has little effect on $k_L a$. From a consideration of the literature presented in Chapter 4, section 5, it might be expected that $k_L a$ would be reduced in this solution. However any reduction in $k_L a$ due to the slight increase in viscosity is probably compensated for by the increase in concentration of ions in the solution. In water $k_L a$ values are extremely sensitive to low concentrations of ions, with increasing concentration increasing $k_L a$ and reducing slightly the dependence of $k_L a$ on the air flow rate, as shown in Chapter 6. CMC contains approximately 7% by weight of sodium ions, the addition of these is probably responsible for the slight increase in the gas hold-up seen in 0.04% CMC when compared with that in water. This causes an increase in the interfacial area which compensates for any reduction in k_L caused by the increase in viscosity. If the results obtained here were compared with those obtained in water containing a large amount of ions, e.g. those presented in figure 6.5, then a decrease in $k_L a$ would be noted.

As the viscosity is further increased, then bubble coalescence rates will be determined primarily by the rheological properties of the liquid, with any effects due to the concentration of ions masked or removed. In 0.1% CMC, shown in figure 8.15, $k_L a$ is reduced by the increasing viscosity when compared with 0.04% CMC, in addition the gas hold-up is reduced. The Reynolds number is still high ($3 - 6 \times 10^3$) indicating that the turbulent regime is fully developed. This results in Po_g values which are less dependent on the impeller speed, than those seen in the

Figure 8.14

$k_L a$, Hold-Up (ε) and the Gassed Power Number (Po_g), versus P/V.

Two Disc Turbines (D=T/2) in 0.04% CMC.

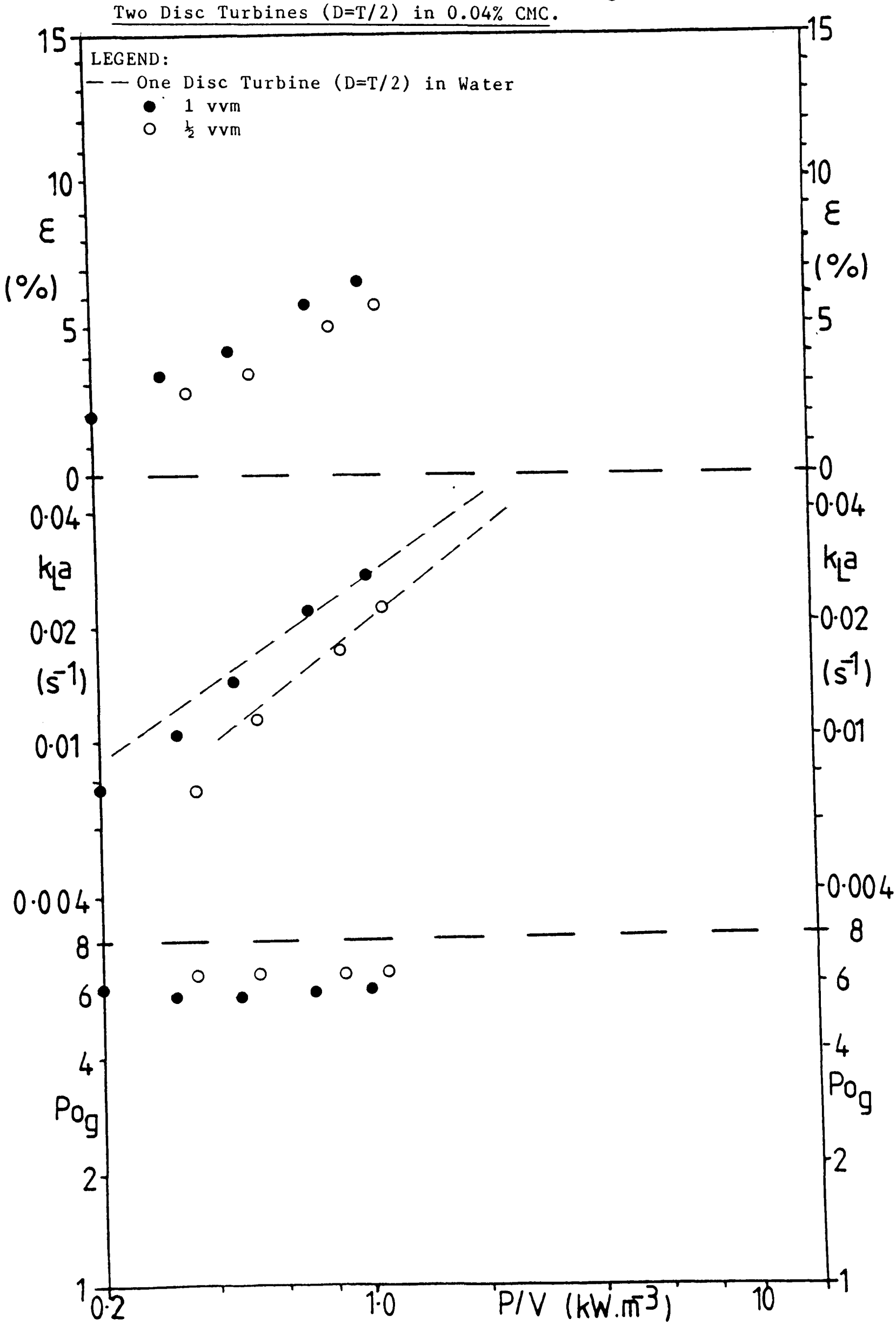

Figure 8.15

$k_L a$, Hold-Up (ε) and the Gassed Power Number (Po_g), versus P/V.

Two Disc Turbines (D=T/2) in 0.1% CMC.

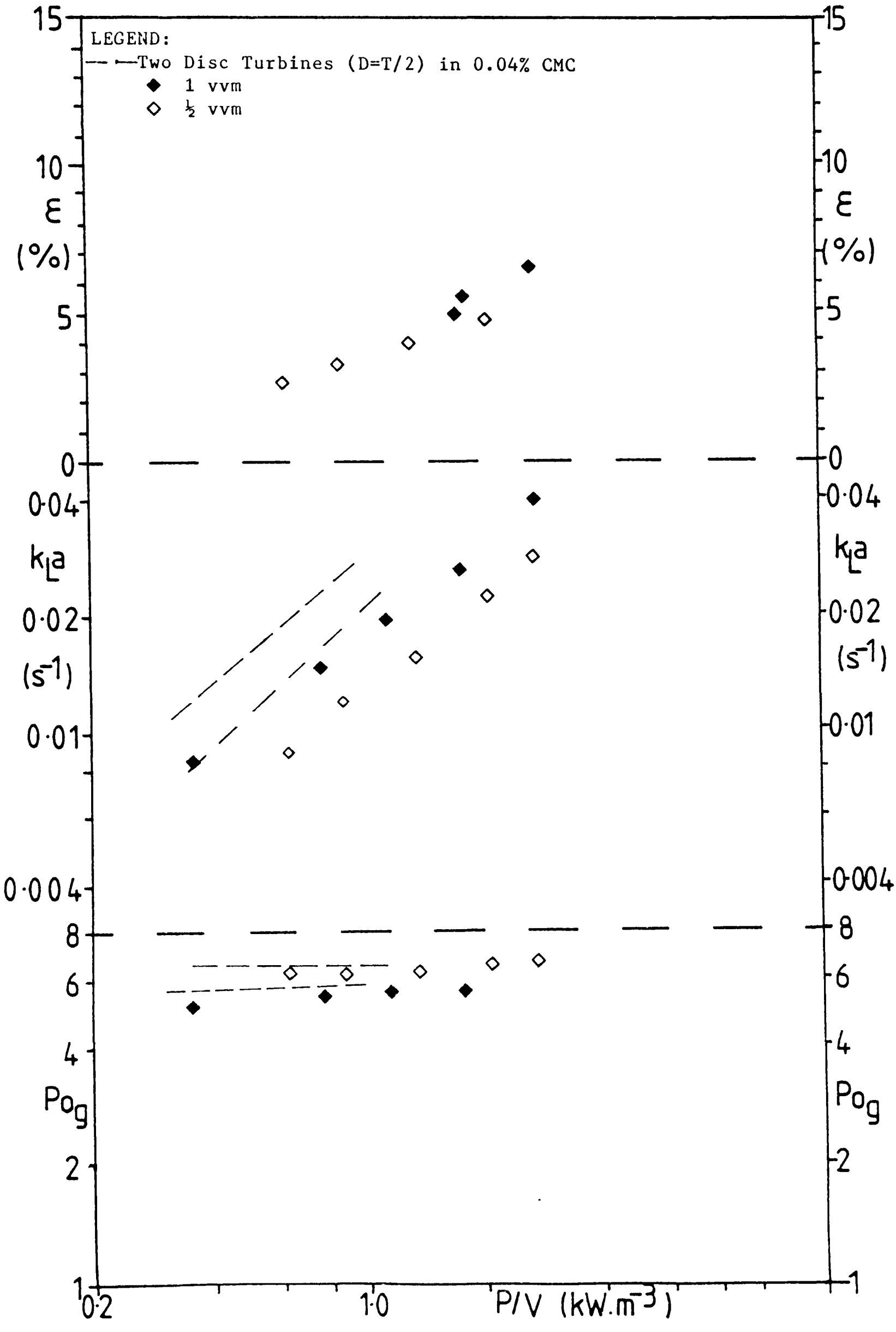

more concentrated CMC solutions (see Chapter 7), and are the same as those found for 0.04% CMC. Thus for a given P/V these two solutions require the same impeller speeds. On increasing the viscosity further the Reynolds number falls and the transitional region is entered. This is accompanied by a reduction in Po_g values which means that for a given P/V the impeller speed must be increased. In 0.2 and 0.35% CMC this does not prevent the reduction in k_La caused by the increasing viscosity, these solutions do however show an increase in the gas hold-up compared with 0.1% CMC, (see figure 8.16 & 8.17). At intermediate CMC concentrations, 0.35, 0.5 and 0.8%, the k_La values obtained are independent of the solution viscosity. Figure 8.18 shows the results obtained in a 0.5% CMC solution. These show very similar k_La and gas hold-up values to those obtained in 0.35% CMC (figure 8.17). In 0.8% (shown in figure 8.4), the hold-up values are much more dependent upon P/V and rise to a higher value than is shown by the 0.35% CMC solution, in addition the dependency of k_La on air flow rate is removed. The 0.8% CMC solution shows similar k_La values to those obtained in 0.5 and 0.35% CMC, particularly at intermediate P/V. This lack of variation of k_La with variations in viscosity does not extend to higher CMC concentrations. In 1.1% CMC, shown in figure 8.19, k_La values are reduced compared with those in 0.8% CMC. In 1.4% CMC the k_La values are reduced even further, as shown in figure 8.5. Although at very high P/V the variation in k_La is small for a large variation in μ_a.

The overall effect of varying μ_a on k_La can be seen in figure 8.20, which shows k_La as a function of μ_a at several different P/V values for the two large disc turbines. For P/V = 1 & 4 $kW.m^{-3}$ the results obtained at two air flow rates are shown, which demonstrate the reduction in dependence of k_La on air flow rate with increasing viscosity. It can be seen that at P/V = 1 $kW.m^{-3}$, the range of constant k_La is reduced compared with that at 4 $kW.m^{-3}$. This is related to the changing slopes of the k_La - P/V

Figure 8.16

$k_L a$, Hold-Up (ε) and the Gassed Power Number (Po_g), versus P/V.

Two Disc Turbines (D=T/2) in 0.2% CMC.

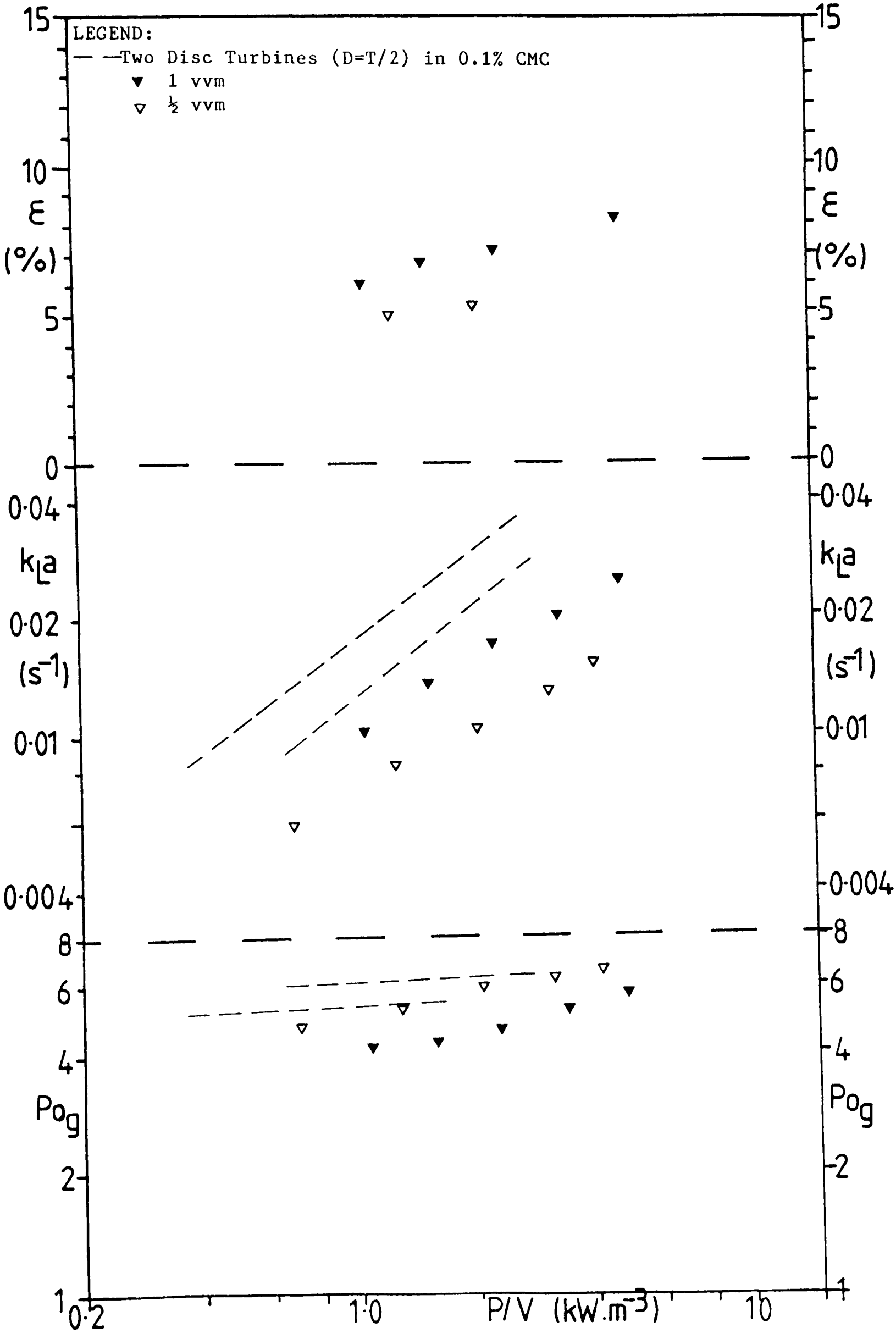

Figure 8.17

$k_L a$, Hold-Up (ε) and the Gassed Power Number (Po_g), versus P/V.
Two Disc Turbines (D=T/2) in 0.35% CMC.

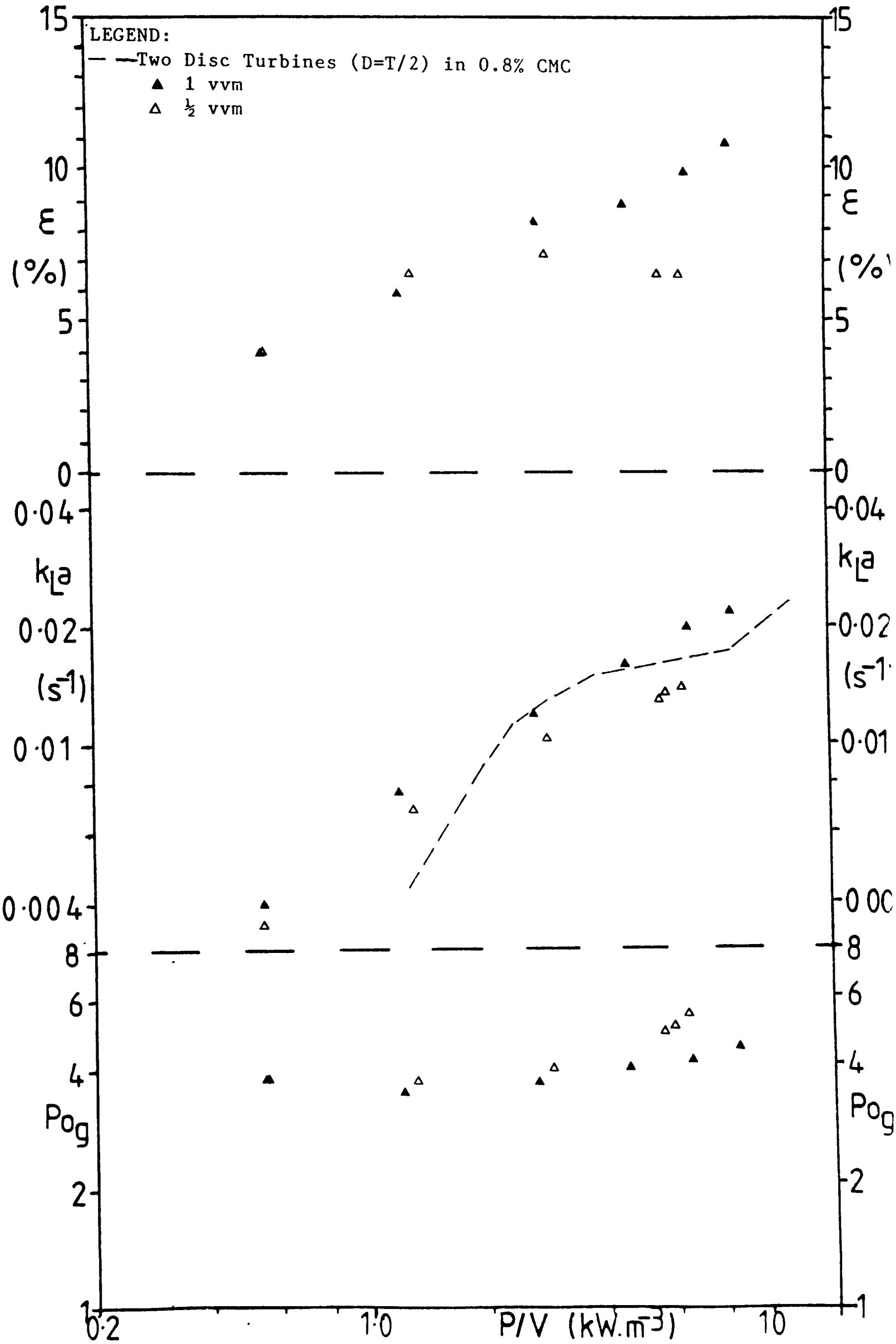

Figure 8.18

$k_L a$, Hold-Up (ε) and the Gassed Power Number (Po_g), versus P/V.
Two Disc Turbines (D=T/2) in 0.5% CMC.

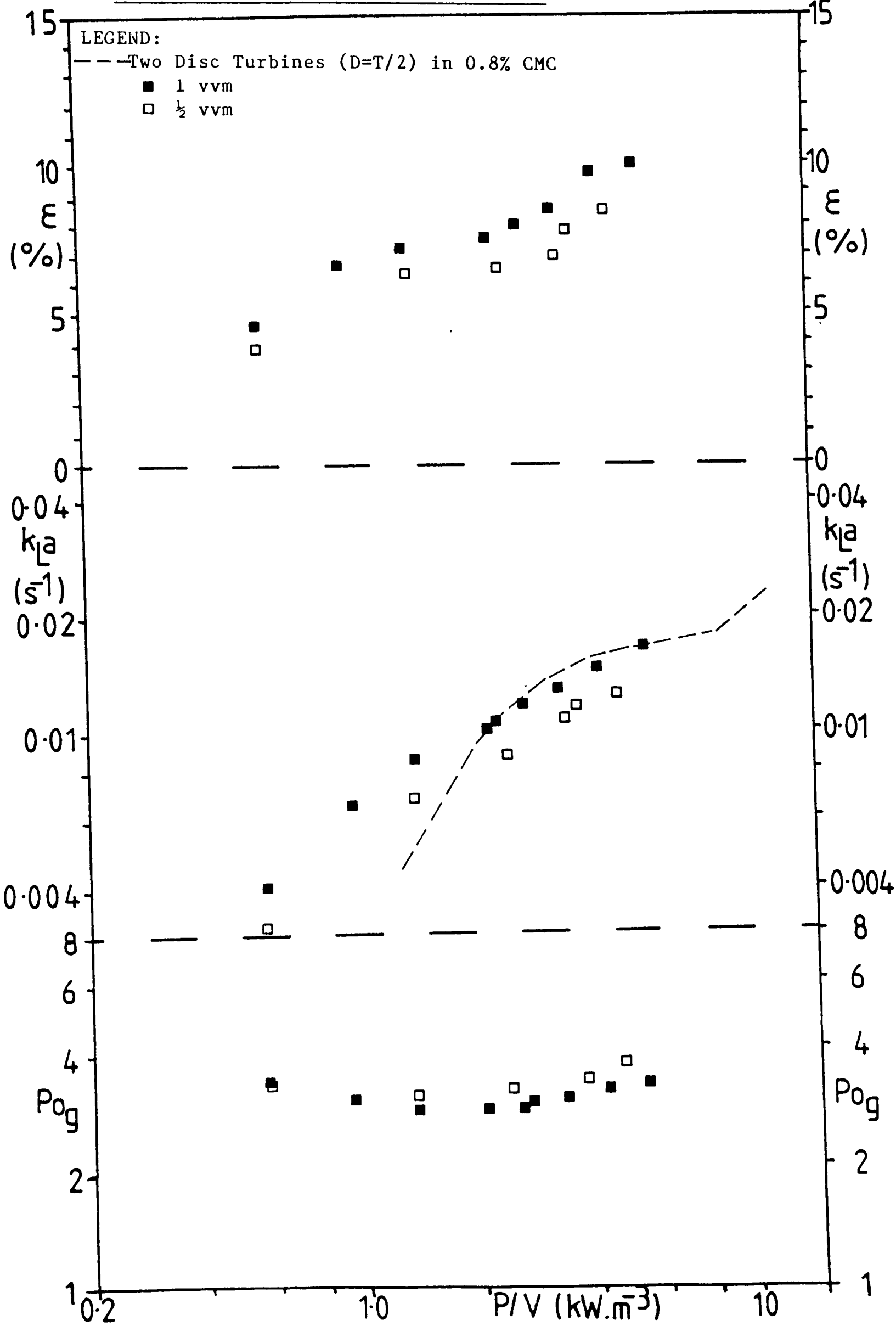

Figure 8.19

$k_L a$, Hold-Up (ε) and the Gassed Power Number (Po_g), versus P/V.

Two Disc Turbines (D=T/2) in 1.1% CMC.

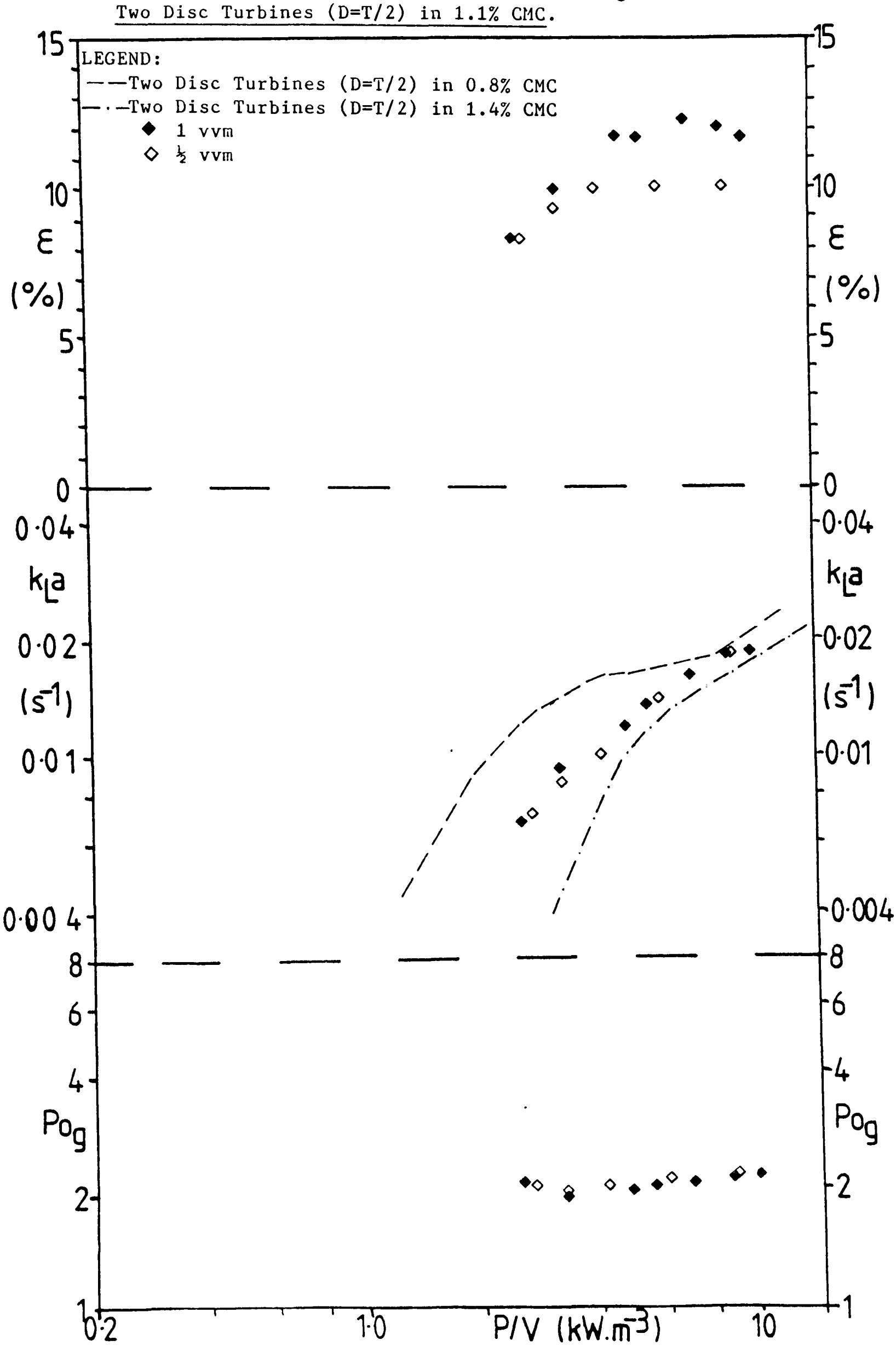

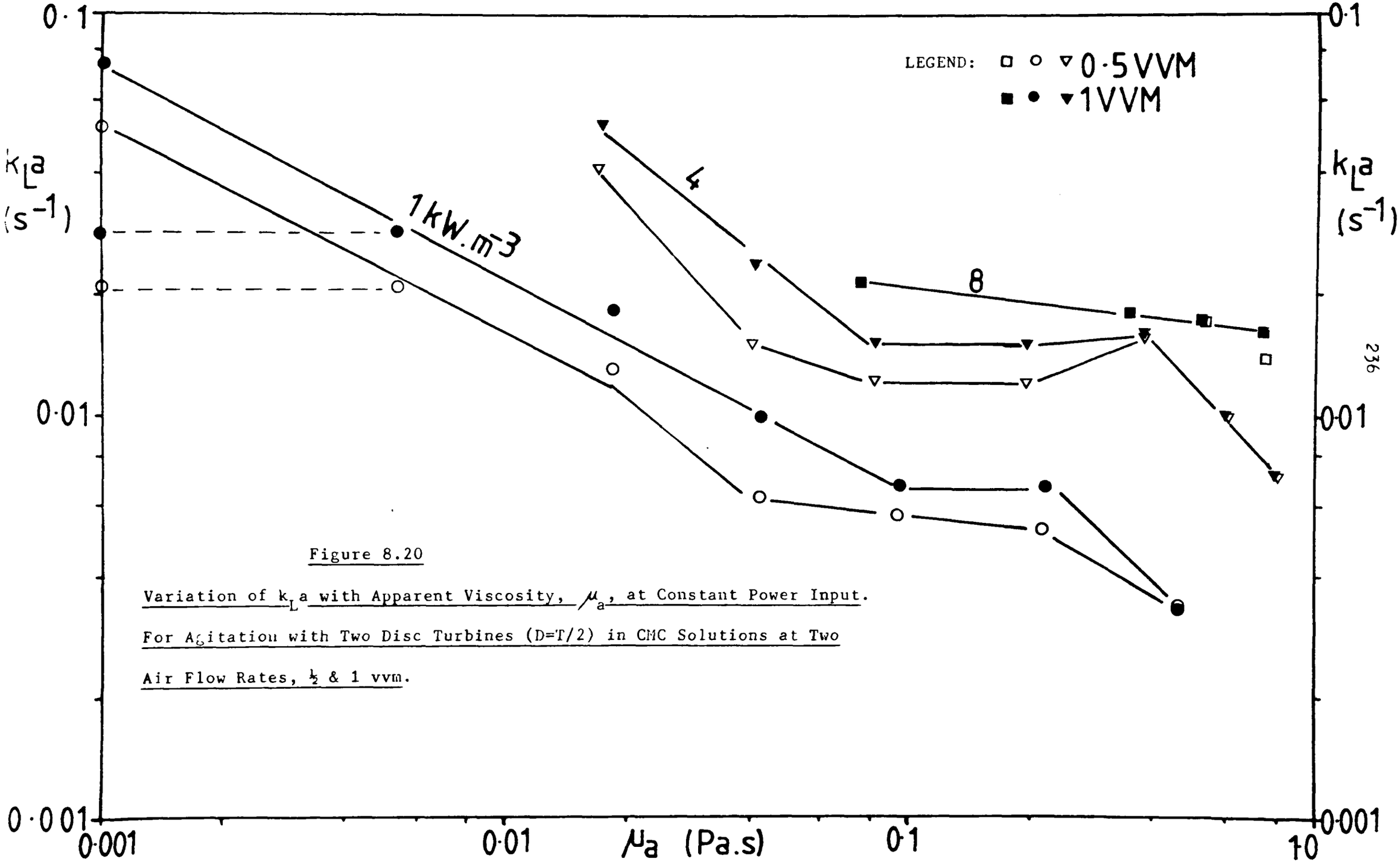

Figure 8.20

Variation of k_La with Apparent Viscosity, μ_a, at Constant Power Input. For Agitation with Two Disc Turbines (D=T/2) in CMC Solutions at Two Air Flow Rates, ½ & 1 vvm.

curves at high CMC concentrations which is in turn related to variations in Po_g and the gas hold-up seen in the solutions, as described in section 8.3. At P/V = 8 $kW.m^{-3}$ k_La is only slightly dependent on μ_a. It would seem that the high intensity of agitation required to give this P/V is responsible for removing any effect which altering the rheological properties has on k_La: As the concentration increases, the hold-up increases, counteracting the reduction in k_La expected from the increasing viscosity. When using a single large disc turbine (D = T/2), or two small disc turbines (D = T/3), k_La is similarly unaffected by changing viscosity in solutions of intermediate viscosity. This can be seen from figures 8.1, 8.7 and 8.21, which show the results obtained when using a single disc turbine in water, 0.8% CMC and 0.4% CMC respectively, and from figures 8.2, 8.6 and 8.22 for the same solutions using two small disc turbines. Here the higher than expected k_La values obtained in 0.8% CMC are matched by increases in the gas hold-up, ϵ, compared with 0.4% CMC. The same applies for two large disc turbines, with ϵ in 0.8% CMC higher than that in lower concentration solutions. This implies that a marked change in behaviour is occurring in the intermediate concentration CMC solutions. At low concentrations ϵ varies linearly with increasing P/V. At higher CMC concentrations (0.5% +) ϵ is more variable, showing plateau regions where altering P/V hardly affects ϵ, as well as regions of decreasing ϵ with increasing P/V. The precise causes of these variations are not known, although the variations in the size of the gas filled cavities within the vessels are thought to be a major factor in the variations in ϵ seen (see Chapter 7, section 3). As this change in behaviour is occurring, it is not suprising that the k_La values obtained are affected. This area of constant k_La - μ_a can be linked with the transition region between laminar and turbulent flow of the Po_g - Re curve, as shown in figure 8.23. At low Re, where Po_g falls with increasing Re, k_La is highly dependent on

Figure 8.21

$k_L a$, Hold-Up (ε) and the Gassed Power Number (Po_g), versus P/V.
One Disc Turbine (D=T/2) in 0.4% CMC.

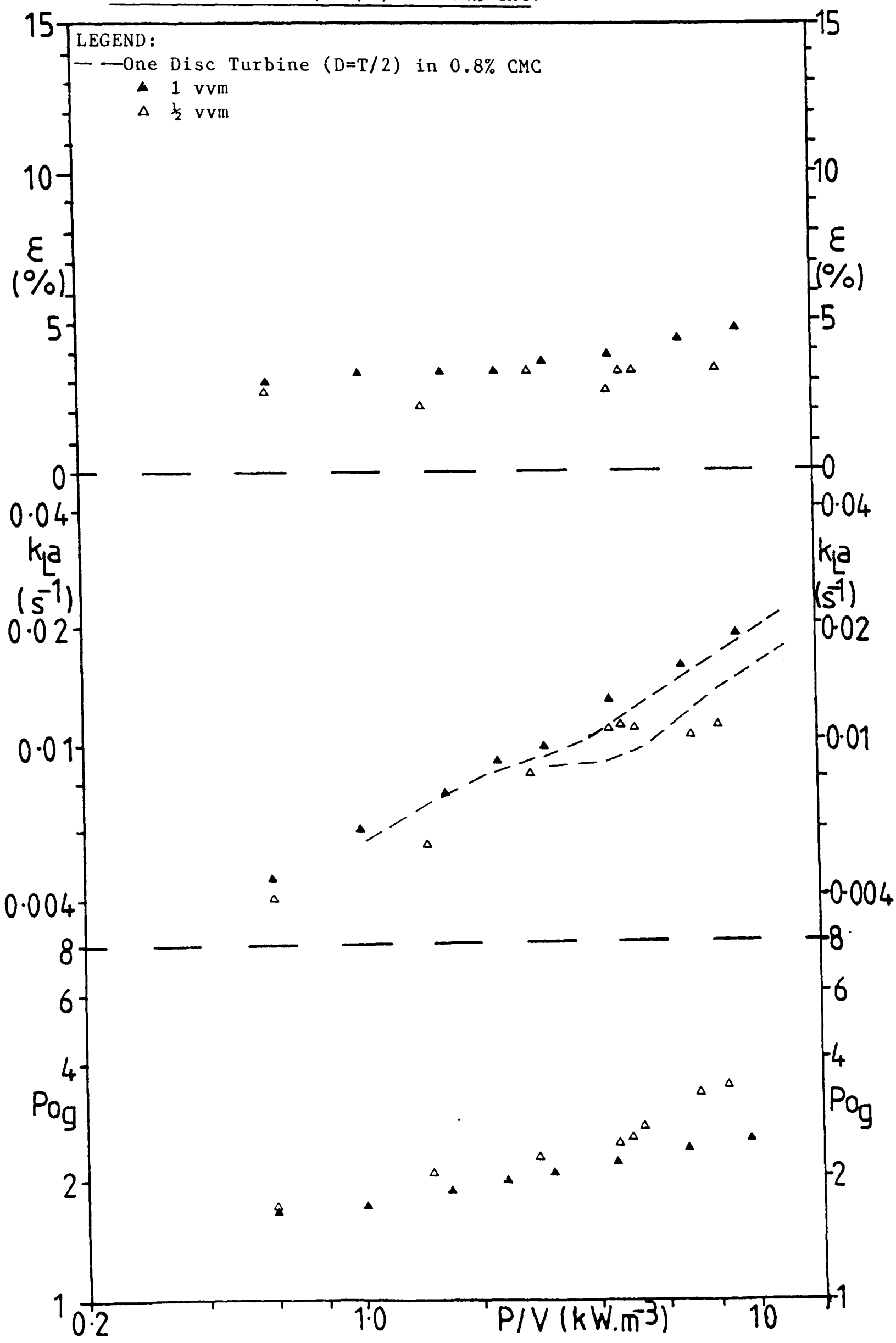

Figure 8.22

$k_L a$, Hold-Up (ϵ) and the Gassed Power Number (Po_g), versus P/V.

Two Disc Turbines (D=T/3) in 0.4% CMC.

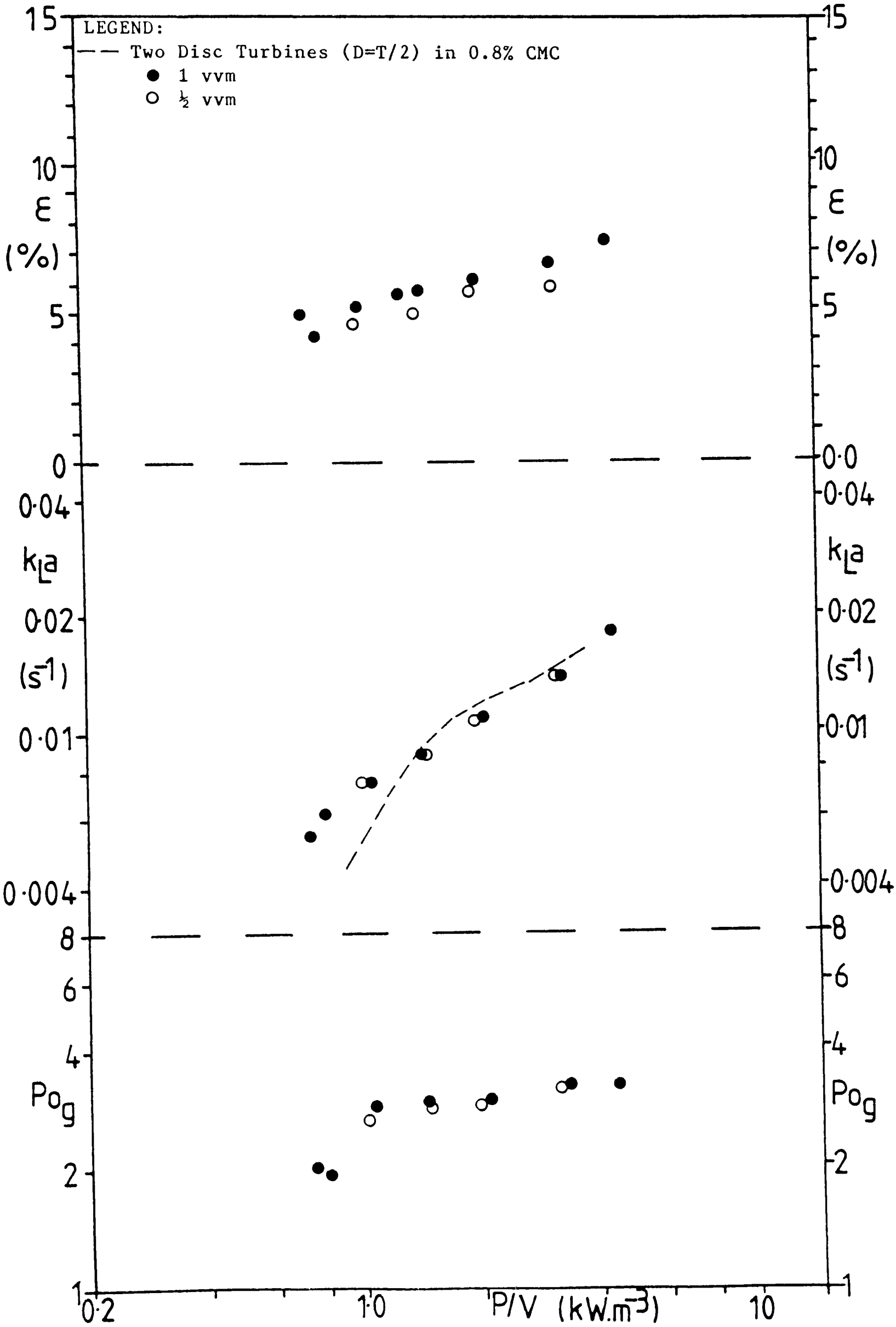

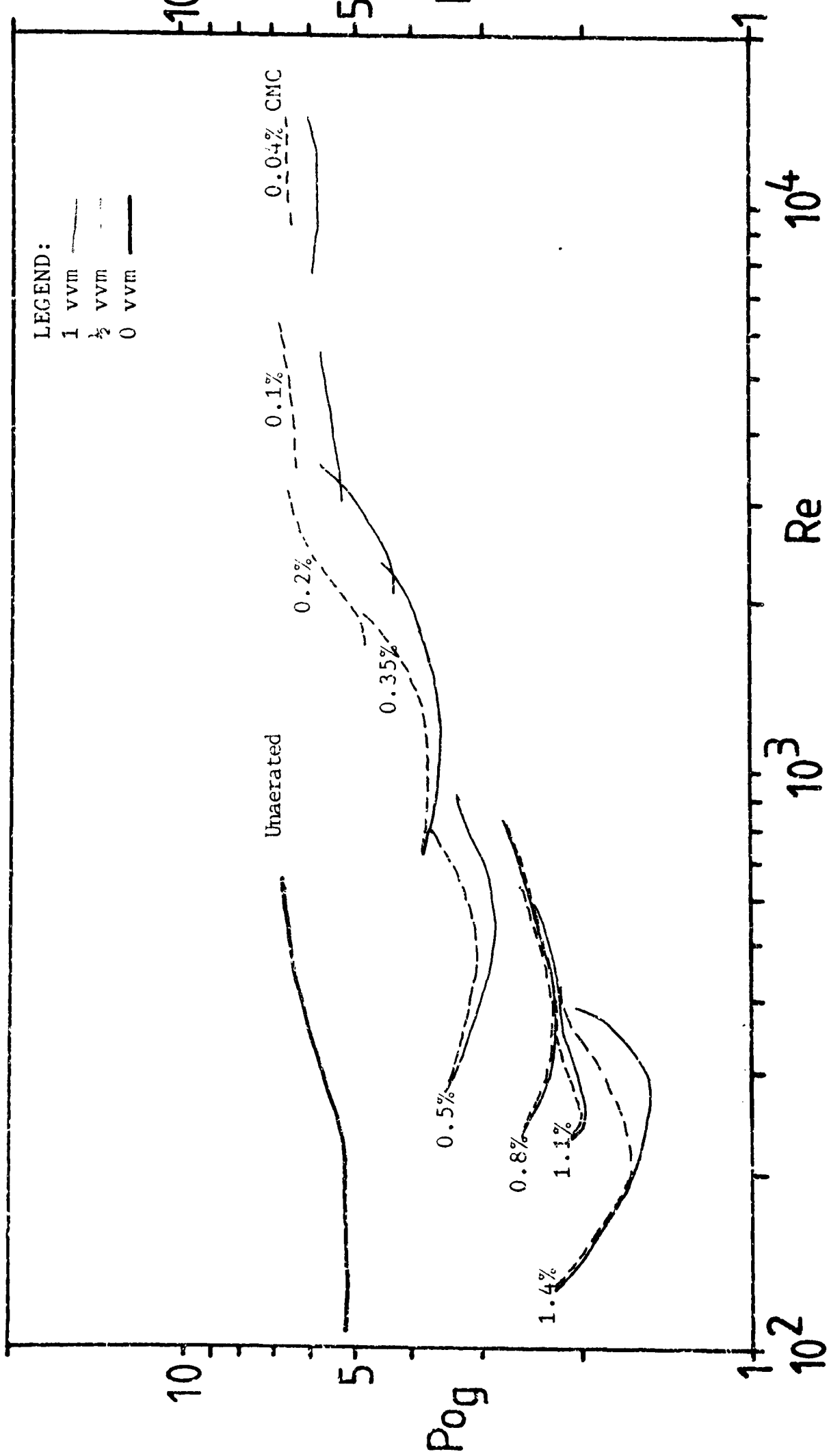

Figure 8.23

Po versus Re for Two Disc Turbines (D=T/2), in Various CMC Solutions
g

μ_a. At intermediate Re, where Po_g rises with increasing Re, k_La remains constant for a given P/V.

8.4.2) Intermigs

The results obtained using Intermigs in water are discussed in section 8.2 and shown in figure 8.3. The results obtained in 0.8 and 1.4% CMC solutions are discussed in section 8.3 and shown in figures 8.10 - 8.13. In addition measurements have been carried out in solutions of 0.2 and 0.4% CMC, these are shown in figures 8.24 and 8.25. When using these impellers the effect of increasing CMC concentrations is to reduce the k_La values, whilst the slope of the k_La - P/V curve increases slightly with increasing solution concentration. Little overlap in measurements between the solutions has occurred, as the range of P/V available in each CMC solution is narrow. However figure 8.26 shows the variation of k_La as a function of μ_a for several power inputs. It can be seen that k_La is increasingly dependent on μ_a at higher viscosities and power inputs, with air flow rate having little effect at any viscosity. No region of constant k_La for varying μ_a occurred, with k_La decreasing for each increase in CMC concentration. This was matched by a decrease in gas hold-up for increasing viscosity at constant P/V, as shown in figure 8.27.

The behaviour of the Intermigs over various CMC concentrations is much more simple than the behaviour of the disc turbines. k_La and hold-up values decrease with increasing μ_a or decreasing P/V when using Intermigs, whereas the corresponding behaviour with disc turbines is complex, with hold-up rising and falling with increasing μ_a or decreasing P/V depending on the flow regime in force at the impeller speeds under consideration. This simple behaviour of the Intermigs is matched by a corresponding simplicity in the Po_g - Re curves. The Po_g data collected during the mass transfer experiments is shown as a function of Re in

Figure 8.24

$k_L a$, Hold-Up (ε) and the Gassed Power Number (Po_g), versus P/V.
Two Intermigs (D=0.58T) in 0.2% CMC.

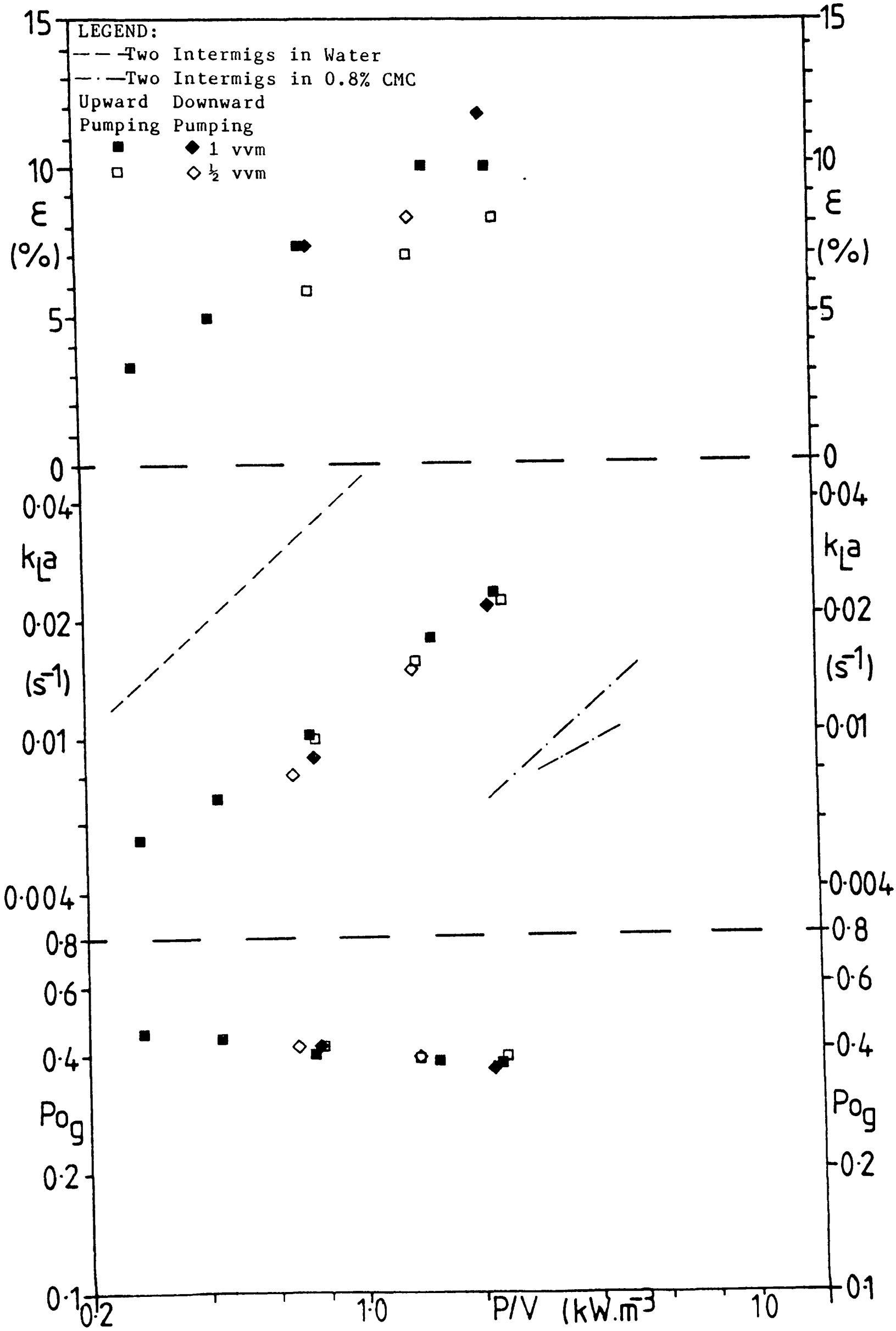

Figure 8.25

$\underline{k_L a}$, Hold-Up (ε) and the Gassed Power Number (Po_g), versus P/V.
Two Intermigs (D=0.58T) in 0.4% CMC.

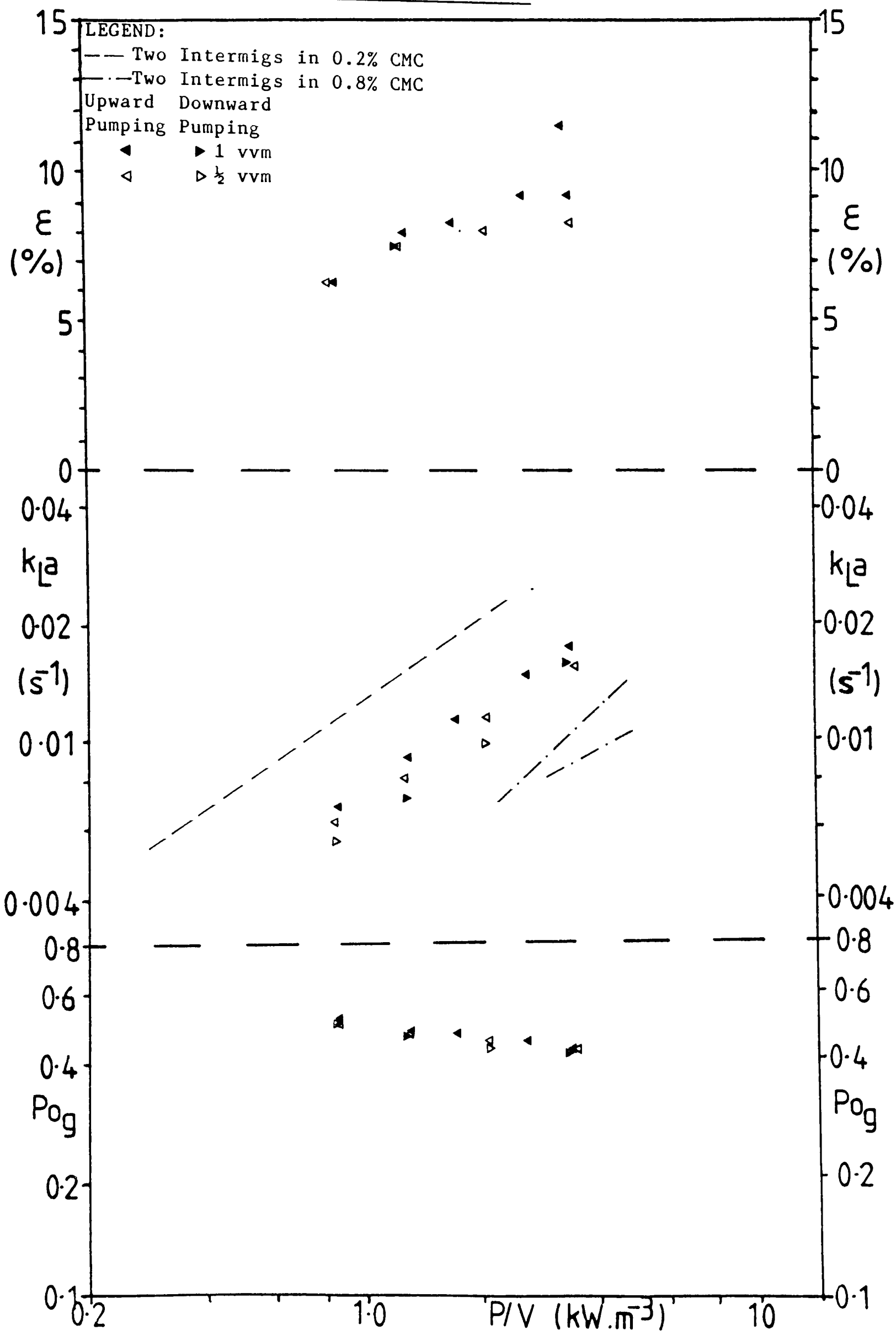

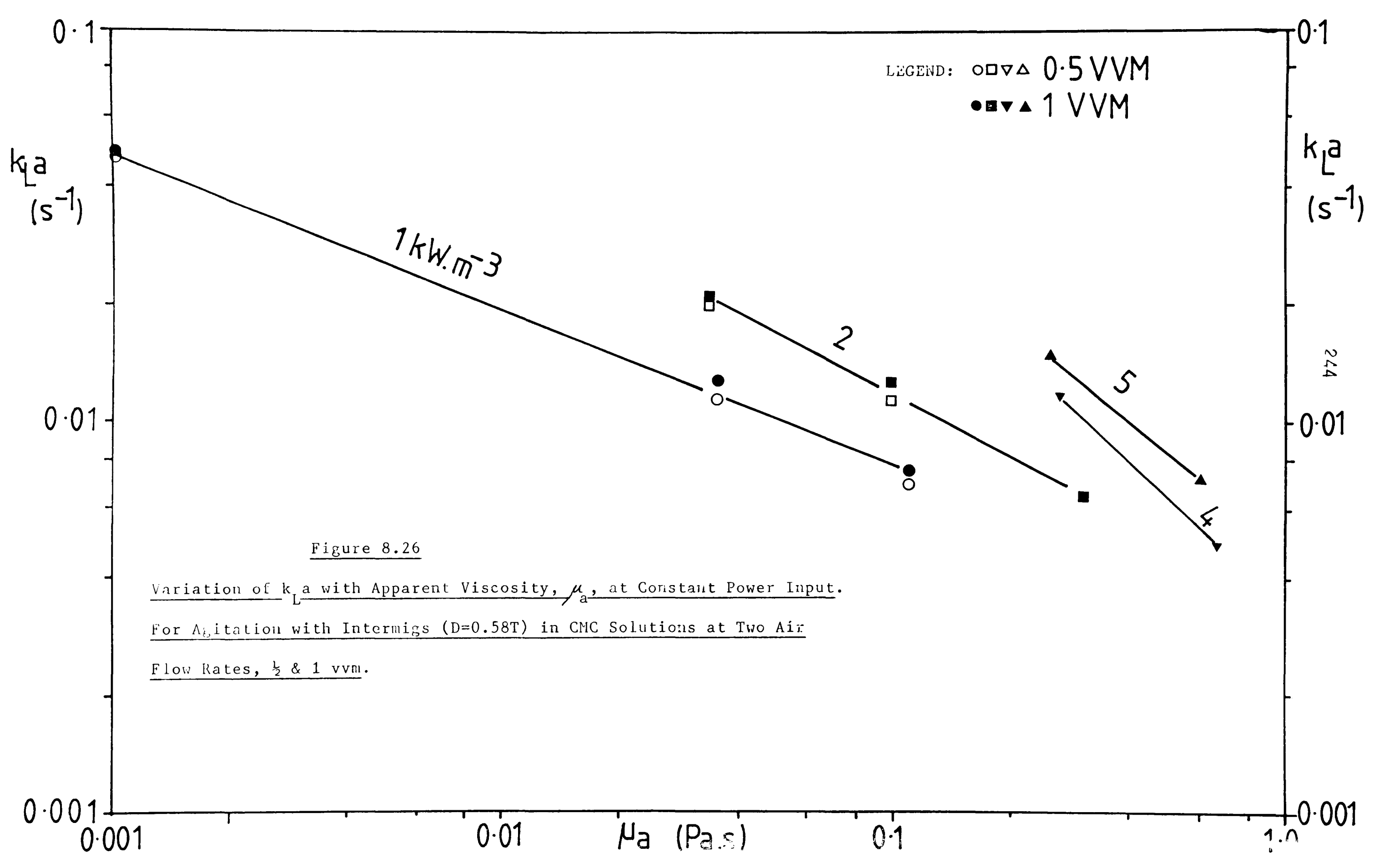

Figure 8.26

Variation of $k_L a$ with Apparent Viscosity, μ_a, at Constant Power Input.

For Agitation with Intermigs (D=0.58T) in CMC Solutions at Two Air Flow Rates, ½ & 1 vvm.

Figure 8.27

Gas Hold-Up, ε, at 1 vvm, versus Power Consumtion, P/V.

For Agitation with Intermigs (D=0.58T) in Various CMC Solutions.

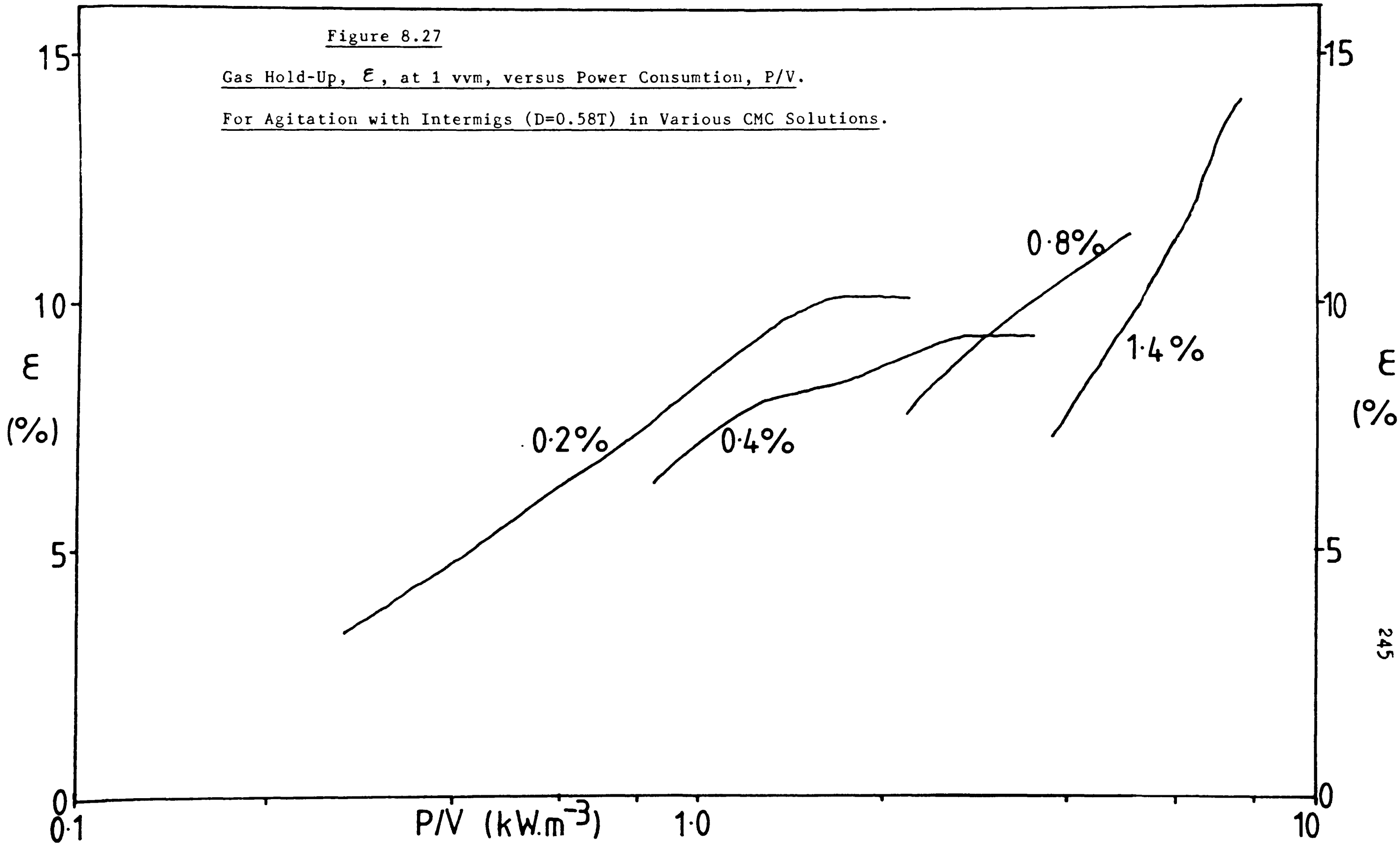

figure 7.13a. In the more concentrated solutions, Po_g falls steadily with increasing Re. Showing no upturn at high Re, possibly because none exists, or because high enough impeller speeds were not reached to show this. In the less concentrated solutions the Po_g - Re curve slopes gently to show lower Po_g at higher Re. No intermediate or transition region occurs, which is the region in which the behaviour of the disc turbines is surprisingly complex.

8.4.3) Conclusions Regarding the Effects of Viscosity

From figures 8.20 and 8.26 it can be seen that the variation in k_La with varying viscosity is a function of the impeller type in use. For disc turbines the slope of the k_La - μ_a curve varies in a complex manner, however, if a line of best fit is taken through the data then $k_La \propto \mu_a^{-0.46}$ at P/V = 1 $kW.m^{-3}$ which is valid for μ_a < 0.5 Pa.s. At higher viscosities, $k_La \propto \mu_a^{-1}$ at P/V = 4 $kW.m^{-3}$ and $k_La \propto \mu_a^{-0.01}$ at P/V = 8 $kW.m^{-3}$. For Intermigs $k_La \propto \mu_a^{-0.48}$ at P/V = 1 $kW.m^{-3}$ and μ_a < 0.10 Pa.s. At higher viscosities the slope of the curve increases, giving $k_La \propto \mu^{-0.9}$ at P/V = 4 $kW.m^{-3}$. Overall for all impeller systems an exponent of - 0.5 is satisfactory for μ_a < 0.5 Pa.s, above this k_La can fall off rapidly at all but the highest P/V.

8.5) Comparison of Mass Transfer Results Obtained Here With Those Presented in the Literature and Correlation of the Results Using Dimensionless Groups

There are several factors which make a direct comparison of the results obtained possible in only a few instances. The most important is that the different studies make use of solutions with differing rheological properties and each covers only a limited range of apparent viscosities. Perez and Sandall[74] produced reliable $k_L a$ values only in low viscosity solutions, with foaming altering the values obtained at higher viscosities. Ranade and Ulbrecht[30] used a measuring method which involved the addition of salts to the solution of interest. This removed any measureable non-Newtonian behaviour and reduced the viscosity. Yagi and Yoshida[49] used more viscous solutions up to an apparent viscosity of μ_a = 0.33 Pa.s, but made no measurement of the power consumption. Hocker[43] did measure the power consumption, but restricted his measurements to solutions of low and intermediate apparent viscosity (μ_a < 0.140 Pa.s). Similarly Kipke[114] restricted his measurements to solutions of high apparent viscosity (μ_a > 0.234 Pa.s). Only Nishikawa et al.[115] covered the whole range of apparent viscosity of interest using CMC solutions of 0 - 6% giving K = 0.001 - 10.8 Pa.s^n and n = 1 to 0.59, which gives μ_a = 0.001 - 2 Pa.s for the shear rates used. With the exception of Ranade and Ulbrecht[30], none of the studies report any measurement of the visco-elastic properties of the solutions, although Yagi and Yoshida[49] do attempt to relate the viscoelasticity of the solutions to the mass transfer results obtained through the use of a Deborah number which relies only on the viscous properties of the solution.

Overall, little raw data is presented from which the individual results can be compared. That which is available is shown in figure 8.28 for CMC solutions of similar apparent viscosities agitated using a single disc turbine. The power consumption for the data of Yagi and Yoshida[49]

Figure 8.28

Comparison of Literature Data with Results Obtained here, for $k_L a$ versus P/V, in Similar CMC Solutions Agitated with a Single Disc Turbine.

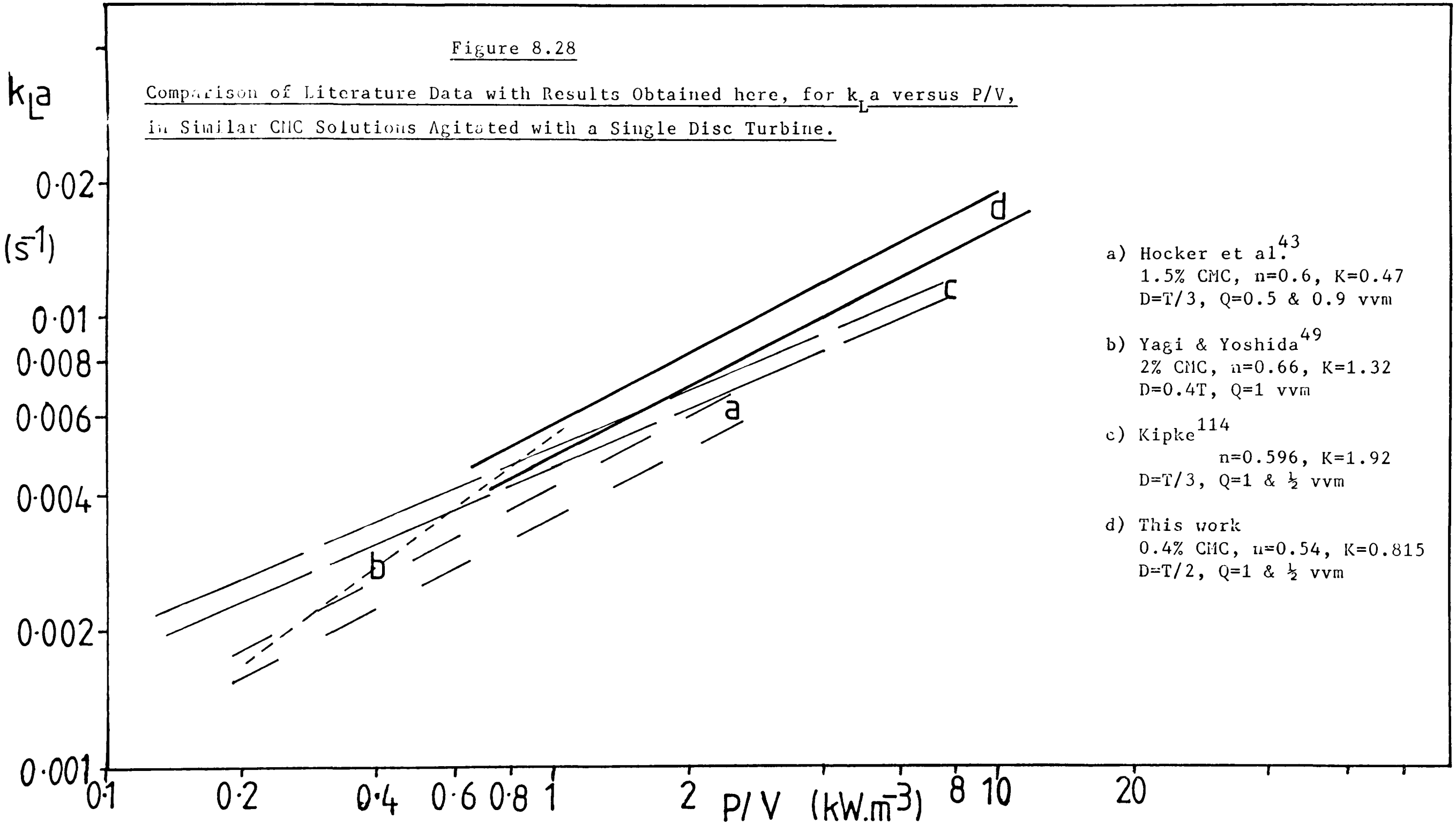

a) Hocker et al.[43]
1.5% CMC, n=0.6, K=0.47
D=T/3, Q=0.5 & 0.9 vvm

b) Yagi & Yoshida[49]
2% CMC, n=0.66, K=1.32
D=0.4T, Q=1 vvm

c) Kipke[114]
n=0.596, K=1.92
D=T/3, Q=1 & ½ vvm

d) This work
0.4% CMC, n=0.54, K=0.815
D=T/2, Q=1 & ½ vvm

has been estimated using Po - Re data for a disc turbine of the same diameter in similar solutions. Similarly the power consumption for the data of Kipke[144] has been estimated by using a value of $Po_g = 1.68$, which can be obtained from Kipkes own results. Reasonable agreement is obtained between the results of the various studies, although different impeller diameters have been used, varying between 0.33 and 0.5 times the tank diameter. In addition the apparent viscosities of the solutions vary over the range 0.092 - 0.374 Pa.s (measured at $N = 5\ s^{-1}$). This lack of variation in k_La over this range of μ_a can be attributed to the use of disc turbines in the transitional flow regime, as shown in the previous sections. The results obtained in this study are marginally higher than those in the literature, while those reported by Hocker et al.[43] are the lowest. These two studies show the same dependence of k_La on the gas flow rate, Q, with the dependence of k_La on Q reduced in the more viscous solutions used by Kipke[114]. Thus supporting the trend noticed in this study and that of Kipke[114], i.e. that increasing viscosity reduces the dependence of k_La on Q.

The data contained in figure 8.28 are the only results which have been obtained in the literature using disc turbines in the viscosity range 0.1 - 0.6 Pa.s. Yagi and Yoshida[49] and Hocker et al.[43] studied solutions of lower viscosity whilst Kipke[114] studied more viscous solutions. Nishikawa et al.[115] used solutions of greater and lower viscosity, but none in this region. Thus no other major study has confirmed the region of constant k_La for changing μ_a which has been seen here.

Further comparison of the results requires the use of correlations of the type reported in Chapter 4, section 5. The majority of the literature results have been correlated using the approach suggested by Zlokarnik[73], including the data of Yagi and Yoshida[49] which has been reinterpreted by Henzler[132]. This approach has been adopted here, and in

addition the variation in $k_L a$ with the parameters P/V, Q and μ_a is shown. Zlokarnik's correlation[73] requires the use of six dimensionless groups, as shown in equation 4.20. If the assumption that bubble coalescence behaviour does not vary markedly in the different CMC solutions is made, then the group Si^* can be eliminated. In addition Yagi and Yoshida[49], Ranade and Ulbrecht[30] and Nishikawa et al.[115] have shown that the surface tension does not vary significantly with varying CMC concentration, allowing the group σ^* to be ignored. This leaves four groups to be considered, as shown in equation 4.24. The diffusion coefficient, D_L, for the CMC solutions has not been measured here, but is considered to have a constant value of 2.0×10^{-9} $m^2.s^{-1}$, at 25°C, as used by Hocker et al.[43], regardless of the solution concentration. This is a reasonable assumption as data reported by Yagi and Yoshida[49] in CMC solutions of varying concentration up to 2% show almost constant values of $D_L = 2.3 \times 10^{-9}$ $m^2.s^{-1}$ at 30°C, similarly Nishikawa et al.[115] show that D_L is only reduced significantly at greater than 4% CMC concentration, below this concentration the value of D_L for water can be used. Multiple regression leads to the dimensionless results shown in table 8.1. In addition the dependence of $k_L a$ on P/V, Q and μ is shown. For two disc turbines (D = T/2) the range of solutions used are divided into groups according to their apparent viscosity, which are then correlated separately, these groups correspond to the different regions of $k_L a$ dependence on μ_a which are shown in the preceding sections. These results can be compared with those presented in the literature, as shown in Chapter 4, section 6, and table 4.1.

The correlations of Hocker et al.[43] and Henzler[132] reduce the number of dimensionless groups to three, through the use of equation 4.27. In order to justify this, the exponent on the group $(Q/V)^*$ must be close to unity. This is given by the value of c_3 in table 8.1. For one disc turbine (D = T/2), $c_3 = 0.80$. If this is set to unity then the correlation

TABLE 8.1

Correlation Equations for the Dependence of $k_L a$ on the Process Variables.

Results Obtained in This Study.

Correlation Equation		$(k_L a)^* = c_1 (P/Q)^{*c_2} . (Q/V)^{*c_3} . Sc^{c_4}$				$k_L a \ (s^{-1}) = c_5 [P/V]^{c_6} (kW.m^{-3}) . [Q/V]^{c_7} (s^{-1}) . \mu_a^{c_8} (Pa.s)$				Viscosities
Agitator Type	CMC Conc. %	c_1	c_2	c_3	c_4	c_5	c_6	c_7	c_8	
One Disc Turbine (D=T/2)	0-0.8	6.1×10^{-4}	0.47	0.80	0.12	0.060	0.47	0.33	-0.26	Low-Intermediate (0.001-0.34 Pa.s)
Two Disc Turbines (D=T/3)	0-0.8	2.2×10^{-4}	0.64	0.77	0.27	0.935	0.64	0.14	-0.23	Low-Intermediate (0.001-0.34 Pa.s)
Two Disc Turbines (D=T/2)	0.04-0.35	1.6×10^{-2}	0.39	0.91	-0.02	0.023	0.39	0.53	-0.31	Low (0.005-0.1 Pa.s)
	0.35-0.80	2.5×10^{-4}	0.37	0.75	0.28	0.006	0.37	0.38	-0.05	Intermediate (0.1-0.5 Pa.s)
	0.80-1.4	6.2×10^{-3}	0.50	0.68	-0.12	0.249	0.50	0.18	-0.56	High (0.4-0.9 Pa.s)
(Overall)	0.04-1.4	1.5×10^{-2}	0.48	0.85	-0.04	0.039	0.48	0.37	-0.29	Overall (0.005-0.9 Pa.s)
Intermigs (D=0.58T)	0-1.4	2.8×10^{-4}	0.45	0.62	0.13	0.175	0.45	0.18	-0.29	(μ = 0.001-0.8 Pa.s)

becomes:

$$K^* = 2.25 \times 10^{-3} . (P/Q)^{*0.51} . Sc^{0.07} \qquad (8.1)$$

This corresponds to $k_La \propto P/V^{0.51} . Q^{0.49} . \mu_a^{-0.27}$, which shows a slightly increased dependency of k_La on P/V, Q and μ_a and in addition increases the scatter in the results slightly. A similar result is found for two disc turbines in CMC solutions of 0.04 - 0.35%. Here $c_3 = 0.91$, which if set to unity produces the correlation:

$$K^* = 0.031 . (P/Q)^{*0.40} . Sc^{-0.05} \qquad (8.2)$$

This also increases the apparent dependence of k_La on the independent variables, i.e. $k_La \propto P/V^{0.40} . Q^{0.60} . \mu_a^{-0.32}$

In the more viscous solutions, a different lower value is found for the constant c_3. This is due to the markedly reduced dependence of k_La on the air flow rate seen in the viscous solutions. Here it is inappropiate to use a correlation such as that used by Hocker et al.[43] and Henzler[132], as the dependence of k_La on the air flow rate is so low. A correlation of the type shown in equation 4.25 is more appropriate. This produces:

$$(k_La)^* = 6.4 \times 10^{-3} . (P/V)^{*0.51} . Sc^{-0.07} \qquad (8.3)$$

As the exponent on the Schmidt number is close to zero, this can be altered to give: $(k_La)^* = 2.6 \times 10^{-3} . (P/V)^{*0.52}$, without significantly increasing the scatter. This gives an overall dependence of $k_La \propto P/V^{0.52} . \mu^{-0.51}$. Further analysis of the data obtained in the most viscous solutions shows that at low power inputs k_La is very highly dependent on P and μ. If data for $k_La < 0.01\ s^{-1}$ is correlated using equation 4.25 for two disc turbines (D = T/2) in these solutions then this results in:

$$(k_L a)^* = 7.1\ (P/V)^{*0.94}.\ Sc^{-0.65} \qquad (8.4)$$

Which corresponds to $k_L a \propto P/V^{0.94}.\ \mu^{-1.3}$. Clearly care is needed when applying these correlations to ensure that the different regions of mass transfer dependence on μ_a, shown in the preceding sections are taken into account.

As these results in the more viscous 0.8 - 1.4% CMC solutions are for a similar range of viscosities to those used by Kipke[114], it is possible to compare the data by using the correlation method chosen by Kipke[114] given in equation 4.33. This gives:

$$K^* = 5.4 \times 10^{-4}.\ (P/Q)^{0.60} \qquad (8.5)$$

Which is similar to the results obtained by Kipke[114] for a single disc turbine and for two Intermig agitators. This does however indicate a much higher dependence of $k_L a$ on the air flow rate and a lower dependence on the viscosity, than is actually found, giving $k_L a \propto P/V^{0.6}.\ Q^{0.4}.\ \mu^{-0.4}$. This may explain the large scatter in the results presented by Kipke[114] and also the scatter in the results when this data is correlated by Henzler[132].

Overall the correlation of the type used by Hocker et al.[43] and Henzler[132] are appropriate when using disc turbines, providing the apparent viscosity does not exceed 0.3 Pa.s. At higher viscosities it is necessary to consider the flow regime in force in the vessel. For the extended laminar regime, where Po_g falls with increasing Re, then the correlation given above in equation 8.4 is correct. In the transition region, where Po_g rises with increasing Re, then the correlation given in table 8.1 for solutions of 0.35 - 0.8% CMC is valid. For Intermigs no such distinction is necessary and the correlation given in the table can be used for all viscosities.

On examination it can be seen that the results obtained in this study when using Intermig agitators and the results obtained when using disc turbines at μ_a < 0.300Pa.s show a lower dependence of k_La on P, Q and μ_a than is found by Hocker et al.[43], Yagi and Yoshida[49] and Henzler[115]. This is in part due to the increased dependence obtained when correlations of the type shown in equation 4.27 are used, as can be seen above for one and two disc turbines (D = T/2). However this can only explain part of the discrepancy, the major effect is probably due to the different measuring methods used. In the literature studies, quoted above, a dynamic gassing out method is used and here a steady state method is used, from a consideration of the likely errors involved in the use of these two methods it becomes apparent that discrepancies will exist. The main problems associated with the dynamic method are outlined in Chapter 4, sections 2.4 & 3. Only those which are likely to alter the apparent dependence of k_La on P, Q and μ_a will be discussed further here. These are:

1) The dynamic method requires assumptions to be made about the gas phase dynamics. It is usual to assume that the gas phase in the vessel is not depleted of the transferring component when calculating C^*. This will introduce error into the results, giving a lower apparent k_La value than actually exists. This error will increase with reducing air flow rate, reducing the k_La values found at low air flow rates more than the reduction at higher air flow rates. Thus k_La is reduced and shows a greater dependence on Q.

2) The response of the dissolved oxygen probe to the oxygen dissolved in the bulk liquid will be controlled in part by the presence of a laminar film of liquid around the probe tip[100], through which the oxygen must diffuse. As this layer becomes thicker the apparent k_La value will be reduced compared with the actual k_La value, due to the measured dissolved oxygen concentration lagging behind the real dissoved oxygen concentration.

Thickening of this laminar liquid layer and reduction in k_La measured/k_La real, will occur for two reasons[22,100]:

a) The solution viscosity increases, this is particularly important where the solutions are shear thinning, as a low shear rate will be associated with proximity to solid surfaces, such as dissolved oxygen probes, causing a higher viscosity at the surface.

b) The impeller speed is reduced. As in a) this will lower the average shear rate within the vessel, so it is of particular importance when shear thinning liquids are used

Thus the k_La measured by the dynamic system will be further reduced by reducing impeller speed (and power consumption) and increasing viscosity. This in turn increases the apparent dependence of k_La on P and μ.

The likely errors in k_La measurement when using a steady state method are described in detail for the work carried out in this study in Appendix 2. The only errors which are likely to affect the dependence of k_La on the process variables, rather than just affecting the accuracy with which k_La is measured are:

1) Increasing air flow rate reduces the accuracy with which the oxygen uptake rate can be measured, as the difference in oxygen concentration between the inlet and exit gas streams is reduced. This is partly offset by a decrease in the dependence on the gas phase dynamics, as the gas phase composition becomes more uniform the choice of plug flow or fully back mixed models becomes irrelevant to the k_La measurement.

2) A change in the impeller speed will alter the response of the dissolved oxygen probe to a given dissolved oxygen concentration, as seen above when using the dynamic method. Thus at low N the probe reading will be reduced compared with the reading for the same dissolved oxygen concentration at high N. This effect can be reduced by careful calibration of the dissolved oxygen probe at all impeller speeds in use, prior to the

measurement of k_La, as described in Chapter 6. In addition this effect is offset by the reduced effect which an error in dissolved oxygen measurement will have at the low dissolved oxygen concentrations found at lower k_La values.

3) Increasing viscosity will affect the probe reading in the same manner as described above for lowering the impeller speed. In addition doubt as to the dissolved oxygen concentration profile in the more viscous liquids can introduce error into the k_La measurement. This is offset by the lower dissolved oxygen concentrations found in the more viscous liquids, due to the lower k_La values. Also the use of more than one dissolved oxygen probe, as carried out here and by Yagi and Yoshida[49] helps to assess the degree of non-uniformity in the dissolved oxygen concentration.

These points are dealt with in more detail in Appendix 2. Overall the steady state method allows ready estimation of the degree of error associated with any variable, which through careful choice of experimental conditions can be eliminated or reduced to a minimum. Thus the results found here may be considered to give a more accurate description of the dependence of k_La on the variables P, Q and μ_a; particularly for the range of agitator configurations and solution viscosities studied. Where fermentations are being considered, this steady state method mimics the conditions found within such a process, making it the method of choice.

CHAPTER 9

CONCLUSIONS AND SUGGESTIONS FOR FURTHER WORK

9.1) Conclusions

The steady state measuring method which has been developed and used here provides an adequate means of obtaining values of the volumetric mass transfer coefficient, $k_L a$, particularly in liquids which are viscous and rheologically complex, e.g. fermentation broths. In addition, the use of a microorganism which is capable of anaerobic fermentation as well as aerobic respiration, such as the yeast used here, can provide an indication of the degree to which the liquid phase is well mixed, when compositional analysis of the gas stream is carried out.

The $k_L a$ values obtained have been found to be dependent on culture variables, such as concentration of microorganisms, substrate feed rate and culture age, however a steady state period in which $k_L a$ does not vary with time was observed where reproduceable values could be obtained. Within this steady state period, the $k_L a$ values obtained are dependent on the rheological properties of the liquid, the gassing rate and the power input, as well as the impeller speed, type and number. In general, $k_L a$ is reduced by increasing apparent viscosity at constant power input, over the range of viscosities examined (0.001 - 0.9 Pa.s). However, there is a region at intermediate viscosities ($0.1 < \mu_a < 0.3$ Pa.s) where $k_L a$ is independent of variations in the apparent viscosity, when agitating with disc turbine impellers. This region corresponds to the transition region between laminar and turbulent flow regimes (Re = 300 - 2000), where the gassed power number, Po_g, increases with increasing Reynolds number, Re, in a given liquid.

At high viscosities ($\mu_a > 0.3$ Pa.s) $k_L a$ is highly dependent on the agitator power input and the viscosity, but is virtually independent of the gassing rate, regardless of the agitation system used. When using

the Intermig impellers at lower viscosities (μ_a < 0.3 Pa.s) k_La remains virtually independent of the gassing rate, although the other impeller systems used all show some dependence of k_La on the gassing rate, at low viscosities.

Adequate gas-liquid mixing was not easily achieved in the most viscous solutions used (1.4% CMC, μ_a = 0.858 Pa.s at $\dot{\gamma}_{AV}$ = 100 s^{-1}), when agitating with a single disc turbine or with two small disc turbines (D = T/3). Thus dual large diameter impellers are required (D $\geq$ T/2), with the highest k_La values achieved by dual disc turbines (D = T/2) for a given power input. In solutions of lower viscosity (0.4 - 0.8% CMC, μ_a = 0.07 - 0.35 Pa.s at $\dot{\gamma}_{AV}$ = 100 s^{-1}), smaller dual disc turbines (D = T/3) give superior mass transfer performance at lower power inputs than the large impellers, due to their higher rotational speed for a given power input. At high power inputs in each solution used, all agitator types tend to give similar mass transfer performance, with the exception of the pitched blade/disc turbine combination in the downward pumping mode and the Intermig impellers, where severe vibration occurred.

The power consumed when agitating the shear thinning viscoelastic liquids is reduced to a much larger extent by gassing, than is seen when agitating Newtonian liquids. In addition the gassed power number, Po_g, is highly dependent on the agitator diameter, which can be linked to the viscoelastic properties of the liquid. The gas hold-up, ε , has been seen to be linked to the value of Po_g, with rising Po_g and falling ε at high impeller speeds. It is postulated that this is linked to the size of the gas filled cavities behind the impeller blades, with variations in k_La in turn linked to the variations in Po_g and ε .

9.2) Suggestions for Further Work

As the oxygen uptake rate is measured here for the vessel as a whole, the values of the volumetric mass transfer coefficient obtained represent global values, integrated over the whole vessel. The differences seen in the point dissolved oxygen concentrations in the more viscous solutions would suggest that localised k_La values may vary markedly. Unfortunately measurement of localised k_La values would prove difficult in the systems of interest, thus analysis of the variation in transfer rates throughout the vessel is limited to measurement of the point dissolved oxygen concentrations and global measurement of the respiratory quotient. In this area provision of more measurements to enable the profiles of the dissolved oxygen concentration to be determined would be of interest, as would further work on the link between efficient bulk mixing and the RQ values obtained.

The vessel geometry used here, with liquid height = width, is popular for laboratory scale work. However there are several reasons why studies carried out in a taller geometry would be beneficial. The major reason is that industrial scale practice favours tall vessels, with the increased pressure due to the hydrostatic head increasing mass transfer rates. In addition use of a taller vessel would allow the effects on the power consumption and mixing due to variation in impeller separation to be examined, with the possible result that impellers which produce axial flow, such as the pitched blade turbine or the Intermig, may provide better mixing and mass transfer coefficients, than impellers which disperse the fluid radially. In conjunction with this, useful information would be provided by an investigation of the parameters which determine the bulk mixing patterns, such as the impeller speed, diameter and separation, the gassing rate and the rheological properties. Of particular interest are the effects of altering these parameters on the type of bulk mixing produced, whether zonal or global, as shown in figure 7.3, patterns A and

B. Measurement of the degree of inter-zonal mixing, e.g. by dye addition or through the use of tracer particles, when mixing pattern B dominates, is of importance, particularly where the vessel being considered has additional material added, e.g. substrate etc., during the course of the process carried out.

Further work using different impeller types would provide information from which an optimum design could be found, for operation over the range of viscosities encountered. Here the separate functions which the impeller must provide result in a compromise, as the bulk mixing of the vessel contents is most easily achieved with large diameter impellers, whereas gas bubble breakup and initial distribution is achieved most readily using small fast impellers. Separation of these two roles, by provision of two agitator systems, or the use of stationary internal fixtures, e.g. draft tubes, which utilise the rising gas bubbles to promote liquid circulation, may provide an interesting avenue of research.

The effects of the viscoelasticity of the liquid on gas dispersion and power consumption, which has been seen to be related to the impeller diameter, warrants further investigation, as does the effect on mixing and mass transfer of other variations in rheological properties, through the use of other model liquids. In particular, maintaining similar apparent viscosities, whilst varying the shear thinning nature of the liquid, i.e. through use of liquids with n close to zero, would provide data of interest, as many industrially important fermentations operate under these conditions. In this case further work is required to assess the effects due to the differing properties of the solutions, depending on whether the complex rheological behaviour is due to the formation of a soluble product which renders the continuous phase viscous, or the growth of filamentous microorganisms, where a semi-solid lattice-work is formed, suspended in an essentially aqueous continuous phase.

Finally, work on a variety of scales is required to assess the applicability of the results found here to the industrial scale.

APPENDIX 1

Determination of $k_L a$ from the Experimental Data

The equation used to determine $k_L a$ from steady state data is derived in Chapter 4, section 1 as:

$$N_A = k_L a \left(C^* - C_L \right) \qquad (4.12)$$

where $k_L a$ is the volumetric mass transfer coefficient of interest (s^{-1})

N_A is the oxygen uptake rate (OUR) for the liquid in the vessel

(moles $O_2 . m^{-3} . s^{-1}$)

C^* is the liquid phase concentration of oxygen which is in equilibrium with the gas phase (moles $O_2 . m^{-3}$)

C_L is the actual concentration of oxygen in the bulk liquid

(moles $O_2 . m^{-3}$)

a) Determination of N_A

This is found from mass balances on the inlet and exit gas streams for the vessel. The inlet stream consists of air at a volumetric flow rate, v_i ($m^3 . s^{-1}$); at pressure, P_i (Pa); and temperature, T_i (K). It is considered to be composed of oxygen, nitrogen and water such that:

$$O_2(i) + N_2(i) + H_2O(i) = 100\%$$

After drying for analytical purposes the assumed composition is:

$$O_2(i) = 21\% \text{ and } N_2(i) = 79\%$$

This removal of water alters the volumetric flow rate, reducing it slightly. In fact the inlet gas stream was assumed to be saturated with water in the compressor at a pressure of 70 psig, T = 20°C, this gave $H_2O(i) = 0.7\%$ as the vapour pressure of water at 20°C is approximately 20 mm Hg and as 70 psig = 3500 mm Hg. Thus v_i (dry) = 0.993 x v_i (wet)

For the exit gas stream water vapour can be ignored, as no measurement

of the volumetric flow rate (v_o) was used and the gas was dried before analysis, giving a composition of:

$$O_2(o) + CO_2(o) + N_2(o) = 100\%$$

with pressure P_o, at temperature T_o.

A mass balance for oxygen provides:

$$N_A = \left[\frac{O_2(i)}{100} \cdot \frac{P_i.v_i}{RT_i} - \frac{O_2(o)}{100} \cdot \frac{P_o.v_o}{RT_o} \right] \frac{1}{V} \qquad (A.1)$$

(moles $O_2.m^{-3}.s^{-1}$)

where V is the volume of liquid within the vessel

R is the gas constant

As accurate measurement of v_o is not possible, due to potential leaks within the system, a mass balance for nitrogen is carried out, assuming that no net accumulation takes place under steady state conditions. This gives:

$$\frac{N_2(i)}{100} \cdot \frac{P_i.v_i}{RT_i} = \frac{N_2(o)}{100} \cdot \frac{P_o.v_o}{RT_o} \qquad (A.2)$$

Substituion of A.2 in A.1 provides:

$$N_A = \frac{1}{V} \left[\frac{P_i.v_i}{RT_i} \cdot \frac{O_2(i)}{100} - \frac{O_2(o)}{100} \cdot \frac{N_2(i)}{100} \cdot \frac{100}{N_2(o)} \cdot \frac{P_i.v_i}{RT_i} \right]$$

$$= \frac{1}{100\ V} \cdot \frac{P_i.v_i}{RT_i} \left[O_2(i) - O_2(o) \cdot \frac{N_2(i)}{N_2(o)} \right] \qquad (A.3)$$

As the inlet gas stream when dried consists only of oxygen and nitrogen, whilst the exit stream also contains carbon dioxide produced by

the yeast in the vessel:

$$N_2(i) = 100 - O_2(i) \qquad (A.4)$$

$$N_2(o) = 100 - O_2(o) - CO_2(o) \qquad (A.5)$$

Substituting A.4 and A.5 in A.3 gives:

$$N_A = \frac{1}{100\ V} \cdot \frac{P_i.v_i}{RT_i} \left[O_2(i) - O_2(o) \frac{100 - O_2(i)}{100 - O_2(o) - CO_2(o)} \right]$$

$$= \frac{1}{100\ V} \cdot \frac{P_i.v_i}{RT_i} \left[\frac{100[O_2(i) - O_2(o)] - O_2(i).CO_2(o)}{100 - O_2(o) - CO_2(o)} \right]$$

(A.6)

Assuming $O_2(i) = 21\%$, let $X = O_2(i) - O_2(o)$, as measured by the oxygen analyser.

let $Y = CO_2(o)$, as measured by the carbon dioxide analyser.

Substitution in A.6 gives:

$$N_A = \frac{P_i.v_i}{RT} \cdot \frac{1}{V} \cdot \frac{X - 0.21Y}{79 + X - Y} \qquad (A.7)$$

With the inlet gas stream rotameter calibrated to give the volumetric flow rate at 1 atmosphere pressure and 20°C:

$$P_i = 1.013 \times 10^5 \text{ Pa}$$

$$R = 8.314 \text{ J.mole}^{-1}.\text{K}^{-1}$$

$$T_i = 293 \text{ K}$$

$$v_i(\text{dry}) = 0.993\ v_i(\text{wet})$$

$$N_A = \frac{1.013 \times 10^5 \times 0.993}{8.314 \times 293} \cdot \frac{v_i}{V} \cdot \frac{X - 0.21Y}{79 + X - Y}$$

For the 20 litre vessel used $V = 20 \times 10^{-3}\ m^3$ and a typical gas

flow rate used is 1 vvm, i.e. 20×10^{-3} $m^3.min^{-1}$.

Example:

If the measured values of X and Y are 0.30 and 0.25% respectively, then:

$$N_A = 41.3 \times \frac{20 \times 10^{-3}}{60} \cdot \frac{1}{20 \times 10^{-3}} \cdot \frac{0.3 - 0.21 \times 0.25}{79 + 0.3 - 0.25}$$

$$= 2.15 \times 10^{-3} \text{ moles } O_2.m^{-3}.s^{-1}$$

which was a value typical of those encountered in the experiments. The carbon dioxide production rate can be found in a similar manner as:

$$CPR = \frac{41.3\ v_i}{V} \cdot \frac{0.79\ Y}{79 + X - Y} \qquad (A.8)$$

which yields for the respiratory quotient:

$$RQ = \frac{CPR}{N_A} = \frac{0.79\ Y}{X - 0.21\ Y} \qquad (A.9)$$

b) Determination of the Driving Force $(C^* - C_L)$

The probes used in the 20 litre vessel were calibrated to read 100% at a vessel temperature, T_v = 25°C and a vessel pressure, P_v of 150 mm Hg above atmospheric pressure. At this temperature and pressure water vapour in the vessel reduces the concentration of oxygen, thus the pressure of oxygen in the gas phase when calibrating the probes is given by:

$$P_{O_2} = \frac{760 + 150 - 24}{760} \times \frac{O_2(i)}{100} \qquad (A.10)$$

$O_2(i)$ is the inlet gas concentration in % and is 21%, thus:

$$P_{O_2} = 0.245 \text{ atm.}$$

Henry's Law constant is 1.268 moles $O_2.m^{-3}.atm\ O_2^{-1}$ @ 25°C (see Chapter 6) giving 100% dissolved oxygen = 0.311 moles $O_2.m^{-3}$ (approximately 10 $g.m^{-3}$)

Thus:

$$C_L = \frac{0.311}{100} \times Z \qquad (A.11)$$

where Z is the probe reading in %.

During the experiments the gas phase oxygen concentration varies according to the oxygen uptake rate. For a fully backmixed vessel, the exit gas composition is assumed to apply to the whole of the gas phase in the vessel, giving:

$$P_{O_2} = 0.245 \times \frac{O_2(o)}{O_2(i)} \quad \text{atm.} \qquad (A.12)$$

$$\text{and } C^* = 0.311 \times \frac{O_2(o)}{O_2(i)}$$

$$= 0.311 \times \frac{21 - X}{21} \qquad (A.13)$$

combining equations A.11 and A.13 gives:

$$(C^* - C_L) = 0.311 \left(\frac{21 - X}{21} - \frac{Z}{100} \right)$$

$$= \frac{0.311}{21} (21 - X - 0.21 Z)$$

$$= 0.01480 (21 - X - 0.21 Z) \qquad (A.14)$$

As H varies with temperature a correction factor, Tc, is incorporated, which enables small minor variations in temperature to be compensated for. H is reduced by 1.56% for each degree rise in temperature, so for a temperature in the vessel of T':

$$Tc = \frac{(25 - T') \times 1.56 + 100}{100} \qquad (A.15)$$

There is no need to correct the dissolved oxygen readings, as the probes were self compensating for temperature, giving:

$$(C^* - C_L) = 0.01480\ Tc\ (\ 21 - X - 0.21\ Z/Tc\ ) \quad (A.16)$$

For plug flow of the gas phase a log mean driving force is used, i.e.

$$\text{DRIVING FORCE} = \frac{(C^*_{in} - C_L) - (C^*_{out} - C_L)}{\ln\left(\frac{C^*_{in} - C_L}{C^*_{out} - C_L}\right)}$$

$$= \frac{0.01480.Tc\ [(\ 21 - 0.21\ Z/Tc\ ) - (\ 21 - X - 0.21\ Z/Tc\ )]}{\ln\left(\frac{21 - 0.21\ Z/Tc}{21 - X - 0.21\ Z/Tc}\right)}$$

$$= 0.01480.Tc.X\ /\ \ln\left[1 + \frac{X}{21 - X - 0.21\ Z/Tc}\right]$$

(A.17)

In practice X was small compared to $O_2(o)$ or $O_2(i)$, with a typical maximum value of 0.6% compared to 21% for $O_2(i)$. Thus the results obtained using a plug flow model are similar to the fully backmixed model.

Example:

$T' = 24°C$; $X = 0.6\%$; $Z = 30\%$ (midway in the range used, 0 - 60%)

$$Tc = \frac{1.56 \times 1 + 100}{100} = 1.0156$$

Fully Backmixed Driving Force $= 0.01480 \times 1.0156\ (\ 20.4 - 0.21 \times 70/1.0156\ )$

$= 0.213$ moles $O_2.m^{-3}$

Plug Flow Driving Force $= 0.01480 \times 1.0156 \times 0.6\ .\ \ln\left[1 + \frac{0.6}{20.4 - 0.21 \times 70/1.0156}\right.$

$= 0.218$ moles $O_2.m^{-3}$

APPENDIX 2

Sources of Error in the Measurement of $k_L a$

Clearly there will be errors in the measurement of $k_L a$ which are due to instrumental imperfections, such as chart recorder accuracy, gauge accuracy etc., which are inherent in any experimental work. These have of course been reduced to a minimum, through use of good quality equipment and will not be discussed further here. In addition there are potential sources of error in the assumptions made in the derivation of the operating equation for $k_L a$, i.e. equation 4.12:

$$N_A = k_L a \ (C^* - C_L) \qquad (4.12)$$

These assumptions are outlined in Chapter 4, where equation 4.12 is derived and in general they are accepted, with equation 4.12 acting as a definition of the parameter sought, i.e. $k_L a$. This leaves only the errors in the measurement of N_A, the oxygen uptake rate (OUR), and the driving force, $(C^* - C_L)$. Each of these is dealt with in turn.

a) Errors in the Determination of N_A

The derivation of N_A in Appendix 1 results in the equation:

$$N_A = \left[\frac{P_i . v_i}{R \ T_i} \right] . \frac{1}{V} . \left[\frac{X - 0.21Y}{79 + X - Y} \right] \qquad (A.7)$$

Clearly variations in atmospheric pressure (P_i) and room temperature (T_i) will directly affect the value of N_A found, by altering the mass flow rate of air into the vessel ($P_i . v_i / R . T_i$). These variations are not likely to be significant over the course of a single experiment, except where it lasts for more than one day, however between individual experiments, carried out in different weather conditions up to 5% error can be introduced. This is mitigated by using an inlet pressure (at the inlet rotameter) of

10 psig, which reduces the effect due to varying atmospheric pressure on the measured inlet flow rate, e.g. a 5% increase in atmospheric pressure results in a 3% increase in inlet pressure. In addition a variation in room temperature of 5°C, which is an extreme value, results in a 2% error in measurement of the inlet mass flow rate. Thus extreme variations in measurement of the inlet mass flow rate will result in up to 5% error in the measurement of N_A, with typical variations producing a smaller error, estimated as $\pm$ 2 - 3%.

Variations in atmospheric pressure will also affect the readings obtained from the oxygen analyser (X) and the carbon dioxide analyser (Y). This occurs when the pressure at which the analysers were calibrated differs from the pressure at which the experimental readings are obtained. In the oxygen analyser this error is removed by using two channels, one for the inlet gas stream and one for the exit gas stream. This means that any alteration of pressure will alter both readings to the same extent, thus the difference reading will effectively remove this error. The analysers are also subject to drifting of the output signal. For the oxygen analyser this was found to be a sinusoidal variation in the difference signal produced, of $\pm$ 0.02% oxygen concentration over a 24 hour period, when passing air through the analysers. For the carbon dioxide analyser the drift was principally due to variations in atmospheric pressure, which affected the full scale reading, giving a 1 - 2% variation in output over a period of 24 hours when passing 5% carbon dioxide through the analyser. The zero reading, obtained using nitrogen gas, was remarkably stable, with no drift observed. Frequent recalibration of the oxygen and carbon dioxide analysers during each experiment reduced these errors. Overall the maximum error in the difference output of the oxygen analyser found during an experiment was 0.01% oxygen, producing an average error of 0.005% oxygen. As a typical minimum reading of X, the oxygen concentration difference was 0.25%, obtained at a high gas flow

rate (1 vvm) under conditions of low $k_L a$, this represents an error of $\pm$ 2% in X, with a worst case error of $\pm$ 4%. From equation A.7 it can be seen that this will have a direct effect on the measurement of N_A. The 1 - 2% maximum error in the measurement of carbon dioxide concentration, Y, will have a smaller effect on N_A, as it is multiplied by 0.21 in equation A.7 before subtraction from X.

Variation of the liquid volume, V, will have a direct effect on the value of N_A. A liquid height of 0.3 m ($\pm$ 0.001 m) at the start of each experiment was maintained. Over the course of each experiment the addition of liquid, by the glucose feed pump, and the removal of liquid, by evaporation and sampling, resulted in a maximum change of liquid height of 0.003 m, introducing a 1% error into the measurement of N_A.

b) Errors in the Determination of the Driving Force $(C^* - C_L)$

From the example in Appendix 1 it can be seen that the error in measurement of the driving force, which is introduced by the assumption that the gas phase is fully backmixed, or in plug flow, is very small under the experimental conditions used here. Thus the use of equation A.14, with the temperature correction of equation A.15 seems reasonable. This still leaves several sources of error; related to the measurement of the solubility of oxygen, the gas phase concentration of oxygen and the liquid phase concentration of oxygen.

The solubility of oxygen in the solutions of CMC containing live yeast is indeterminate, with the assumption being that it is equal to the solubility in water (see Chapter 4, section 4). This assumption is likely to introduce a large error into the measurement of the driving force. A consideration of the effects of salts etc. on the solubility of oxygen suggests that the assumption overestimates the solubility, possibly by as much as 10%. However this error will be consistent for all the measurements carried out here, as the addition of CMC has a

negligible effect on the solubility of oxygen (see Chapter 4). Thus for internal comparison it has no effect, whilst direct comparison with the results of other workers, is highly dependent on geometry, solution characteristics etc., all of which affect $k_L a$.

Variations in atmospheric pressure will affect the solubility of oxygen. With increases in pressure raising its solubility according to Henry's Law (see Chapter 4, section 1). This will have a direct effect on the driving force measurement, introducing errors on the same scale as outlined above for the measurement of N_A. It should be noted that this dual effect of pressure variation on N_A and $(C^* - C_L)$ will tend to cancel out the overall effect on $k_L a$, as a rise in pressure will raise N_A and raise the driving force by virtually the same degree.

The error in estimating X, the difference in inlet and exit oxygen concentrations in the gas phase will have only a very minor effect on C^*, providing X is small, as is the case in the experiments carried out here. If X is large then 21 - X becomes smaller and an error in X will introduce error into the measurement of C^*. This will be mitigated by the increased accuracy with which X can be measured, however assumptions made about the gas phase mixing may then be invalid, introducing further error.

Error in the measurement of the liquid phase oxygen concentration can have a large effect on the value of the driving force and may stem from different sources. The larger the value of C_L, then the smaller is the difference $(C^* - C_L)$, hence as C_L rises the error introduced has a large effect. For example a 5% error in measuring C_L, when C_L is only $0.1 \times C^*$ will introduce less than 1% error in the measurement of the driving force. If C_L is $0.9 \times C^*$, then a similar 5% error produces a 45 - 55% error in the driving force. For this reason an upper limit was placed on C_L of $0.6 \times C^*$, corresponding to a dissolved oxygen reading of approximately 60%. At this limit a 1% error in the measurement of

C_L produces a 1.5% error in the measurement of the driving force, which was considered to be an acceptable limit. Errors in the measurement of C_L may stem from several sources. The most important being incorrect calibration of the dissolved oxygen electrode, drift in electrode calibration, electrode malfunction, temperature variations, differing liquid velocities across the probe tip, gas bubbles adhering to the probe tip or variations in dissolved oxygen concentration as a function of the position in the liquid. These sources of error are minimised by careful experimental method: Checking the calibration readings at all impeller speeds removes the error due to differing liquid velocities, allowing accurate calibration to within 1%. The calibration drift was estimated to be less than 2% per week, which is longer that the time scale of the experiments, with calibration before and after the experiment carried out where possible. Electrode malfunctions were usually due to a punctured membrane, which allowed the elctrolyte to leak out; slow response, due to oxide formation on the silver anode; gas bubbles within the electrode, which caused rapid fluctuations in the output, particularly when the pressure on the membrane varied; or flat batteries, which was indicated on the display of the meter. These malfunctions could generally be avoided by frequent inspection and servicing of the electrodes.

The temperature variations were allowed for by using electrodes with built in temperature compensation. In addition the equation used to determine the driving force has a temperature correction factor to allow for the differing solubility of oxygen (see Appendix 1). The presence of gas bubbles adhering to the probe and increasing the measured dissolved oxygen concentration occurred when the liquid velocity across the probe tip was low. In these circumstances the output of the electrode was erratic, showing sharp spikes in dissolved oxygen concentration. The probe which was used to provide the reading from which C_L was determined was not generally susceptible to this effect as it was always in a region

of high liquid flow near to the impellers.

Variation of dissolved oxygen concentration in different parts of the vessel occurred in the more viscous solutions used, as described in Chapter 7,section 4. However its effects on the measurement of k_La were minimised, as it occurs only in the more viscous solutions where low k_La values are encountered. Under these circumstances the dissolved oxygen concentration is low and an error in its estimation is not increased when determining the driving force. For example, if the dissolved oxygen concentration near the impellers is 5%, whilst that in the extremes of the vessel is 0%, then the average value will be between 0 - 5%. Use of a figure of 2½%, i.e. the mean of the two readings, will give a maximum error of 2½% in determining the driving force. In practice it is possible to estimate the likely average value of dissolved oxygen concentration throughout the vessel, from the readings given by the three electrodes and knowledge regarding the degree of liquid mixing present at the relevant impeller speed. This knowledge is gained through visual observation of the liquid mixing prior to addition of the yeast. In general only the extremes of the vessel became stagnant at the impeller speeds of interest, thus the overall dissolved oxygen concentration is likely to be near to that found in the region of the impellers.

Examination of k_La values at lower and higher impeller speeds also provides information regarding the accuracy of measurement of the driving force when the dissolved oxygen concentration is dependent on position within the vessel. At higher speeds, the dissolved oxygen concentration is uniform, allowing accurate measurement of the driving force. At lower speeds the dissolved oxygen concentration is uniformly zero, again allowing accurate measurement of the driving force. Clearly interpolation to intermediate impeller speeds is subjective, but the results obtained are reasonably consistent.

Overall an error of up to $\pm$ 3% in measurement of the driving force may be expected at non-zero dissolved oxygen concentrations, which coupled with the errors in measurement of the oxygen uptake rate, N_A, leads to a potential error in k_La measurement of up to $\pm$ 5%. This will be reduced within each individual experiment, where the relative error may be negligible, due to the repetition of individual readings.

N.B. This appendix has not dealt with errors which occur due to variations in k_La itself. k_La is dependent on the solution composition, principally through the effects which the composition has on the surface properties of the liquid, which affect coalescence rates, equilibrium bubble size, diffusion coefficients etc. As has been described in Chapter 6, variations in composition occur with time in the cultures used, which causes variations in k_La. These variations may also occur between individual experiments. Repetition of experiments has showed that reproduceable results, to within $\pm$ 10% are obtainable in the CMC solutions used, which is acceptable considering the difficulty in reproducing the rheological properties exactly (see Chapter 6). Figure A.1 shows the results of two separate experiments conducted in 1.4% CMC. As the rheological properties of the two solutions were slightly different, the dependence of k_La on P/V shows some scatter. This is eliminated in figure A.1 by plotting k_La versus Reynolds number. In water similar reproduceability was obtained, which is shown by the results presented in figure 6.5, which were obtained in several different experiments.

Figure A.1 Variation of $k_L a$ with Reynolds number, Re. Two separate experiments, both in 1.4% CMC.

LEGEND:

1 vvm	½ vvm	
●	○	Solution 1: n = 0.324, K = 19.3 Pa.s^n
■	□	Solution 2: n = 0.333, K = 19.3 Pa.s^n

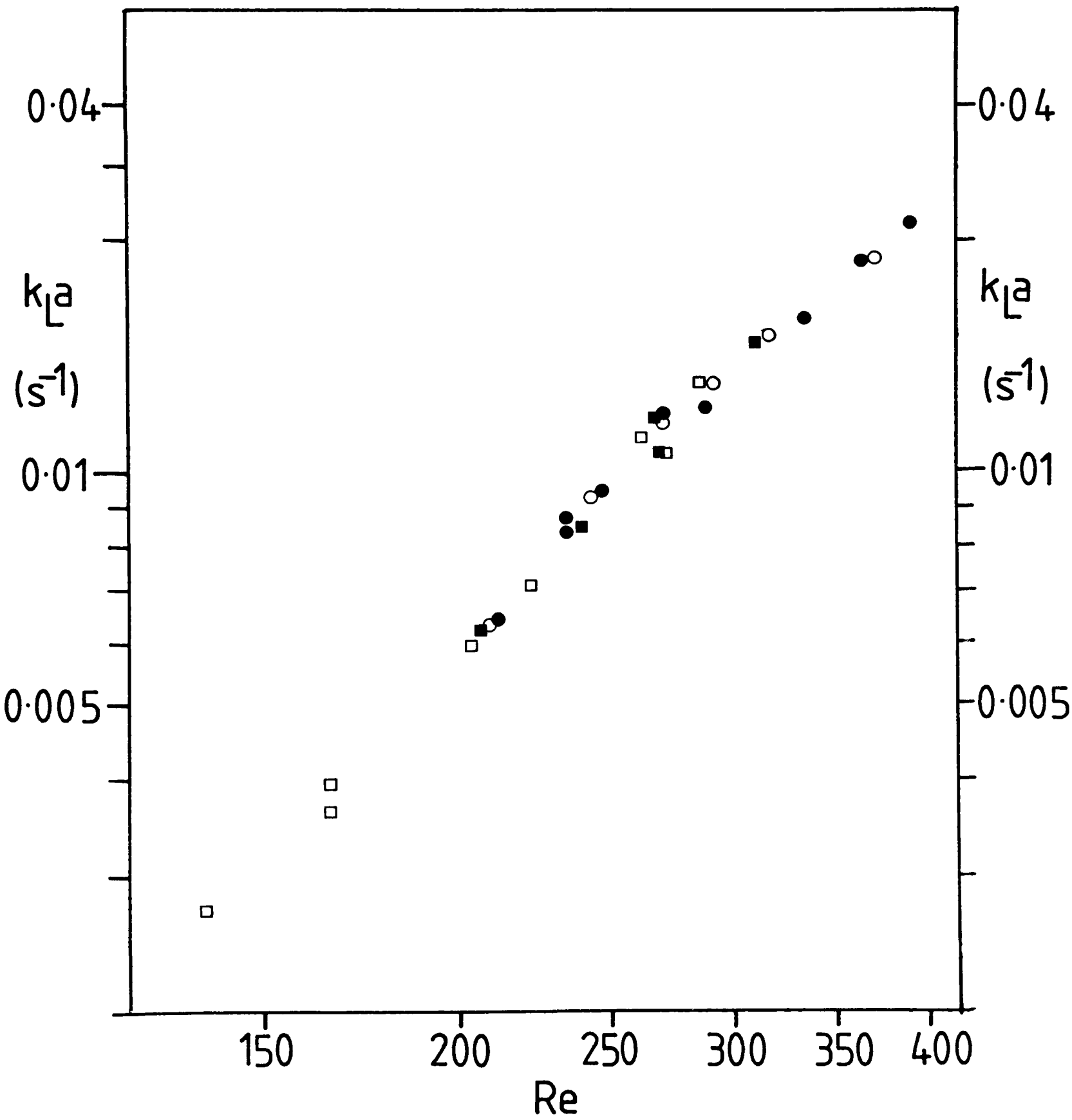

NOMENCLATURE

a	-	gas liquid interfacial area per unit volume of liquid	m^{-1}
A'	-	gas-liquid interfacial area	m^2
A	-	constant, equation 2.12	$Pa.s^b$
b	-	exponent, equation 2.12	-
C	-	oxygen concentration (see subscripts)	$Moles.m^{-3}$
C*	-	liquid phase oxygen concentration in equilibrium with the gas phase	$Moles.m^{-3}$
CPR	-	carbon dioxide production rate	$Moles.m^{-3}.s^{-1}$
c	-	impeller clearance above base of tank	m
d	-	distance of element from shaft	m
D	-	impeller diameter	m
D_L	-	Molecular diffusion coefficient of gas in liquid	$m^2.s^{-1}$
D_m	-	general diffusion coefficient	$m^2.s^{-1}$
De	-	Deborah number, equation 3.15	-
F	-	normal force	N
Fl_g	-	aeration number, equation 3.11	-
Fr	-	Froude number, equation 3.10	-
g	-	gravitational acceleration	$m.s.^{-2}$
G_T	-	torque on cone or plate	N.m
Ga	-	Galilei number, equation 3.12	-
H_l	-	liquid height	m
H	-	Henry's law constant	pressure/concn.
J	-	creep compliance	$m^2.N^{-1}$
J_N	-	Newtonian compliance	m^2N^{-1}

J_o	-	instantaneous compliance	$m^2.N^{-1}$
J_R	-	retarded compliance	$m^2.N^{-1}$
k_s	-	agitator shear rate constant	-
k_c	-	general mass transfer coefficient	$m.s^{-1}$
k_G	-	gas phase mass transfer coefficient	$m.s.^{-1}$
k_L	-	liquid phase mass transfer coefficient	$m.s.^{-1}$
k_La	-	volumetric mass transfer coefficient	s^{-1}
k_La^*	-	dimensionless volumetric mass transfer coefficient, equation 4.21	-
K	-	consistency index	$Pa.s^n$
K*	-	dimensionless mass transfer and gas flow rate number, equation 4.28	-
L	-	characteristic length of system .	m
M_G	-	mass flow rate of gas	$kg.s.^{-1}$
n	-	flow behaviour index	-
N	-	rotational speed of the agitator	s^{-1}
N_A	-	overall mass flux	$Moles.m^{-3}.s^{-1}$
N_1	-	first normal stress difference	$N.m^{-2}$
N_2	-	second normal stress difference	$N.m^{-2}$
OUR	-	oxygen uptake rate	$Moles.m^{-3}.s^{-1}$
p	-	partial pressure (see subscripts)	$N.m^{-2}$
P	-	power imput to the agitator	W
P'	-	power input due to gassing	W
Po	-	power number, equation 3.9	-
Po_g	-	gassed power number	-
P_{in}, P_{out}		inlet and exit gas pressures	$N.m^{-2}$
P_{ij}	-	stress tensor	$N.m^{-2}$
(P/Q)*	-	dimensionless power input and gas flow rate equation 4.22	-
(P/V)*	-	dimensionless power input per unit volume equation 4.26	-

Q	-	volumetric gas flow rate	$m^3.s^{-1}$
(Q/V)*	-	dimensionless gas flow rate per unit volume equation 4.23	-
r	-	rate of mass transfer	$Moles.s.^{-1}$
r_c	-	volumetric rate of oxygen consumption	$Moles.m^{-3}.s^{-1}$
R	-	gas constant	$J.K.^{-1}Mole^{-1}$
Rc	-	radius of cone	m
R_1R_2	-	radius of inner and outer coaxial cylinders	m
Re	-	Reynolds Number, equation 3.6	-
Re_c	-	coaxial cylinder Reynolds number, equation 2.15	-
RQ	-	respiratory quotient	-
s	-	seperation between impellers	m
Sc	-	Schmidt number, equation, 4.18	-
Sh	-	Sherwood number, equation 4.16	-
Sh'	-	modified Sherwood number, equation 4.17	-
Si	-	description of bubble coalescence	-
Si*	-	dimensionless number describing coalescence	-
t	-	torque on impeller shaft	N.m
t_0, t_1	-	times	s
t_p	-	characteristic process time	s
T	-	tank diameter	m
v_s	-	superficial gas velocity	$m.s^{-1}$
v_1, v_2, v_3		velocity components	$m.s.^{-1}$
V	-	liquid volume	m^3
Wi	-	Weissenberg number, equation 3.13	-

GREEK SYMBOLS

γ	-	strain	-
$\dot{\gamma}$	-	shear rate or rate of strain	s^{-1}
$\dot{\gamma}_r$	-	representative shear rate	s^{-1}
$\dot{\gamma}_{av}$	-	average shear rate	s^{-1}
ϵ	-	hold-up (voume of bubbles/volume of liquid)	-
θ	-	cone angle	radians
λ	-	characteristic material time (or fluid relaxation time)	s
μ	-	Newtonian viscosity	Pa.s.
μ_a	-	apparent viscosity	Pa.s
μ_o	-	apparent viscosity at zero shear rate	Pa.s
μ_w	-	viscosity of water	Pa.s.
μ_g	-	viscosity of gas phase	Pa.s
μ_r	-	representative viscosity	Pa.s
μ_∞	-	apparent viscosity at infinite shear rate	Pa.s
ρ	-	density of liquid	$k_g.m^{-3}$
σ	-	interfacial or surface tension	$N.,^{-2}$
σ^*	-	dimensionless interfacial tension, equation 4.23a	$N.m^{-2}$
τ	-	shear stress	$N.m^{-2}$
τ_y	-	yield stress	$N.m^{-2}$
Ω	-	angular velocity	$radians.s^{-1}$

SUBSCRIPTS

g	-	gassed
G	-	gas phase
i	-	interface
L	-	liquid phase
BC	-	bubble cloud
CD	-	complete gas dispersion

REFERENCES

1. Bhavaraju, S.M., Russell, T.W.F. and Blanch, H.W. A.I.Ch.E. J. 24, 454 (1978)

2. LeGrys, G.A. Chem. Eng. Sci. 33, 83 (1978)

3. Anderson, C., LeGrys, G.A. and Solomons , G.L. The Chem. Engr. 377, 43 (1982)

4. Skelland, A.H.P. "Non-Newtonian Flow and Heat Transfer", Wiley and Sons (1967)

5. Sherman, P. "Industrial Rheology", Academic Press (1970)

6. Whorlow, R.W. "Rheological Techniques", John Wiley and Sons (1980)

7. Walters, K. "Rheometry", Chapman and Hall (1975)

8. Walters, K. "Rheometry: Industrial Applications", John Wiley and Sons, Research Studies Press (1980)

9. Boger, D.V. J. Non-Newt. Fluid Mech. 3, 87 (1977-1978)

10. Boger, D.V. "Rheology" Vol 1, p 195. 8th Int. Congress on Rheology, Naples (1980)

11. Cheng, D. C-H. Chem. Eng. Sci. 23, 895 (1968)

12. Roels, J.A., Van Den Berg, J. and Voncken, R.M. Biotechnol. Bioeng. 16, 181 (1974)

13. Schugerl, K. Adv. in Biochem. Eng. 19, 71 (1981)

14. Reuss, M., Debus, D. and Zoll G. The Chem. Engr. 381, 233 (1982)

15. Charles, M. Adv. in Biochem. Eng. 8, 1 (1978)

16. Metz, B., Kossen, N.W.F. and van Suijdam, J.C. Adv. in Biochem. Eng. 11, 103 (1979)

17. Bongenaar, J.J.T.M., Kossen, N.W.F., Metz, B. and Meijboom, F.W. Biotechnol. Bioeng. 15, 201 (1973)

18. Blakeborough, N., McManamy, W.I. and Tart, K.R. Trans. Instn. Chem. Eng. 56, 127 (1978)

19. LeDuy, A., Marson, A.A. and Coupal, B. Biotechnol. Bioeng. 16, 61 (1974)

20. Pace, G.W. and Righelato, R.C. Adv. in Biochem. Eng. 15, 41 (1980)

21. Smith, I.H. and Pace, G.W. J. Chem. Tech. Biotechnol. 32, 119 (1982)

22. Solomon, J. Ph.D. Thesis, University of London (1980)

23. Metzner, A.B. and Otto, R.E. A.I.Ch.E. J. 3 , 3 (1957)

24. Metzner, A.B. Feehs, R.H., Ramos , H.L., Otto, R.E. and Tuthill, J.D. A.I.Ch.E. J. 7, 3 (1961)

25. Calderbank, P.H. and Moo-Young, M.B. Trans. Instn. Chem. Eng. 37, 26 (1959)

26. Calderbank, P.H. and Moo-Young, M.B. Trans. Instn. Chem. Eng. 39, 337 (1961)

27. Ducla, J.M., Desplanches, H. and Chevalier, J.L. Chem. Eng. Commun. 21, 29 (1983)

28. Ranade, V.R. and Ulbrecht, J. Second European Conference on Mixing (BHRA), Cambridge, F6-83 (1977)

29. Hocker, H. and Langer, G. Rheol. Acta. 16, 400 (1977)

30. Ranade, V.R. and Ulbrecht, J.J. A.I.Ch.E. J. 24, 796 (1978)

31. Ulbrecht, J. The Chem. Engr. J. 286, 347 (1974)

32. Metzner, A.B. and Taylor, J.S. A.I.Ch.E. J. 6, 109 (1960)

33. Sachs, J.P. and Rushton, J.H. Chem. Eng. Prog. 50, 597 (1954)

34. Joshi, J.B., Pandit, A.B. and Sharma, M.M. Chem. Eng. Sci. 37, 813 (1982)

35. Codleski, E.S. and Smith, J.C. A.I.Ch.E. J. 8, 617 (1962)

36. Paca, J., Ettler, P. and Gregr, V. J. Appl. Chem. Biotech. 26, 309 (1976)

37. Einsele, A. and Finn, R.K. Ind. Eng. Chem. Process Des. Dev. 19, 600 (1980)

38. Rushton, J.H., Costick, E.W. and Everett, H.J. Chem. Eng. Prog. 46, 395 (1950)

39. Bates, R.L., Fondy, P.L. and Corpstein, R.R. Ind. Eng. Chem. (PDD) 2, 310 (1963)

40. Solomon , J., Nienow, A.W. and Pace, G.W. I. Chem. E. Symp. no.64, A1 (1981)

41. Wichterle, K. and Wein, O. Int. Chem. Eng. 21, no.1, 116 (1981)

42. Nienow, A.W., Wisdom, D.J., Solomon, J., Machon, V. and Vlcek, J. Chem. Eng. Comm. 19, 273 (1983)

43. Hocker, H., Langer, G. and Werner, U. Ger. Chem. Eng. 4, 51 (1981)

44. Prud'homme, R.K. and Shaqfeh, E. A.I.Ch.E. J. 30, 485 (1984)

45. Van't Riet, K. and Smith, J.M. Chem. Eng. Sci. 28, 1031 (1973)

46. Bruijn, W., Van't Riet, K. and Smith, J.M. Trans. Instn. Chem. Eng. 52, 88 (1974)

47. Nienow, A.W. and Wisdom, D.J. Chem. Eng. Sci. 29, 1994 (1974)

48. Nienow, A.W., Wisdom, D.J. and Middleton, J.C. Second European Conference on Mixing (BHRA), Cambridge, F1-1 (1977)

49. Yagi, H. and Yoshida, F. Ind. Eng. Chem. (PDD) 14, 488 (1975)

50. Acharya, A. and Ulbrecht, J.J. A.I.Ch.E. J. 24, 348 (1978)

51. Blakeborough, N. and Sambamurthy, K. J. Appl. Chem. 14, 413 (1964)

52. Edney, H.G.S. and Edwards, M.F. Trans. Instn. Chem. Eng. 54, 160 (1976)

53. Hixson, A.W. and Gaden, E.L. Ind. Eng. Chem. 42, 1792 (1950)

54. Bailey, J.E. and Ollis, D.F. "Biochemical Engineering Fundamentals", McGraw-Hill (1977)

55. Shah, Y.T. and Sharma, M.M. Trans. Instn. Chem. Eng. 54, 1 (1976)

56. Danckwerts, P.V. Ind. Eng. Chem. 43, 1460 (1951)

57. Nienow, A.W. "Symposium on the Profitable Aeration of Waste Water" (BHRA), London, Paper 1 (1980)

58. Levenspiel, O. "Chemical Reaction Engineering", John Wiley and Sons (1972)

59. Levenspiel, O. and Godfrey, J.H. Chem. Eng. Sci. 29, 1723 (1974)

60. Calderbank, P.H., Johnson, D.S.L. and Loudon, J. Chem. Eng. Sci. 25, 235 (1970)

61. Koide, K., Orito, Y. and Hora, Y. Chem. Eng. Sci. 29, 417 (1974)

62. Elstner, F. and Onken, U. Ger. Chem. Eng. 4, 84 (1981)

63. Calderbank, P.H. Trans. Instn. Chem. Eng. 36, 443 (1958)

64. Sridhar, T. and Potter, O.E. Chem. Eng. Sci. 35, 683 (1980)

65. Reith, T. and Beek, W.J. Trans. Instn. Chem. Eng. 48, T63 (1970)

66. Keitel, G. and Onken, U. Chem. Eng. Sci. 37, 1635 (1982)

67. Kawecki, W., Reith, T., van Heuven, J.W. and Beek, W.J. Chem. Eng. Sci. 22, 1519 (1967)

68. Joshi, J.B. and Sharma, M.M. Trans. Instn, Chem. Eng. 54, 42 (1976)

69. Mehta, V.D. and Sharma, M.M. Chem. Eng. Sci. 26, 461 (1971)

70. Joshi, J.B. and Kale, D.D. Chem. Eng. Comm. 3, 15 (1979)

71. Van't Riet, K. Ind. Eng. Chem. (PDD) 18, 357 (1979)

72. Heineken, F.G. Biotechnol. Bioeng. 13, 599 (1971)

73. Zlokarnik, M. Adv. Biochem. Eng. 8, 133 (1978)

74. Perez, J.F. and Sandall, O.C. A.I.Ch.E. J. 20, 770 (1974)

75. Voigt, J. and Schugerl, K. Chem. Eng. Sci. 34, 1221 (1979)

76. Konig, B., Lippert, J. and Schugerl, K. Ger. Chem. Eng. 2, 371 (1979)

77. Keitel, G. and Onken, U. Chem. Eng. Sci. 36, 1927 (1981)

78. Wang, D.I.C., Cooney, C.L., Demain , A.L., Dunnill, P., Humphrey, A.E. and Lilly , M.D. "Fermentation and Enzyme Technology", John Wiley and Sons (1979)

79. Kappeli, O. and Fiechter, A. Biotechnol. Letters 3, 541 (1981)

80. Spriet, J.A., Botterman, J.H., De Buyser, D.R., De Visscher, P.L. and Vandamme, E.J. Biotechnol. Bioeng. 24, 1605 (1982)

81. Votruba, J., Sobotka, M. and Prokop, A. Biotechnol. Bioeng. 19, 1553 (1977)

82. Kappeli, O. and Fiechter, A. Biotechnol. Bioeng. 22, 1509 (1980)

83. Tsao, G.T. Biotechnol. Bioeng. 12, 51 (1970)

84. Tsao, G.T. Chem. Eng. Sci. 27, 1593 (1972)

85. Tsao, G.T. Biotechnol. Bioeng. 19, 557 (1977)

86. Tsao, G.T. Biotechnol. Bioeng. 20, 157 (1978)

87. Lozowski, D., Langa, J., Andrews, G.F. and Stroeve, P. Chem. Eng. Comm. 6, 349 (1980)

88. Sobotka, M., Votruba, J. and Prokop, A. Biotechnol. Bioeng. 23, 1193 (1981)

89. Yagi, H. and Yoshida, F. Biotechnol. Bioeng. 17, 1083 (1975)

90. Yagi, H. and Yoshida, F. Biotechnol. Bioeng. 19, 561 (1977)

91. Merchuk, J.C. Biotechnol. Bioeng. 19, 1885 (1977)

92. Linek, V. and Benes, P. Biotechnol. Bioeng. 19, 565 (1977)

93. Brian, P.L.T., Vivian, J.E. and Mayr, S.T. Ind. Eng. Chem. Fundam. 10, 75 (1971)

94. Buchholtz, R., Luttman, R., Zakrzewski, W. and Schugerl, K. J. Chem. Tech. Biotechnol. 31, 435 (1981)

95. Bandyopadhyay, B., Humphrey, A.E. and Taguchi, H. Biotechnol. Bioeng. 9, 533 (1967)

96. Mignone, C.F. and Ertola, R.J. J. Chem. Tech. Biotechnol. 34B, 121 (1984)

97. Spriet, J.A. and Botterman, J.H. J. Chem. Tech. Biotechnol. 34A, 137 (1984)

98. Heineken, F.G. Biotechnol. Bioeng. 12, 145 (1970)

99. Lee, Y.H. and Tsao, G.T. Adv. Biochem. Eng. 13, 35 (1979)

100. Dang, N.D.P., Karrer, D.A. and Dunn, I.J. Biotechnol. Bioeng. 19, 853 (1977)

101. Aiba, S. and Huang, S.Y. Chem. Eng. Sci. 24, 1149 (1969)

102. Linek, V. and Benes, P. Biotechnol. Bioeng. 19, 741 (1977)

103. Linek, V. and Vacek, V. Biotechnol. Bioeng. 18, 1537 (1976)

104. Linek, V. and Vacek, V. Biotechnol. Bioeng. 19, 983 (1977)

105. Linek, V. and Benes, P. Biotechnol. Bioeng. 20, 903 (1978)

106. Shoiya, S. and Dunn, I.J. Chem. Eng. Sci. 33, 1529 (1978)

107. Lopes de Figueiredo, M.M. and Calderbank, P.H. Chem. Eng. Sci. 34, 1333, (1979)

108. Dunn, I.J. and Einsele, A. J. Appl. Chem. Biotechnol. 25, 707 (1975)

109. Shoiya, S. and Dunn, I.J. Chem. Eng. Comm. 3, 41 (1979)

110. Linek, V. and Vacek, V. Chem. Eng. Sci. 37, 1425 (1982)

111. Chapman, C.M., Gibilaro, L.G. and Nienow, A.W. Chem. Eng. Sci. 37, 891 (1982)

112. Vardar, F. and Lilly, M.D. Biotechnol. Bioeng. 24, 1711 (1982)

113. Sridhar, T. and Potter, D.E. Ind. Eng. Chem. Fund. 19, 21 (1980)

114. Kipke, K. International Symposium on Mixing, Mons (1978)

115. Nishikawa, M., Nakamura, M. and Hashimato, K. J. Chem. Eng. Japan 14, 227 (1981)

116. Tanaka, H. Biotechnol. Bioeng. 24, 425 (1982)

117. Manfredini, R. and Cavallera, V. Biotechnol. Bioeng. 25, 3115 (1983)

118. Nakanoh, M. and Yoshida, F. Biotechnol. Bioeng. 25, 1653 (1983)

119. Votruba, J. and Sobotka, M. Biotechnol. Bioeng. 18, 1815 (1976)

120. Votruba, J., Sobotka, M. and Prokop, A. Biotechnol. Bioeng. 19, 435 (1977)

121. Votruba, J., Sobotka, M. and Prokop, A. Biotechnol. Bioeng. 20, 913 (1978)

122. Linek, V. and Vacek, V. Biotechnol. Bioeng. 20, 305 (1978)

123. Heijnen, J.J., Van't Riet, K. and Wolthius, A.J. Biotechnol. Bioeng. 22, 1945 (1980)

124. Schumpe, A. and Quicker, G. Adv. Biochem. Eng. 24, 1 (1982))

125. Schumpe, A., Adler, I. and Deckwer, W.D. Biotechnol. Bioeng. 20, 145, (1978)

126. International Critical Tables, 3, 272, McGraw-Hill, New York (1928)

127. "Standard Methods for the Examination of Water and Waste Water", 13th Ed., American Public Health Assoc. and American Waterwork Assoc. and Pollution Federation, Eds. American Public Health Assoc., New York, p474 (1971)

128. Hikita, H., Asai, S. and Azuma, Y. Can. J. of Chem. Eng. 56, 371 (1978)

129. Quicker, G., Schumpe, A., Konig, B. and Deckwer, W.D. Biotechnol. Bioeng. 23, 635 (1981)

130. Kappeli, O. and Fiechter, A. Biotechnol. Bioeng. 23, 1897 (1981)

131. Sideman, S., Hortacsu, O. and Fulton, J.W. Ind. Eng. Chem. 58, No 7, 32 (1966)

132. Henzler, H.J. Chem. Ing. Techn. 52, 643 (1980)

133. Nagata, S., Nishikawa, M., Tada, H. and Gotoh, S. J. Chem. Eng. Japan 4, 72 (1971)

134. Paca, J., Ettler, P. and Gregr, V. J. Ferment. Technol. 56, 144 (1978)

135. Jurecic, R., Berovic, M., Steiner, W. and Koloini, T. Can. J. Chem. Eng. 62, 334 (1984)

136. Kok, R. and Zajic, J.E. Biotechnol. Bioeng. 17, 273 (1975)

137. Jones, R.P., Pamment, N. and Greenfield, P.F. Proc. Biochem. 16, 42 (1981)

138. E.B.C. Analytica Microbiologica, Method 2.2.2.3. "Methylene Blue Staining". J. Inst. Brew. 83, 109 (1977)

139. Patel, Y.R. Ph.D. Thesis, University of Birmingham (1983)

140. Vogel, A.I. "Text Book of Quantitative Inorganic Analysis: Theory and Practice", 3rd Edn. Longmans (1962)

141. Wasan, D.T., Lynch, M.A., Chad, K.J. and Srinivasan, N. A.I.Ch.E. J. 18, 928 (1972)

142. Oladimaji, S. M.Sc. Thesis, Dept. of Chem. Eng., University of Birmingham (1981)

143. Miller, G.L. Anal. Chem. 65, 426 (1959)

144. Andrews, S.P.S. Trans. Instn. Chem. Eng. 60, 3 (1982)

145. Hocker, H., Langer, G. and Werner, U. Chem. Ing. Techn. 52, 916 (1980)

146. Allsford, K. Ph.D. Thesis, University of Birmingham (1985)

147. Kuboi, R. and Nienow, A.W. Fourth European Conference on Mixing (BHRA) Leeuwenhurst, 247 (1982)

148. Kipke, K.D. Fourth European Conference on Mixing (BHRA) Leeuwenhorst, 355 (1982)

149. Sittig, W. J. Chem. Tech. Biotechnol. 32, 47 (1982)

150. Moo-Young, M. and Blanch, H.W. Adv. Biochem. Eng. 19, 1 (1981)

151. Furukawa, K., Heinzle, E. and Dunn, I.J. Biotechnol. Bioeng. 25, 2293 (1983)

152. Moraine, R.A. and Rogovin, P. Biotechnol. Bioeng. 15, 225 (1973)

153. Jones, R.P. and Greenfield, P.F. Enz. Microb. Technol. 4, 210 (1982)

154. Barford, J.P. and Hall, R.J. Biotechnol. Bioeng. 21, 609 (1979)

155. Judat, H. Ger. Chem. Eng. 5, 357 (1982)